Fuel Cell Power Plant Integrated Systems Evaluation

Keywords:
Fuel Cells
Molten Carbonate
Power Plant

EPRI

EPRI EM-1670
Project 1085-1
Final Report
January 1981

Prepared by
General Electric Company
Schenectady, New York

ELECTRIC POWER RESEARCH INSTITUTE

Fuel Cell Power Plant Integrated Systems Evaluation

EM-1670
Research Project 1085-1

Final Report, January 1981

Prepared by

GENERAL ELECTRIC COMPANY
Energy Systems Program Department
One River Road
Schenectady, New York 12345

Principal Investigators
T. L. Bonds
M. H. Dawes
A. W. Schnacke
L. W. Spradlin

Prepared for

Electric Power Research Institute
3412 Hillview Avenue
Palo Alto, California 94304

EPRI Project Manager
B. R. Mehta

Fuel Cells and Chemical Energy Conversion Program
Energy Management and Utilization Division

ORDERING INFORMATION

Requests for copies of this report should be directed to Research Reports Center (RRC), Box 50490, Palo Alto, CA 94303, (415) 965-4081. There is no charge for reports requested by EPRI member utilities and affiliates, contributing nonmembers, U.S. utility associations, U.S. government agencies (federal, state, and local), media, and foreign organizations with which EPRI has an information exchange agreement. On request, RRC will send a catalog of EPRI reports.

NOTICE

Prepared by
General Electric Company
Schenectady, New York

ABSTRACT

Carbonate fuel cell power plants are attractive candidates for future power generation applications. One application of these plants would be central stations (675 MW) fueled by coal. Another would be small dispersed generation plants (5 MW) fueled by oil, probably with reject heat utilitization. This report presents an extension of efforts reported in Interim Report (EPRI No. 1097) dated June 1979, and describes the activities conducted to define power plant configurations for these two applications.

Plant capital costs and cost of electricity were evaluated for both plants and these have been compared with cost goals. Performance sensitivity studies have led to an improvement in plant cycle efficiency and have considered the important design constraints. Parametric variations and the impact on the plant and components are discussed. Alternate oil-fired cycles as well as several alternate coal gasifiers are examined to show effects on plant performance. A steam injection and anode recirculation study was also performed.

A cost sensitivity evaluation was performed for both plants for variations in design parameters and/or design assumptions on the cost of electricity. The objective was to seek the minimum cost of electricity in those cases where design freedom existed, or to evaluate the importance of an assumption in those cases where design freedom did not exist. The vital connection between these results, the technology development goals, and the sensitivity of plant economics is discussed.

Through this work, the economic attractiveness of the coal-fired plant is confirmed, and a scenario in which the dispersed oil-fired plant with reject heat recovery is established. Performance for the coal-fired plant (6669 Btu/kWh) exceeds the study goal (6800 Btu/kWh) significantly, and the oil-fired plant performance (7627 Btu/kWh) is very close to the study goal (7500 Btu/kWh).

The development of a finite slice computer model of the carbonate fuel cell is reported and an initial parametric cell and plant performance study was performed using the model.

Preliminary subsystem description sheets and plant layout arrangements are presented.

EPRI PERSPECTIVE

PROJECT DESCRIPTION

Molten carbonate fuel cell (MCFC) power plants could be an attractive generating option due to their high inherent efficiency coupled with their benign environmental characteristics. Such power plants are being considered for application both as baseload, central station generators integrated with coal gasifiers and as intermediate duty, dispersed generators fueled by distillate fuel or natural gas. The efficiency and cost of these power plants are determined to a large degree by the ability to fully integrate the fuel cell power section with the fuel processor and other power plant subsystems. The ability to utilize waste heat streams to preheat reactants or produce auxiliary power is important to the overall power plant cost and efficiency.

This project (RP1085-1) evaluated integrated MCFC power plant configurations that would result in reference designs for the respective applications. The cost and performance of these two reference design cycles were subsequently analyzed to determine optimum, integrated design configurations which could achieve or exceed desired efficiency and cost goals. This final system analysis report describes the results of these analyses.

PROJECT OBJECTIVES

The general objective of EPRI's MCFC program is to develop practical, thermally cyclable, high-performance, cost-effective components and subsystems, which can be integrated into large central power stations or dispersed power (and heat) generators. For this project, targets of 50% efficiency (6800 Btu/kWh heat rate) and a total capital cost (1978 dollars) of $800/kW were established for the central station baseload plant, and 45.5% efficiency (7500 Btu/kWh heat rate) and a total capital cost (1978 dollars) of $300/kW were established for the dispersed, intermediate duty power plant.

The specific objectives addressed in this report were:

- To develop optimum MCFC power plant designs based upon cost and efficiency
- To determine cost and performance sensitivities to a range of design and operating parameters
- To evaluate impact on cost and efficiency of alternative coal gasifiers

PROJECT RESULTS

An oxygen-blown Texaco coal gasifier fueled by Illinois No. 6 coal and thermally integrated with MCFC topping cycle and a partially cascaded 2400 psig/950°F/950°F steam bottoming cycle was selected as the reference baseload (675 MW) central power plant. This reference plant achieved a 6700 Btu/kWh heat rate (51.2% efficiency) versus a 6800 Btu/kWh heat rate (50% efficiency) goal. A preliminary cost assessment of this 675 MW coal-fired plant indicated total capital requirement (TCR) of $846/kW versus a capital cost goal of $800/kW (both in 1978 dollars). Recent detail cost estimates (RP239-2, EPRI Final Report AP-1543) for a similar 1430 MW power plant fueled by 10,000 STPD coal reported TCR of $749/kW (1976 dollars). Considering the preliminary nature of these cost estimates, the capital cost estimates of the coal-fired MCFC plant appear to be in excellent agreement and close to the program goal.

The above TCR analysis assumed that the interim replacement cost of fuel cell stacks at 40,000-operating-hour intervals will be treated as an operation and maintenance (O&M) cost. The interim replacement costs could also be capitalized. It is also important to note that the fuel cell stacks at the end of 40,000-hour design life would still generate power, though at slightly less than design efficiency, for an extended period. At 70% capacity factor, the different accounting procedures could impact the capital costs and first-year cost of electricity (COE) as follows (1978 dollars):

	Interim Replacement Costs Treated as O&M Costs	Equivalent TCR by Capitalizing 100% Fuel Cell Replacement Costs
Capital costs ($/kW)	846	1014
First year COE (mills/kWh)	42.6	46.7

Cost and performance sensitivity analysis for the central station power plant indicated that (1) the fuel cell design optimized at 150 ASF/0.768 VDC and (2) power plant economics were not adversely impacted by either increasing sulfur content of the coal or by a significant increase in sulfur removal requirements.

Technoeconomic comparisons of MCFC power plants employing a Texaco entrained coal gasifier versus those with Shell-Koppers (entrained-bed), U-Gas (fluidized-bed), and British Gas Slagging (moving-bed) gasifiers suggested that high-temperature, entrained-bed gasifiers with highest level of conversion of coal into ($CO + H_2$) tend to offer attractive heat rates and the lowest cost of electricity. Within the accuracy of such estimates and early developmental nature of these gasifiers, all four gasifiers appeared to be acceptable for integrating with MCFC power plants.

The initial cost and performance analysis of an oil-fueled dispersed MCFC power plant (4.5 MW) did not achieve the cost and performance targets. The calculated heat rate was 7890 Btu/kWh versus a 7500 Btu/kWh goal, and the estimated plant capital costs of $641/kW exceeded the $300/kW goal. A better understanding (by the contractor) of the fuel reformer and its integration with the fuel cell subsystem is required to approach realistic efficiency and competitive cost levels.

B. R. Mehta, Project Manager
Energy Management and Utilization Division

CONTENTS

ILLUSTRATIONS

TABLES

Section 1

EXECUTIVE SUMMARY

OVERALL PROGRAM

The work described in this final report was performed by the General Electric Company under EPRI Contract #RP 1085-1, "Molten Carbonate Fuel Cell Power Plant System Evaluation". The scope of this program was to define power plant cost and performance goals for central coal-fired stations and for dispersed oil-fired plants and then to define and evaluate plant design concepts against those goals. These activities continued the work reported in the June 1979 Interim Report, EPRI No. EM 1097 (2-1).

The overall plant cost goal for the reference 675 MW coal-fired power plant was established by determining the annual ownership cost that is attractive to the utility industry. At a selected capacity factor of 70%, a value of $340/kW/yr or less was determined as the requirement to compete with other coal-fired technologies such as the Integrated Gasification Combined Cycle power plant. An equivalent total capital requirement in 1978 dollars of $700 million or $1036/kW is then calculated for a central 675 MW coal-fired plant.

Subsystem cost goals were then derived from the review and appropriate scaling and adjustment of previously published costing studies and data. Bottom-up cost estimates were not performed in this study. The plant subsystem cost goals for the reference 675 MW coal-fired power plant developed in this study are shown in Table 1-1. Using these subsystem goals, overall plant cost goals were generated as shown in the economic summary given in Table 1-2.

Table 1-1

COAL-FIRED PLANT SUBSYSTEM COST GOALS

Plant Selection	Material	Labor	A&E Fee	Sales Tax	Total Cost	Contingencies Process	Contingencies Project	Total Plant Investment $	$/kW
Coal Handling	6,250	4,900	1,271	312	12,733	-	1,273	14,006	20.7
Oxidant Feed	35,000	24,350	6,810	1,750	67,910	-	6,791	74,701	110.8
Gasification and Ash Handling	7,000	5,250	1,400	350	14,000	700	1,400	16,100	23.8
Gas Cooling	25,000	8,900	4,015	1,250	39,165	1,958	3,917	45,040	66.7
Acid Gas Removal	25,000	8,000	3,925	1,250	38,175	-	3,818	41,993	62.2
Steam Bottoming Cycle	42,928	22,220	7,588	2,146	74,882	-	7,488	82,370	122.0
Fuel Cell Modules and Turbines	76,249	8,732	10,404	3,812	99,197	4,960	9,920	114,077	169.0
Inverter System	20,585	4,381	3,011	1,029	29,006	-	2,901	31,907	47.3
Electrical System	9,235	6,745	1,829	462	18,271	-	1,827	20,098	29.8
Land, Improvements, Misc.	21,415	18,015	4,478	1,071	44,979	-	4,398	49,477	73.3
Total	268,662	111,493	44,731	13,432	438,318	9,068	43,833	489,769	725.6

Notes: 1. All above figures are thousands of 1978 dollars.
2. Plant output = 675 MW (ac) Net

Table 1-2

PLANT COST GOALS - ECONOMIC SUMMARY
(1978 Dollars)

	$1000	$/kW	%
Total Plant Investment	489,769	725.6	85.8
Prepaid Royalties	2,456	3.6	0.4
Preproduction Costs	12,148	18.0	2.1
Inventory Capital	4,758	7.1	0.8
Initial Catalyst & Chemicals	292	0.4	0.1
Allowance for Funds in Construction	61,402	91.0	10.8
Total Capital Requirement (TCR)	570,825	845.7	100.0
Increment for Interim Replacement	113,632	168.3	
Equivalent Total Capital Requirement (ETCR)	684,457	1014.0	

The MCFC coal-fired power plant capital cost study goal available at the beginning of this study was $800/kW (1978 dollars).

Oil-fired power plant cost goals for several scenarios were determined and studies for both oil-fired and coal-fired applications were performed to evaluate the effects of different cycle and component assumptions on overall plant cost and performance. The studies for this period included:

- Cost and performance sensitivity evaluation of the large central station coal-fired power plant at 675 MW capacity.
- Cost and performance sensitivity evaluation of the small dispersed oil-fired power plant of 5 MW capacity.
- Development and initial cell evaluation of the finite slice (nodal) MCFC computer model.
- Evaluation of the performance of coal-fired systems using alternate gasifiers.
- Parametric evaluation of steam injection and anode recirculation for carbon formation control.
- Evaluation of the performance of alternate oil-fired systems using various reformer operating conditions.
- Analysis and evaluation of the cleanup system design.

REFERENCE PLANT EVALUATIONS

The work reported here focused upon developing cost information for the reference plants and determining the sensitivity of the costs to the various plant parameters. Based upon the cost sensitivity information, the plant configurations and goals were updated. The approach adopted for the plant evaluations is summarized as follows:

- Evaluation of plant capital costs based upon published report data.
- Establishment of plant operating cost and cost of electricity.
- Assessment of plant cost goals.
- Study of sensitivity of plant costs to key plant parameters and key assumptions.
- Updating of plant performance based on sensitivity results.
- Preparation of preliminary subsystem descriptions.
- Preparation of conceptual plant layout drawings.

COAL-FIRED PLANT

The plant studied had 675 MW(ac) capacity and was fueled by an oxygen-blown Texaco gasifier. It included a partially cascaded bottoming cycle, described in Case 1 in the interim report (2-1).

The first-year cost of electricity, assuming 70% capacity factor and $\$1.43/10^6$ Btu coal, was found to be 46.7 mills/kWh which, for a heat rate of 6669 Btu/kWh, consisted of the elements shown in Table 1-3:

Table 1-3

COAL-FIRED PLANT COST OF ELECTRICITY (70% Capacity Factor)

	First Year mills/kWh	%
Levelized Fixed Charges-Plant Investment	27.4	58.7
Fuel Cell Replacement Allowance	6.0	12.8
Fuel ($1.43/$10^6$ Btu coal)	9.6	20.6
O&M	3.7	7.9
	46.7	100.0

Cost Sensitivity Study

The cost evaluation results were used as the basis for a cost sensitivity evaluation in which the sensitivity of the cost of electricity to important design parameters and assumptions was determined.

The major findings were:

- Increasing fuel cell current density above the design value of 160 mA/cm^2 leads to improvement in the cost of electricity up to 5% at a peak value of about 300 mA/cm^2. Reduction below this design value can result in a 5% increase at a level of 120 mA/cm^2.
- Increased current density can, to some extent, compensate for the adverse economic impact of excessive polarization loss, assuming linear polarization behavior.
- The power plant will remain economically attractive over a wide range of coal sulfur content. A change from 3% coal sulfur content to 4%, as an example, results in an increase in the cost of electricity of 2%.
- Acid gas removal subsystem costs can change significantly without significantly altering the cost of electricity. Variations in acid gas removal costs of ±50% will change the cost of electricity by ±3.5%.
- The coal-fired plant cost of electricity optimizes at 180% excess fuel cell air flow.

Performance Sensitivity

The plant cycle was studies to determine sensitivity to key parametric variations. Major findings were:

- The fuel cell air flow and pressure selected were 180% excess air and 100 psia pressure. Operation above 180% reduces plant efficiency and also raises raw gas cooler metal temperature above a safe 800^{o}F level.

- The 50% anode recirculation ratio level was selected. This was a compromise between plant performance and carbon suppression in the fuel cell anode.

- If methane is assumed not to form in the anode, the plant optimizes at an anode recirculation ratio of 0.5, the minimum level needed to establish a carbon-free gas equilibrium in the anode.

- The reference steam cycle (2400 psi/950^{o}F/950^{o}F) can be upgraded to 2400 psi/1000^{o}F/1000^{o}F without significantly affecting the maximum temperature of the steam in the high temperature steam generator heat exchanger. This will permit a 38% steam turbine generator efficiency at a condenser pressure level as high as 3" Hg.

- Overall plant efficiency changes with increased fuel cell current density at the rate of approximately 1% per 50 mA/cm^{2}, assuming 0.7 Ω/cm^{2} polarization losses.

Coal-Fired Power Plant Performance

Based on the prior sensitivity studies, the power plant performance was updated, and new flow sheet data were calculated.

The coal-fired plant efficiency, as a result of the study, was updated to 51.2% (6669 Btu/kWh). This was achieved while meeting all of the constraints imposed. It exceeds the program goal of 50% (6800 Btu/kWh).

Alternate Coal Gasifier Evaluation

Three alternate gasifier systems were studied to assess overall performance and cost values in comparison with the reference design; the Shell-Koppers (entrained) system, the IGT U-Gas (fluidized) system and the British Gas Slagger (moving bed) system. Using updated Texaco gasifier cycle data, an overall comparison was made. The normalized results are shown in Table 1-4 (details in Appendix F).

Table 1-4

SYSTEM ECONOMIC COMPARISON OF ALTERNATE GASIFIERS

	Texaco	British Gas Slagger	IGT U-Gas	Shell Koppers
Total Plant Investment 1978 ($1000)	1.0	0.977	0.910	0.961
Equivalent Total Capital Requirement ($1000)	1.0	0.977	0.910	0.961
Cost of Electricity mills/kWh	1.0	0.985	0.949	0.968
$\frac{(CO + H_2)}{\text{Coal HHV Input}}$ Cold Gas Efficiency(%)	1.0	0.919	0.862	1.04
$\frac{\text{Net Electric Output(\%)}}{\text{Coal HHV Input}}$	1.0	0.987	0.932	1.02

These results show that the most important gasifier parameter for MCFC combined cycle efficiency is the ratio of the heating value of the $CO+H_2$ in the product gas to the heating value of the coal. The output ratio $\frac{\text{Electrical Output}}{\text{Coal HHV Input}}$ of the fuel cell, the largest contributor to system output, is approximately proportional to this heating value ratio. The gas turbine generator output ratio is approximately proportional to the ratio of the total gas heating value to the heating value of the coal, since the turbine air/gas flows are proportional to the total quantity of fuel gas handled by the system. Gas turbine generator gross output also increases with the pressure ratio of the fuel gas expander. Heat transferred to the steam is the difference between the coal energy input and the sum of fuel cell and gas turbine generator outputs plus losses including the largest loss, stack loss. The stack loss ratio increases with the ratio of total gas heating value to the heating value of the coal.

Overall conclusions from the study are:

- The Shell-Koppers and Texaco high temperature entrained bed gasifiers have a significant performance advantage for the MCFC combined cycle application over the U-Gas (fluidized bed) gasifier, and a small advantage over the British Gas Slagger (moving bed) gasifier. The superior performance of the entrained bed gasifier relates directly to a higher $CO+H_2$ cold gas efficiency.

- The British Gas Slagger gasifier, operating with total recycle of tar and condensable hydrocarbons, has a very high overall product gas cold gas efficiency (0.95), and also a moderately high $CO+H_2$ cold gas efficiency (0.70). These characteristics result in a potential for 50% efficiency of a combined cycle system using this gasifier.

- A wide range of gasifiers appears to be acceptable from a cost standpoint. The results for the BGC gasifier power plant show that the cost of recovering condensable hydrocarbons (tars, oils, phenols, naptha) has a negligible effect on the overall capital cost and the cost of electricity.

- The U-Gas gasifier power plant has the lowest cost of electricity despite higher operating expenses because of the lower capital needs of its gasification, gas cooling subsystems.

- Capital cost variations dominate the economics of each of these power plants compared to the fuel, operating and maintenance expenses. Fixed charges amount to approximately 70% of the total cost of electricity.

MCFC Parametric Evaluation

An extension of General Electric's molten carbonate fuel cell modeling efforts, reported previously, resulted in the development of a finite slice (nodal) model (Appendix D) and simulation of the fuel cell and associated MCFC subsystem. In the development of the earlier lumped parameter fuel cell model, described in EPRI EM-1097, June 1979, the simplified model was intended to represent general parametric relationships, as opposed to detailed behavior of the fuel cell.

Use of the finite slice model developed in the recent efforts provided more insight into the predicted behavior of the cell itself and more accurately represented its performance characteristics in the overall system. Of special interest are the predictions of temperature distributions (anode gas, cathode gas, cell/electrolyte) within the fuel cell as a function of flow configuration and operating conditions. For example, in the earlier lumped parameter model, it was assumed that the temperature of the two exit gas streams from the cell were essentially at the same temperature as the cell itself, based on assumed vigorous heat transfer characteristics. Calculated results from the finite slice model, however indicated that this previous assumption was not valid and that previous conclusions regarding heat removal in the anode and cathode gas streams were imprecise.

Preliminary results from the finite slice model showed that the higher cell efficiency associated with counterflow operation is accompanied by a temperature profile within the cell that has undesirable peaks and gradients compared to those for co-flow operation. These and other results, including an examination of predicted characteristics for crossflow operation, revealed characteristics that would not be predicted from the lumped parameter model. System implications associated with choice of flow arrangement and planned method of operation require careful study. The developed MCFC subsystem model, with the finite slice representation of the fuel cell, is useful in determining answers to important system-related questions.

Parametric runs were made using the MCFC subsystem simulation with the finite slice fuel cell model. The results provided a preliminary indication of subsystem operational interrelationships as well as the detailed bahavior of the key fuel cell parameters under different conditions. Three cell flow configurations were investigated; co-flow, counterflow, and crossflow. A comparison of the results for the three flow configurations yields several observations and conclusions about the indicated trends:

- For a given fuel and oxidant utilization (e.g., 0.85), cell efficiency increases as fuel flow (and power output) decrease. This increase in efficiency is most marked for the counterflow configuration and is least for the co-flow case.
- As flow is decreased (at constant utilization), the terminal voltage changes least for the co-flow configuration (about 3% for a 75% decrease in fuel flow). For the counterflow configuration, the voltage increases approximately 13%.
- The distribution of local current density in the cell is most uniform for the counterflow configuration, and the pattern is relatively unaffected by a reduction in fuel flow.
- The distribution of temperature within the cell is an important consideration and differs significantly as a function of flow configuration.

Steam Injection and Anode Recirculation Studies

Using the nodal fuel cell model, the use of steam injection and anode recirculation was investigated as a method of preventing carbon formation at the anode inlet to be compared with anode recirculation only. The nodal fuel cell model indicated that water vapor injection can be used either alone, or in conjunction with anode recirculation, as a means of preventing carbon formation at the anode inlet. The use of water vapor injection generally results in an increase in cell efficiency up to a value of approximately 0.30 water vapor, with a peak efficiency of 47.3%

occurring in the range of 0.20 to 0.30 water vapor, and anode recirculation of 0.2 or less, but within this range of operating conditions the peak cell efficiencies do not appear to be significantly different.

OIL-FIRED PLANT

In the interim report, a small oil-fired plant (5 MW) for dispersed application was described. The plant gasifies #2 fuel oil in an autothermal reformer. Sulfur is removed by a zinc oxide reactor. Power is generated only with fuel cells; a turbocompressor with no net power output uses the fuel cell waste heat to drive the requisite air compressors.

Cost Evaluation

A Total Capital Requirement of $810.4/kW was determined through evaluation and scaling of existing published data. These results are shown in Table 1-5.

Table 1-5

OIL-FIRED PLANT COST EVALUATION
(Plant Output 4.5 MW (AC) Net)

	$/kW*	%
Land and Improvements, Structures and Miscellaneous Equipment	43.2	6.7
Fuel Handling and Processing	110.2	17.2
Fuel Cell Subsystem	250.4	39.0
Turbocompressor	54.0	8.6
Electrical System	103.6	16.2
Total	561.4	100.0
Capital Charges	80.0	
Increment for Fuel Cell Replacement	169.0	
Equivalent Total Capital Requirement (ETCR)	810.4	

Notes: 1) * Per plant kW (AC) Net
2) 1978 Dollars

The fuel cell subsystem is clearly the predominant cost, accounting for 39% of plant cost. Within the fuel cell subsystem, the fuel cells stacks are the major item.

The first year cost of electricity from this oil-fired plant is 79.5 mills/kWh, as indicated in Table 1-6:

Table 1-6

OIL-FIRED PLANT COST OF ELECTRICITY
(50% Capacity Factor)

	mills/kWh	%
Levelized Fixed Charges-Plant Investment	26.4	33.2
Fuel Cell Replacement Allowance	7.0	8.9
Fuel ($4.74/$10^6$ Btu) Oil	37.4	47.0
O&M	8.7	10.9
Total	79.5	100.0

The fuel cell replacement allowance, while certainly not negligible, can be seen to be a smaller percentage (9%) of the total than in the coal-fired case. The impact of using a premium fuel is apparent in this cost of electricity breakdown.

Plant Cost Goals

The original cost goal established in 1978 dollars for this plant was $300/kW; however, this was evaluated on the basis of competing in the utility system. This early evaluation did not make adequate recognition of the plant's unique ability to be sited in a dispersed urban area, nor did it place value on the high grade reject heat available. The predicted costs of alternate advanced competing power plants, used to establish the goal, have also changed since selection of the original goal.

An updated evaluation was made of the plant cost goals; this justifies increasing the cost goal to $525/kW. We believe that this goal is achievable through continuing technology development and is dependent on realization of the assumed savings or credits.

Performance Sensitivity

An integrated performance sensitivity study was conducted on the oil-fired plant to establish the feasibility of improved plant efficiency. This focused on interactions between reformer conditions and fuel cell conditions that related fuel cell and reformer pressure effects associated with carbon deposition in the fuel cell and in the reformer. The sensitivity study became a multivariable trade-off with the objective of searching for the best efficiency.

The major conclusions were:

- Cathode recirculation (50%) permits a reduction in the amount of excess cathode air needed for cooling; the resultant increase in cathode CO_2 concentration increases plant efficiency.
- A reduction in reformer steam flow will increase the tendency to deposit carbon in the fuel cell anode, which can be controlled by a reduction in system pressure. This can lead to an improved plant performance, although presently constrained by reformer operating limitations.
- Plant efficiency increases vary slightly with increased reformer operating temperatures.
- The power plant efficiency goal of 45.5% is reasonable and could be exceeded if reformer development programs are successful at low air to fuel ratios.

Cost Sensitivity Study

To find the minimum cost of electricity, a cost sensitivity study was performed by adjusting several key plant parameters.

The major findings were:

- The cost of electricity would be reduced only 2% by increasing the fuel cell design current density from 160 mA/cm^2 to 190 mA/cm^2. The impact of reducing current density below 150 mA/cm^2 is important in establishing technology development goals. Reduction to 100 mA/cm^2 showed a 20% increase in the cost of electricity.
- A change in fuel sulfur content from 0.22% design value to 0.5% increased cost of electricity by 8.6 mills/kWh.
- A change in excess air from the original 300% to 60% produced a 2% reduction in cost of electricity.

Oil-Fired Power Plant Performance

The various performance and cost sensitivity studies described herein have improved the efficiency to a value of 44.8% (7627 Btu/kWh) as compared with the study goal of 45.5% (7500 Btu/kWh).

Modest improvement in reformer performance through technology development would cause the plant to exceed the performance goal.

Alternate Oil-Fired System Cycles

A cycle design approach different from that in previous studies was investigated to define new theoretical possibilities for achieving high fuel cell performance in the oil-fired plant. Two alternate forms of a cycle employing an oil steam reformer thermally coupled by heat transfer to a combustor of anode discharge gas were defined. The result is a potential improvement that would dramatically increase the reformer fuel conversion and the fuel cell efficiency.

Although the No. 2 oil steam reformer component required by this approach is not yet realizable as a practical device, these cycles indicate new levels of fuel cell and overall cycle efficiency that are theoretically achievable with No. 2 oil fuel, and which may be, at the present state of the steam reforming art, actually achievable with methane and light hydrocarbon fuels.

Section 2

COAL-FIRED PLANT EVALUATION

INTRODUCTION

This section of the report describes a sequence of studies conducted on a Molten Carbonate Fuel Cell (MCFC) power plant using coal as its source of energy. The general approach has been to select a cycle configuration and then improve that plant through a series of cost and performance evaluations. Finally, preliminary subsystem description sheets have been prepared.

The previous interim report (2-1) described several coal-fired power plant cycle options. The plant shown below in Figure 2-1 (Case 1 in Reference 2-1) was selected for the studies described herein. This cycle employs a 600 psia Texaco-type entrained gasifier with oxygen as the oxidant feed. After cooling, the fuel gas is cleaned of sulfur impurities via a Selexol-based cleanup system with a zinc oxide polisher, and following regenerative heating is expanded to the fuel cell pressure of 100 psia. The fuel cell has anode reactant gas recirculation to prevent carbon buildup, and cathode reactant gas recirculation to remove heat. The anode exhaust is passed through a catalytic burner to provide CO_2 for the cathode. Spent cathode gases are expanded through a turbocompressor, which provides electrical power and pressurizes the cathode air supply. A steam turbine is driven by heat rejected from three locations – cathode recycle, gasifier and cathode exhaust – in the cycle. A more detailed description of the plant can be found within this section under the subheading "Coal Plant Description."

Figure 2-2 shows the work flow plan adopted for these studies. Two different costing methods were used. The first, described as the ECAS method, follows the methodology used by the United Technologies Corporation (UTC) MCFC portion of the ECAS study (2-2). The second method, described as the EPRI method, is as prescribed by the EPRI Technical Assessment Guide (TAG). The most significant difference between the ECAS and EPRI methods is the evaluation of the cost for replacement fuel cells. Details of both cost methods are given in Appendix B.

For the establishment and evaluation of system and subsystem goals, EPRI's 1979 TAG was used as a guideline for the cost sensitivity studies.

COST EVALUATION

Cost evaluations were made using utility (2-4) accounting methods, and compared with cost estimates based on ECAS (2-2) techniques. The data base was obtained from several different sources listed below:

- Economic Studies of Coal Gasification Combined Cycle Systems for Electric Generation, Fluor Engineers and Constructors, Inc., EPRI Report No. AF 642, January 1978 (2-3).
- Energy Conversion Alternatives Study (ECAS), United Technologies Phase II Final Report, NASA Report No. CR 134955, FCR-0237 (2-2).
- Molten Carbonate Fuel Cell Power System Evaluation - Gas Cleanup System and Sulfur Plant. J.C. Dart & Associates, May 9, 1979 (2-5).
- Cogeneration Technical Alternatives Study (CTAS), Interim Oral Briefing, General Electric Co., Contract No. DEN 3-31, December 7, 1978.
- Cogeneration Technical Alternatives Study, Final Oral Briefing, General Electric Co., Contract No. DEN 3-31, April 27, 1979.
- Advanced Power Cycles and their potential for Electrical Energy Generation. General Electric Company, Corporate Research and Development, April 1978.
- Energy Conversion Alternatives Study (ECAS) Summary Report, General Electric Company, NASA Report No. TM-73871, September 1977.
- Technical Memo: Fuel Cell Task Force Comparison of Capital and Operating Costs of a Molten Carbonate Fuel Cell Integrated with a Low Btu Gasifier and GE-ECAS & Power Plant Concepts. H.E. Gerlaugh, General Electric Company, October 5, 1976.

The first two citations provided the bulk of the data base since the systems costed were similar to our reference systems. In addition, these references contained sufficient subsystem cost details to evolve appropriate scaling changes to match our reference plants. The third citation was used as the cost basis for cleanup system.

Procedures and Assumptions Used for Plant Costing

The significant procedures and assumptions inherent in the two costing methods are discussed in Appendix B.

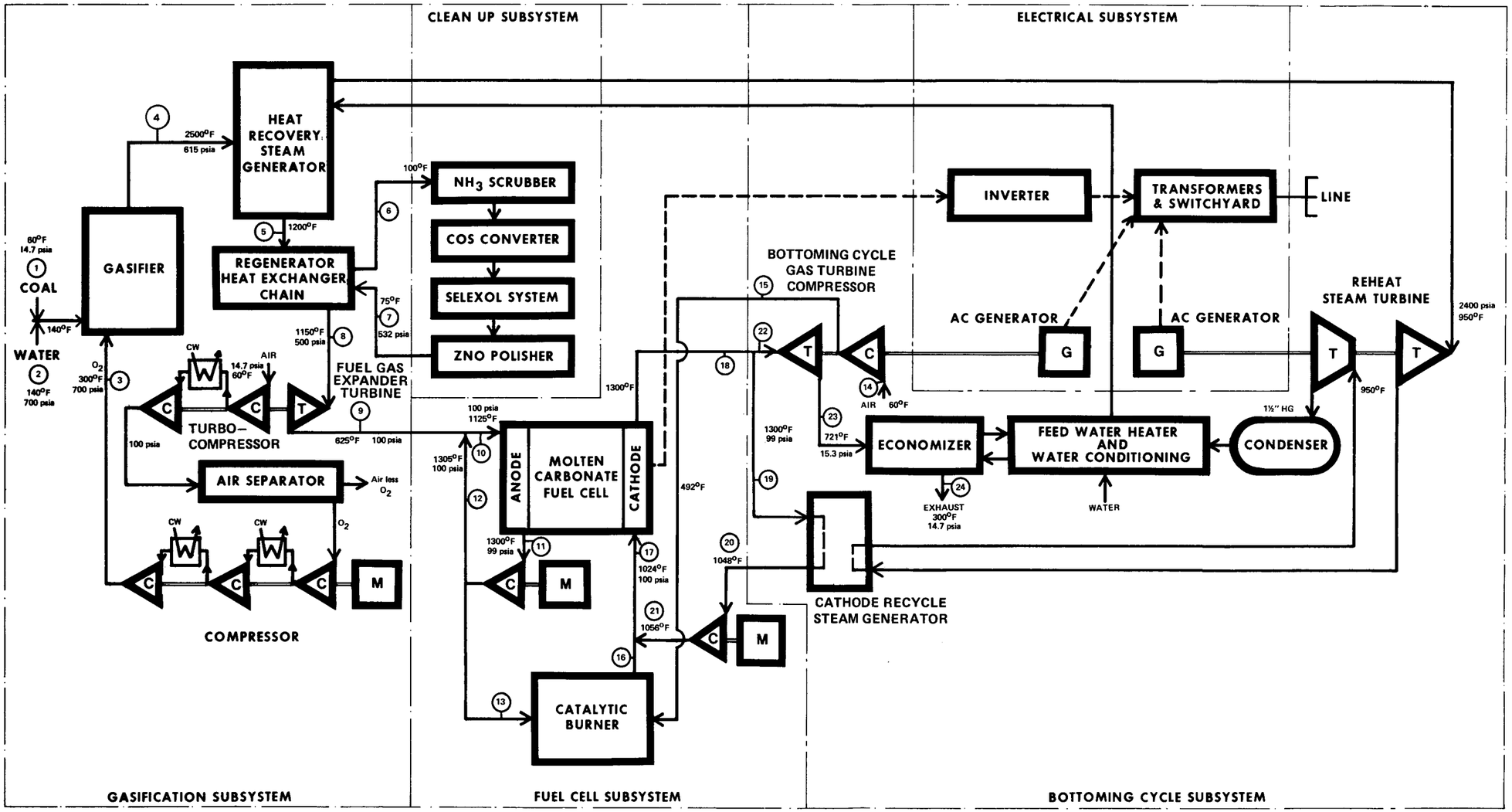

Figure 2-1. A Coal-Fired Molten Carbonate Fuel Cell Power Plant With an Oxygen-Blown Gasification System and a Partially Cascaded Bottoming Cycle

Blank Page

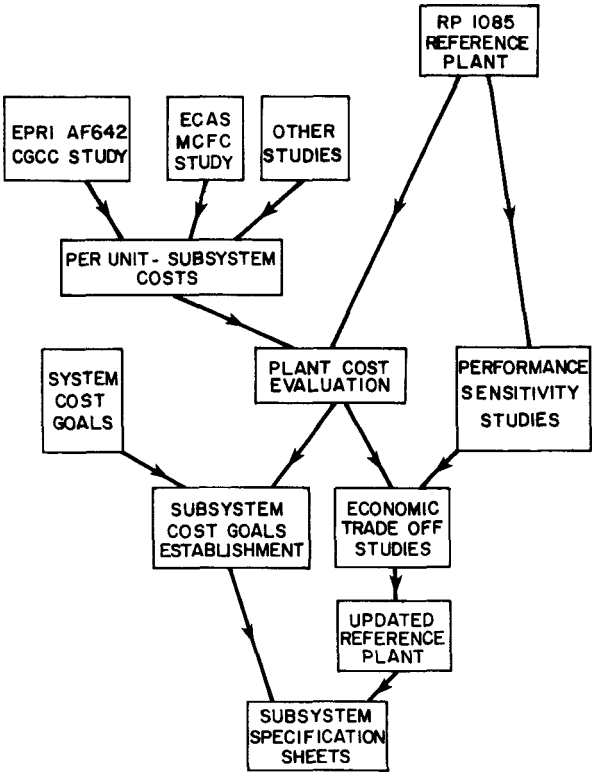

Figure 2-2. Coal-Fired Plant Cost Studies Work Plan

Coal-Fired Plant Cost Evaluation Scaling Factors

In using plant costs generated in one study to evaluate those of another study, it is vital to use appropriate scaling factors. This requires identifying the plant operating parameters which have the most significant influence on plant cost, and then selecting a relationship between changes in that parametric value and the particular component or subsystem cost. If the system is not to be costed from a raw materials basis, then the selection of the scaling factors becomes somewhat judgmental. For this study, each component or subsystem cost was scaled proportionally to a single key parameter. Table 2-1 summarizes the data source and cost scaling parameter used for each plant component cost. These component costs were then further evaluated using the two different costing methods (EPRI AND ECAS) described in Appendix B.

PLANT COST GOALS

Completion of the plant cost evaluation permits a reevaluation of plant cost goals, and an estimate of the subsystem cost goals needed to meet that plant goal.

Table 2-1

COAL-FIRED PLANT - COMPONENT COST DATA SOURCES AND SCALING FACTORS

Subsystem	Source	Scaling Factors
• Land, Improvements, Structures & Misc. Equip.	ECAS Report (2-2)	Change in Plant MW Output
• Fuel Handling and Processing		
- Coal Handling	EPRI AF-642 (2-3)	Change in Coal Flow Rate
- Oxidant Feed	EPRI AF-642	Change in Coal Flow Rate
Gasification & Ash Handling	EPRI AF-642	Change in Coal Flow Rate
- Gas Cooling	EPRI AF-642	Change in Coal Flow Rate
- Acid Sulfur Recovery	J.C. Dart Report (2-6)	Change in Coal Flow Rate
- Sulfur Storage Removal & Transfer	ECAS Report	Change in Coal Flow Rate
• Fuel Cell Subsystem		
- Fuel Cell Turbocompressor	EPRI 1979 TAG (2-4)	Change in Turbine Output
- Balance of Fuel Cell Subsystem	ECAS Report	Change in Fuel Cell AC Output
• Steam Bottoming Cycle	EPRI AF-642	Change in Steam Turbine Cycle Output
• Electrical Plant Equipment		
- Inverter	ECAS Report	Change in Fuel Cell AC Output
- Steam Plant Accessory Electrical Equipment	ECAS Report	Change in Steam Cycle Output
- Balance of Electrical Plant	ECAS Report	Change in Plant MW Output
• Operating and Maintenance Costs		
- Coal Gasification and Desulfurization	EPRI AF-642	Change in Equipment Investment
- Balance of O&M Costs	EPRI AF-642 + ECAS Report	Plant MW Coal Flow Various

Note: All baseline costs were escalated to mid 1978 dollars, with 6.5%/Year inflation rate

The method used for establishing the coal plant cost goal is to determine the annual ownership cost that is economically attractive to the ultimate utility user. This requires identification of "competing" technologies from which the MCFC power plant may be selected.

Reference to the EPRI publication, "Technical Assessment Guide" (2-4) suggests that among the conventional technologies, the two current technology plants to be considered are coal-fired steam plant with flue gas desulfurization (FGD) and nuclear plants. Among the advanced technologies, three plants to be considered are liquid metal fast breeder reactors (LMFBR), atmospheric fluidized bed (AFB) steam generation with steam turbine, and integrated gasification combined cycle (IGCC) (entrained bed gasifier).

The same reference provides the cost and performance data shown in Table 2-2.

Table 2-2

POWER PLANT ASSESSMENT DATA

	Capital Cost $/kW	Fuel Cost $/10^6 Btu	O&M Cost Fixed $/kW/yr	O&M Cost Variable mills/kWh	Heat Rate Btu/kWh
Nuclear	818	0.44	3.10	1.5	10,400
Coal w FGD	730	1.43	12.9	3.5	9,450
AFB	700	1.43	10.8	6.05	9,950
IGCC	815	1.43	14.4	1.5	8,980
LMFBR	1023	0.44	3.10	1.5	9,000

Notes:
- East Central Region
- Private Utility
- 1978 dollars
- Coal Cost based on 1980 delivered prices extrapolated from 1985 & 1990
- EPRI "Technical Assessment Guide," 1979 issue

These may be reduced to an annual cost of ownership for each capacity factor selected using a 30-year levelized cost; the result is shown in Figure 2-3.

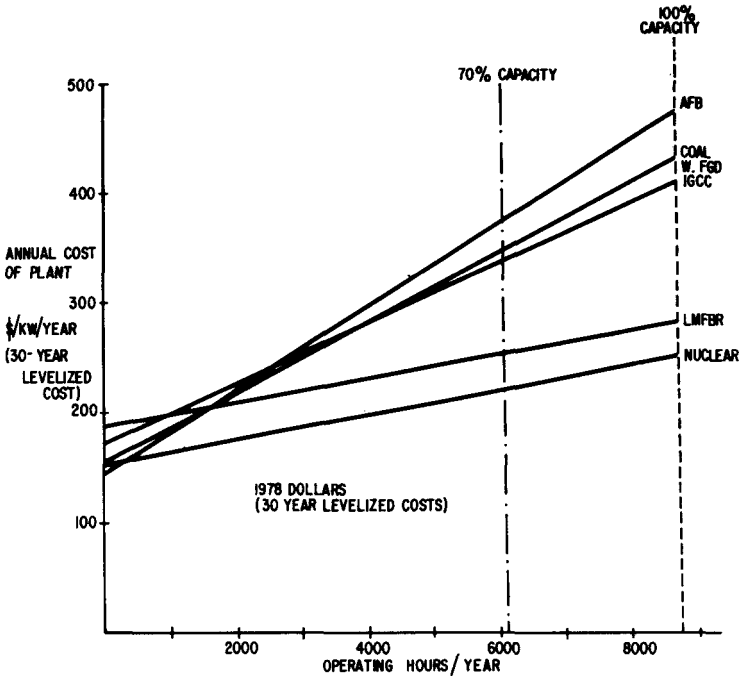

Figure 2-3. Central Power Plants - Cost Comparison

At the selected capacity level of 70%, the MCFC plant must have an annual cost of $340/kW/yr or less to be more attractive than the Integrated Gasification Combined Cycle plant. That plant, incidentally, incorporates an oxygen-blown Texaco gasifier based fuel supply. Establishment of this annual cost of $340/kW/yr now permits establishment of subsystem cost goals which will lead to an economically attractive plant. These subsystem cost goals may become development goals of equal importance to the technology development goals.

Use of the same fuel and O&M costs (as in the Appendix B-EPRI method) gives an allocation of annual costs as follows:

		k$/year
30-year levelized coal cost		75,153
Fixed O&M		26,608
Variable O&M		1,901
		103,662
Levelized fixed charges		125,838
$340/kW/year x 675 MW	=	229,500

From this, an equivalent total capital requirement goal (including increment for interim fuel cell replacement) of 1036 $/kW is calculated. The predicted equivalent capital cost obtained from the initial cost evaluation described previously (Appendix B) is within 10% of this goal.

Subsystem Goals

In the establishment of subsystem goals, the plant cost evaluation has modest process contingencies added. Using this approach, the subsystem goals that have been adopted are shown in Table 2-3.

Using these subsystem goals, the plant economic summary shown in Table 2-4 has been developed. This summary includes contingency of 5% for each of the following:

- Gasification and ash handling
- Gas cooling
- Fuel cell modules and turbines

10% project contingency has been added to all systems.

It may be seen that this approach yields a plant cost which will be competitively attractive with alternate coal-fired plants.

PERFORMANCE SENSITIVITY STUDY

The sensitivity of the coal-fired plant efficiency to variations in certain cycle parameters was investigated. The parameters involved include:

- Fuel cell pressure level
- Fuel cell excess air ratio
- Anode recirculation ratio
- Steam cycle efficiency
- Fuel cell current density

In this section of the report the results of the coal plant performance sensitivity studies are presented and discussed.

Table 2-3

PLANT COST GOALS

Plant Section	Material	Labor	A&E Fee	Sales Tax	Total Cost	Contingencies		Total Plant Investment $	$/kW
						Process	Project		
Coal Handling	6,250	4,900	1,271	312	12,733	-	1,273	14,006	20.7
Oxidant Feed	35,000	24,350	6,810	1,750	67,910	-	6,791	74,701	110.7
Gasification and Ash Handling	7,000	5,250	1,400	350	14,000	700	1,400	16,100	23.8
Gas Cooling	25,000	8,900	4,015	1,250	39,165	1,958	3,917	45,040	66.7
Acid Gas Removal	25,000	8,000	3,925	1,250	38,175	-	3,818	41,993	62.2
Steam Bottoming Cycle	42,928	22,220	7,588	2,146	74,882	-	7,488	82,370	122.0
Fuel Cell Modules and Turbines	76,249	8,732	10,404	3,812	99,197	4,960	9,920	114,077	169.0
Inverter System	20,585	4,381	3,011	1,029	29,006	-	2,901	31,907	47.3
Electrical System	9,235	6,745	1,829	462	18,271	-	1,827	20,098	29.8
Land, Improves, & Misc.	21,415	18,015	4,478	1,071	44,979	-	4,498	49,477	73.3
Total	268,662	111,493	44,731	13,432	438,318	7,618	43,833	489,769	725.5

Notes: 1. All above figures are thousands of 1978 dollars.
2. Plant output = 675 MW (ac) Net

Table 2-4

PLANT COST GOALS - ECONOMIC SUMMARY
Plant Output - 675 MW (AC) Net

	10^3 $	$/kW
Total Plant Investment	489,769	725.6
Prepaid Royalties	2,456	3.6
Preproduction Costs	12,148	18.0
Inventory Capital	4,758	7.1
Initial Catalyst & Chemicals	292	0.4
Allowance for Funds in Construction	61,402	91.0
Total Capital Requirement (TCR)	570,825	845.7
Increment for Interim Replacement of Fuel Cells	113,632	168.3
Equivalent Total Capital Requirement (ETCR)	684,457	1014.0

ALL COSTS ON THIS PAGE ARE IN YEAR MID 1978 DOLLARS

Summary Description of Cycle

The cycle is illustrated in Figure 2-1. Fuel gas generated in the oxygen-blown gasifier is cooled to a temperature of 1200°F in a heat recovery steam generator, and is then further cooled to the level of the Selexol acid gas removal process by heat transfer to the clean gas returning to the fuel cell. The clean gas at a temperature of 1150°F and a pressure of 500 psia is admitted to a turbine, which delivers power to the oxygen plant air compressor, and is reduced in pressure by expansion through this turbine to the fuel cell pressure level. The fuel gas temperature at the turbine discharge is below a suitable minimum level for admission to the fuel cell anode. Heating is accomplished by mixing the clean fuel gas with recirculated anode discharge gas. This recirculation/gas mixing process, in addition to heating the incoming fuel gas, also raises the concentration of H_2O and CO_2 to levels such that carbon formation does not occur in the anode gas passage; methane formation is also inhibited. H_2O and CO_2 are formed by the electrochemical reactions and additional H_2 and CO_2 are formed by the reaction of CO and H_2O. Fuel

utilization in the anode is held to a constant level of 85%. The gas exhaust stream from the anode, containing unreacted H_2 and CO, is passed through the catalytic burner into which air is introduced from the discharge of pressurizing gas turbine compressor. At the cathode inlet, flow streams from the catalytic burner, the gas turbine discharge, and the cathode discharge are mixed. The stream from the cathode discharge is recirculated through a steam generator heat exchanger.

It is recognized that the use of recirculation loops for both the anode and the cathode flow streams complicates the design. However, the sensitivity of fuel cell voltage to changes in reactant/product concentrations caused by recirculation is much stronger for the anode than for the cathode. One reason for this is that the net cathode flow is two to three times that of the anode. Therefore a given value of recirculation ratio results in a higher recirculation loop flow and lower ΔT for a given rate of heat rejection in the cathode than in the anode. Thus, in order to maximize system efficiency, a minimum level recirculation flow, sufficient only to prevent anode inlet carbon formation, was selected for the anode and a larger recirculation flow, suitable for rejection of the fuel cell waste heat, was selected for the cathode.

The net outflow stream from the cathode is passed to the inlet of the bottoming cycle gas turbine generator, and the exhaust from the turbine is cooled in an economizer heat exchanger before being passed to the stack.

The gross plant output is produced by the sum of the outputs from the fuel cell, the bottoming cycle gas turbine, the fuel gas expander turbine, and the bottoming cycle steam turbine, for which steam is generated in three separate heat exchangers: the economizer (FW heating, plus, in the case of the higher excess air ratios, some evaporation); the gasifier discharge HRSG (completion of FW heating, plus vaporation, and in the case of the higher excess air ratios, partial superheating); and the cathode recirculation loop heat exchanger (superheating and reheating). Net plant output is the difference between gross output and the parasitic power. The parasitic power, including power for the air separation plant air and oxygen compressor, power for the Selexol cleanup system (pumps, refrigeration compressor), power for coal handling and for gasifier operation, compressor power for fuel cell recirculation, steam plant parasitic power, and other miscellaneous parasitic power, has been estimated at 7% of the coal HHV input energy.

Carbon and Methane Formation

A potential problem of concern to the MCFC power plant is the formation of carbon and methane in the clean fuel gas steam flowing to the fuel cell from the gas cleanup process. This problem is particularly critical at the anode inlet where the entering fuel gas first comes into contact with the nickel catalyst surfaces. Carbon and methane may also form in the regenerative heat exchangers located between the cleanup system and the fuel cell. Equilibrium considerations indicate that the tendency for formation of both carbon and methane is aggravated by elevated pressure and low temperature, while the kinetics of these reactions are accelerated by increased temperature. Removal of H_2O from the fuel gas by the cleanup process also increases the tendency for carbon and methane formation.

The approach which has been taken toward the carbon/methane problem in the present study is the following:

- It has been assumed that neither carbon nor methane will form in the clean gas stream in the heat exchanger upstream of the fuel cell. This assumption is sound at temperatures below approximately $900^{o}F$ because of slow kinetics; however at temperatures between $900^{o}F$ and $1150^{o}F$, the assumption is less safe, particularly with respect to carbon. If carbon formation should occur, a minor modification of the cycle involving reduction of the $1150^{o}F$ temperature at the fuel cell expander inlet and a corresponding reduction in the gasifier discharge HRSG gas outlet temperature can be made with a small resulting loss in cycle efficiency. Loss in fuel gas expander output will be partially compensated by an increase in steam cycle output.

- The effects of variations in fuel cell anode recirculation ratio on carbon and methane formation at the anode inlet have been analyzed assuming chemical equilibrium at the anode inlet. A minimum recirculation ratio has been assumed which results in no carbon in the equilibrium mixture.

- The effect on cycle efficiency of variations in anode recirculation ratio has been calculated. This includes changes in fuel cell output and offsetting changes in steam cycle output. Also the amount of methane formation, assuming equilibrium at the anode inlet, has been calculated as a function of anode recirculation ratio, and the effect of this on cycle efficiency has been determined, assuming that methane is electrochemically inert and that no methane reforming occurs in the anode. This represents an absolute "worst case" set of assumptions.

- A tabulation of the effect of methane formation, under the above conservative assumptions, on the efficiency of a cycle which has been optimized on the basis of no methane formation, has been prepared. The optimized cycle efficiency is reduced approximately one point if methane formation is assumed.

- Figure 2-11 shows the effect of anode recirculation ratio on efficiency over a range of fuel cell pressures.

The effects of both pressure and anode recirculation ratio on fuel cell output are seen to reverse in direction depending upon whether methane is or is not formed. However, the fuel cell pressure level for peak overall cycle efficiency is approximately 100 psia on the basis of either assumption regarding methane.

Study Assumptions

For all of the reference cycle variations considered in the study the following assumptions apply:

- The fuel gas stream supplied to the fuel gas expander turbine inlet has the gas species molar concentrations shown below:

(lb Moles/lb Coal)

CO	CO_2	H_2	H_2O
.04588	.00602	.3117	.002

  The pressure/temperature of this gas is 500 psia/1150^{o}F.

- The temperature of the fuel cell anode and cathode discharge streams is 1300^{o}F.

- The overall anode utilization ratio of CO and H_2 is .85 (outside the recirculation loop). For cases involving methane formation this factor covers both electrochemical conversion and methanation.

- Gas turbine/compressor efficiencies are .92/.88.

- The reference steam cycle is a 2400 psig/1000^{o}F/1000^{o}F non extraction reheat cycle with a steam turbine generator efficiency of .38.

- The fuel cell polarization is .7 Ω/cm^2.

- The Coal HHV (High Heat Value) is 12235 Btu/lb. (as received).

Fuel Cell Pressure

The effects of fuel cell pressure variation may be discussed in terms of the several independent phenomena:

- Increasing fuel cell pressure has the effect of increasing fuel cell voltage in accordance with the Nernst equation. As indicated by Figure 2-4, this effect is strongest at pressure levels below 8 atmospheres. Above this the rate of rise of fuel cell output with pressure falls off.

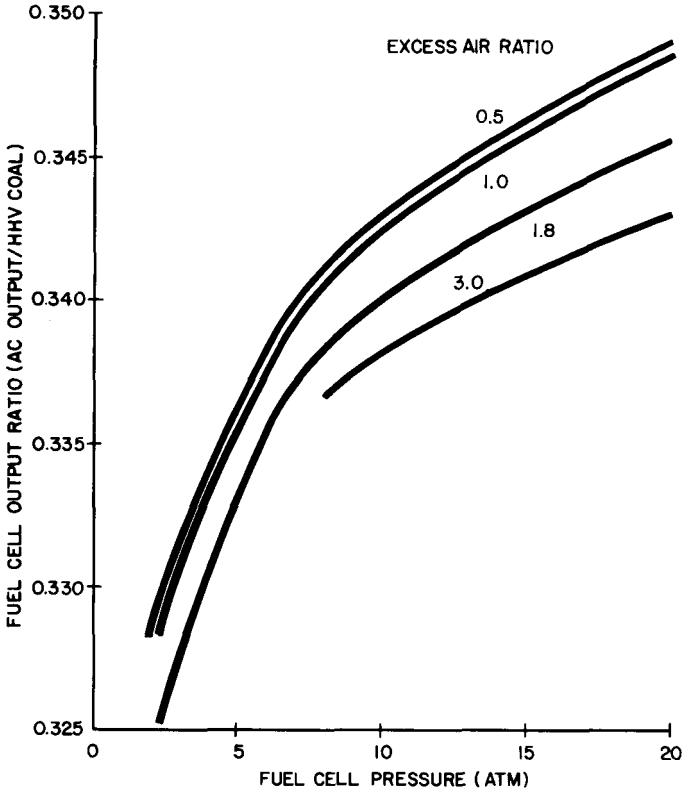

Figure 2-4. Fuel Cell Output Ratio vs. Fuel Cell Pressure and Excess Air Ratio

- The fuel cell pressure affects the outputs from the bottoming cycle gas turbine and from the fuel gas expander, the inlet of which is assumed to be held at a constant level. As shown by Figure 2-5 the sum of these outputs maximizes at a fuel cell pressure of approximately 7.5 atmospheres. This pressure level corresponds to the optimum pressure ratio for the gas turbine cycle at the assumed 1300^{0}F turbine inlet temperature. The difference between the turbine output and the compressor input maximizes at this pressure ratio.

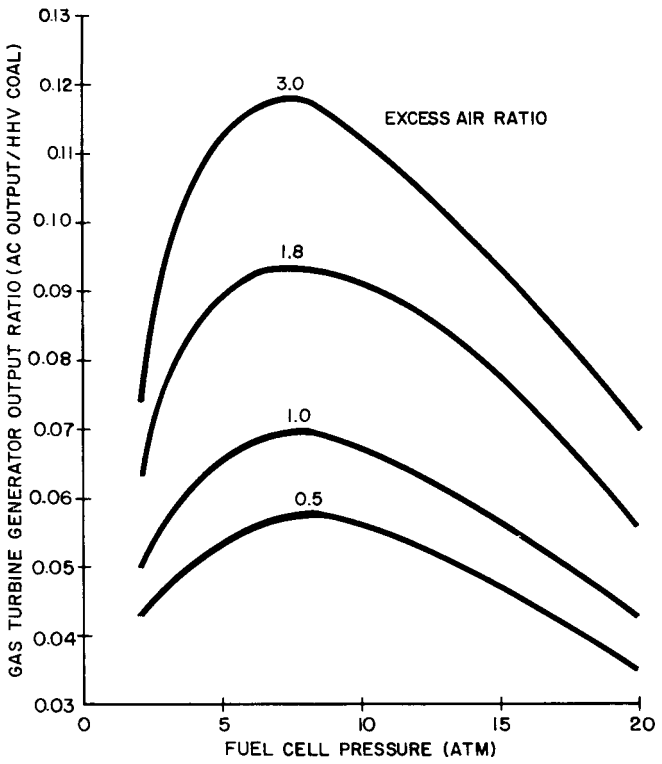

Figure 2-5. Gas Turbine Generator Output Ratio vs. Fuel Cell Pressure and Excess Air Ratio (Included Fuel Gas Expander Turbine Output)

- The fuel cell pressure affects the contributions to steam generation made by the economizer/heat exchanger downstream of the bottoming cycle gas turbine and by the cathode recycle steam generator. The variation of steam cycle output shown on Figure 2-6 reflects the algebraic sum of these two effects. As fuel cell pressure is increased the gas turbine pressure ratio increases resulting in a larger turbine ΔT, a lower temperature at the economizer inlet, and reduced heat input to the steam. However, this effect is offset by the increase in energy input to the fuel cell from the bottoming cycle gas turbine compressor which occurs when pressure ratio is increased, and also by the increase in fuel cell expander discharge temperature which occurs when the fuel cell pressure is increased and the expander pressure ratio reduced. Both of these effects result in a requirement for increased fuel cell heat rejection to the cathode recirculation loop heat exchanger. The relative magnitude of these separate effects is influenced by the level of excess air, as shown in Figure 2-6.

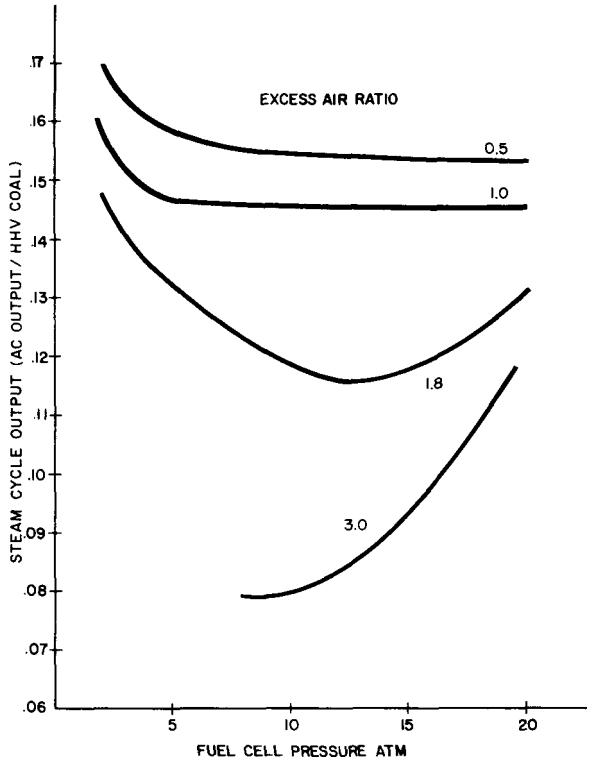

Figure 2-6. Steam Cycle Output Ratio vs. Fuel Cell Pressure and Excess Air Ratio

The combined effects of fuel cell pressure variation on the output ratios of the fuel cell, gas turbine, and steam turbine are indicated in Figure 2-7 which shows the variation of plant efficiency with fuel cell pressure. This figure indicates an optimum pressure level of approximately 6.8 atmospheres for 180% excess air and a slightly higher optimum pressure for 100% excess air.

Excess Air

Excess air is defined as the fraction of air flow in the fuel cell cathode above the minimum that would be required to completely react the anode fuel. The fuel cell excess air ratio, like the fuel cell pressure level, has an effect on the output ratios of the fuel cell, the gas turbine, and the steam turbine. The excess air ratio affects the fuel cell output through effects on O_2 and CO_2 concentrations in the cathode flow stream. The fuel cell output maximizes at an excess air ratio of approximately 75%. Below this level output decreases because of reduced CO_2

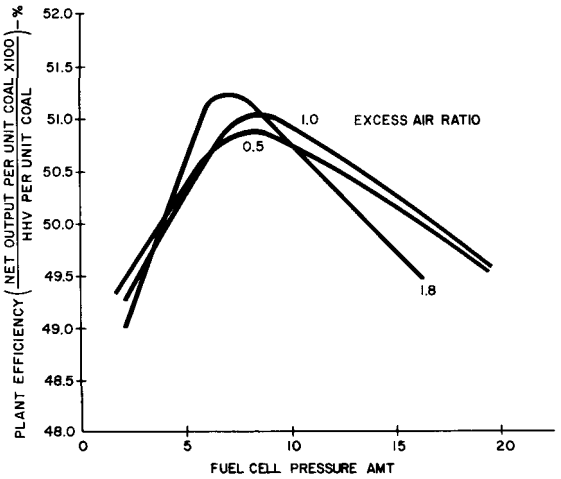

Figure 2-7. Plant Net Output Efficiency vs. Fuel Cell Pressure and Excess Air Ratio

concentration. However for variations of excess air ratio between 50% and 180% the effect on fuel cell voltage is small, as shown by Figure 2-4.

Excess air ratio has a major effect on gas turbine output, since this ratio directly affects the flow rate handled by the gas turbine. This is shown by Figure 2-5.

The effect of excess air ratio on heat input to the steam cycle, is to reduce heat input to the steam as the excess air ratio is increased. This occurs as the superposition of three effects. First, increased air increases direct air cooling of the fuel cell and reduces the requirement for fuel cell heat rejection to the cathode recirculation heat exchanger. This effect is greatest at low pressure levels where the air supply temperature is low. Second, increased air increases the gas flow rate through the economizer and thereby tends to increase heat input to the economizer. However, at high excess air flow rates the economizer gas discharge temperature is forced to increase by the necessity of maintaining an adequate pinch point ΔT for heat transfer between the gas and the steam under conditions of a high ratio of gas flow to steam flow. This reduces heat input to the steam. This effect is strong at intermediate pressure as the economizer inlet temperature is reduced to levels such that all the heat input is to feedwater with no vaporization duty. Under these conditions there is no need to raise the stack

temperature. This combined with the effect of elevated pressure on the cathode recirculation steam generator accounts for the rising portions of the 180% and 300% excess air curves shown in Figure 2-6.

As indicated in Figure 2-7, overall plant efficiency maximizes at an excess air ratio of approximately 180% for a fuel cell pressure level of approximately 6.8 atmospheres. However, the difference in plant efficiency at optimum pressure for excess air ratios of 180% and 50% is less than 0.5% and the difference between the 180% excess air peak and the 100% peak is only about 0.2%. At 180% excess air some superheat duty is required in the gasifier discharge steam generator with a peak steam temperature of approximately 800^{o}F. At 100% excess air the maximum steam temperature is the saturation level of 660^{o}F.

The material shown in Figures 2-5 through 2-7 is replotted in Figures 2-8 through 2-10, assuming a fixed fuel cell pressure of 6.8 atmospheres. The optimum plant efficiency at 180% excess air becomes apparent in Figure 2-11. The limitation of the economizer pinch point ΔT can be seen to take effect above 180% in Figure 2-9 non-linearly.

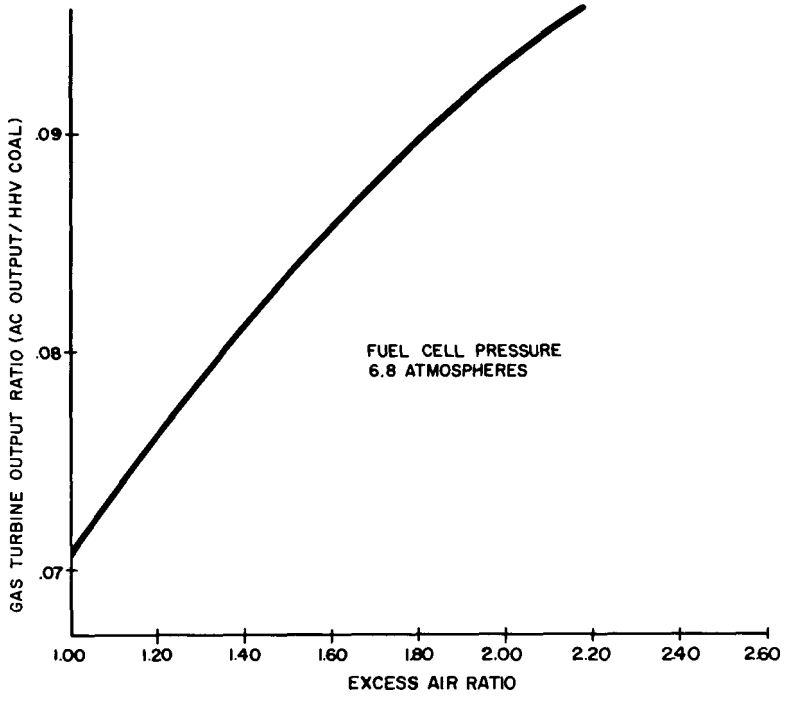

Figure 2-8. Gas Turbine Output Ratio vs. Fuel Cell Excess Air Ratio

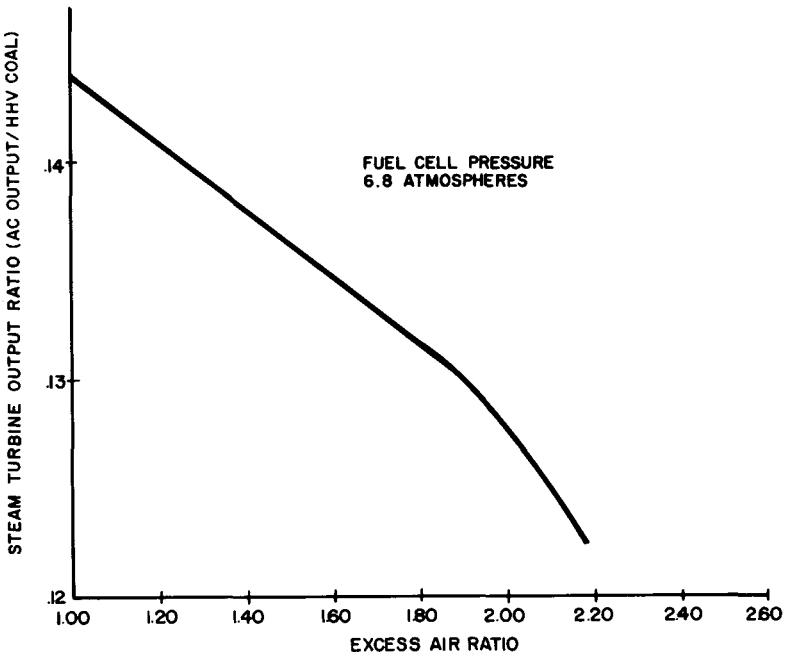

Figure 2-9. Steam Turbine Output vs. Fuel Cell Excess Air Ratio

Anode Recirculation Ratio (ARCR)

The anode recirculation ratio is the proportion of anode exit gas flow that is recirculated back to the anode inlet. The rationale for the selection of reference cycle anode and cathode recirculation ratios was the following:

- A minimum level anode recirculation ratio, sufficient only to prevent carbon formation and to heat the incoming fuel gas, was selected.
- A minimum level cathode recirculation ratio, sufficient only to satisfy the fuel cell heat rejection requirement and to establish a cathode inlet stream temperature of 1024^{0}F, was selected.

Under the assumption that methane will not form at the anode inlet, or under the assumption that if methane forms it will be reformed during passage through the anode, the above procedure provides maximum fuel cell efficiency.

The effect of variation in the anode recirculation ratio on the fuel cell output ratio is shown in Figure 2-11. These curves, which are based on the assumption

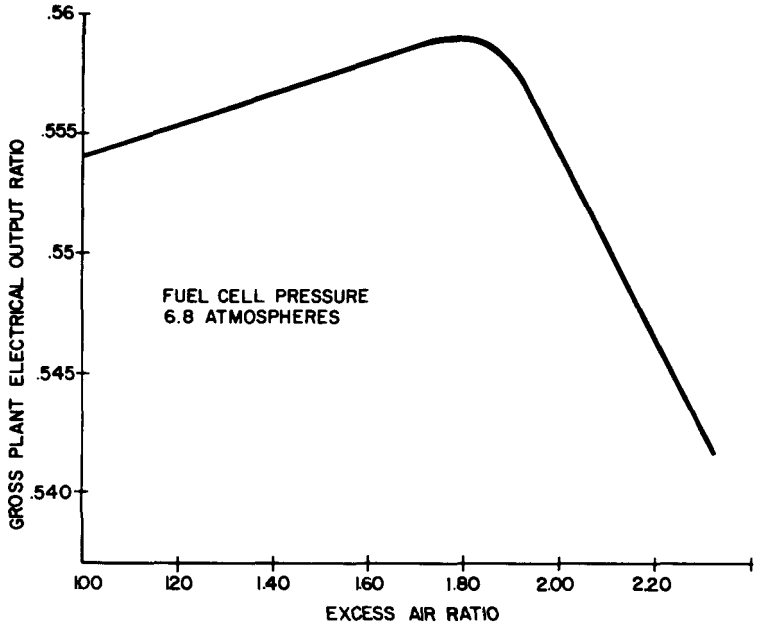

Figure 2-10. Gross Plant Electric Output Ratio vs. Fuel Cell Excess Air Ratio

that methane will not form, indicate a drop in fuel cell output of approximately 2.5% for a change in recirculation ratio from 0.5 to 0.7. Since the energy represented by this drop in fuel cell useful output is transferred to the steam through the recirculation loop heat exchanger, and is converted at the steam cycle efficiency of 38%, the net loss to the overall cycle is approximately 0.8%. The loss results from a drop in fuel cell voltage associated with changes in the reactant/product concentrations in the anode inlet stream.

If methane is assumed to form at the anode inlet, the optimum anode recirculation ratio is increased. This is indicated by the curves of Figure 2-12. The reason for this is that the equilibrium mole fraction of methane in the anode inlet stream is reduced by increased concentrations of H_2O and CO_2 associated with increased recirculation ratio. Methane formation removes H_2 and CO from the anode flow thereby reducing the amount of CO and H_2 which can react electrochemically.

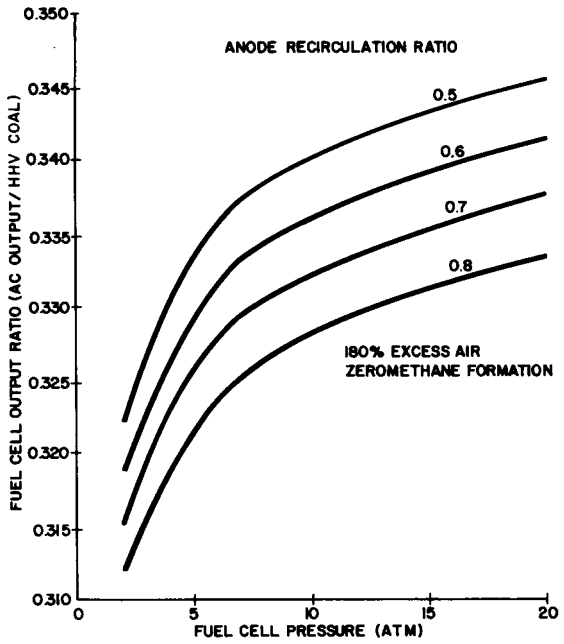

Figure 2-11. Effect of Fuel Cell Pressure and Anode Recirculation Ratio on Fuel Cell Output Ratio

As shown by the curves of Figure 2-12 the increase in fuel cell output ratio associated with an increase in recirculation ratio from 0.5 to 0.8, under the assumption of equilibrium methane formation, is greatest at the higher pressure levels. This results from the fact that increased pressure promotes increased methane formation.

Table 2-5 summarizes alternative system optimizations made for the assumptions of no methane formation vs equilibrium methane formation. If methane is formed, a high recirculation ratio (0.7) is desired to limit the equilibrium concentration to a negligible level and thereby to maximize the fuel cell output ratio. Thus the relationship between recirculation ratio and fuel cell output ratio, under the assumption of equilibrium methane formation is the reverse of that which applied under the assumption of no methane formation. The difference in net plant efficiency, after allowance is made for steam cycle conversion of the incremental fuel cell loss, is approximately 0.8 percent.

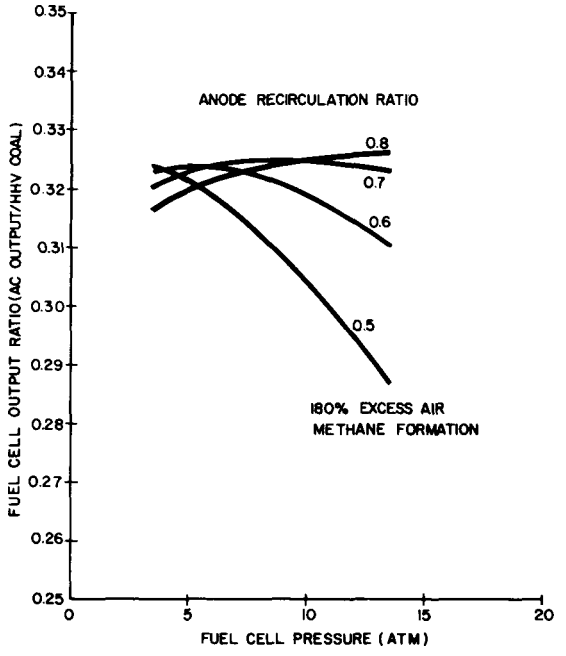

Figure 2-12. Effect of Fuel Cell Pressure and Anode Recirculation Ratio on Fuel Cell Output Ratio (Assumption of Equilibrium Methane Formation)

Table 2-5

EFFECT OF METHANE FORMATION ON PERFORMANCE AT OPTIMIZED CONDITIONS (180% Excess Air, 6.8 Atm.)

	Fuel Cell Output	Optimum ARCR	Steam TB Output	Gas TB Output	Plant Efficiency
METHANE NOT FORMED	.337	0.5	.126	.094	.512
METHANE FORMED	.325	0.7	.130	.094	.504

It is to be noted that an anode recirculation ratio of 0.7 corresponds to a sufficiently high recirculation flow rate that the fuel cell heat rejection heat

exchanger may be located in the anode recirculation stream and that cathode recirculation can be eliminated. This appears to be a significant simplification, which, if the assumption of equilibrium methane formation is correct, can be achieved without penalty to the overall system efficiency.

Steam Cycle Efficiency

The effect of steam cycle efficiency on plant efficiency is shown in Figure 2-13. Variation in steam turbine generator output ratio is simply the product of the variation in steam cycle efficiency and the steam cycle heat input ratio. A reduction in steam cycle efficiency from 38% for a 2400 psi reheat cycle to 30% for an 800 psi non-reheat cycle results in a 3% gain in plant efficiency in the reference cycle because the power produced by the more efficient fuel cell is increased.

Effect of Fuel Cell Current Density

The effect of fuel cell current density on plant efficiency is shown in Figure 2-14. Variation in fuel cell output ratio is calculated as the product of the current

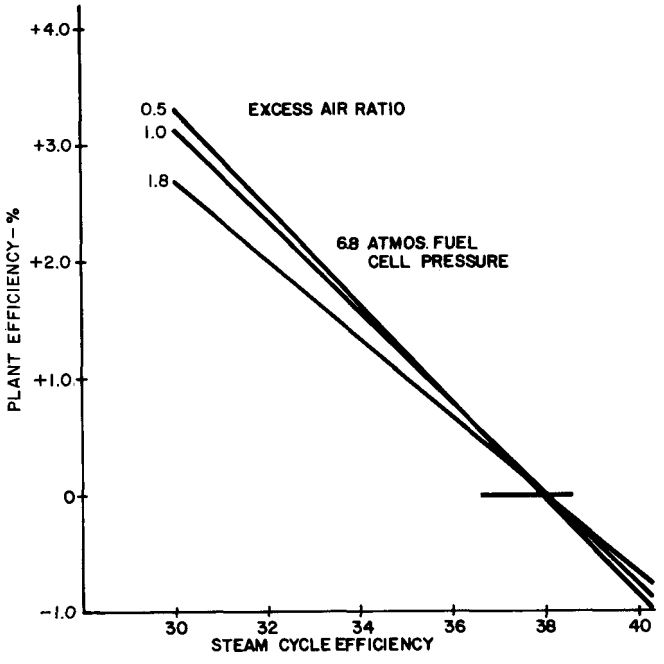

Figure 2-13. Effect of Steam Cycle Efficiency on Plant Efficiency

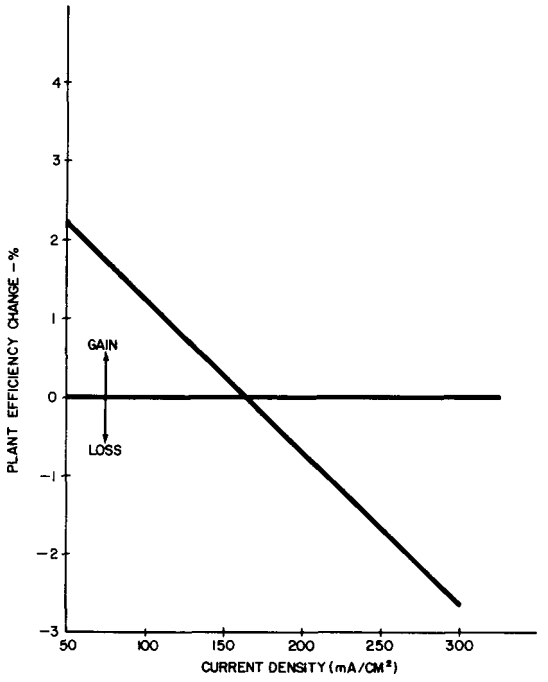

Figure 2-14. Effect of Fuel Cell Current Density on Plant Efficiency

density variation, the assumed polarization factor of 0.7 Ω/cm^2, and a constant times the electrochemically reacted moles of H_2 and CO per pound of coal divided by the coal HHV.

Conclusions

From the performance sensitivity study reported above the following conclusions can be drawn:

- The reference design, based on 6.8 atmospheres fuel cell pressure, 100% excess air, and 0.5 anode recirculation ratio, is close to the optimum design from the standpoint of overall plant efficiency.
- An efficiency gain of approximately 0.25% results from an increase in the reference cycle excess air ratio from 100% to 180%.
- The optimum fuel cell pressure level varies slightly with excess air ratio, from 6.8 atmospheres at 180% excess air to 8 atmospheres at 100% excess air. However for 100% excess air the overall efficiency variation for the range of pressure between 6.8 and 8 atmospheres is less than 0.1 percent.

- If methane is assumed not to form in the anode, the plant optimizes at an anode recirculation ratio of 0.5, the minimum level needed to establish a carbon-free gas equilibrium in the anode.

- If methane is assumed to form in equilibrium quantity at the anode inlet, the optimum anode recirculation ratio is increased from 0.5 to 0.7 and the overall efficiency is reduced by 0.8%. This recirculation ratio inherently establishes a carbon-free gas equilibrium in the anode.

- The optimum cathode recirculation ratio is that value which establishes a minimum acceptable cathode inlet temperature of 1000°F.

- The reference steam cycle (2400 psi/950°F/950°F) can be upgraded to 2400 psi/1000°F/1000°F without significantly affecting the maximum temperature of the steam in the high temperature steam generator heat exchanger. This will permit a 38% steam turbine generator efficiency at a condenser pressure level as high as 3" Hg.

- Overall plant efficiency changes with increased fuel cell current density at the rate of approximately 1% per 50 mA/cm^2, assuming 0.7 Ω/cm^2 polarization losses.

COST SENSITIVITY STUDY

Evaluation of plant costs by subsystem and examination of the sensitivity of plant performance to parametric variations permits an assessment of parameter effects on the cost of electricity (COE). This section summarizes these cost sensitivity evaluations and it will be noted that some changes to the studied plant operation conditions have been made. The cost sensitivity studies described are as follows:

- Fuel cell current density
- Fuel cell excess air
- Coal sulfur content
- Bottoming cycle options
- Fuel cell polarization loss assumption
- Fuel cell cost assumption
- Cleanup subsystem cost assumption

In order to evaluate the sensitivity of COE to a given parametric variation, the impacts on capital cost, fuel cost and O&M cost must be determined. The final cost impact is related directly to plant efficiency which has been discussed in the previous section.

For the purposes of the cost sensitivity study, the ECAS cost method (Appendix B) was used. The somewhat simpler "adders" to the capital cost ease the task of sensitivity evaluation. The EPRI accounting method (Appendix B) would produce minor differences, but the qualitative results, the guidelines for system design and the goals for technology development would be essentially the same.

As noted earlier, COE consists of the contributions of capital cost, fuel cost and O&M cost.

The subsystem capital costs are taken from Appendix B and then scaled according to an assumed parametric impact. The relationship used is as follows:

Revised Subsystem Cost

$$\frac{\text{Revised Subsystem Cost}}{\text{Reference Subsystem Cost}} = \left[\frac{\text{Revised key parameter value}}{\text{Reference parameter value}}\right]^{(\text{exponent})}$$

Where:

Revised	-	refers to the subsystem under the conditions being evaluated.
Reference	-	refers to the subsystem conditions prior to the perturbation.
Key Parameters	-	is the parameter judged to be determining subsystem cost; it may not be the same parameter for which the system sensitivity is being studied.
Exponent	-	A factor between minus one and plus one, based on historical cost data and industry experience.

The value of 'exponent' for each plant subsystem is, of course, quite important to the outcome of the cost sensitivity results. In each case, the value of exponent was carefully selected based on one or more of the following considerations:

- Reports of similar scaling studies
- Cost estimating texts
- Theoretical derivations
- Manufacturers' data

Table 2-6 lists the key parameters and exponents used for each subsystem for each sensitivity study.

Table 2-6

COST SENSITIVITY STUDY - KEY PARAMETERS AND EXPONENTS

Subsystem Study	Current Density	Fuel Cell Excess Air	Coal Sulfur Content	Bottoming Cycle	Fuel Cell Polarization
	Key Parameters (Exponent)				
Land, Improvements Structures and Miscellaneous Equipment	Fixed (0)	Fixed (0)	Fixed (0)	Fixed (0)	Fixed (0)
Fuel Handling	Plant Efficiency (-1.0)	Plant Efficiency (-1.0)	Fixed (0)	Plant Efficiency (-1.0)	Plant Efficiency (-1.0)
Fuel Processing	Plant Efficiency (-0.7)	Plant Efficiency (-0.7)	Coal Sulfur% (1.0)	Plant Efficiency (-0.7)	Plant Efficiency (-0.7)
Fuel Cell Stacks, Vessels, Burners, Piping, Etc.	Fuel Cell Area (1.0)	Fuel Cell Area (1.0)	Fixed (0)	Fuel Cell Output (1.0)	Fuel Cell Area (1.0)
Fuel Cell Recirculation Pump	Fixed (1.0)	Cathode Flow (1.0)	Fixed (0)	Fuel Cell Output (1.0)	Fixed (1.0)
Fuel Cell Turbocompressor	Fixed (0)	Turbine Flow (1.0)	Fixed (0)	Steam Cycle Output (0.8)	Fixed (1.0)
Steam Bottoming Cycle	Steam Cycle Output (0.8)	Steam Cycle Output (0.8)	Fixed (0)	Steam Cycle Output (0.8)	Steam Cycle Output (0.8)
Inverter System	Fuel Cell Output (1.0)	Fuel Cell Output (1.0)	Fixed (0)	Fuel Cell Output (1.0)	Fuel Cell Output (1.0)
Balance of Electrical	Fixed (0)	Fixed (0)	Fixed (0)	Fixed (0)	Fixed (0)

For this study, the parameters and exponents selected and shown in this table are judgmental; as the plant design moves to a more detailed phase, it will be appropriate to repeat these evaluations in a more detailed way. Specifically, at such time as plant costs are defined by means of specific vendor quotes, then sensitivities should similarly be reevaluated.

Following are discussions of the individual sensitivities. The individual subsystem cost variations in each case generally are not shown, but use of the equation shown earlier and the information in Table 2-20 will yield them.

Current Density

For the plant described, a current density of 161.5 mA/cm^2 was used as a design value. The previous section of this report (Figure 2-14) showed the effect of current density on plant efficiency.

The corresponding changes in subsystem outputs are given by

$$\Delta(\text{Fuel Cell Output}) = 0.613 \times \frac{(\text{Fuel Cell Output})}{(\text{Fuel Cell Efficiency})} \times \frac{(\Delta\text{Plant Efficiency})}{(\text{Plant Efficiency})}$$

$$\Delta(\text{Steam Cycle Output}) = -\Delta(\text{Fuel Cell Output})$$

Additionally, fuel cell area is given by:

$$\text{Fuel cell area} = \frac{(\text{Fuel Cell Output})}{(\text{Fuel Cell Voltage}) \times (\text{Current Density})}$$

Subsystem O&M costs are assumed to vary parametrically in the same way as subsystem costs. Fuel cost, of course, is inversely proportional to plant efficiency.

Figure 2-15 shows the resultant effect of fuel cell design current density on cost of electricity. It will be observed that a theoretical minimum exists as a density of about 320 mA/cm^2. However, two factors have to be considered before a decision could be made to operate at that value. First, experimental results to date indicate severe difficulty may be encountered at current densities that high. Second, the difference in COE between the minimum (37.8 mills/kWh) and the current design value (39.7 mills/kWh) is small; certainly within the limits of accuracy of the evaluation.

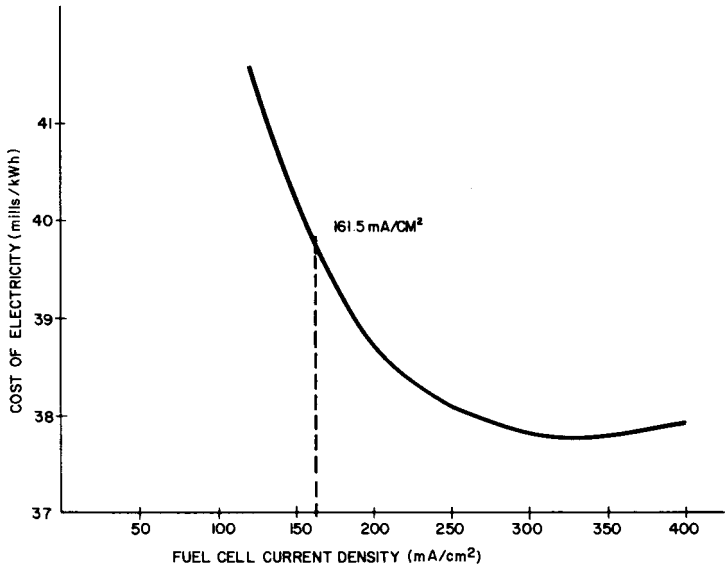

Figure 2-15. Sensitivity of Cost of Electricity to Current Density

Fuel Cell Excess Air

The plant design on which the cost sensitivity studies were based used a value of 1.0 excess air ratio. Figure 2-10 in the previous section (Performance Sensitivity Study), indicated that plant performance steadily increases with increasing excess air flow to a maximum at 1.8. However, Figure 2-8 indicated that the gas turbine output, and therefore its cost, also increases. The cost sensitivity study combines these effects to determine where the cost of electricity is lowest.

The costs of the subsystems are assumed to vary with current density in a manner similar to that described earlier. In addition, however, the cathode recirculation pump cost is assumed to vary proportionally with cathode flow, and gas turbine cost with turbine flow.

Figure 2-16 shows the result of the cost sensitivity study with a shallow optimum at 180% excess air. As was discussed earlier under Performance Sensitivities, this point also coincides with a modest amount of superheating duty present in the steam generator.

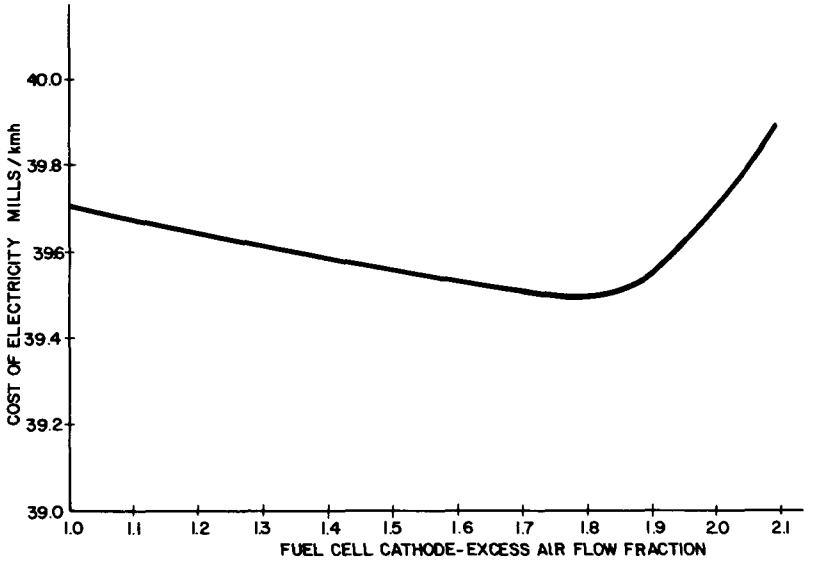

Figure 2-16. Sensitivity of Cost of Electricity to Fuel Cell Excess Air

The peak steam temperature of 800°F was selected as a conservative limit, this constrains excess air to ≤180%. The reference plant design will be modified to reflect the 180% excess air operation, and technology development goals modified to reflect the different inlet oxidant concentrations.

Coal Sulfur Content

This evaluation is not an optimization or trade-off in the same sense as the earlier two studies, but is an estimation of the cost impact of designing for use with a differing coal sulfur content. A ground rule for this evaluation was that the equipment selections were unaltered.

As noted on Table 2-6, the only capital cost that is assumed to vary is that of the Acid Gas Removal and Sulfur Recovery portion of the Fuel Processing system. O&M costs related to this system are also presumed to vary. Cost variations are assumed to be proportional to coal sulfur content.

Figure 2-17 shows the sensitivity of COE plotted against variations in coal sulfur content. The rather modest gradient of this line suggests that this plant will be attractive for a wide range of design value coal sulfur contents.

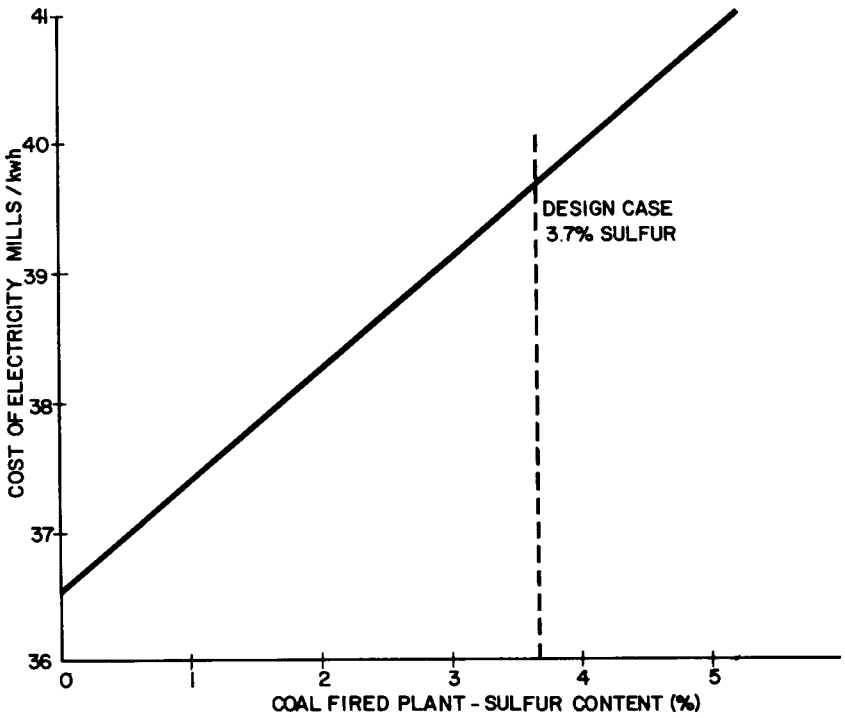

Figure 2-17. Sensitivity of Cost of Electricity to Coal Sulfur Content

Bottoming Cycle Options

The earlier General Electric Study (2-1) showed a performance advantage of 1.4 percentage points through use of a reheat turbine as the expander for the fuel cell turbocompressor. Assuming that the reheat turbocompressor costs 75% more than the simple cycle machine and that O&M costs increased by 50%, it will be seen that although some small economic benefit is noted, it is clearly insufficient to warrant the increased plant complexity under these assumed cost factors. The result of the evaluation is shown in Table 2-7.

Fuel Cell Polarization (Performance)

It has been assumed that the fuel cell polarization is linear and 0.7 Ω/cm^2. This was established in the 1976 UTC-ECAS Study (2-2) as being a reasonable cell development goal, and current cell research work maintains this as a goal. However, it is appropriate to assess the impact of the fuel cell development efforts falling short of or exceeding this goal. To this end, an assessment was made of the sensitivity of COE to the combined parametric effects of polarization and design current density.

Table 2-7

COST SENSITIVITY OF REHEAT VS SIMPLE CYCLE TURBOCOMPRESSOR*
(MID 1978 COSTS)

	Capital Cost (10^6\$)	Cost of Fuel (mills/kWh)	O&M Cost (mills/kWh)	COE (mills/kWh)
Simple Cycle	337.28	6.73	3.76	39.72
Reheat	337.03	6.60	3.83	39.66

*See also Appendix B

Figure 2-18 shows the result of assuming different polarizations from zero to 1.6 Ω/cm^2. The reference case used elsewhere in this study is 0.7 Ω/cm^2. It will be observed that the optimum current density decreases as polarization increases. This is to be expected since a lower current density and hence larger cell area must be maintained to achieve an optimum fuel cell efficiency.

The most significant result of this study is the apparent sensitivity of plant economics to fuel cell polarization (performance). There appears to be a strong incentive to improve performance. The uppermost curve (1.6 Ω/cm^2) is similar to current cell performance and optimizes at a current density close to that assumed for the reference plant of this study.

Fuel Cell Cost Assumption

Figure 2-19 shows the sensitivity of cost of electricity to the assumed fuel cell cost for fixed current density and polarization assumptions. In conducting this study the impact on material costs for fuel cell replacement is also scaled. This plot suggests that some latitude exists; a 38% increase in cost causes only a 5% increase in COE. The ±5% COE change limits are also shown as Figure 2-19.

Three of the previous cost of electricity sensitivity assessments are plotted on Figure 2-20. This is presented in order to be able to make a qualitative judgment with regard to the relative effects of the major fuel cell parameters. In addition this plot indicates the extent to which one parameter could be adjusted to compensate for changes in other parameters.

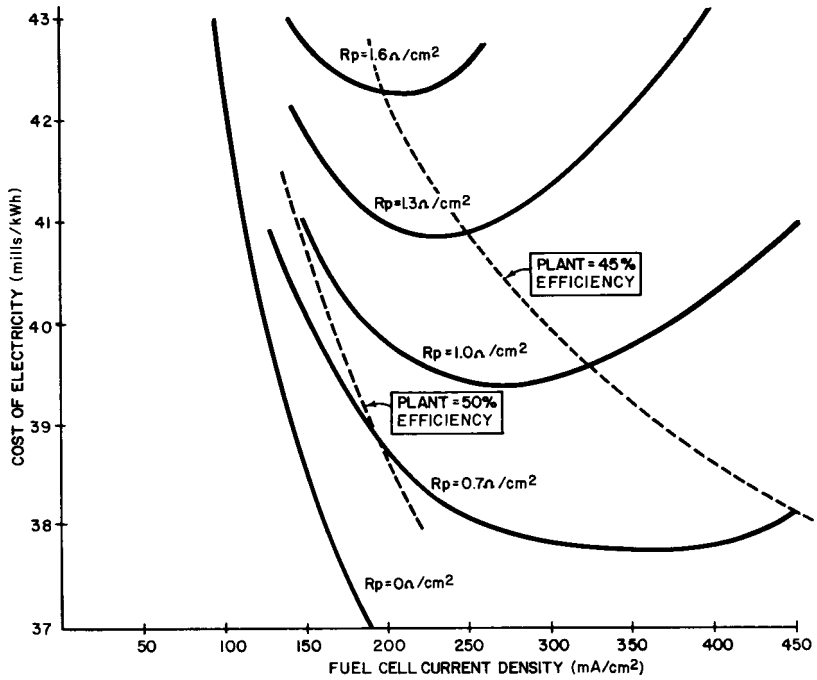

Figure 2-18. Cost of Electricity Sensitivity to Fuel Polarization Loss and Current Density

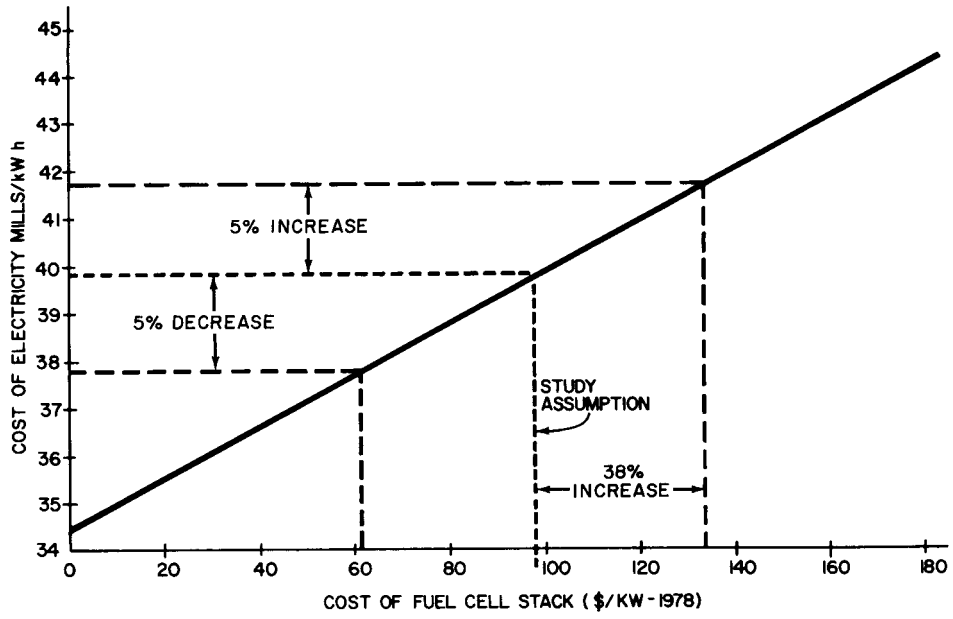

Figure 2-19. Sensitivity of Cost of Electricity to Fuel Cell Cost Assumption

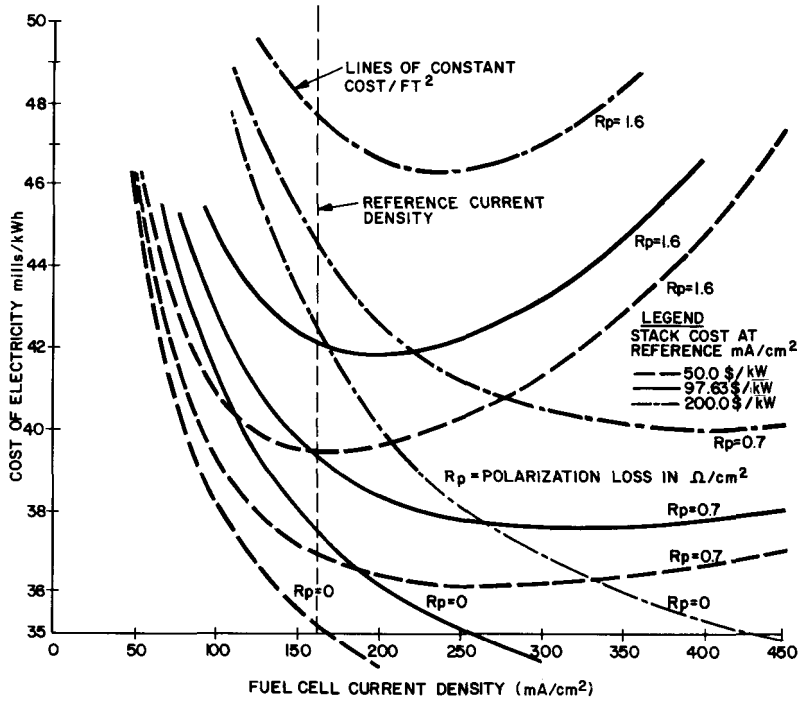

Figure 2-20. Sensitivity of Cost of Electricity to Fuel Cell Cost, Current Density and Polarization Assumption

It is now apparent that fuel cell stack cost is a powerful lever in compensating for excessively large polarization or too small current density. As an example, a fuel cell stack which cost $50/kW (compared with the assumed study value of $97.63/kW) would yield the same COE at over twice the polarization loss. Note also, however, that at $200/kW the COE currently assumed can not be achieved at under 200 mA/cm^2, and that would be with a polarization-free cell.

Cleanup Subsystem Cost Assumption

Approximately 10% of the plant capital cost is the acid gas removal subsystem. That cost was established on the basis of scaling a chemical industry installation estimate. It does not reflect savings from repetitively produced equipment.

Figure 2-21 shows the sensitivity of the cost of electricity to the assumed acid gas removal subsystem cost. This subsystem cost has only a small impact on the cost of electricity. Specifically, the subsystem cost can nearly double and have only a 5% increase in COE. Conversely, the incentive for cost reduction, while present, is not as great as it is for the fuel cell stack.

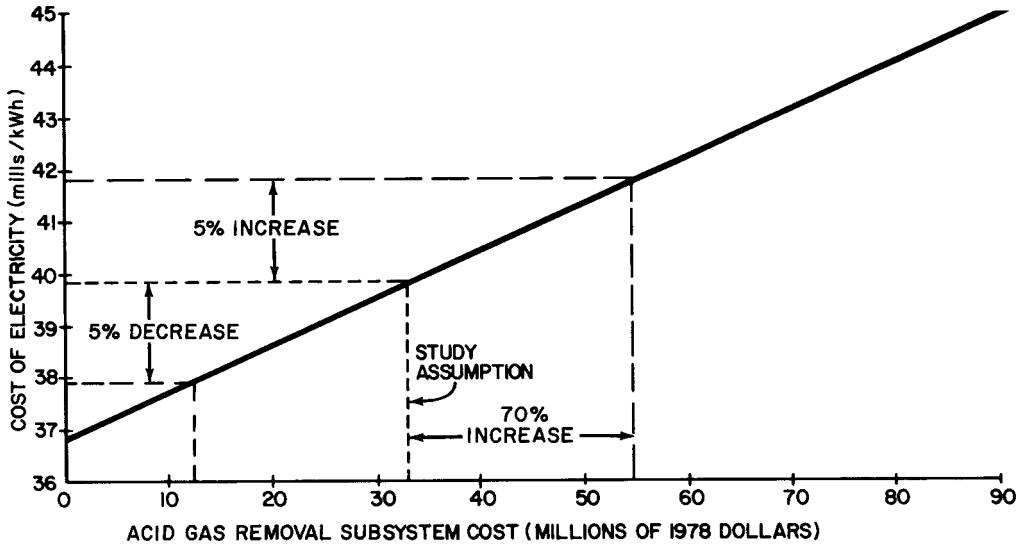

Figure 2-21. Sensitivity of Cost of Electricity to Acid Gas Removal Subsystem Cost

Conclusions

A review of the preceding cost sensitivities allows some important conclusions to be drawn. These conclusions relate not only to design of the coal-fired power plant, but also to the establishment of goals for technology development. The major conclusions are listed below.

- Some improvement in COE could be achieved by operating the fuel cell at higher current densities. The benefit is small (4.8% improvement in COE in moving from design value to optimum); and the optimum is high ($320\ mA/cm^2$) in comparison with state-of-the-art cells ($150\ mA/cm^2$).
- The cost penalty of designing below $150\ mA/cm^2$ is severe, establishing a lower threshold for technology development.
- The power plant COE optimizes at 180% excess fuel cell air flow which coincides with a steam generator metal temperature of $800^{o}F$. The plant design will be modified to reflect this.
- The power plant will remain economically attractive over quite a wide range of coal sulfur contents.
- The small improvement that results in the cost of electricity would not make the use of a reheat expander on the fuel cell turbocompressor attractive.

- There is considerable incentive to improve fuel cell performance (reduce polarization). To a limited extent, however, increasing the operating current density can compensate for poorer performance.

- Fuel cell stack cost has a small effect on cost of electricity when varied independently of other parameters. However, when the plant is reoptimized with respect to current density, cost is a powerful lever in compensating for excessive polarization and vice-versa. As above, reduced fuel cell stack cost permits operation at low current density for a given polarization loss.

- Acid gas removal subsystem costs can change significantly without significantly altering the COE.

COAL-FIRED MOLTEN CARBONATE FUEL CELL POWER PLANT DESCRIPTION

An overall conceptual description of the selected coal-fired fuel cell power plant configuration is given in the following section in the form of:

- Updated goals and requirements.

- A description of the cycle and the hardware components involved.

- The summary of operating characteristics of the plant.

- A conceptual plant layout drawing and a discussion of the rationale for its design.

- Preliminary subsystem specification descriptions defining performance requirements and implementation characteristics.

Power Plant Requirements and Goals

Requirements and goals for the coal-fired fuel cell plant were outlined at the beginning of this study to provide a framework within which the system evaluations were to be performed. They are summarized in Table 2–8 and include the updated heat rate resulting from improvements in the cycle.

The specified fuel is Illinois #6 coal, representative of the highly-caking Eastern Bituminous coals which the plant will handle. Table 2-9 gives the composition of Illinois #6.

Regulations have not established definitive environmental standards for the construction and operation of a coal-fired fuel cell power plant. Lacking specific emission standards, the typical practice is to extrapolate standards for equipment that the plant might displace. Table 2-10 gives the existing environmental limits applicable to a new or modified large coal-fired combustion facility. Table 2-10 also compares these limits with those projected to 1985 by General Electric and others. These projected standards are the design basis for the reference plant.

Table 2-8

GENERAL DESIGN REQUIREMENT AND GOALS FOR A COAL-FIRED INTEGRATED FUEL CELL POWER PLANT

Requirements		
1.	Central Station Power Plant	
2.	Power Level	675 MW(e) AC Net
3.	Fuel	Illinois #6 Coal
4.	Site Characteristics	"Middletown" Except for Cooling Tower Heat Rejection
5.	Environmental	Projected 1985 Federal Requirements
Goals		
1.	Base Load Duty with Daily* Load Following Capability	
2.	Heat Rate	6800 Btu/kWh
3.	Plant Availability	85%
4.	Life (75% capacity factor)	
	Fuel Cell Stacks	6 Years
	Balance of Plant	30 Years

*Large load changes within 2 hours
Small load changes at a rate of 2%/minute

Table 2-9

COMPOSITE OF ILLINOIS #6 COAL

Proximate Analysis (Wt. %)	
Moisture	4.2
Volatile Matter	34.2
Fixed Carbon	52.0
Ash	9.6
	100.0

Ultimate Analysis - DAF (Wt. %)	
Carbon	77.26
Hydrogen	5.92
Oxygen	11.14
Nitrogen	1.39
Sulfur	4.29
	100.00

Higher Heating Value (HHV)	12,235 Btu/lb (as received)
Lower Heating Value (LHV)	11,709 Btu/lb (as received)

Table 2-10

CURRENT AND PROJECTED EMISSION STANDARDS
FOR THE COAL-FIRED PLANT

Pollutant	Current Standards	Projected 1985 Federal Requirements
SO_x	1.2 lb/10^6 Btu	90% Removal (0.7 lb/10^6 Btu)
NO_x	0.7 lb/10^6 Btu	0.6 lb/10^6 Btu
TSP	0.1 lb/10^6 Btu	0.03 lb/10^6 Btu

Cycle Description

This cycle, shown in Figure 2-1, is generally described as an oxygen-blown system with a partially cascaded bottoming cycle.

The fuel for this system is derived from an oxygen-blown Texaco gasifier fed with a coal/water slurry. Gasifier effluent passes through the high temperature steam generator which incorporates an initial radiant section followed by a convection section. Slag and particulates are removed through lockhoppers. Steam generation duty includes completion of feedwater heating, vaporization, and partial superheating. From the steam generator, the raw fuel gas passes through the regenerative heat exchanger train where it cools to approximately 100°F and water vapor condenses. The cleanup system is a Selexol physical absorption system including an NH_3 scrubber, COS converter, both gas and absorbent refrigeration units, an H_2S absorber and a steam stripper regenerator. A hydraulic pump-turbine unit conserves pumping power in the absorbent liquid flow circuit. There will be five turbocompressor units, each with its own economizer, and also five heat recovery steam generators, one associated with each gasifier. The number of cathode heat exchangers is undetermined at this time, however it will probably be one per turbocompressor for a total of five in the plant. There will be one steam turbine generator for the plant.

The clean fuel gas leaves the Selexol system and passes back through the regenerative heat exchanger train. The clean gas is expanded through a turbine to the fuel cell pressure level of 100 psi. This turbine supplies the compressor power

for the air separation unit. Oxidant-supply parasitic power is required for the motor driven, intercooled, oxygen compressor. Fuel gas leaving the turbine is heated by a stream of anode outlet gas for entrance into the fuel cell anode. In addition to heating the incoming fuel, the anode recirculation also establishes a carbon-free equilibrium mixture at the anode inlet.

From the anode discharge the fuel gas enters the catalytic burner which receives a portion of the discharge air from the gas turbine compressor. Before entering the cathodes, gas discharging from the catalytic burner mixes with the makeup and recirculating air streams. The duty of the recirculation flow heat exchanger is superheating and reheating. The feedwater heater economizer downstream of the turbine adds heat to the steam. This system has an efficiency (based on the assumption of no methane generation in the fuel cell) of 51.2% (6669 Btu/kWh). Table 2-11 shows the various plant electrical outputs and electrical losses.

Table 2-11

ELECTRIC POWER OUTPUT SUMMARY
(watts per unit coal HHV)

Fuel Cell DC Output	.3416	
Less Inverter Loss	.0068	
Fuel Cell AC Output		.3348
Gas Turbine Shaft Output	.0953	
Alternator Losses	.0014	
Gas Turbine Generator AC Output		.0939
Steam Turbine Net Shaft Output After Delivery of Energy to FW Pump	.1301	
Alternator Losses	.0020	
Steam Turbine Generator AC Output		.1281
Total Plant Gross AC Output		.5568
Parasitic Power		
Oxidant Supply (in excess of air compressor)	.02	
Other	.025	
TOTAL		.0450
Net Plant AC Output		.5118

Table 2-12 lists the major power plant operating parameters, while Table 2-13 summarizes the energy balance in the fuel gas stream on its passage through the plant. The schematic diagram in Figure 2-1 shows all of the major cycle conditions which are also listed in Tables 2-14 and 2-15.

Reference Plant Description

A single, plan view, conceptual layout has been generated for the coal fired fuel cell power plants. The layout depicts the power plant and its subsystem and reflects preliminary evaluation of configuration alternatives. It is shown in Figure 2-22.

The concept consists of major subsystem islands which are interconnected by piping or conveyors. The islands are grouped in descending order based on their potential for energy loss by means of heat and pressure dissipation. The first four islands represent areas where heat loss is a very important consideration, especially for the 2500^{o}F gasifier. The last five islands represent areas with less potential for undesirable heat loss.

- Gasification Island
- Steam Turbine-Generator Island
- Fuel Cell Island with Turbocompressors
- Heat Exchanger Island with High Pressure Oxidant/Fuel Turbocompressors
- Oxygen Supply Island
- Fuel Gas Cleanup System Island
- Inverter/Power Conditioning Island
- Balance of Plant
- Coal and Ash Handling

The power plant consists of five independent power units with each unit containing a set of gasifiers, fuel cells, cleanup apparatus, gas turbines, power conditioning apparatus and other equipment. The single steam turbine is the only exception to the modularized concept.

An electrical inverter island is located near the fuel cell islands. It contains the DC to AC inverters and other electrical apparatus needed for converting the direct current supplied by the fuel cell to alternating current and otherwise transforming

Table 2-12

POWER PLANT OPERATING PARAMETERS

Coal Feed (lb/hr)	367814		Steam Turbine Shaft Output	171.6	MW
(MWt)	1319		Steam Turbine Alternator Losses	2.6	MW
Gasifier Efficiency			Steam Turbine Net Output	169.0	MW
(H_2+CO+CH_4)	.7730		Steam Turbine Efficiency	38%	
(H_2+CO)	.7703		Electric Power Output (MWe)		
Fuel Cell Voltage (DC)	.7685		Fuel Cell (AC) (MWe)	442	
Fuel Cell Efficiency (bases on HHV of H_2+CO supplied at anode inlet)	.4435		Gas Turbine - Generator (MWe)	124	
H_2+CO Fuel Utilization	.85		Steam Turbine - Generator (MWe)	169	
Turbocompressor Shaft Output	125.7	MW	TOTAL (MWe)	735	
Turbocompressor Shaft Losses	1.7	MW	Parasitic Power (MWe)	60	
Turbocompressor Net Output	124.0	MW	Net Plant Power Output (MWe)	675	
			Power Plant Heat Rate (Btu/kWh)	6669	

Table 2-13

SYSTEM GAS STREAM ENERGY BALANCE

Energy Inputs To Gas Stream	
Coal HHV	1.000
Sensible Heat Inputs to Gasifier	
H_2O	.003
Coal	.002
Oxygen	.003
	1.008

Energy Outputs From Gas Stream	
Fuel Cell DC Output	.3416
Gas Turbine Shaft Output	.0953
Heat Transferred to Steam	.3373
Energy Delivered to Oxygen Plant Air Compressor	.0270
Cleanup Heat Loss	.0538
Stack Loss	.1363
Other Heat Loss	.0167
Total	1.008

Table 2-14

COAL-FIRED PLANT FLOW SHEET DATA

Stream No.	1	2	3	4	7	9	10	11	12	15	17	18	19	23	24
Stream ID	Coal	Water to Gasifier	Oxidant to Gasifier	Gasifier Exit	Cleanup Exit	Turbine Exit	Anode Inlet	Anode Exit	Anode Recir.	Fuel Cell Air	Cathode Inlet	Cathode Exit	Subsystem Recir.	Turbine Exit	Vent
Temperature (^{o}F)	140	140	300	2500	75	625	1125	1300	1305	492	1024	1300	1300	721	300
Pressure (psia)	14.7	700	700	615	532	100	100	99	100	100	100	99	99	15.3	14.7
Gas Composition (Mole Fraction)															
CO				.4245	.5397	.5397	.2506	.0544	.0544						
H_2				.2884	.3668	.3668	.1257	.0224	.0224						
CO_2			.0871	.0708	.0708	.4682	.7256	.7256		.1346	.0869	.0869	.0869	.0869	
CH_4				.0008											
O_2			.9799							.2100	.1459	.1291	.1291	.1291	.1291
N_2			.0151	.0066						.7900	.6686	.7285	.7285	.7285	.7285
Ar			.0050	.0012											
H_2S				.0101											
COS				.0006											
NH_3				.0019											
H_2O		1.000		.1788	.0227	.0227	.1555	.1976	.1976		.0409	.0555	.0555	.0555	.0555
Total Flow (10^3lb-mole/hr)		8.9883	9.6371	39.7580	31.2820	31.2820	86.6683	110.7725	55.3863	202.5582	439.3909	403.2345	183.5748	219.6597	219.6597
Total Flow (10^6lb/hr)	.36781	.16179	.30819	.80248	.60586	.60586	2.65794	4.10423	2.05211	5.87419	13.28225	11.83601	5.38841	6.44760	6.44760
Enthalpy Flow (10^6Btu/hr)	4509.1	12.9	16.5	4474.8	3483.8	3616.1	5099.2	2900.1	1454.7	609.4	3655.0	4319.7	1966.6	1299.9	616.1

Note: Stream Numbers and pressure/temperature conditions are shown in Figure 2-1.

Table 2-15

BOTTOMING CYCLE SUBSYSTEM FLOW SHEET DATA
(whole plant basis)

Stream No.	4	5	18	22	19	20	15	23	24
Steam ID	Gasifier Exit	HRSG Exit	Cathode Exit	Turbine Inlet	Hx Inlet	Cathode Recycle	Air to Fuel Cell	Turbine Exhaust	Stack
Temperature (^{O}F)	2500	1200	1300	1300	1300	1048	492	721	300
Pressure (Psia)	615	584	99	99	99	95	100	15.3	14.7
Gas Composition (Mole Fraction)									
O_2	--	--	.1291	.1291	.1291	.1291	.2100	.1291	.1291
CO	.4245	.4245	--	--	--	--		--	--
H_2	.2884	.2884	--	--	--	--		--	--
CO_2	.0871	.0871	.0869	.0869	.0869	.0869		.0869	.0869
CH_4	.0008	.0008	--						
N_2	.0066	.0066	.7285	.7285	.7285	.7285	.7900	.7285	.7285
Ar	.0012	.0012	--	--	--	--		--	--
H_zS	.0101	.0101	--	--	--				
COS	.0006	.0006	--	--	--				
NH_3	.0019	.0019	--	--	--				
H_2O	.1788	.1788	.0555	.0555	.0555	.0555		.0555	.0555
Total Flow (10^3 lb-mol/HR)	39.758	39.758	403.2345	219.6597	183.5748	183.5748	202.5582	219.6597	219.6597
Enthalpy Flow (10^6 Btu/HR)	4474.8	2509.5	4319.7	2353.1	1966.6	1585.3	609.4	1299.9	616.1

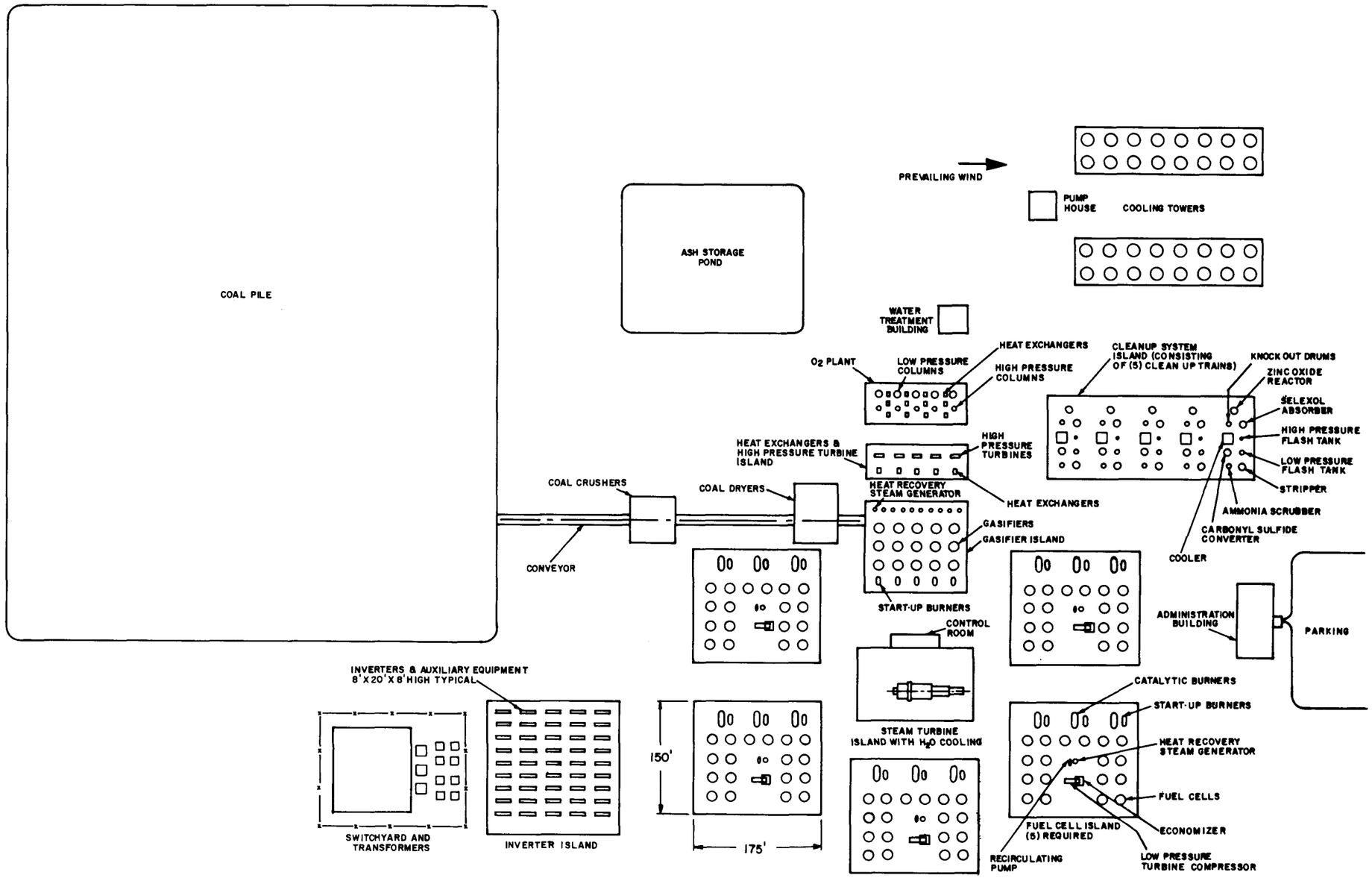

Figure 2-22. Coal-Fired Molten Carbonate Fuel Cell 675 MW Power Plant

Blank Page

the three component power outputs to a single electric output suitable for use in a utility power grid. Miscellaneous balance of plant equipment, such as the steam cycle cooling towers, is positioned in lower priority locations; i.e., further from the center of the plant.

The coal and ash handling island consists of a 60-day coal storage area, a recessed ash storage pond, coal crushers, coal dryers, conveyors and auxiliary equipment. This equipment is placed in areas away from the center of the plant.

The rationale for the configuration shown is two-fold. First, the number of independent power units (5) is selected to achieve a power plant availability of 85%, which has been identified as a practical goal of a baseload duty cycle power plant. Secondly, the islands are located to minimize the length of high temperature and high flow rate piping between islands, thereby keeping down energy losses as well as expense. The gasifiers and their HRSG's contain the highest temperature gases in the plant, and carry high flow rates of fuel gas as well as steam. Hence, the components are placed together in the gasifier island which then is located in the center of the plant to achieve close proximity to the other high temperature/flow components. The next highest gas temperatures occur in the regenerative heat exchangers and high pressure turbines; hence, these components are placed in an island adjacent to the gasifier island. Since the high pressure turbines supply compressor power for the oxygen plants, the oxygen plant island is located nearby, away from the center of the plant. The low temperature cleanup system is also placed nearby for close proximity to the regenerative heat exchangers that cool and reheat the fuel gas for cleanup.

The steam turbine generator island is placed in the center of the arrangement to achieve close proximity to the steam system heat sources which are located in the gasifier island and the five fuel cell islands. The fuel cell islands are symmetrically arranged around the steam turbine island. Each fuel cell island contains 18 fuel cells clustered around the fuel cell bottoming cycle equipment to achieve short piping runs for the high temperature, very high flow piping between the fuel cell modules, turbomachinery, steam generator and economizer. The inverter/electrical island is placed nearby for close access to power sources. The coal and ash handling and balance of plant equipment are placed in less central locations since they have no potential for significant heat loss and need to be close to

the perimeter of the complex for access to rail transportation. The oblique orientation and remote location of the cooling towers promotes effective use of the prevailing wind.

Approximate sizes for the various components were established based on scoping calculations and published information as described below. Gasifier size was checked by scoping calculations, and gasifier and syn-gas cooler sizes consistent with published information were used. The fuel cell island steam generators were sized based on approximate heat transfer and an assumed heat transfer coefficient of 25 Btu/hr-ft^2-^{o}F.

Sizes of the cleanup system components were estimated based on scoping calculations considering flow rates and assumed values for parameters such as catalyst packing density, heat exchanger tube density, and component internal flow passage density. The zinc oxide reactor size is based on assumed inlet plant cpacity factor and six months' catalyst replacement interval. Major vessels in the oxygen plant were sized based on oxygen supply rate requirements and assumed parameters such as distilled nitrogen gas velocity of 10 ft/sec and 90% flowpath obstruction by trays. Miscellaneous heat exchanger sizes were determined from published literature or sized based on approximate heat transfer calculations. Turbomachinery sizes for the bottoming cycle and oxygen plant were estimated based on scaling commercially available equipment, considering flow rates and configuration limitations.

The fuel cell gasification system reference plant consists of a Texaco gasifier and a particulate scrubber for solids removal operating in five parallel trains as outlined in the EPRI AF-642 (2-1) report. The gas purification system consists of an ammonia scrubber. the Selexol solvent system and the zinc oxide trim unit. The sulfur recovery plant uses the Claus process with a Beavon tail gas cleanup. A more detailed description of the cleanup system equipment is given in Appendix A.

Subsystem Descriptions

Preliminary definition of the subsystems for the coal-fired plant was prepared in the form of description sheets. These sheets will form the basis for continuous

updating as the designs mature. The subsystems covered are listed below. A control subsystem will be added later.

- Fuel Cell Subsystem
- Gasification Subsystem
- Gas Cleanup Subsystem
- Bottoming Cycle Subsystem
- Electrical Subsystem
- Balance of Plant Subsystem

Fuel Cell Subsystem Descriptions

Function:

The fuel cell subsystem electrochemically converts process clean low Btu gas, produced from coal to electrical power.

Requirements and Desired Characteristics:

• Current Density	100-200 mA/cm^2
• Fuel Cell Efficiency (H_2+CO) Content	>.40
• Clean Gas Flow Rate	.61 x 10^6 lbs/hr (whole plant)
• Fuel Gas (H_2 + CO) Mole Fraction	51.4%
• Oxidant Composition	Air
• Cooling	Cathode Recirculation
• CO_2 Source	Catalytic Burner on Anode Exit Gas
• Carbon Suppression	Minimum Required Anode Recirculation

Reference Plant Implementation:

The fuel cell subsystem consists of a number of fuel cell stacks in which the electrochemical conversion process takes place. Equipment associated with the fuel cell includes recirculating compressors, a catalytic burner to oxidize vent gas from the fuel cell anode, and a heat exchanger for transferring fuel cell waste heat to the steam turbine bottoming cycle.

Several full cell stacks are arranged within a module, each module being a rail shippable pressure vessel with pipe connections, and producing 5 MW (dc) electrical output. The pressure vessel is 13 feet in diameter and 20 feet long.

Stack assemblies will be connected in series/parallel combinations within each module, and modules will also be connected to give the appropriate voltage/current for the inverter subsystem.

The fuel cell recirculating compressors are driven by steam turbines. The catalytic burners utilize a precious metal catalyst amounting to 0.3% by weight supported on a ceramic material.

Reference Plant Performance:

- Fuel Cell Efficiency based on (H_2+CO content) 44.35%
- Fuel Cell Voltage (per cell) 0.7685V
- Fuel Cell Current Density 161.5 mA/cm^2

Gasification Subsystem Description

Function:

The gasification subsystem converts coal to a raw fuel gas.

Requirements and Desired Characteristics:

- Coal Feed Rate 367814 lbs/hr
- Efficiency (H_2+CO HHV/Coal HHV) >76%
- Raw Gas Temperature $\leq 2500^{o}F$
- Methane Production Negligible
- Tars and Condensable Hydrocarbons Negligible
- Blast Temperature $<1200^{o}F$
- Raw Gas Heating Value >2500 Btu/lb

Reference Plant Implementation:

Five Texaco entrained bed gasifiers employing a feed of pulverized coal slurried in water are used in the reference plant. A particulate separator in the raw gas cooler captures much of the particulate material for recycle, thus avoiding excessive inefficiency due to char particle loss.

Raw gases are cooled to 1200°F by the raw gas cooler which performs final feedwater heating and partial vaporization. Since the gas will be cooled below the ash fusion temperature, the HRSG will be provided with lockhoppers for ash removal on a periodic basis.

The oxygen used in the blast is produced by an air separation plant operating at 100 psia, and boosted to 700 psi by a motor driven compressor. The 100 psi level air compressor is driven by the expansion of the clean fuel gas.

Reference Plant Performance:

- Gasifier Efficiency
  - (H_2 + CO + CH_4) content 77.3%
  - (H_2 + CO) content 77.0%
- Raw Gas Heating Value 2547 Btu/lb

Gas Cleanup Subsystem Description

Function:

The gas cleanup subsystem provides gas which contains less than 1 ppm sulfur and keeps all emissions exiting the cleanup system within acceptable environmental limits.

Requirements and Desired Characteristics:

- Clean Gas Flow Rate $.61 \times 10^6$ lbs/hr
- Clean Gas Exit Temperature <75 °F
- Sulfur in Clean Gas <1 ppm
- Ash in Fuel Gas Negligible
- Loss of CO_2 in Cleanup System Minimum
- Consumables Minimum

Reference Plant Implementation:

The clean up system is a Selexol physical absorbent system including an ammonia scrubber, both gas and absorbent refrigeration units, a zinc oxide unit, heat exchangers and a steam stripper regenerator. The absorber operates at approximately

560 psi/40^{o}F, and the regenerator operates at approximately 25 psi/220^{o}F. The regenerator requires 0.3 pounds of 50 psi steam per pound of coal, which it extracts from the steam turbine. A hydraulic pump-turbine unit conserves pumping power in the absorbent liquid flow circuit.

Raw fuel gas in the subsystem is cooled to about 105^{o}F before entering an ammonia scrubber where all the ammonia contained in the gas stream is stripped out with water. The ammonia-free gas then enters the Selexol system where the H_2S and COS are essentially absorbed. The clean gas stream from the Selexol unit is heated to about 750^{o}F before entering a zinc oxide polisher which will further reduce the sulfur content of the gas stream to less than 1 ppm.

Reference Plant Performance (per unit coal HHV):

- Heat Loss in Cleanup System .0582
- Electric Power Loss in Cleanup System .009
- Energy Flow of Gas Leaving Cleanup System .7615
- Total Sulfur Content in Exit Gas <1 ppm

Bottoming Cycle Subsystem Description

Function:

The bottoming cycle subsystem converts the sensible energy of the fuel cell discharge stream to AC electricity and supplies compressed air to the fuel cell.

Requirements and Desired Characteristics:
(whole plant basis)

- Fuel Cell Discharge Stream:
  - Temperature: 1300^{o}F
  - Flow Rate: 11.8 x 10^{7} lbs/hr
- Air to Fuel Cell:
  - Temperature: 485^{o}F
  - Pressure: 100 psia
- Raw Gas Cooling:
  - Temperature: 2500^{o}F in, 1200^{o}F out
  - Flow Rate: 8 x 10^{5} lbs/hr
  - Maximum Metal Temperature 800^{o}F

Balance of Plant Subsystem Description

Function:

The balance of plant subsystem provides service buildings, compressed air systems, inter island piping and wiring, auxiliary boilers and accessories, water systems, a startup fuel oil system, liquid waste treatment system, power plant fire protection system, and other plant utilities including heating, ventilating and air conditioning, equipment handling and plant communications.

Requirements and Desired Characteristics:

To be determined.

Electrical Subsystem Description

Function:

The electrical subsystem converts the DC output of the fuel cell to AC power; steps up the AC output voltage of the turbine generators to transmission levels; and distributes power to various plant electrical auxiliaries.

Requirements and Desired Characteristics:

• Net Fuel Cell Output - DC	451 MW
• Net Steam Turbine Generator Output - AC	169 MW
• Net Gas Turbine - Compressor - Generator Output - AC	124 MW
• Net Parasitic Electric Power - AC	59.3 MW
• DC to AC Conversion Efficiency	>.98

Reference Plant Implementation:

The electrical plant equipment for the integrated coal gasifier/fuel cell power plant consists of the fuel cell island electrical equipment, which takes the DC output of the fuel cell, converts it to 3-phase 60 Hz AC power and steps it up to transmission voltages; the steam turbine and gas turbine island electrical equipment which steps up the AC output of the turbine generator to transmission levels; and the auxiliary system which provides electrical power to plant auxiliaries. The DC/AC inverter is of the solid state type.

The number, type, and switch interconnection of the inverters is an important issue intimately concerned with the availability of the plant, and the failure and aging characteristics of the fuel cell. In addition, the inverters will establish the operating load characteristics of the fuel cell modules and those of the plant.

REFERENCES

2-1. Fuel Cell Power Plant Integrated Systems Evaluation, General Electric Company, EPRI Report No. 1097, June 1979.

2-2. "Integrated Coal Gasifier/Molten Carbonate Fuel Cell Power Plant Conceptual Design and Implementation Assessment," Energy Conversion Alternatives Study (ECAS United Technologies Phase II Final Report, Report No. FCR-0237.

2-3. Economic Studies of Coal Gasification Combined Cycle Systems for Electric Generation, Fluor Engineers and Constructors, Inc., EPRI Report No. AF 642, January 1978.

2-4. Technical Assessment Guide, EPRI Report No. PS-1201-SR, July 1979.

2-5. Molten Carbonate Fuel Cell Power System Evaluation - Gas Cleanup System and Sulfur Plant. J.C. Dart & Associates, May 9, 1979.

2-6. Economics of Current and Advanced Gasification Processes for Fuel Gas Production, Fluor Engineers and Constructors, Inc., EPRI AF 244, July 1976.

2-7. Private Communication from Shell I.P.M., B.V., The Hague Netherlands to D.J. Ahner, General Electric Company, Schenectady, N.Y.

2-8. Fuel Cell Power Plant Integrated Systems Evaluation, General Electric Company, October 1979 (Draft prepared for EPRI).

Section 3

OIL-FIRED PLANT EVALUATION

INTRODUCTION

This section describes the results of studies directed toward improving the definition of an oil-fired molten carbonate fuel cell power plant. This power plant is directed toward dispersed applications. The dispersed nature permits use of the waste heat.

The cycle under consideration is shown in Figure 3-1, and is the oil-fired plant described in Reference (3-1). Cycle data shown is for the latest study using a steam to carbon ratio of 2.0. Performance sensitivity studies performed earlier in the program and discussed in this section were for a steam to carbon ratio of 1.51. This cycle employs an autothermal reformer to convert the #2 fuel oil into a fuel gas with the sulfur bearing gases removed by a zinc oxide bed. Air for the autothermal reformer is supplied by a turbocompressor and heated, following compression, by the reformer exit gases. Water, recovered from the cycle, is also heated to become superheated steam by the reformer exit gases prior to injection into the reformer. A process heat exchanger is used to cool the fuel cell, through reducing the anode exit gas temperature prior to reintroducing it into the cathode as a CO_2 source. Cathode exit gases are expanded to provide turbocompressor power.

COST EVALUATION

Cost Data Base and Methodology

The cost data base used for the oil-fired plant was obtained from the different sources listed herein. The methodology and assumptions used are the same as for the coal-fired plant.

- Preliminary Costs Analysis Molten Carbonate Fuel Cell Power Plant Utilizing No. 2 Fuel Oil Feed Stock. J.W. Harrison, General Electric Aircraft Equipment Division, October 1, 1976.
- Advanced Technology Fuel Cell Program. EPRI EM-956, Project 114-2, December 1978.

- Assessment of Fuel Processing Systems for Dispersed Fuel Cell Power Plants. EPRI EM-1010, Project 1041-1, March 1979.
- Assessment of Fuel Processing Alternatives for Fuel Oil Cell Power Generation. EPRI EM-570, Project 919-1, September 1977.
- An Assessment of the Fuel Cell's Role in Small Utilities. EPRI AF 696, Project 918, February 1978.
- Autothermal and Steam Reforming of Distillate Fuel Oils, National Fuel Cell Seminar, John Housman (JPL), July 1978.
- Process Plant Estimating Evaluation and Control, Kenneth M. Guthrie, 1974.
- Assessment of Industrial Applications for On-Site Fuel Cell Cogeneration Systems. Arthur D. Little, Inc. Contract No. NAS 3-20818.
- 4.41 and 25 MWe CTAS Oil-Fired Molten Carbonate Fuel Cell Power Plant. T.L. Bonds, General Electric Co., Energy Systems Programs Department, November 15, 1978.
- Assessment of Fuel Processing Systems for Dispersed Fuel Cell Power Plants. EPRI Project 1041-1, December 1979.

Scaling Factors

The cost evaluation in this section was conducted by scaling cost estimates from published reports.

Table 3-1 summarizes the data source, scaling parameters and exponential scale factors used for each component or system cost estimate. The total power plant cost was then evaluated using two different cost accumulation methods described in Appendix C.

Assessment of Cost Goals

An evaluation of oil-fired power plant cost is presented in Appendix C. The cost evaluation estimates an equivalent total capital requirement (ETCR) at $3,650,000 for a 4.5 MW plant; i.e., $811/kW. The ETCR includes an amount representative of the purchase of fuel cells for the life of the plant. A&E and other fees, sales tax, process contingencies on development items and project contingencies on all charges. The cost evaluation assumed production of 100 power plants per year.

If cost goal of $525/kW for an oil-fired dual energy use system MCFC power plant is assumed, based on economic equivalence with an oil-fired combined cycle power

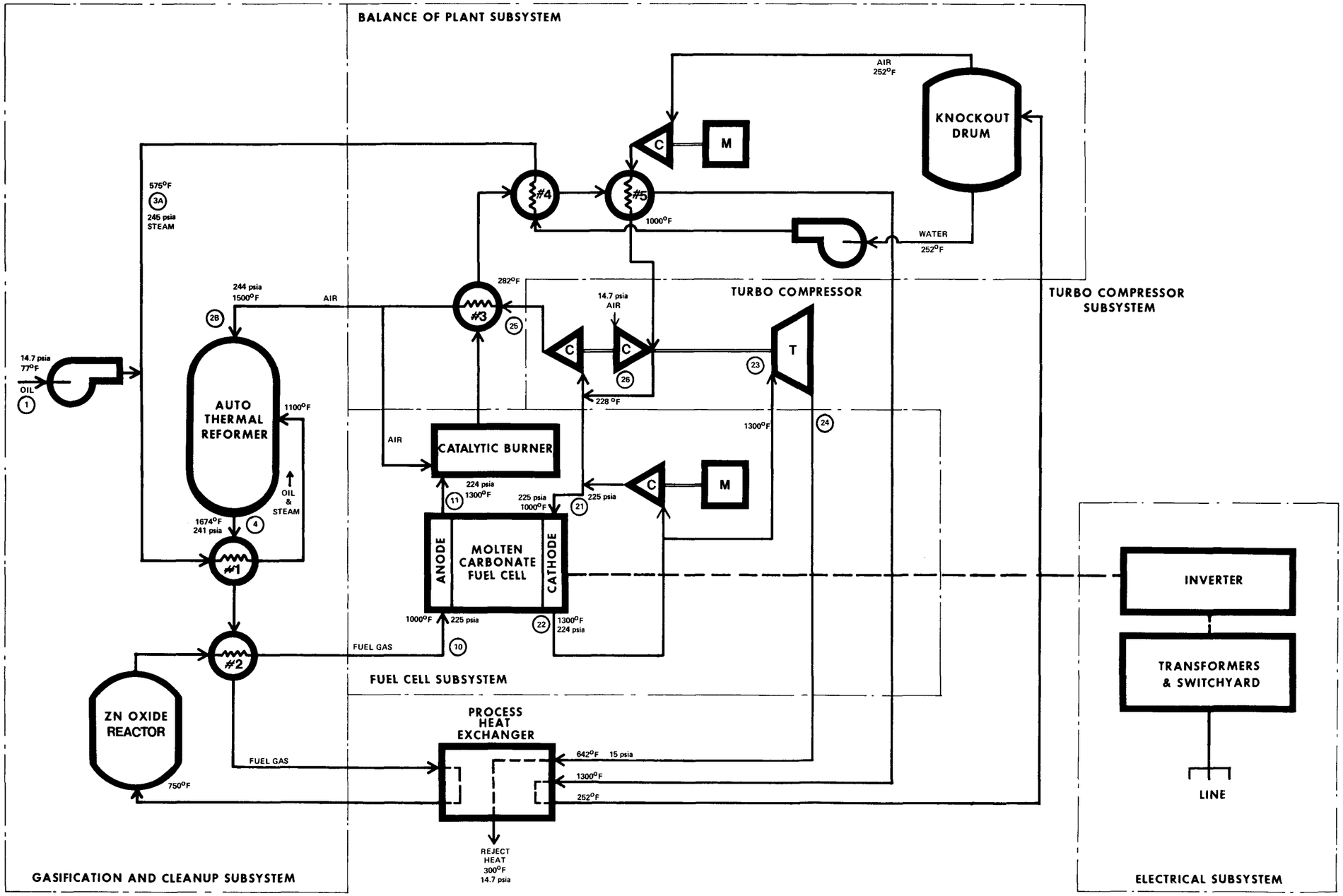

Figure 3-1. Oil-fired Molten Carbonate Fuel Cell Power Plant

Blank Page

Table 3-1

OIL-FIRED PLANT USING THE TECHNICAL ASSESSMENT GUIDE
Cost Data Sources and Scaling Factors

Subsystem	Source	Scaling Parameters*	Scaling Exponents
• Improvements, Structures, etc.			
- Improvements & Misc. Equipment	ECAS Report (2-2)	Plant MW Output	
- Structures	ECAS Report	Judgmental (2/5 of ECAS) Plant MW Output	1
• Fuel Processor Subsystem**			
- Oil Reformer	EPRI EM1010 by KTI	Judgmental (2.3 of KTI) Oil Flow (Btu/h) Production Rate (100/yr)	NA 1 .14
- Heat Exchangers, Vessels, Instrumentation, Piping	(Alternate verification using NASPCR135429 by A.D. Little)	Numbers of HX or Vessels Oil Flow Production Rate (100/yr)	1 1 .14
- Pumps, Skid, Painting, Misc.		Oil Flow Production Rate (100/yr)	1 .14
• Fuel Cell Subsystem	ECAS Report	Exclude Burner Catalyst ($6K) Fuel Cell DC Output Voltage	 1
• Fuel Cell Turbocompressor	Manufacturer Data	Judgmental (booster comp - add 2.5) Flow Rate Production Rate (150/yr)	NA .25 .44
• Electrical Plant Equipment	ECAS Report	Exclude Stm Plant & Diesel Gen	
- Inverter		Fuel Cell DC Output	1
- Balance of Electrical Plant		Plant MW Output	
• Process Contingencies			
- Reformer Vessel & Control Instr.	ECAS Report/EPRI Guidelines	15% of Total Cost Including Tax and Fee	
- High Temperature Heat Exchangers		15% of Cost for 2 of 6 HX's	
- Fuel Cell Module		50% of Cost for Stacks, Vessel and Instr.	
- Inverter Subsystem		10% of Total Cost	
• Project Contingencies	EPRI TAG (2-4)	15% of Process Plant & Facilities	1
• Fixed Operating Cost	EPRI TAG	Labor at 4 h/wk	1
• Variable Operating Cost	EPRI TAG		
- Oil Cost	EPRI TAG Guide	$4.74/MBtu	
- Reformer Catalyst	EPRI EM1010 by KTI		
- Sulfur Sorbent	Unit Cost per J. Dart Report EPRI EM570 by Catalytica	Sulfur Flow Rate via Oil Spec	
- Burner Catalyst	ECAS Report	Use mills/kWh	
- Waste Disposal	Same as Sulfur Sorbent	$4/ton of Sulfur Sorbent	
• Prepaid Royalties	EPRI TAG	0.5% of Process Plant Investment	
• Preproduction Costs	EPRI TAG	Per Guidelines	
• Inventory Capital	EPRI TAG	Per Guidelines	
• Initial Catalyst & Chemicals	EPRI Guidelines ZnO Cost per J. Dart Report EPRI EM1010 by KTI ECAS Report	Same as ECAS Method Capital Costs	1
• Allowance for Funds During Construction	EPRI TAG	0.1249 x Total Plant Investment	
• Land	ECAS Report (alternate land cost calculation)	Plant MW Output	

*All Baseline Costs Were Escalated to Mid 1978 Dollars, with 6.5%/Year Inflation Rate.
**Engineering and Contingency Costs Applied Uniformly to Components.

plant, the question arises as to whether the cost goal could be met, and how should subsystem goals be allocated to meet this goal.

First, consider the impact of an increase in the production from 100 to 200 power plants. Significant cost reductions can be made for the fuel processor system and turbocompressor by doubling their production. The exponential scale factor for fuel processing equipment cost versus production rate is estimated as 0.14 based on Reference (3-3). The exponential scale factor for turbocompressor cost versus production rate is estimated as 0.44 based on manufacturer data. A reduction in flow rate is also scaled to the 0.25 power. The estimated cost impact for doubling production rate is shown in Table 3-2:

Table 3-2

PRODUCTION POWER PLANT COST PROJECTIONS

Production Power Plants	100th	200th	Learning Factor
Fuel Processing Equipment Cost (1000$)	443	402	0.14
Turbocompressor (1000$)	211	128	0.44

Costs are tabulated by system and without contingencies for all except the fuel cell system (Table 3-3). It is assumed that cost reductions will not be achieved for the inverter system, electrical system and real estate improvements, structures and miscellaneous equipment. The cost goal of $525/kW establishes an ETCR of $2.36 million for the plant and the cost goals for the individual subsystems can then be deduced.

This tabulation indicates a cost bogey of $1,240,000 for fuel cells and replacements in a 4.5 MWe power plant, based on the total plant cost goal of $2,363,000 ($525/kW). Fuel cell system cost was estimated in Appendix C at $692,000 for the initial system and $547,000 for interim replacement, without contingencies, totaling $1,239,000. This is comparable to total fuel cell cost target of $1,240,000. Elimination of the fuel cell contingency is consistent with equipment in production.

The total plant cost goal of $525/kW for a dual energy use system MCFC power plant is therefore concluded to be a reasonable and potentially achievable goal.

Table 3-3

OIL-FIRED PLANT COST GOALS

	Cost ($10^3$$)	$/kW
Fuel Processor System	402	89.3
Turbocompressor	154	34.2
Inverter System	268	59.6
Electrical System	108	24.0
Improvements, Structures, etc.	191	42.4
Subtotal (without fuel cells)	1123	249.5
Fuel Cell Cost (Balance)	1240	275.5
Total Plant Cost (ETCR) for 200 Plants	2363	525

ALL COSTS ON THIS PAGE ARE IN MID 1978 DOLLARS

PERFORMANCE SENSITIVITY STUDY

Using the reference design concept, performance sensitivity analyses have been performed to identify the effect of key fuel cell operating parameters on plant performance. Other parameters having a direct and substantial impact on fuel cell performance were also identified and investigated; namely reformer operating conditions. Performance sensitivity analysis is the first step in refining the power plant operating condition (flows, temperature, etc.) to achieve higher efficiency, higher reliability and lower cost. This work was performed using a steam to carbon ratio of 1.51. Later work assumed a steam to carbon ratio of 2.0, the data for which are reflected in Figure 3-1.

This section presents the results of studies conducted to determine the sensitivity of oil-fired power plant performance to the following operating parameters:

- Fuel Cell Pressure
- Current Density
- Fuel Cell Air Flow
- Cathode Recirculation Flow
- Anode Recirculation Flow

- Reformer Air/Carbon Flow Rates
- Reformer Steam/Carbon Flow Ratio
- Reformer Pressure
- Reformer Exit Temperature
- Reformer Charge Temperature
- Anode Methanation

Performance of the fuel cell and power plant is determined based on assumptions and ground rules established in previous performance analyses and reiterated herein. Carbon deposition in the fuel cell is assumed to occur according to equilibrium theory; although this assumption results in a possibly conservative performance calculation, the assumption is warranted by the absolute necessity to avoid carbon fouling in the fuel cell and downstream equipment. Methane formation is assumed not to occur except in analyses which are aimed specifically at calculating the performance effects of methane formation in the fuel cell anode. In such cases, methane equilibrium at the anode inlet with no subsequent reforming is assumed as a worst case. Reformer operating characteristics are calculated using equilibrium theory.

The ECAS study (2-2) identified 161.5 mA/cm^2 (150 A/ft^2) as a development goal for current density and this value is used as a reference except where current is noted as a study variable. Present testing programs have demonstrated the feasibility of utilization in excess of 80%; hence, an overall utilization of 85% has been selected for the anode and as a maximum for the cathode. Polarization losses are estimated at 0.7 Ω/cm^2 based on the ECAS study (2-2).

DC to AC inverter efficiency has been selected as 0.98. The following temperatures have been selected for use:

- Gas exit temperatures - 1300^oF
- Gas inlet temperatures - 1000^oF

Fuel Cell Pressure

Pressure is varied downward from the reference design value of 133 psia to a minimum value of 23 psia without the use of anode recirculation. Pressure is varied

upward to a peak value of 200 psia using anode recirculation only to the degree needed to prevent carbon formation in the anode inlet. Minor adjustments in cathode cooling air flow are used to maintain constant inlet and exit gas temperatures. The results are depicted in Figure 3-2 which gives fuel cell and power plant efficiency, respectively, as functions of fuel cell pressure. The figure indicates that the 133 psia fuel cell pressure is optimum for the reformer operating conditions used in the reference design; i.e., fuel cell efficiency is highest at 133 psia. As fuel cell pressure is decreased below 133 psia, efficiency goes down according to the Nernst effect. As fuel cell pressure is increased above 133 psia, anode recirculation is needed to prevent carbon formation in the anode; the net result is a decrease in efficiency due to dilution of the anode inlet stream. Fuel cell and power plant efficiencies are related by Eq. 3-1 where inverter efficiency is assumed to be 98%.

$$\eta \text{ power plant} = \eta \text{ fuel cell} \times \eta \text{ reformer} \times \eta \text{ inverter} \qquad (3\text{–}1)$$

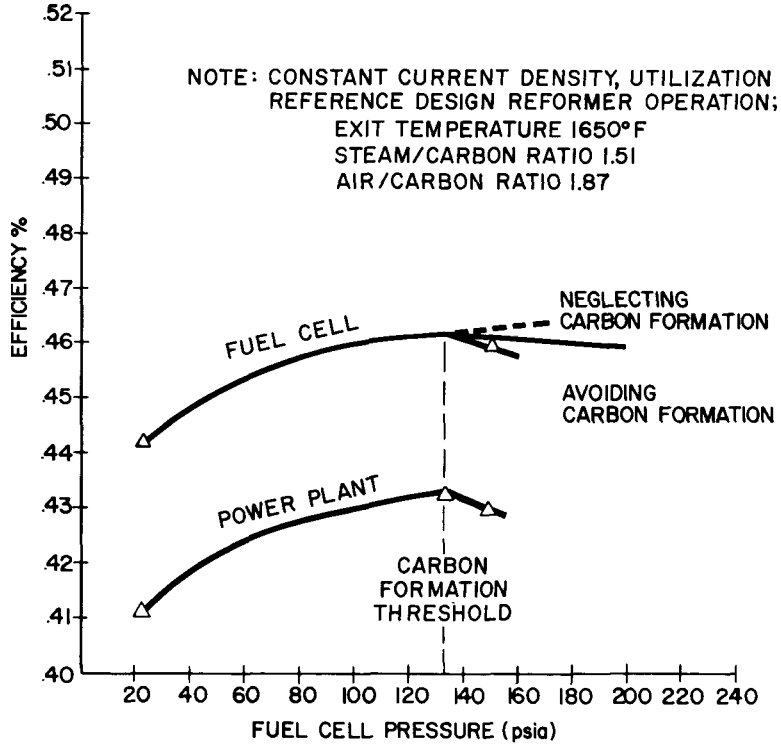

Figure 3-2. Efficiency vs. Pressure

It should be noted that the optimum value for fuel cell pressure depends on reformer operating conditions, reformer pressure being only one parameter. However, based on reference design reformer flow rates and temperatures, the fuel cell pressure selected for the reference design is a well optimized value. The impact of varying additional reformer operating parameters is presented subsequently.

Fuel Cell Air Flow and Cathode Recirculation

In the reference design concept, fuel cell heat rejection is accomplished by excess air flow through the cathode. This sensitivity analysis is aimed at determining the benefit of cooling the fuel cell with a combination of cathode recirculaiton and air flow. Fuel cell air flow is varied downward from the reference design case, and cathode recirculation is used to maintain constant inlet and exit gas temperatures. These flows are varied until a lack of oxygen causes cathode utilization to exceed the 85% limit. Otherwise, reference design operating conditions are used, including no anode recirculation. The results are depicted in Figure 3-3 which gives fuel cell and power plant efficiency, respectively. Peak efficiency is achieved at a cathode recirculation ratio of about 0.45; i.e., 45% of the cathode exit gas is recirculated back to the cathode inlet. The corresponding air flow rate is about 2.0 lb-mole/lb-mole of anode fuel gas (100% excess air. Efficiency is improved by about 0.6% compared to reference design conditions. The conclusion is that cathode recirculation is a more efficient cooling mechanism than excess cathode air flow, provided that sufficient air is supplied to support the chemical need for oxygen at cathode utilization of 50% or less.

Anode Recirculation

In the study reference design concept, fuel cell pressure is limited to 133 psia to avoid carbon deposition, and fuel cell heat rejection is accomplished by excess air flow through the cathode. This sensitivity analysis is aimed at determining the effect of employing anode recirculation to allow carbon-free operation at increased pressure and determining the performance effect of cooling via anode recirculation compared to the other fuel cell cooling mechanisms (cathode recirculation and air flow). The first question is resolved by the results of the pressure sensitivity analysis depicted in Figure 3-3 and discussed herein. These figures indicate that anode recirculation dilutes the anode inlet stream, causing a decrease in fuel cell efficiency which more than offsets the Nernst increase in

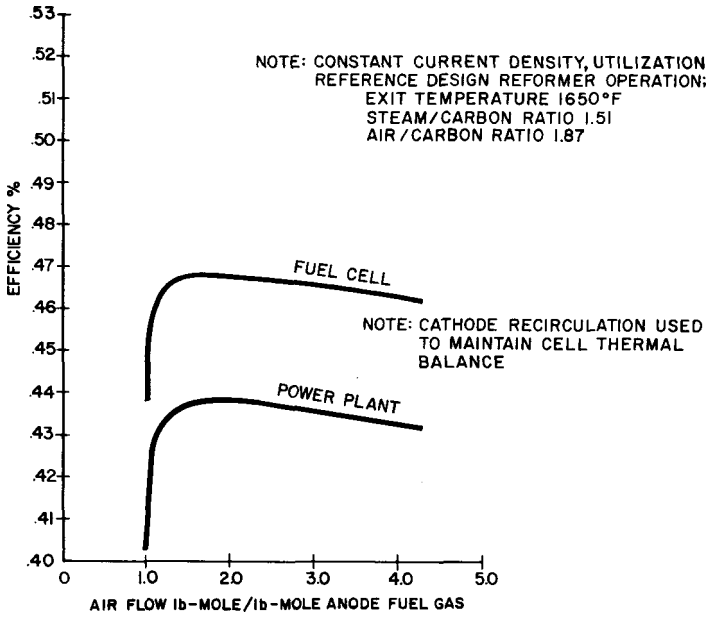

Figure 3-3. Efficiency vs. Air Flow

efficiency due to an increase in pressure. The net effect is a decrease in fuel cell efficiency and power plant efficiency.

The performance effect of cooling via anode recirculation is determined by varying anode recirculation and adjusting air flow to maintain constant inlet and exit gas temperatures. These parameters are varied until a lack of oxygen causes cathode utilization to exceed the 85% limit, which results in a rapidly declining fuel cell efficiency. Otherwise, reference design operating conditions are used except that two values of cathode recirculation are considered. The analysis is performed for the reference design value of zero cathode recirculation, and the analysis is repeated for a cathode recirculation value of 0.45 which was selected as a near-optimum value as shown in Figure 3-4. The results of both analyses are shown in Figure 3-4, which depicts fuel cell and power plant efficiency, respectively, as functions of anode recirculation ratio; i.e., the fraction of anode exit gas which is recirculated back to the anode inlet. The results show a decrease in efficiency with anode recirculation. The initial decrease in efficiency is caused by dilution of the fuel content of the anode inlet gas; the second more dramatic decrease in efficiency is caused by oxygen starvation in the cathode chamber.

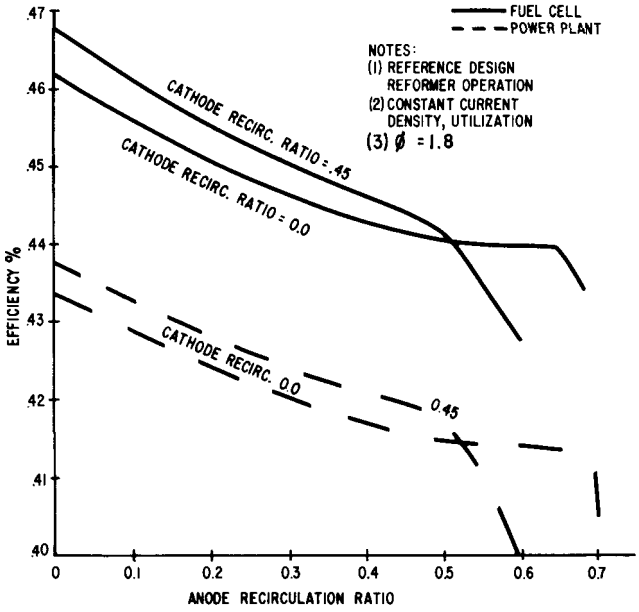

Figure 3-4. Power Plant Efficiency vs. Anode Recirculation

The conclusion is that anode recirculation is the least attractive of the three alternate cooling mechanisms. Peak power plant efficiency is achieved using cathode recirculation as the primary cooling mechanism, cathode air flow as a secondary cooling mechanism, and no anode recirculation.

Current Density

In previous performance calculations a fuel cell current density of 161.5 mA/cm^2 (150 A/ft^2) is used. The objective of this sensitivity study is to determine the relationship of fuel cell and power plant efficiency to variable current density. The results of primary interest are given in Figure 3-5 in which cathode air flow is varied to maintain constant inlet and exit gas temperatures of 1000^{o}F and 1300^{o}F, respectively, as in the reference design. Fuel cell pressure is included as a parametric variable. Otherwise, reference design operating conditions are used, including no anode or cathode recirculation. Figure 3-5 shows fuel cell and power plant efficiency versus current density for various fuel cell pressures.

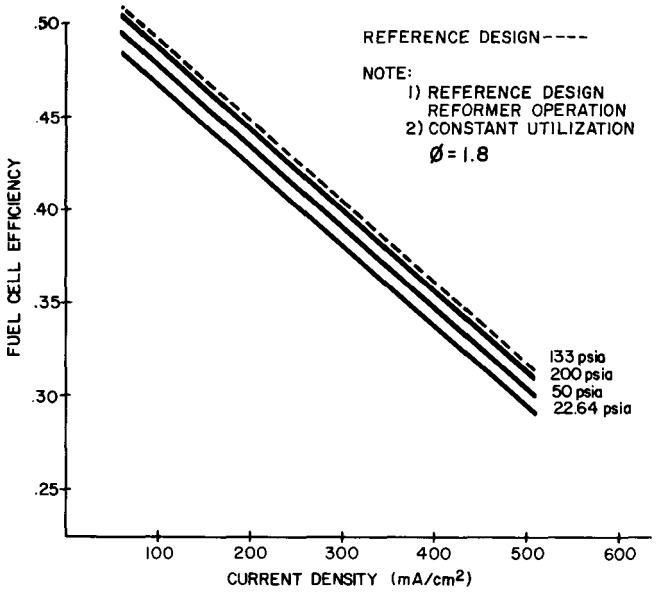

Figure 3-5. Power Plant Efficiency vs. Current Density and Pressure

Figures 3-6 and 3-7 depict the sensitivity of efficiency and current density with the use of cathode recirculation rather than air as the dominant cooling mechanism. These figures indicate that there is no significant coupling effect between variation in the cooling mechanism and variations in current density; hence, their effects on performance should be additive.

Reformer Operating Conditions

Three reformer operating parameters were considered for sensitivity analyses. An evaluation of reformer performance was made for each parameter. Detailed fuel cell and power plant performance sensitivity was studied for parameters with significant flexibility and potential for improved efficiency. The parameters considered were:

- Inlet air to fuel ratio
- Inlet steam to fuel ratio
- Pressure
- Exit temperature
- Charge temperature

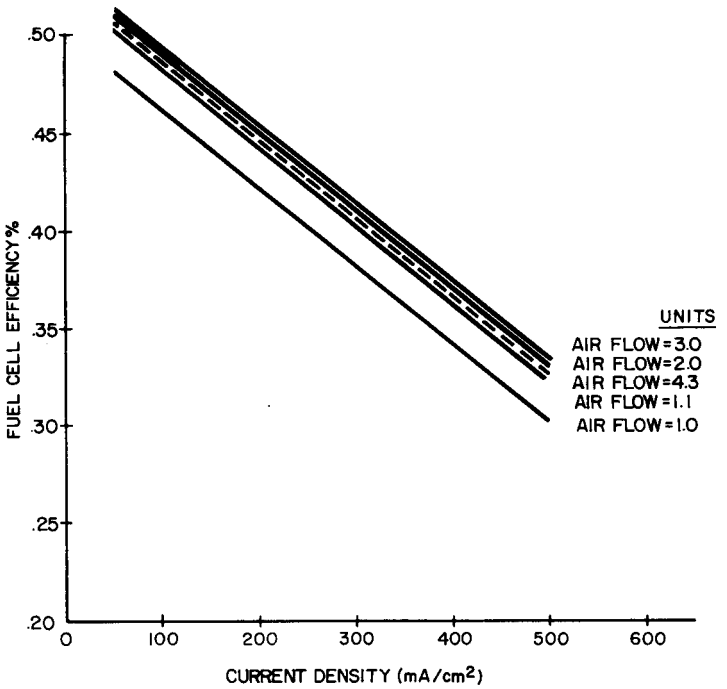

Figure 3-6. Fuel Cell Efficiency vs. Current Density and Cathode Air Flow

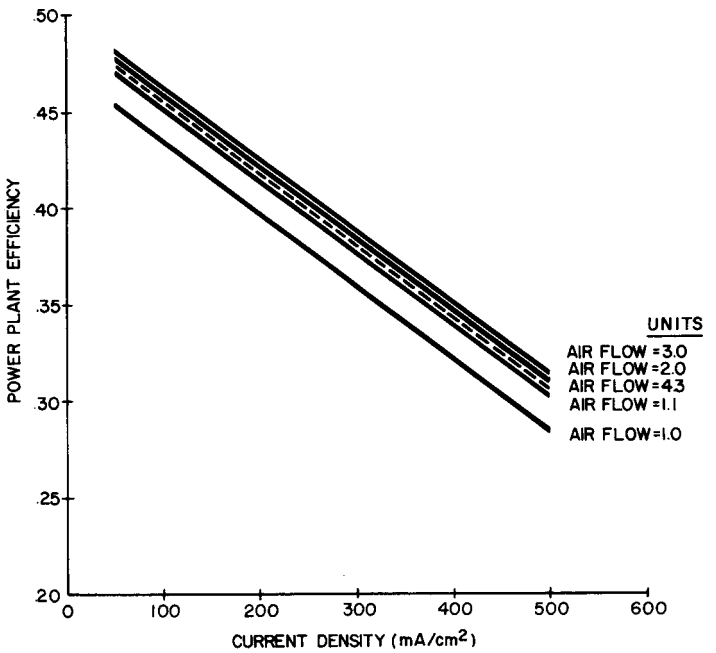

Figure 3-7. Power Plant Efficiencies vs. Current Density and Cathode Air Flow

Reformer Air Flow

Reducing reformer air flow (and combustion) is the most straightforward way of increasing reformer efficiency. Sensible heat supplied from the power plant system is substituted for combustion. In system installation, reformer performance is limited by the peak temperature available for heating the air (about 1700°F at the catalytic burner exit). However, a more severe limitation on reducing the fraction of fuel combusted is carbon deposition, found in experimental work with heavy oil fuel feedstocks. Carbon deposition in the reformer causes soot to form on the catalyst, leading to eventual plugging. The soot problem establishes an empirical, state-of-the-art limit on the improvement in reformer performance as summarized in Figure 3-8. The data points shown represent data produced by the Jet Propulsion Laboratory (JPL) (3-4) in autothermal reformer development. Although the precise value of this experimental minimum air condition is not well defined, its value appears to be in the range of 1.6 to 1.8 air to carbon molar ratio, as depicted in Figure 3-9. The figure also shows the theoretical soot disposition boundaries as calculated by General Electric and JPL. The occurrence (in terms of decreasing air/carbon ratio) of an experimental soot boundary relative to the equilibrium prediction is noteworthy. Additionally, a large increase in steam/carbon ratio does not appear to help. This implies that the sooting problem is the result of fuel decomposition (cracking) or heterogeneous partial oxidation.

The significant conclusion is that a more restrictive soot limit exists in practice than in theory. Figure 3-8 shows, as a circled point, that the autothermal reformer prediction for the reference design oil-fired plant is on the carbon-free side of the experimental boundary. Since the minimum permissible value for air flow is estimated at 1.8 air to carbon molar ratio plus a judgmental safety margin the current reference design air flow is nearly optimum, and a detailed performance sensitivity analysis for different reformer air flow is not warranted since the cost impact would be negligible.

Reformer Steam Flow

Reformer steam flow variation by itself affects both reformer activity (H_2 and CO production) and fuel cell efficiency. Although equilibrium calculations predict that increasing the reformer steam flow enhances reformer efficiency and soot control, fuel cell efficiency suffers significantly with increased steam flow because the increase in steam reduces the concentration of hydrogen and carbon monoxide in the anode inlet gas. At fixed pressure and neglecting carbon formation, the loss in fuel cell efficiency is greater than the gain in reformer efficiency as shown in Figure 3-10.

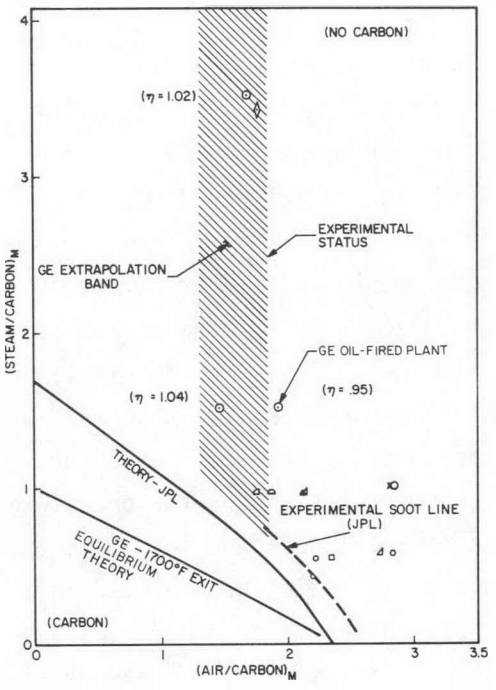

Figure 3-8. Autothermal Reformer Soot Line

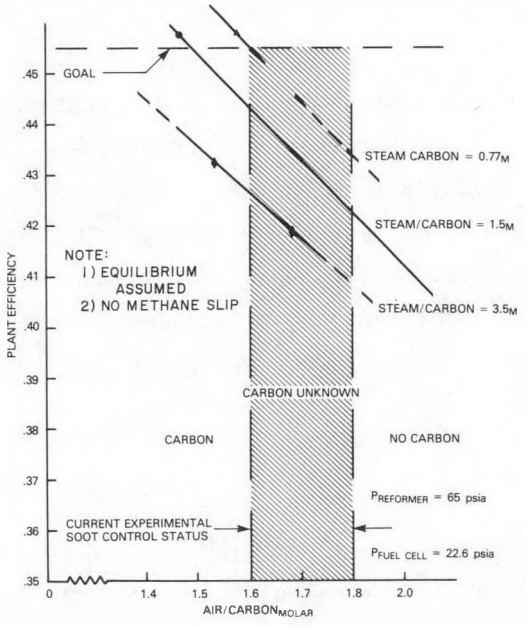

Figure 3-9. Oil-Fired Power Plant Efficiency

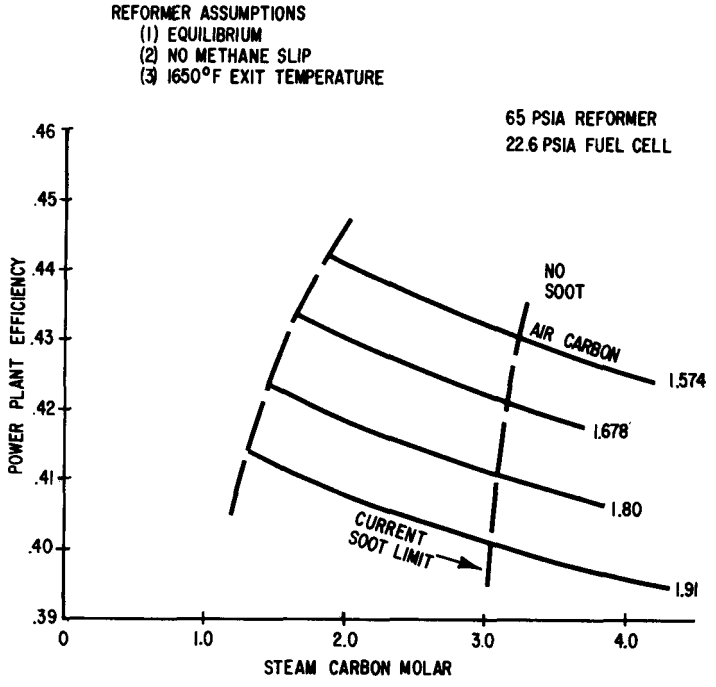

Figure 3-10. Power Plant Efficiency vs. Reformer Steam and Air Flows - Low Pressure

However, an increase in reformer steam flow increases the threshold pressure for carbon formation in the fuel cell anode, thereby allowing the fuel cell to be operated at higher pressures which tend to increase fuel cell efficiency. Thus there is a coupling effect between reformer steam flow and fuel cell operating pressure, and a true optimization requires that steam flow and pressure be analyzed jointly. A necessary step in this procedure is to establish a relationship between the maximum permissible fuel cell pressure, as limited by carbon formation in the anode and reformer steam flow. This is shown in Figure 3-11. Inherent in this is the assumption that the pressure effect on the reformer is negligible, since reformer and fuel cell pressures are related; analysis has confirmed this assumption to be reasonable. This curve can also be viewed as the minimum permissible steam flow for a given fuel cell pressure.

A trade-off study between system pressure and reformer steam flow was conducted by selecting near optimum values for systems parameters as determined in the previous sensitivity studies. The following values were selected:

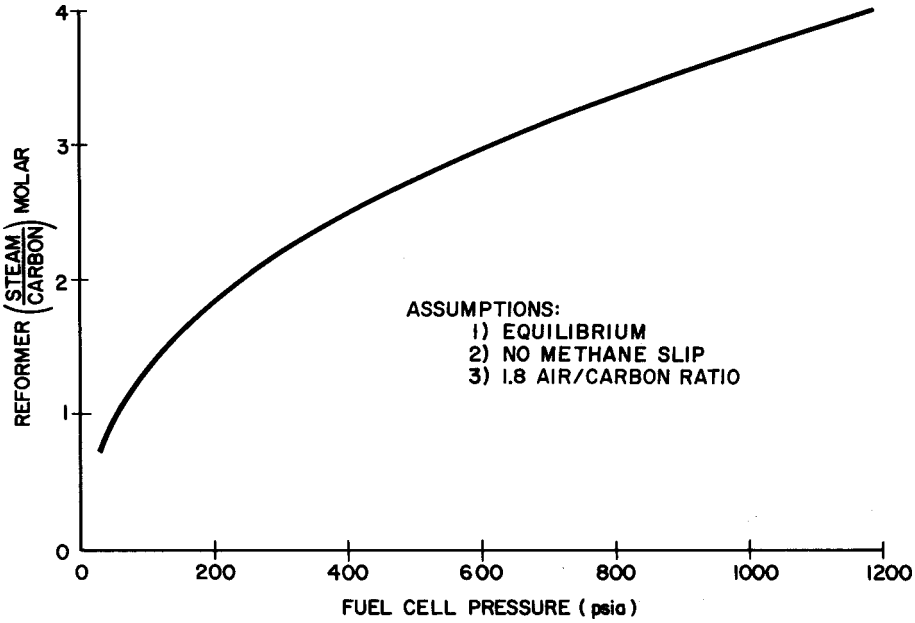

Figure 3-11. Reformer Steam Flow Criterion

Current Density	162.5 mA/cm^2
Tentative Cathode Recirculation Ratio	0.5
Reformer Air/Carbon Mole Ratio	1.8
Tentative Reformer Exit Temperature	1650^{o}F
Reformer Steam Flow	Minimum

The proportionality factor between reformer pressure and fuel cell pressure was established based on estimated pressure losses through the intervening components as follows:

	% Pressure Loss
Reformer Exit Nozzle	1
Heat Exchangers (4)	8 (2 each)
ZnO Reactor	7

$P_{\text{fuel cell}} = .8492\ P_{\text{reformer}}$

Turbomachinery output and losses are a consideration in establishing the range of pressures to be analyzed. The case of net turbomachinery electricity output has not been considered for the oil-fired plant, hence, turbomachinery considerations dictate upper and lower limits for power plant pressure.

A peak fuel cell pressure of 400 psi was selected for the trade-off study based on maintaining a margin for turbomachinery power in order to accommodate transient power plant operation.

For a selected fuel cell pressure, the minimum reformer steam flow to avoid carbon deposition in the fuel cell anode was derived as shown in Figure 3-11. The reformer pressure was computed and the integrated system was analyzed using the computer models described (3-1). Keeping the reformer steam flow constant, the fuel cell pressure and reformer pressure were then refined by iterative analysis to achieve maximum pressure as limited by anode carbon deposition.

The procedure was repeated for a wide range of fuel cell pressures with a specific value for steam/carbon ratio for each pressure, not necessarily restricted to state-of-the-art limitations.

The results are given in Table 3-4 and Figure 3-12. Table 3-4 indicates that the adverse effect of high pressure on reformer efficiency is not substantial but is significant enough to offset the Nernst effect for fuel cell pressures over 100 psia. The mole fractions of H_2 and CO are, of course, significantly higher at lower reformer steam flows as shown in Figure 3-13. The theoretical increase in fuel cell efficiency with increasing pressure (and steam flow) is also affected by the use of cathode recirculation cooling which yields greater benefits for lower anode flow rates; i.e., lower reformer steam flows which dictate lower pressures. The net effect is that power plant efficiency decreases with system pressure as shown in Figure 3-12.

Reformer Exit Temperature

An evaluation of the effect of varying reformer exit temperature on reformer performance is shown in Figure 3-13, which depicts reformer hydrogen plus carbon monoxide production versus exit temperature for selected reformer steam flow conditions. The sum of hydrogen and carbon monoxide is selected as the meaningful parameter since these are the only combustibles converted to electric output by the fuel cell.

Table 3-4

TRADE-OFF STUDY DATA

CASE	A	B	C	D	E	F	G	H
REFORMER DATA								
Air/Carbon (mole)	1.8	1.8	1.8	1.8	1.8	1.8	1.8	1.8
Steam Carbon (mole)	2.5	1.65	1.33	0.8	1.33	0.8	0.8	0.8
Pressure (psia)	471	180	112	37.6	112	37.6	37.6	37.6
Air Inlet Temperature (^{o}F)	1417	1315	1290	1259	1600	1600	1500	1500
Exit Temperature (^{o}F)	1650	1650	1650	1650	1745	1792	1743	1743
Efficiency*	.9606	.9670	.9683	.9694	.9696	.9698	.9697	.9697
FUEL CELL DATA								
Pressure (psia)	408	153	95	32	94	32	32	32
Cathode Recirculation Ratio	0.5	0.5	0.5	0.5	0.5	0.5	0.5	.545
Efficiency*	.4632	.4670	.4683	.4700	.4701	.4707	.4707	.4709
POWER PLANT EFFICIENCY	.4361	.4426	.4444	.4465	.4467	.4473	.4473	.4475

*Efficiencies include H_2, CO and CH_4
No Methane Slip

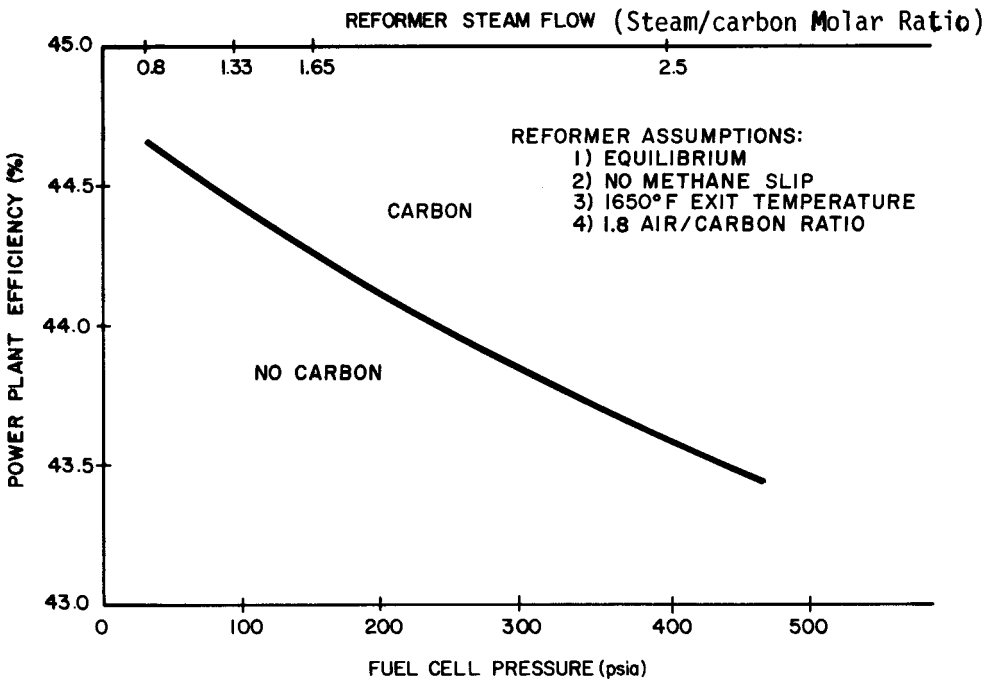

Figure 3-12. Power Plant Efficiency Pressure and Reformer Steam Flow

The sensitivity studies indicate that a small increase in reformer (and fuel cell) efficiency can be attained by increasing the reformer exit temperature, thereby increasing the mole fractions of H_2 and CO. Figure 3-13 shows the effect of reformer exit temperature on product gas composition. The results shown in Figure 3-13 are based on the combined effects of reformer pressure and steam flow rather than a single parameter analysis, which indicates a similar increase in reformer efficiency at constant pressure as shown in Figure 3-15.

The increase in reformer exit temperature is achieved by increasing the reformer air inlet temperature, and the corresponding results are presented in Figure 3-14 which shows power plant efficiency versus reformer air inlet temperature. The data shown represent the low pressure system. Peak reformer air inlet temperature is limited by practical constraints such as heat exchanger and catalytic burner metal temperatures. Plant efficiency is higher at low system pressures, but the change in efficiency is diminished as the reformer air inlet temperature is increased as

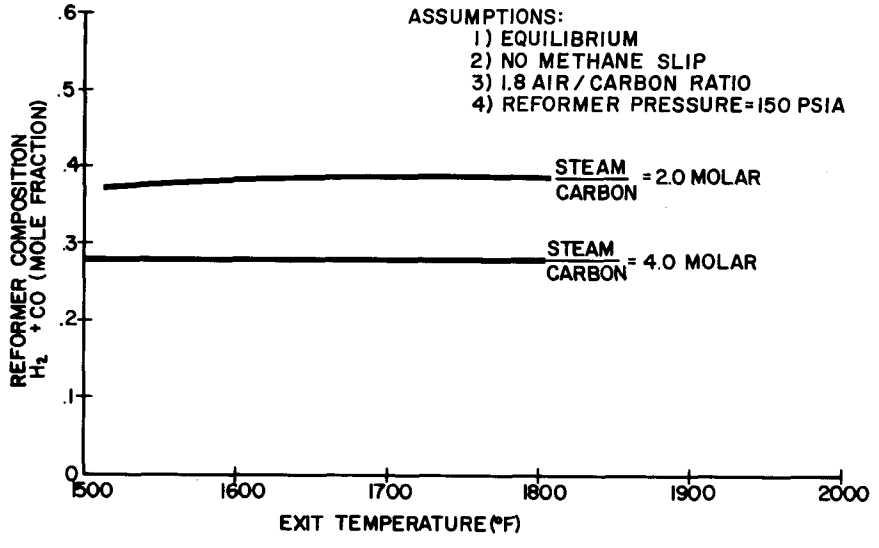

Figure 3-13. Reformer Output vs. Exit Temperature

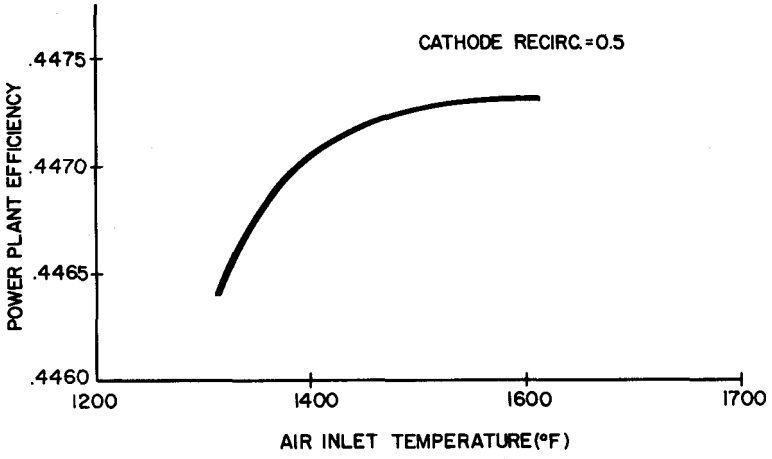

Figure 3-14. Power Plant Efficiency vs. Reformer Inlet Temperatures

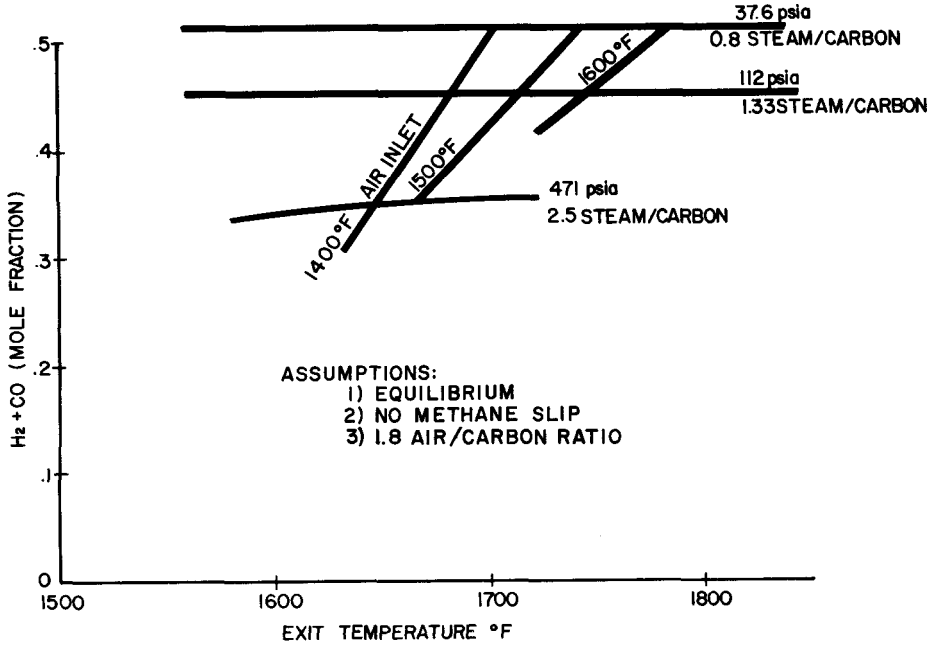

Figure 3-15. Reformer H_2 + CO Output vs. Steam Flow Exit Temperature and Pressure

illustrated by cases C to E compared to cases D to F in Table 3-4. As inlet air temperature is increased to 1600^{O}F, power plant efficiency for the low steam flow condition increases from 44.65% to 44.73%, compared to an increase from 44.44% to 44.67% for the higher steam flow condition.

The reason for the greater increase in plant efficiency for the higher steam flow cases is the greater increase in the concentrations of H_2 and CO in the reformer gas product gas. However, power plant efficiency appears to be higher for the low steam flow (low pressure) condition at any reasonable reformer air inlet temperature.

Conclusions for Performance Sensitivity

- The current reference design fuel cell pressure is about optimum for the given reformer operating conditions; however, an integrated combined evaluation of fuel cell and reformer operating conditions indicates that fuel cell and reformer pressures should be set at about 15 atmospheres for peak power plant efficiency as limited by reformer steam to carbon ratio.
- Efficiency of the current reference design plant can be increased about 0.6% using 50% cathode recirculation as a cooling mechanism. Efficiency of a low pressure system can be comparably increased using cathode recirculation.
- Anode recirculation generally causes such a loss in efficiency that other methods of carbon control are preferred; e.g., reducing fuel cell pressure.
- Efficiency decreases linearly with current density.
- Reformer steam flow and system pressure can be reduced simultaneously, consistent with fuel cell carbon formation limits to achieve an increase in plant efficiency.
- Plant efficiency increases very slightly with increased reformer operating temperatures as controlled by inlet temperature.
- The power plant efficiency goal of 45.5% is reasonable and could be exceeded if reformer development programs are successful at low air to fuel ratios.

COST SENSITIVITY STUDY

This section examines the impact of plant capital cost and cost of electricity when certain operating parameters are varied. Performance sensitivity studies are presented previously indicate the relative importance for various operating parameters in terms of their impact on plant performance. This section adds cost considerations to that performance sensitivity, and thus permits selection of certain plant parameters. The following key parameters have been selected for cost sensitivity study:

- Current Density
- Fuel Cell Air Flow
- Fuel Sulfur Content

Procedures

The results of the cost evaluation are used for all subsystem and component costs. Costs for the fuel cell heat exchanger and the cathode recirculation pump, required in the excess air study, are found in References (3-5) and (3-6), respectively.

Study Methodology

The cost figures presented earlier in the cost evaluation are for a 4.5 MW (AC Net) plant. Therefore, in order to facilitate their use in the sensitivity analysis, the total MW output (4.5) is held constant throughout the sensitivity studies. The results of the oil-fired plant performance sensitivity study are used for all performance information.

Table 3-5 is a summary of the subsystems considered to have a cost impact as each of the parameters is varied. The table also gives the scaling parameter used for each subsystem and the exponential scaling factor. As in the case of the coal-fired plant (Section 2), the value of the "exponent" used in scaling has been established in each case on the basis of one or more of the following:

- Similar cost scaling studies
- Costing texts
- Theoretical derivations
- Manufacturers' data

The subsystems referred to in this table correspond to those subsystem breakdowns in the cost study using the ECAS method (Appendix C), which is more readily applicable to a cost sensitivity analysis than the EPRI method, due to its subsystem breakdown and less complex adders.

For the oil-fired plant, fuel cell and plant efficiency are directly proportional. Thus, when assessing the cost impact of a particular parametric change, either efficiency may be used as a gauge of component size. For example, when evaluating the effect of current density on fuel processor cost, the change in fuel cell efficiency can be used; at first glance a more direct approach would be the use of plant efficiency to reflect oil throughput at constant output but, as noted, this is equivalent. In general, fuel cell efficiency is more readily computed and is thus used.

Table 3-5

COST SENSITIVITY KEY PARAMETERS
OIL-FIRED CASE

Parameter Being Varied	Subsystems Considered	Scaling Parameters	Exponential Scaling Factor
Current Density	- Fuel Processing Subsystem	1/η	0.7
	- Fuel Cell Subsystem	Area	1
	- Fuel Cell Turbocompressor	1/η	0.25
	- O&M Cost of Sulfur Sorbent	1/η	1
	- Cost of Fuel	1/η	1
Fuel Specification	- Sulfur Sorbent	Sulfur	1
	- Sorbent Vessel	Content	0.7
	- O&M Cost of Fuel Processing System		1
Excess Air	- Fuel Cell Turbocompressor Subsystem	3 Flowrates	0.25
	- Fuel Processing Subsystem	1/η	0.7
	- Fuel Cell Piping Cost	Cathode flow	1
	- Balance of Fuel Cell Subsystem	1/η	1
	- Cathode Heat Exchanger	Thermal duty	1
	- Cathode Recirculation Pump	Recirc. ratio	0.25
	- O&M Cost of Fuel Processing Subsystem	1/η	1
	- Cost of Fuel	1/η	1

η = fuel cell efficiency based on HHV of (H_2+CO)

Fuel Specification

The only component cost that is scaled in the fuel processing system is the zinc oxide reactor, which includes both vessel and sulfur sorbent. The zinc oxide reactor and the O&M costs of the fuel processing system are scaled by the sulfur content of the fuel.

Excess Air

In varying excess air flow to the fuel cell several turbomachinery costs are affected. The following breakdown is assumed for the fuel cell turbocompressor subsystem: 40% for turbine, 40% for fuel cell compressor, and 20% for reformer compressor. These costs are then scaled by the three respective turbine and compressor flow rates, keeping electric output constant. At a constant plant output, as excess air increases, fuel cell efficiency decreases and flow rates through the fuel cell increase. Fuel cell piping costs are scaled by cathode inlet flow rates. The balance of the

fuel cell subsystem, the O&M cost of the fuel processing system, and the cost of fuel are scaled by fuel cell efficiency. Where a cathode heat exchanger is needed, its cost is scaled by thermal duty. Cathode recirculation compressor cost is scaled by the cathode exit gas recirculation ratio. This assumes a fixed power plan pressure.

Current Density

In keeping the total plant output constant, all subsystems except the fuel cell subsystem are scaled by fuel cell efficiency, which is proportional to the overall plant efficiency. As current density is increased, fuel cell efficiency is decreased. The fuel cell subsystem is scaled by the change in area, since for a given output, fuel cell area decreases as current density is increased.

Equation 3-2 is used to calculate fuel cell area:

$$ft^2 \text{ (Cell Area)} = \frac{\text{(output)} \quad W(DC)}{\text{(voltage) } V(DC) \times \text{(current density) amps/ft}^2} \qquad (3\text{–}2)$$

The effect of varying current density on the capital cost and cost of electricity is illustrated on a normalized cost basis in Figures 3-16 and 3-17 respectively. As can be seen in Figure 3-16, as the current density is increased beyond the reference point (162 mA/cm^2), there is a reduction in capital cost. This reduction in cost is largely due to the decreased cost of the fuel cell subsystem, which is 40% of the total capital cost (not including contingencies). For example, as current density is increased from the reference to 300 mA/cm^2 the cost of the fuel cell subsystem drops by about $220,000. However, as the current density is decreased to 100 mA/cm^2, the cost of the fuel cell subsystem increases by approximately $360,000 from the reference case.

The cost of electricity (COE) can be expressed as three component expenses: capital fuel, operating-maintenance.

$$COE = COE_{capital} + COE_{fuel} + COE_{operating \text{ and } maintenance}$$

Figure 3-17 shows that a minimum cost of electricity can be reached at a current density of approximately 190 mA/cm^2. Beyond this point capital cost is decreased by higher current densities, but operating and maintenance costs and the cost of fuel

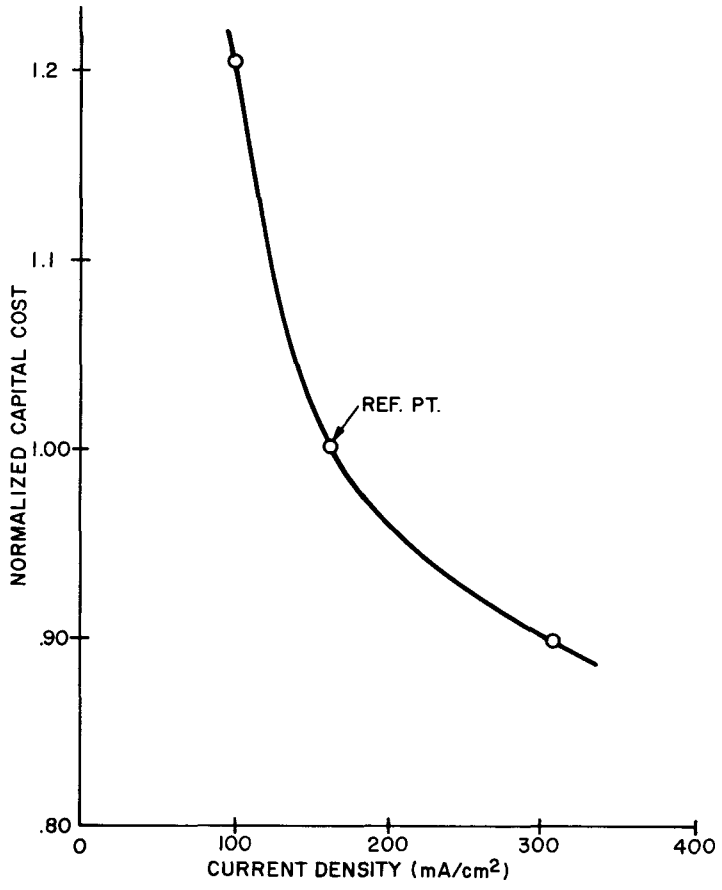

Figure 3-16. Normalized Capital Cost vs. Current Density

are increased by higher current densities due to a loss in fuel cell efficiency. The net effect is an increase in cost of electricity as current density increases beyond 190 mA/cm^2.

Sulfur Content

Figure 3-18 illustrates the impact on capital cost and the cost of electricity when the sulfur content of the fuel is changed. As the sulfur level of the fuel is increased, both capital cost and cost of electricity increase. The indicated increase is due exclusively to the cost impact on the cleanup system, both capital and operating. As the sulfur level is raised from the reference point of 0.22% to 0.5% sulfur, cost of the cleanup system increases by approximately $100,000 and the O&M cost of the cleanup system goes up by 8.6 mills/kWh.

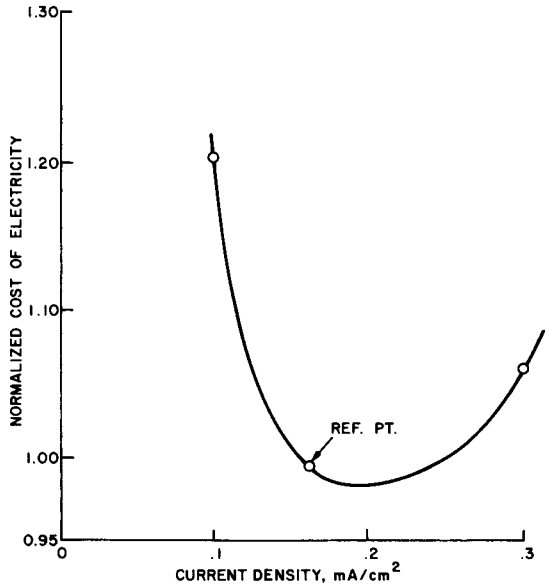

Figure 3-17. Oil-Fired Plant – Normalized Cost of Electricity vs. Current Density

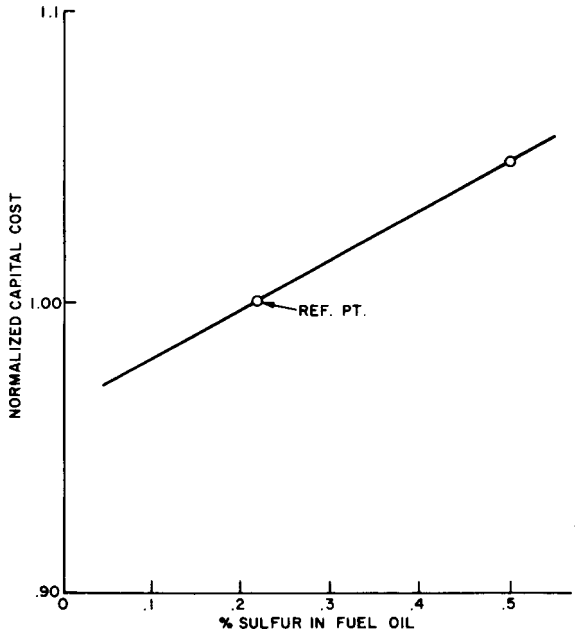

Figure 3-18. Normalized Capital Cost vs. Sulfur Content of Fuel

Excess Air

Figures 3-19 and 3-20 give normalized capital cost and cost of electricity as a function of excess air to the fuel cell. Figure 3-19 shows that plant capital cost is decreased by decreasing fuel cell air flow from the reference case at 322% excess air flow. A major subsystem cost which influences this trend is the fuel cell subsystem. However, the dominant effect in this case is the overall reduction in capital cost due to improved power plant efficiency and reduced air flows. As excess air is decreased from the reference to 100% excess air, cost of the fuel cell subsystem is reduced by $8,000. However, cost of the turbocompressor system decreases by $24,000 and the cathode gas heat exchanger is eliminated, at a savings of $23,000.

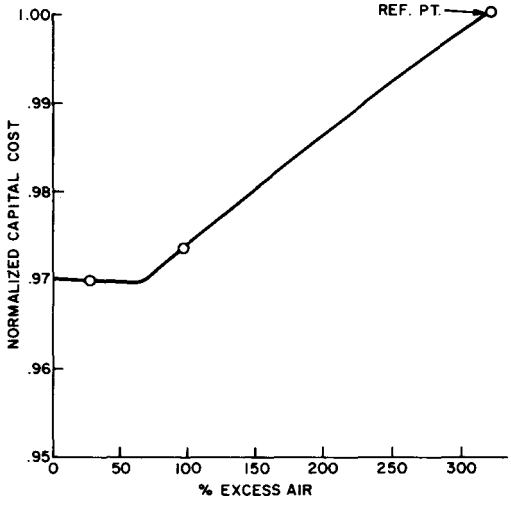

Figure 3-19. Normalized Capital Cost vs. Excess Air

In addition, fuel and operating costs are directly reduced by the improved power plant efficiency at reduced air flows. It can be seen from Figure 3-20 that a minimum cost of electricity is reached between 50% and 100% excess air, which might be expected since the optimum plant efficiency is reached between 90% and 100% excess air. As the capital cost is reduced, the value of air flow at minimum cost of electricity would approach the value of air flow at peak power plant efficiency. Specifically, as economically competitive capital cost goals are achieved, the most cost-effective air flow will be about the same as the air flow at peak plant efficiency.

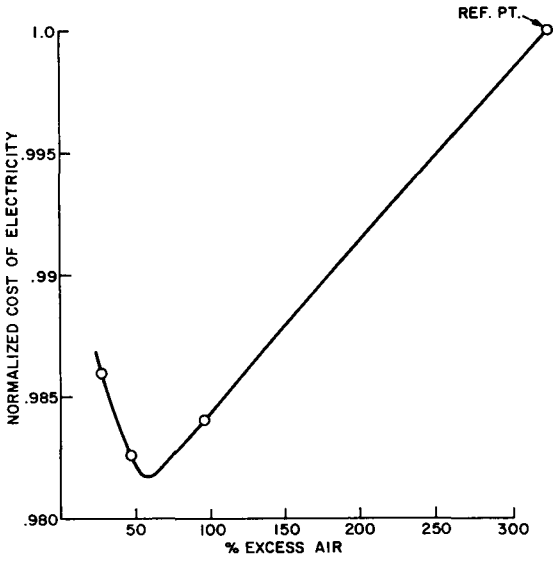

Figure 3-20. Normalized Cost of Electricity vs. Excess Air

Conclusions

The cost evaluation studies described previously permit the following conclusions to be drawn related to the selection of plant operating parameters and the impact of design changes.

- The design value of current density used has been 161.5 mA/cm^2 as in the ECAS study (2-2). This study shows a minimum cost of electricity is encountered at 190 mA/cm^2; however, the improvement is only 1%. Since the uncertainty in the studies is larger, no specific change is justified. However, as noted in the earlier discussion (Section 2) related to the coal-fired plant, in evaluating technology goals, it will be appropriate to note that moderate increases in current density have little impact, but below 150 mA/cm^2, the cost impact of reducing current density is significant.

- The zinc oxide reactor represents a significant percentage of the plant cost, thus the impact of fuel sulfur content is large on plant cost of electricity.

- The cost sensitivity study indicated a 2% improvement in cost of electricity in moving from the 300% excess air used in the reference case to an optimum at about 60% excess air. The improvement is due to the impact of reduced fuel cost through improvement in plant efficiency.

OIL-FIRED MOLTEN CARBONATE FUEL CELL POWER PLANT DESCRIPTION

The foregoing material has described a series of performance and cost studies designed to improve the performance and cost attractiveness of the oil-fired molten

carbonate fuel cell power plant. This plant was initially evaluated in a series of studies reported in the previous Interim Report (3-1), and in that work an overall efficiency of 43.3% (7890 Btu/kWh heat rate) was reported.

This section describes the current requirements, goal, cycle configuration and characteristics, and gives a brief description of a conceptual plant design as well as preliminary subsystem specifications.

Power Plant Requirements and Goals

Table 3-6 lists general design requirements and goals for the oil-fired power plant. The specified fuel is #2 heating oil of the composition given in Table 3-7.

Table 3-6

GENERAL DESIGN REQUIREMENTS AND GOALS FOR THE OIL-FIRED MOLTEN CARBONATE FUEL CELL POWER PLANT

Requirements	
Dispersed Station Plant (Industrial Application)	Utility Owned and Operated
Power Level	4.5 MWe (AC) Net
Fuel	# 2 Fuel Oil
Site Characteristics	"Middletown" Modified for Industrial Application
Environmental	Projected 1985 Federal Requirements
Goals	
Intermediate Load Duty with Hourly Load Following Capability	
Heat Rate	7500 Btu/kWh
Plant Availability	90%
Life (50% Capacity Factor)	
Fuel Cell Stacks	9 Years
Balance of Plant	30 Years

Table 3-7

COMPOSITION OF NO. 2 FUEL OIL

	%
Ash	0.01
Sulfur	0.22 Max
Hydrogen	12.60
Carbon	87.30
Nitrogen	0.006
Oxygen	0.04
Higher Heating Value	19280 Btu/lb

Table 3-8 lists existing environmental limits applicable to the oil-fired power plant, along with projected limits for the 1985 time period.

Table 3-8

CURRENT AND PROJECTED EMISSIONS STANDARDS FOR OIL-FIRED PLANT

Pollutant	Current Standards	Projected 1985 Federal Requirements
SO_x	0.8 $lb/10^6$ Btu	0.2 $lb/10^6$ Btu
NO_x	0.3 $lb/10^6$ Btu	0.15 $lb/10^6$ Btu
TSP	0.1 $lb/10^6$ Btu	0.03 $lb/10^6$ Btu

As shown in Table 3-6, a heat rate of 7500 Btu/kWh and an availability of 90% are the targets for the oil-fired plant. Table 3-9 summarizes the control goals for the intermediate load oil-fired plant.

Table 3-9

CONTROL GOALS FOR THE
INTERMEDIATE LOAD OIL-FIRED PLANT

Daily Load Following

Able to load and unload up from 25 to 100% of nameplate MW rating in 1 minute or less

Module shutdown not required

Startup/Shutdown

Startup: Cold startup in several hours; hot startup in 1 hour

Shutdown: 100% to zero load in 1 hour

Life: 40,000 hours

Frequency Governing

Respond +1.3% − 0.7% of unit nameplate rating in seconds in prompt, stable fashion

Maximum deadband of 0.06% frequency

Maximum overall steady-state regulation of 5%

Abnormal Conditions

Complete load rejection (breakers opening)

Partial load rejection (from power system breakup)

Sustained abnormal voltage or frequency operation

Cycle Description and Reference Plant Data

Referring to the process flow diagram, Figure 3-1, the fuel (#2 Oil) mixes with steam and passes through a heat exchanger where the mixture heats to 1100^{o}F. The steam/oil mixture is then fed into the autothermal reformer (ATR). The heat used to raise the temperature of the mixture is extracted from the reformer exit gas, and the heat used to generate the steam is extracted from the fuel cell anode vent gas. The ATR is also fed by 1500^{o}F air which has been heated by the fuel cell anode vent gas after it has been combusted in a catalytic burner to remove the remaining combustibles.

The mixture of steam and oil vapor reacts with the air in the autothermal reformer and the product gas exits at 1674°F. The hot gas is cooled to 750°F as it passes through the heat exchangers and is piped to a zinc oxide polisher where the sulfur compounds are chemically removed from the fuel gas. The clean fuel gas then recirculates through a heat exchanger where hot fuel from the ATR reheats it to 1000°F.

This hydrogen-rich gas is fed into the anode side of the fuel cell. Meanwhile, the cathode side of the fuel cell is fed with 1000°F air from the turbocompressor and the cathode recirculation loop. Some of the hydrogen and carbon monoxide in the fuel gas reacts in the fuel cell to create electrical power. Heat is extracted from the fuel cell by the anode and cathode exhaust gases. The hot cathode exhaust preheats the cathode inlet gas to the proper temperature and then exits the system by powering the turbine of the turbocompressor set.

The anode exhaust gas passes through a catalytic burner to remove the remaining combustibles. It is then passed to a knockout drum to recover water. The balance of the cold anode exhaust gas is mixed with compressed air and reheated to 1000°F. This mixture, rich with oxygen and carbon dioxide, is fed to the cathode side of the fuel cell where much of the oxygen and carbon dioxide is consumed.

The fuel cell module, consisting of multiple stacks, is assumed to be a single, factory-assembled, self-contained pressure vessel. Two modules have been assumed for layout purposes to give dimensions more compatible with shipping requirements. Although here is conceptual commonality with the individual modules chosen in the coal-fired plants, current differences in operating pressure, method of heat rejection, and fuel gas heating value (amount of heat rejection) are significant.

A reformer air inlet temperature was selected at 1500°F based on judgment of peak feasible heat exchanger operating temperature; the 1500°F air inlet temperature is comparable to a reformer inlet temperature of about 1300°F for the mixed stream (air, oil and steam). Current analyses as described earlier indicate that reformer operating conditions can be adjusted to give very little difference in plant efficiency versus pressure.

It should be noted that there are potential benefits for operating at higher pressures such as a general decrease in component sizes and higher temperatures for cogeneration heat from the water knockout system. An evaluation of optimum operating pressure is contingent upon a cost sensitivity analysis of system pressure.

Should methane formation in the anode turn out to be a real problem, the loss in power plant efficiency would be about 5.9 percentage points at worst, based on calculating methane formation at the updated reference design operating conditions. However, should component test programs identify significant methane formation in the fuel cell anode, the system design tradeoffs would need to be repeated to identify more optimum operating conditions for which the performance penalty would be less.

Table 3-10 and Table 3-11 summarize the oil-fired plant performance results from the studies described in this section.

Table 3-10

OIL-FIRED REFERENCE PLANT
(Reformer Approach to Equilibrium)

Oil Feed (lb/h)	1843
(MWt)	10.41
Reformer Efficiency (%)	
(H_2+CO+CH_4) Content	96.2
(H_2+CO) Content	93.5
Fuel Cell Voltage (V)	0.822
Fuel Cell Efficiency (%)	
(H_2+CO+CH_4) Content	45.8
(H_2+CO) Content	47.2
DC to AC Inverter Efficiency	98
Power Plant Efficiency	43.2
Power Plant Heat Rate (Btu/kWh)	7896
Net Power Output (MWe AC)	4.5

Table 3-11

OIL-FIRED PLANT MATERIAL AND ENERGY BALANCE
(Refer to Figure 3-1 for Stream Numbers)

Stream Number	1	3A	2B	4	10	11	21	22	23	24
Stream ID	Oil	Steam	Air to Reformer	Reformer Exit	Anode Inlet	Anode Exit	Cathode Inlet	Cathode Exit	Turbine Inlet	Vent
Temperature (^{o}F	77	575	1500	1674	1000	1300	1000	1300	1300	642
Pressure (psia)	14.7	245	244	241	225	224	225	224		15
Gas Composition (Mole Fraction)										
O_2			.2100				.1283	.1031	.1031	.1031
CO				.1039	.1039	.0171	.0000	.0000	.0000	.0000
H_2				.2817	.2817	.0265	.0000	.0000	.0000	.0000
CO_2				.0832	.0832	.3707	.1385	.0735	.0735	.0735
CH_4				.0039	.0039	.0029	.0000	.0000	.0000	.0000
N_2			.7855	.2682	.2682	.2022	.6742	.7576	.7576	.7576
A_r			.0045	.0031	.0031	.0023	.0028	.0028	.0028	.0028
H_2S				.0002	.0000	.0000	.0000	.0000	.0000	.0000
H_2O				.2556	.2556	.3782	.0560	.0629	.0629	.0629
Total Flow $\frac{lb - Moles}{h}$		267.7	241.7	701.0	700.9	980.7	3145.5	2800.9	1820.5	1820.5
Total Flow lb/h	1843	4819.0	6975.9	13637.9	13629.5	27445.1	94932.1	81141.7	52742.0	52742.0
Energy Flow $\frac{10^6 Btu}{h}$	35.542	6.145	2.571	46.857	42.700	23.413	26.256	29.871	19.416	9.827

Power Plant Description

A single, plan view, conceptual layout has been generated for the dispersed application, oil-fired molten carbonate fuel cell power plant. The oil-fired configuration is expected to serve as a small output, load-following power plant with capability of supplying industrial heat, or for use in close proximity urban applications.

The layout (Figure 3-21) shows a concept of an almost completely skid-mounted power plant to accent the need for factory assembly and minimum field installation and checkout time. No in-depth evaluation was made of this concept but it indicates sufficient advantage to warrant further study.

The two fuel cell modules, shown skid mounted, would be shipped separately either as total assemblies or for partial field assembly. Studies of on-site servicing versus factory rebuild should be performed later to better assess initial installation costs as well as service and replacement costs. Although there is conceptual

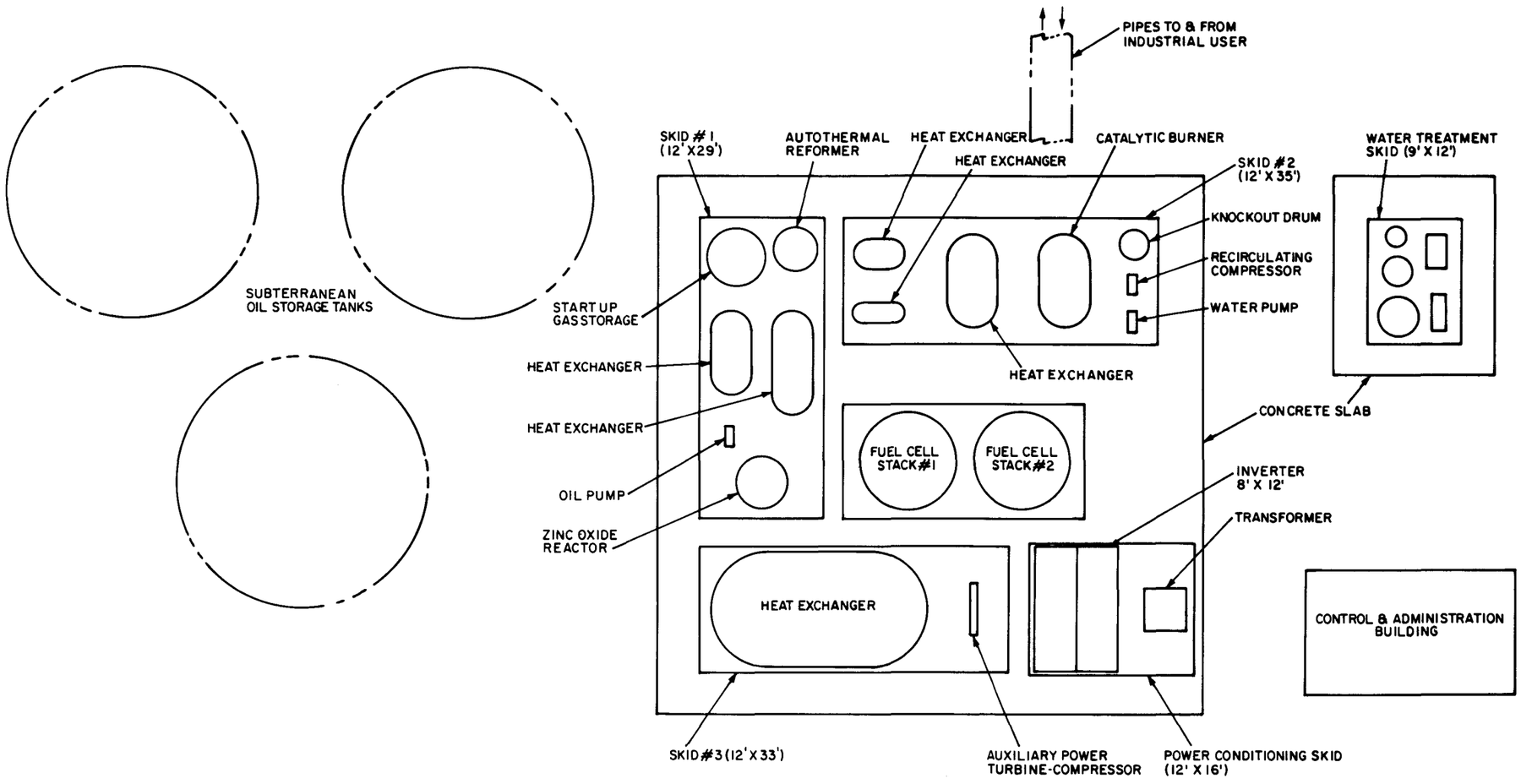

Figure 3-21. Oil-Fired Molten Carbonate Fuel Cell 4.5 MW Power Plant

Blank Page

commonality with the individual fuel cell modules chosen for the coal-fired plant, current differences in operating pressure, methods of heat rejection, and fuel gas heating value are significant.

Subsystem Descriptions

Preliminary definition of the subsystems for the oil-fired plant was prepared in the form of description sheets. These sheets will form the basis for continuous updating as the designs mature. The subsystems covered are listed herein. A control subsystem will be added later.

- Fuel Cell Subsystem
- Reformer Subsystem
- Gas Cleanup Subsystem
- Turbocompressor Subsystem
- Electrical Subsystem
- Balance of Plant Subsystem

Fuel Cell Subsystem Description

Function:

The fuel cell subsystem creates electrical power from the clean fuel gas and provides a source of water for use in the gasification subsystem.

Requirements and Desired Characteristics:

• Current density	100-200 mA/cm^2
• Fuel Cell Efficiency (H_2 + CO) Content	>0.40
• Fuel Gas Flow Rate	13629 lb/h
• Fuel Gas (H_2 + CO) Mole Fraction	51.4%
• Oxidant Composition	Air
• Cooling	Excess Cathode Air and Cathode Recycle
• Carbon Suppression	Cell Pressure

Reference Plant Implementation:

The fuel cell subsystem consists of a number of fuel cell stacks in which the electrochemical conversion process takes place. Several fuel cells stacks are arranged

within a single pressure vessel. The stacks are mounted inside, with pipe flanges on the outside for connection. Fuel cell stacks in the pressure vessel will be connected in a suitable series/parallel combination to provide appropriate electrical characteristics to the inverter subsystem while supporting plant reliability and availability goals. Two pressure vessels have been shown in the reference design, Figure 3-21.

A single catalytic burner is used to oxidize unburned fuel gas in the anode exhaust. This gas is cooled in heat exchanger(s) to provide a water source, and then flows to the cathode as a CO_2 source.

Reference Plant Performance:

- Fuel Cell Efficiency Based on (H_2 + CO) Content — 47.2%
- Fuel Cell Voltage — 0.822
- Fuel Cell Current Density — 161.5 mA/cm^2
- Fuel Utilization — 85%

Reformer Subsystem Description

Function:

The reformer subsystem converts #2 fuel oil to a raw fuel gas.

Requirements and Design Characteristics:

- Oil Feed: Flow Rate — 1843 lb/h
- Reformer Efficiency — 94%
- Hydrocarbon Formation — Negligible
- Raw Gas Temperature — 1750°F
- Raw Gas Heating Value — 2750 Btu/lb

Reference Plant Implementation:

The subsystem consists of an autothermal reformer, air supply preheat exchangers, #2 fuel oil supply system with preheat exchangers and a steam flashing system in the #2 fuel oil supply line.

The autothermal reformer features a large diameter adiabatic reactor; the exothermic and endothermic chemical reactions take place simultaneously in the same reaction chamber in such a way that the required reaction temperature is maintained without external heating of the catalyst bed.

In the process, superheated steam and fuel oil are vaporized, mixed, and preheated to 1100°F. This is then mixed with preheated air at a temperature of 1500°F. The oxygen reacts exothermically with the hydrocarbons, at the same time endothermic steam hydrocarbon reactions take place and limit the temperature rise caused by the exothermic reactions. The gases are forced through fixed bed catalysts which results in essentially complete conversion of the hydrocarbons to hydrogen and carbon oxides. This gas then proceeds to the cleanup system.

Reference Plant Performance:

- Reformer Efficiency
  - (H_2 + CO + CH_4) Content 96.97%
  - (H_2 + CO) Content 96.90%
- Raw Gas High Heating Value 2897 Btu/lb

Gas Cleanup Subsystem Description

Function:

The gas cleanup subsystem desulfurizes the fuel gas to a sulfur level acceptable by the fuel cell.

Requirements and Desired Characteristics:

- Gas Flow Rate 13627 lb/h
- Concentration of Sulfur in Clean Gas Stream <1 ppm

Reference Plant Implementation:

The gas cleanup subsystem consists of a zinc oxide catalyst reactor. The 750°F gas from the gasification subsystem enters the zinc oxide catalyst reactor, where H_2S is absorbed by zinc oxide pellets, thereby reducing H_2S content in the fuel gas to less than 1 ppm of sulfur.

The reference plant design currently employs a single zinc oxide reactor vessel. However, later plant reliability, maintainability and availability studies may show some advantage in using two or even three vessels.

- Sulfur Absorption Capacity of Zinc Oxide — 20% wt
- Rate of Use of Zinc Oxide — 1800 lb/wk
- Replacement Rate of Zinc Oxide — 770 ft^3 semi-annually

Turbocompressor Subsystem Description

Function:

The turbocompressor subsystem recovers the power from the fuel cell discharge stream and supplies compressed air to the fuel cell and autothermal reformer.

Requirements and Desired Characteristics:

- Fuel Cell Subsystem Discharge Stream:
  - Temperature — 1300°F
  - Pressure — 224 psia
  - Flow Rate — 41417 lb/h
- Air to Reformer:
  - Pressure — 244 psia
  - Flow Rate — 6976 lb/h
- Air to Catalytic Combustor:
  - Pressure — 244 psia
  - Flow Rate — 7020 lb/h
- Air to Fuel Cell:
  - Pressure — 225 psia
  - Flow Rate — 25900 lb/h
- Efficiencies:
  - Compressor — 90%
  - Turbine — 92%

Reference Plant Implementation:

The hot cathode exhaust gas exits the system through an auxiliary power turbine. The turbine exhaust is passed to an industrial user for heat recovery.

The power generated by the turbine is used to drive a two-stage compressor. Intermediate pressure air is used for the fuel cell cathode and the higher pressure air is used in the reformer.

Electrical Subsystem Description

Function:

The electrical subsystem converts the DC output of the fuel cell to AC power and steps it up to transmission voltages.

Requirements and Desired Characteristics:

• DC to AC Inverter Efficiency	98%
• Fuel Cell Power Output – DC	4.59 MW

Reference Plant Performance:

• DC to AC Efficiency	98%
• Fuel Cell Voltage (per cell)	0.822
• Net Power Output (MWe AC)	4.50

Reference Plant Implementation:

The electrical plant equipment for the oil-fired plant consists of the fuel cell island electrical equipment, which collects the DC output of the fuel cell, converts it to 3 phase 60 Hz AC power and steps it up to transmission voltages. The DC/AC inverter is of the solid state type.

Balance of Plant Subsystem Description

Function:

Balance of plant subsystem provides service buildings, compressed air systems inter-island piping and wiring, water systems, startup fuel oil system, power plant fire protection system, and other plant utilities, including heating, ventilating and air conditioning and equipment handling. Also included are miscellaneous heat exchangers, drums, and pumps required to support the recovery of water from the anode exhaust stream for use in the gasification subsystem.

Requirements and Desired Characteristics:

To be determined.

REFERENCES

3-1. Fuel Cell Power Plant Integrated Systems Evaluation, General Electric Company, EPRI Report No. EM 1097, June 1979.

3-2. Economic Assessment of the Utilization of Fuel Cells in Electric Utility Systems, Public Service Electric and Gas Company, EPRI Report No. EM 336.

3-3. Assessment of Fuel Processing Systems for Dispersed Fuel Cell Power Plants, Kinetics Technology Incorporated, EPRI Report No. EM 1010. March 1979.

3-4. Autothermal and Steam Reforming of Distillate Fuel Oils, National Fuel Cell Seminar, John Housman (JPL), July 1978.

3-5. Process Plant Estimating Evaluation and Control, Kenneth M. Guthrie, 1974.

3-6. Plant Design and Economics for Chemical Engineers, Max S. Peters and Klaus D. Timmerhaus, 1958.

Appendix A

CLEANUP EQUIPMENT DESCRIPTION

PACKED AMMONIA ABSORBER (Figure A-1)

Process gas containing ammonia from the particulate scrubber overhead is fed to the bottom of a packed tower; water is brought in through a liquid distributor at the top. The purpose of the packing is to provide mixing and to afford surface area for ammonia water contact. Ammonia-free gas is taken off the top, and the ammonia-rich liquid is recycled back to the particulate scrubber.

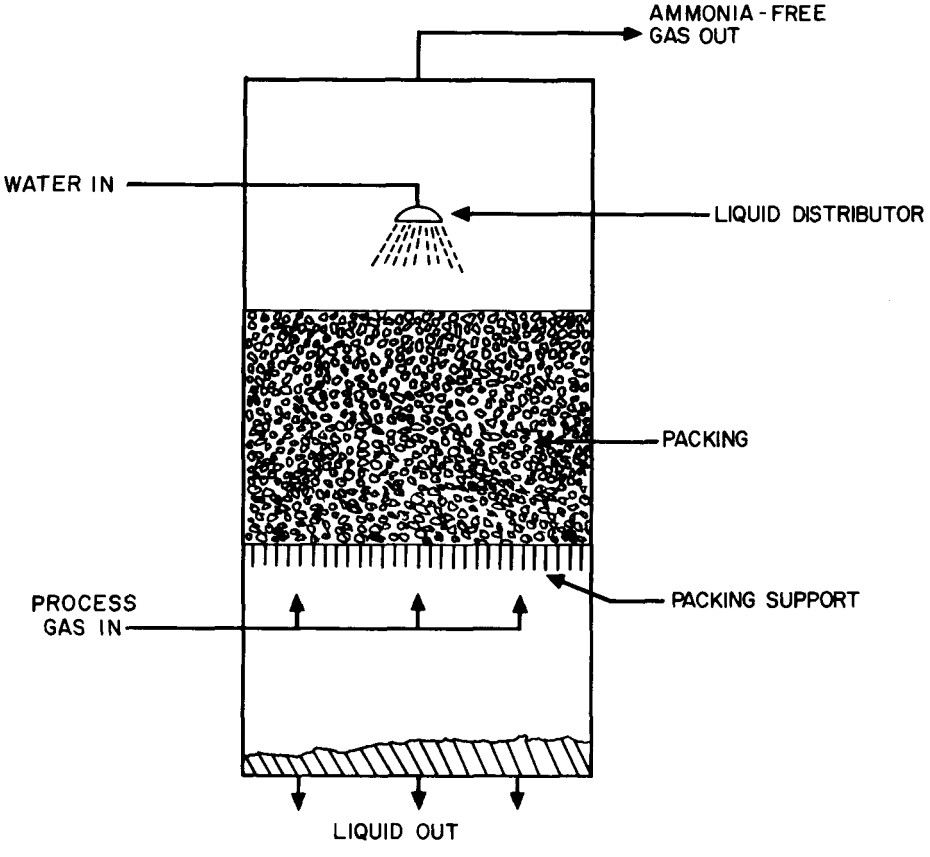

Figure A-1. Packed Ammonia Scrubber

SELEXOL SOLVENT SYSTEM (Figure A-2)

The Selexol Process was developed to remove acid gas components from gas streams by physical absorption. The solvent, dimethyl ether of polyethylene glycol, (trade name Selexol Solvent), has a strong preference for sulfur-based compounds, particularly H_2S.

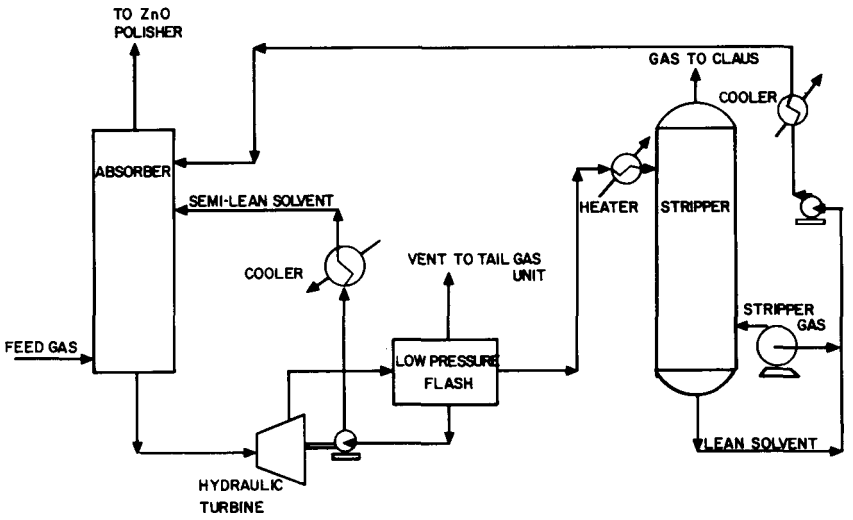

Figure A-2. Simplified Selexol System

For the chosen reference design, it was necessary to modify the Selexol system in order to bring the total sulfur content in the product gas down to <2 ppm. Since the Selexol Solvent is a better absorber of H_2S than COS, the concentration of COS in the gas stream will control the solvent circulation rate. Therefore, for the increased sulfur retention necessary, a high solvent circulation rate will be required. In addition, due to the Selexol Solvent's affinity for H_2S, a larger amount of steam or stripping gas is necessary to produce an essentially H_2S-free solvent recycle to the absorber.

Feed gas from the ammonia absorber enters the bottom of the Selexol absorber at a temperature of about $105^{o}F$. Here the H_2S and COS, along with a large portion of the CO_2, are absorbed to give a product gas which contains <1 ppm total sulfur. This product fuel gas exits at the top of the absorber. Sulfur-rich solvent exits at the absorber bottom and goes through a hydraulic turbine where the pressure is

reduced. The stream is then sent to a low pressure flash where the flashed gases are sent to the Claus unit or vented to the Beavon tail gas unit for cleanup. A portion of the semi-lean solvent is then cooled down and recycled back to an intermediate section in the absorber. The remainder is then heated and sent to the top of the stripper, which is operated at an elevated temperature. The solvent is then stripped, using nitrogen which enters the bottom. The nitrogen comes from the air separation plant. Lean solvent which exits the stripper bottom is cooled and recycled to the top of the absorber. Acid gas exits from the top of the stripper and is sent to the Claus unit. Overall heat effects are minimized by very low absorption heat and specific solvent heat of only 0.5 Btu/#/^{o}F. No provisions for solvent reclamation are needed since the solvent has a very low vapor pressure and exhibits no thermal degradation.

SULFUR GUARD SYSTEM

Complete removal of sulfur from a gas stream by process units employing chemical solutions may not be realized at all times. This can be brought about by upsets in their normal operation which may allow sulfur carryover. Also some organic sulfur compounds in low concentrations, which are difficult to detect, may not be completely extracted in the acid gas removal unit.

To protect any downstream operation sensitive to sulfur compounds, the industrial practice is to install a reactive solid which retains the sulfur or sulfur compounds. The most universally used material is a highly active zinc oxide.

The operation is carried out at operating temperature and pressure ranges up to 400^{o}C (752^{o}F) and 1200 psi respectively. For a desulfurizer guard case, a gas hourly space rate (V_g/V_c/Hr) up to 20,000/hr is used. The zinc oxide is more reactive at the higher temperatures. The higher space rate operation is carried out at the higher pressure conditions. Steam in the gas reduces the ultimate capacity. At a low gas saturation temperature of <100^{o}F, a loading of the ZnO up to 15 wt% sulfur can be obtained without sulfur breakthrough in a one-reactor design.

For the reference plant, a ZnO trim unit is designed to operate on each of the three fuel gas trains following the Selexol unit to insure there will be no sulfur carryover into the fuel cell. The design conditions are as follows:

Inlet Gas Conditions

Sulfur Content (avg.)	2 ppm (wt)
Saturation Temperature	<105°F
Gas Temperature (nominal)	750°F
Gas Pressure (nominal)	517 psig

Design Condition for ZnO

Gas Hourly Space Velocity	10,000 hr^{-1}
Volume (ZnO)	343 Cu Ft
Expected Life	1 Year

Reactor Size

Diameter	8' 0"
Shell Height	9' 6"

MODIFIED CLAUS UNIT (Figure A-3)

The reduction of H_2S to elemental sulfur is an old, well-established fixed bed catalytic process which has been used successfully for several decades. It is based on the following reaction:

$$2\ H_2S + SO_2 \rightleftharpoons 3S + 2H_2O + 35\ kcal \qquad (1)$$

The catalyst is a fairly inexpensive aluminum oxide (Al_2O_3) generally used in a special form, 5-10 mm in diameter. Depending on operating conditions, conversion based on H_2S of 98% or more can be achieved with a good approach to equilibrium at relatively low temperatures.

For an acid gas in which the sulfur is primarily H_2S, partial combustion to SO_2 must be carried out ahead of the Claus reactor in which the following reactions are involved:

$$H_2S + 3/2O_2 \rightleftharpoons SO_2 + H_2O + 124\ kcal \qquad (2)$$

$$H_2S + 1/2O_2 \rightleftharpoons S + H_2O + 53\ kcal \qquad (3)$$

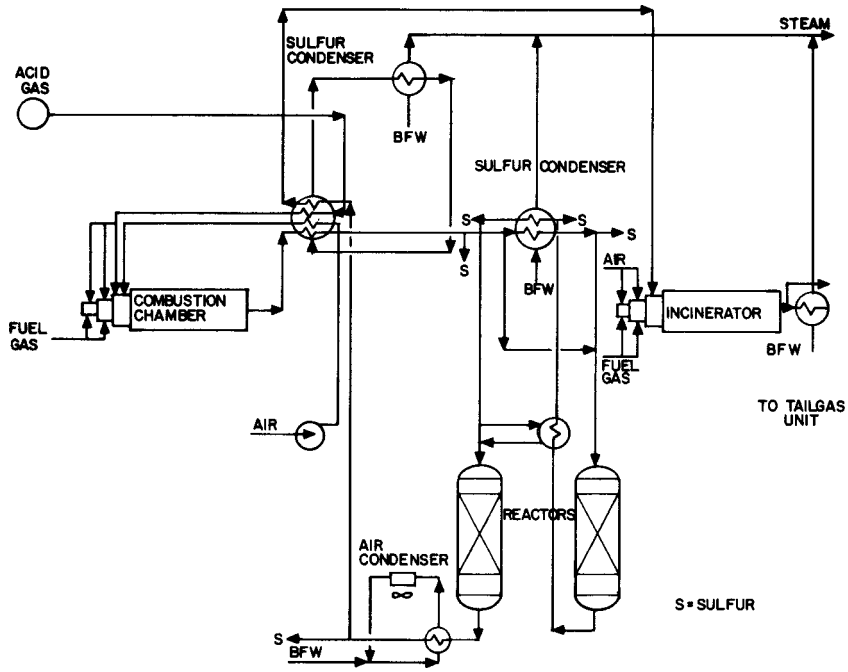

Figure A-3. Preheated Claus Process

Many engineering modifications for improved heat and sulfur recovery have been developed as energy costs and environmental restrictions have increased. Many of these modifications are proprietary. No attempt has been made in this study to evaluate the optimum Claus process for the fuel cell system. However, the process description herein should be representative of a typical Claus plant which is shown in Figure A-3.

Acid gas feed and process air are preheated by heat exchange with the exit gas from the combustion chamber. The preheated acid gases and process air are introduced into a combusion chamber where they react according to reactions (2) and (3). Preheating of the various streams is controlled by the combustion gas temperature, the condensing sulfur, and the medium pressure steam generator. The sensible heat available in the effluent combustion gas is also sufficient for reheating the sulfur-lean process gas to the incinerator to improve thermal efficiency. Synthetic organic liquids can be used as the transfer medium in the closed cycle system.

The process gas, leaving the combustion chamber after the sulfur condensers, enters the Claus reactor. The inlet temperature is controlled by a bypass around the second sulfur condenser.

The required reaction temperature in the Claus reactor is set so as to reduce the COS and CS_2 in the acid gas according to the following reactions:

$$CS_2 + 2H_2O \rightleftharpoons CO_2 + 2H_2S \quad \text{(Hydrolysis)} \qquad (4)$$

$$COS + H_2 \rightleftharpoons CO + H_2S \quad \text{(Hydrogenation)} \qquad (5)$$

In the Claus reactor, the H_2S reacts with SO_2 according to reaction (1) with nearly equilibrium conditions at operating temperatures.

The reactor effluent is cooled to effect final removal of the sulfur before discharging into an incinerator.

In order to attain high sulfur removal approaching 98 to 99% of the sulfur from an acid gas stream, a second or third Claus reactor can be incorporated into the design. In such a modification the effluent from the first Claus reactor is preheated to the required temperature by counter current heat exchange with the effluent gas from the first reactor. The operating temperature of the second reactor is kept as low as possible to preclude sulfur condensing on the catalyst and to obtain a higher conversion by a more favorable equilibrium condition for reaction (1). Accordingly, this temperature is about 15-20^{o}C above the sulfur dewpoint.

Process gas leaving the final Claus reactor is cooled in a sulfur condenser to a temperature approaching the sulfur solidification point. This gas is then further processed in special separators for agglomeration of haze and separation of droplets to an incinerator for thermal post treatment. In this incinerator, the H_2S, COS, CS_2, S, CO and H_2 still contained in the gas will be oxidized completely with an adequate air supply. Dependent on plant size and incinerator temperature, offgas is cooled to stack gas temperature either in a waste heat boiler or by means of quench air. Heat from sulfur condensers and waste heat boiler is used for generation of medium pressure steam.

Low pressure steam of 10-15 psig from the sulfur condenser downstream of the second reactor is condensed in an air-cooled/water-cooled condenser. Resulting sulfur flows through steam jacket seal pipes to a sulfur pit where it is discharged by submerged pumps.

In the reference plant design, however, it is proposed to use a tail gas cleanup unit for ultimate sulfur recovery and to meet environmental constraints which would be impossible to attain using only the modified Claus process. The tail gas unit is described herein.

BEAVON TAIL GAS UNIT (Figure A-4)

The feed to the Beavon Unit will be the tail gas from the Claus sulfur recovery system.

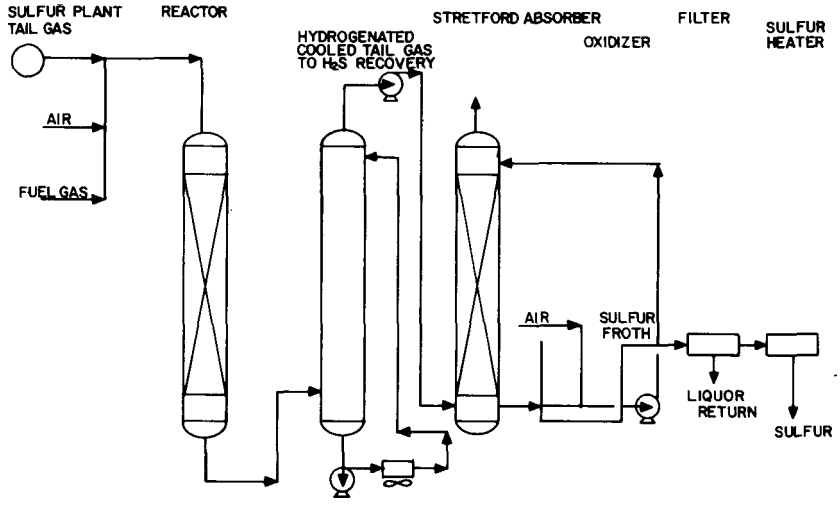

Figure A-4. Beavon Tail Gas Unit

In the first catalytic portion of the process all sulfur compounds in the Claus tail gas (SO_2, S_x, COS, CS_2) are converted to H_2S. The tail gas is heated to reaction temperature by mixing with hot combustion products of fuel gas and air. This combustion may be carried out with a deficiency of air if the tail gas does not contain sufficient H_2 and CO to reduce all of the SO_2 and S_x to H_2S. The heated gas mixture is then passed through a catalyst bed where all sulfur compounds are converted to H_2S by hydrogenation and hydrolysis. The hydrogenated gas stream is cooled by direct contact with a slightly alkaline buffer solution before entering the H_2S removal portion of the process.

The Stretford process is then used to remove H_2S from the hydrogenated tail gas. This process involves absorption of the H_2S in an oxidizing alkaline solution.

The oxidizing agents in the solution convert the H_2S to elemental sulfur, then are regenerated by air oxidation, which floats the sulfur off as a slurry. This sulfur slurry is then filtered, washed and melted to recover the Stretford solution and produce a high purity sulfur product.

The pressure drop for the treated gas is 2 to 3 psi; all pressures are near atmospheric. Operating temperatures are 550-750^{o}F for the hydrogenation reactor and 70-120^{o}F for the Stretford section. The treated gas stream contains <100 ppm of total sulfur compounds and <10 ppm of H_2S. Spent oxidizer air is odorless, since it contains only air and water vapor and does not require incineration.

CLEANUP SYSTEM DESIGN UPDATE

A continuation of study was performed to enhance the level of detail in the previously defined cleanup system (A-1) and to integrate the new gas purification system into the reference fuel cell plant design.

Process units which are involved in the raw gas handling and gas purification system are shown in the process diagram, Figure A-5. The gasification-raw gas handling system consists of a Texaco entrained bed gasifier, cyclone separators, two heat recovery steam generators, two heat exchangers and a particulate scrubber for complete solids removal. The gas purification system consists of a COS conversion unit, gas cooling section, ammonia absorber, the Selexol solvent system and a zinc oxide polisher. The sulfur recovery plant uses the Claus process with a Beavon tail gas cleanup. For purposes of this study, it has been assumed that the gasification-raw gas handling system operates in five parallel trains and the gas purification system in three. These numbers are based on the Fluor report but could change as studies continue.

The major modification made to the reference cleanup system is the addition of the COS conversion unit. This unit converts COS to H_2S by reacting it with steam in the presence of a catalyst. Because the Selexol system is more selective to H_2S than COS, it is expected that this modification will reduce the cost of the Selexol as well as reduce the absorption rates of the other gas constituents due to the lowered solvent recirculation rates.

For this study, no extensive analysis has been made of the sulfur recovery plant, since it does not directly affect the gas composition entering the fuel cell.

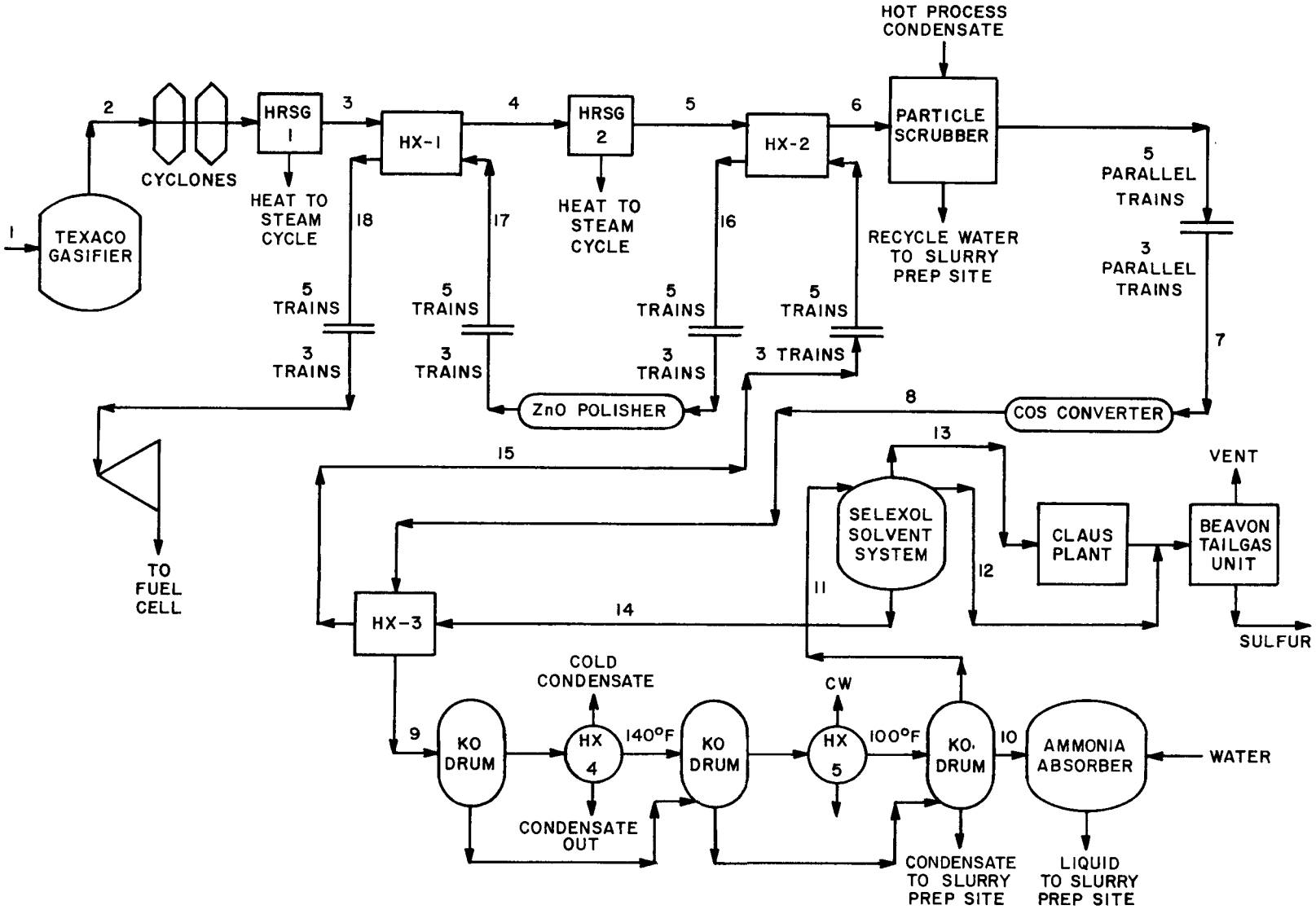

Figure A-5. Process Flow Diagram

Included in this study is an arrangement of the heat exchangers for what was previously called the regenerative heat exchanger train. The gas cooling section of the plant is similar to that described in the Fluor report. Also, heat balances indicate the need for a second heat recovery steam generator within the cleanup system. A reasonable location for this unit was chosen; however, its placement within the cleanup system is optional.

SYSTEM DESCRIPTION

Table A-1 gives stream compositions, temperatures and pressures, along with the total flow rates (from all trains) and the total energy flow in Btu's/hour and as a fraction of the coal higher heating value. This table is for the original reference case (A-1) of 371417 # coal/hr. Table A-2 gives similar information for the updated reference case (A-2) with a coal flow of 367810 # coal/hr.

Gasifier effluent enters cyclone separators where slag and large particles are removed from the gas stream. Raw fuel gas then passes through the first heat recovery steam generator where it exits at a temperature of 1200^{o}F. Raw gas is then cooled to a temperature of 940^{o}F in HX1 before entering the second steam generator where it exits at a temperature of 764^{o}F. Raw gas is further cooled in HX-2 to a temperature of $\simeq$350^{o}F before entering the particulate scrubber, where all particles are stripped from the gas, using water. Process water exiting the unit will be sent to the slurry preparation section of the plant. Fuel gas will exit the particle scrubber at its dew point temperature and pressure of 350^{o}F and 550 psia. The five particulate scrubbers' effluent streams discharge into a header where the flow per train is increased by reducing the number of trains to three. Solids-free fuel gas then enters the COS unit which is operated at a temperature of approximately 350^{o}F. Based on information received concerning the COS conversion catalyst operating at our stream conditions and composition, all COS contained in the gas stream, except 4 ppm, will be converted to H_2S in this unit. The heat effects are negligible, due to the very low concentration of COS. In addition, the water/gas shift reaction is considered not to occur, since the operating temperature of the COS unit does not favor this reaction. Fuel gas exits the COS unit and proceeds to the gas cooling section where it is cooled in a series of heat exchangers HX3, HX4 and HX5 to a temperature of 100^{o}F prior to entering the ammonia absorber. In this unit all ammonia contained in the gas stream is absorbed in water. The ammonia-rich liquid which exits the absorber is recycled back to the slurry preparation section of the plant. The ammonia-free gas enters the Selexol system where the total sulfur content of the gas is brought down to less than 1 ppm, which is

Table A-1

MCFC COAL-FIRED POWER PLANT REFERENCE CASE PROCESS FLOW DATA

STREAM NUMBER	1	2	3	4	5	6	7	8	9	10	11	12 & 13	14	15	16	17	18
STREAM ID	Coal Feed	Gasifier Effluent	Raw Gas HRSG 1 Outlet	Raw Gas Hx 1 Outlet	Raw Gas HRGS 2 Outlet	Raw Gas Hx 2 Outlet	Particle Scrubber Exit	COS Unit Outlet	Fuel Gas To Gas Cooling	Ammonia Absorber Inlet	Ammonia Absorber Outlet	Acid Gas and Vent Gas	Selexol Product Gas	Hx-2 Inlet Clean Gas	ZnO Polisher Inlet	ZnO Polisher Outlet	Turbine Inlet
Temperature (^{O}F)		2430	1200	940	764	352	350	350	320	100	100	100	100	148	750	750	1150
Pressure (PSIA)		615	597	585	568	557	550	540	529	496	490	-	485	475	466	456	447
Gas Composition (Mole Tract)																	
H_2		.2884	→	→	→	→	.2638	.2638	→	.3523	.0511	.3865	→	→	.3865	→	
N_2		.0066	→	→	→	→	.0060	.0060	→	.0048	.0018	.0051	→	→	.0051	→	
H_2O		.1788	→	→	→	→	.2489	.2484	→	.0020	.0192	.00003	→	→	.00003	→	
CO		.4245	→	→	→	→	.3883	.3883	→	.5185	.1635	.5589	→	→	.5589	→	
CO_2		.0871	→	→	→	→	.0797	.0802	→	.1071	.6368	.0468	→	→	.0468	→	
CH_4		.0008	→	→	→	→	.0007	.0007	→	.0010	.0008	.0010	→	→	.0010	→	
H_2S		.0100	→	→	→	→	.0091	.0097	→	.0129	.1266	-	→	→	-	→	
COS		.0006	→	→	→	→	.0005	4 ppm	→	4 ppm	.0001	.6 ppm	→	→	-	→	
NH_3		.0020	→	→	→	→	.0018	.0018	→	-	-	-	→	→	-	→	
Ar		.0012	→	→	→	→	.0011	.0011	→	.0015	.0002	.0016	→	→	.0016	→	
Number of Trains	5	5	5	5	5	5	3	3	3	3	3	3	3	5	3	3	3
Total Flow (lb Moles/hr)		40145.0	→	→	→	→	43893	43893	→	32867.4	3359.1	29508.9	→	→	→	→	
Total Flow (10^3 lbs/hr)	371.417	809.68	→	→	→	→	877.15	877.15	→	675.82	123.83	551.99	→	→	→	→	
Total Energy Flow (MBtu/hr)	4544.2	4511.26	4062.43	4002.86	3917.10	3785.41	3861.32	3680.89	3850.85	3777.27	3573.64	104.52	3436.35	3446.45	3575.51	3575.51	3665.52
Energy Flow As A Fraction Of Coal HHV	1.000	.993	.894	.881	.862	.833	.850	.850	.847	.831	.786	.023	.756	.758	.787	.787	.807

Blank Page

Table A-2

MCFC COAL-FIRED POWER PLANT UPDATED REFERENCE PROCESS FLOW DATA

STREAM NUMBER	1	2	3	4	5	6	7	8	9	10	11	12 & 13	14	15	16	17	18
STREAM ID	Coal Feed	Gasifier Effluent	Raw Gas HRSG 1 Outlet	Raw Gas Hx 1 Outlet	Raw Gas HRGS 2 Outlet	Raw Gas Hx 2 Outlet	Particle Scrubber Exit	COS Unit Outlet	Fuel Gas To Gas Cooling	Ammonia Absorber Inlet	Ammonia Absorber Outlet	Acid Gas and Vent Gas	Selexol Product Gas	Hx-2 Inlet Clean Gas	ZnO Polisher Inlet	ZnO Polisher Outlet	Turbine Inlet
Temperature (^{o}F)		2430	1200	940	764	352	350	350	329	100	100	100	100	148	750	750	1150
Pressure (PSIA)		615	597	585	568	557	550	540	529	496	490	-	485	475	466	456	447
Gas Composition (Mole Tract)																	
H_2		.2884	→	→	→	→	.2638	.2638	→	.3523	.0511	.3865	→	→	.3865	→	
N_2		.0066	→	→	→	→	.0060	.0060	→	.0048	.0018	.0051	→	→	.0051	→	
H_2O		.1788	→	→	→	→	.2489	.2484	→	.0020	.0192	.00003	→	→	.00003	→	
CO		.4245	→	→	→	→	.3883	.3883	→	.5185	.1635	.5589	→	→	.5589	→	
CO_2		.0871	→	→	→	→	.0797	.0802	→	.1071	.6368	.0468	→	→	.0468	→	
CH_4		.0008	→	→	→	→	.0007	.0007	→	.0010	.0008	.0010	→	→	.0010	→	
H_2S		.0100	→	→	→	→	.0091	.0097	→	.0129	.1266	-	→	→	-	→	
COS		.0006	→	→	→	→	.0005	4 ppm	→	4 ppm	.0001	.6 ppm	→	→	-	→	
NH_3		.002	→	→	→	→	.0018	.0018	→	-	-	-	→	→	-	→	
Ar		.0012	→	→	→	→	.0011	.0011	→	.0015	.0002	.0016	→	→	.0016	→	
Number of Trains	5	5	5	5	5	5	3	3	3	3	3	3	3	5	3	3	3
Total Flow (lb Moles/hr)		39755.0	→	→	→	→	43466.74	43466.74	→	32548.21	3326.48	29222.3	→	→	→	→	
Total Flow (10^3 lbs/hr)	367.81	801.82	→	→	→	→	868.63	868.63	→	669.26	122.63	546.63	→	→	→	→	
Total Energy Flow (MBtu/hr)	4500.15	4467.45	4022.98	3963.99	3879.06	3748.65	3823.82	2823.40	3813.45	3740.59	3538.93	103.50	3402.98	3412.98	3540.79	3540.79	3629.92
Energy Flow As A Fraction Of Coal HHV	1.000	.993	.894	.881	.862	.833	.850	.850	.847	.831	.786	.023	.756	.758	.787	.787	.807

Blank Page

required by the fuel cell. Heat balances also indicate that there is a heat loss of approximately 27 MBtu/hr in the Selexol for the original reference case and a ≈32 MBtu/hr loss for the updated case. These heat losses are assumed to be the result of piping and equipment losses within the Selexol system.

Detailed information on the Selexol process was not available due to the proprietary nature of the process; therefore the gas composition leaving the Selexol system was calculated by estimating the distribution coefficient for each component within the absorber. This estimation was based on the relative absorption ratios of each component as given in the Fluor report.

$$Ki = \frac{Yi}{Xi}$$

where Ki = the distribution coefficient

Yi = mole fraction of species i contained in the vapor

Xi = mole fraction of species i contained in the liquid
(moles of species i absorbed)

Based on this, iterative calculations were made until the total sulfur content of the fuel gas was less than 1 ppm.

The product gas leaving the Selexol is heated in heat exchangers HX3 and HX2 to a temperature of 750^{o}F before entering the zinc oxide trim unit. At this temperature, a maximum sulfur retention capacity can be expected. This unit will act primarily as a guard and remove any sulfur that is still contained in the gas stream. The stream leaving the ZnO unit will be heated in HX1 to a temperature of 1150^{o}F before entering the high pressure turbine.

The calculated heat to stream for case (1) is approximately 535 MBtu/hr and for case (2) is ≈519 MBtu/hr. The effect on net plant efficiency is negligible.

The acid gas from the Selexol then proceeds to the Claus plant. The acid gas feed and process air are preheated to reaction temperature by heat exchange with the exit gas from the Claus combustion chamber. Also, combustible gases contained in the Selexol acid gas stream supply a portion of the heat needed in this process.

In the Claus plant approximately 95% of the sulfur-containing compounds in the acid gas will be converted to elemental sulfur. Tail gas from the Claus will enter the Beavon tail gas cleanup. In the Beavon, a sufficient amount of the remaining sulfur compounds will be converted to elemental sulfur to produce a vent to the atmosphere that contains <100 ppm of total sulfur, which is within environmental regulations.

DISCUSSION OF RESULTS

A water/gas shift converter is under consideration as a possible solution to the carbon formation problem occurring at the fuel cell inlet.

This unit would convert CO to CO_2 and H_2 by reacting it with steam in the presence of a catalyst by the reaction

$$CO + H_2O \rightleftharpoons CO_2 + H_2$$

In the shift converter the reaction will proceed until equilibrium is reached; if further conversion is desired the gas must be cooled and allowed to pass through a second shift reactor. Therefore, the amount of CO which is converted is a function of the number of catalyst beds in the system.

This concept appears beneficial in reducing the carbon formation problem because it will increase the concentration of H_2 to the fuel cell and reduce the concentration of CO, which if present in high-enough concentration could promote the Boudart Carbon reaction ($2\ CO \rightarrow C + CO_2$). The optimum amount of CO that is converted will have to be determined.

Another consideration with this scheme is the possibility of recovering a clean stream of CO_2. It has been proposed that this stream be recycled to the anode inlet in an attempt to prevent carbon formation.

With the use of the C-H-O ternary diagram (Figure A-6), scoping studies indicate that CO_2 recirculation would not prevent carbon formation, rather it would bring the gas closer to the carbon-forming range by increasing the concentration of carbon atoms.

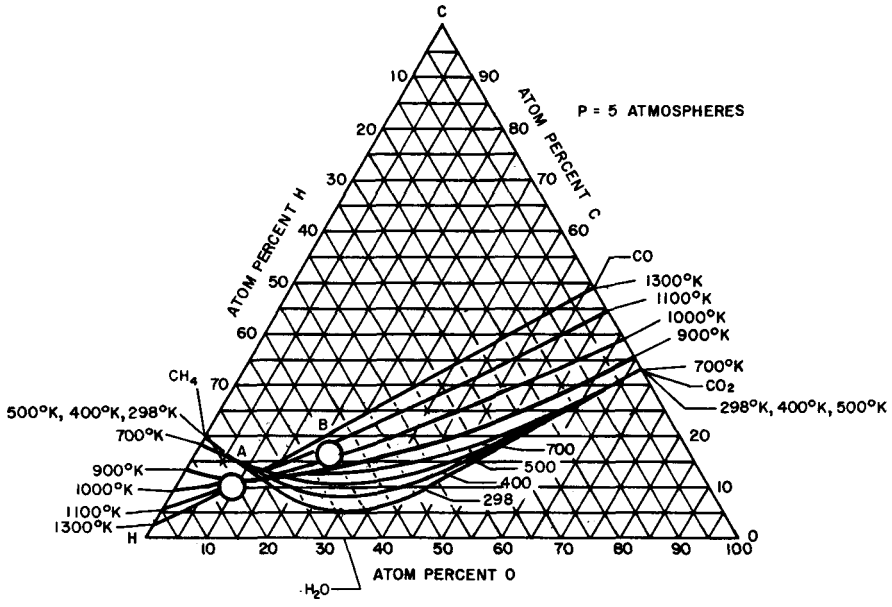

Figure A-6. Carbon deposition boundaries for the C-H-O system at a total pressure of 5 atm (1).

Point A on the diagram represents shifted fuel gas, neglecting CO_2. Point B represents the same gas, but leaving in CO_2. At the fuel cell operating temperature of $\simeq 1100^{o}F$ ($\simeq 900^{o}K$) it can be seen that Point B lies in the carbon-forming range, while Point A lies slightly below.

Based on this analysis it appears as though the removal of CO_2 from the shifted gas stream, and not recirculation, would be most beneficial in preventing carbon formation.

REFERENCES

A-1 Molten Carbonate Fuel Cell Power System Evaluation - Gas Cleanup System and Sulfur Plant, J. C. Dart and Associates. May 9, 1979.

A-2 Economic Studies of Coal Gasification Combined Cycle Systems for Electric Power Generation, EPRI AF642, Fluor Engineers. January 1978.

Appendix B

COAL-FIRED POWER PLANT COSTING
(ECAS and EPRI Methods)

PROCEDURES AND ASSUMPTIONS

- The cost data used was obtained from the different references listed on Page 2-2.
- Both the acid gas removal and the sulfur recovery systems are treated as one code of account.
- Fuel cell modules and combustion turbines are treated as one code of account.
- The electrical subsystem excluding inverter systems has been treated as one code of account.
- The plant section previously entitled steam, condensate and BFW, has been renamed as the steam bottoming cycle code of account.
- The plant section entitled general facilities has been redefined as the land, improvements, structures, and miscellaneous equipment code of account.
- A 3 yr construction period is assumed with no escalation or interest during this period.
- A&E Fees are assumed to be 12 1/2% on materials and 10% on labor.
- Sales tax is assumed to be 5% on materials.
- A 70% operating capacity factor is assumed for the coal-fired plant, 50% is used for the oil-fired plant.
- Contingencies for the coal-fired plant are assumed as follows:

  - Process Contingencies

Gasification and Ash Handling	12.5%
Gas Cooling	15.0%
Acid Gas Removal and Sulfur Recovery	0.1%
Fuel Cell Modules and Gas Turbine	50.0%
Inverter System	10.0%

  - Project Contingency

    10% of each plant section

ECAS Method Assumptions

- A&E Services and Contingency assumed as the fixed percentage of total subsystem costs (24.5%).
- Escalation and interest during the five-year construction is assumed to be 48.7%.
- A 65% operating capacity factor is assumed.

Cost Evaluation-ECAS Method

Table B-1 presents a plant capital cost estimate summary which gives the installed cost for each plant system including A&E services, contingencies, escalation and interest during construction for the coal-fired central station power plant (675 MW). On a mid 1978 basis the plant has a total installed cost of $1043/kW. Tables B-2, B-3, B-4, B-5 and B-6 each give a component cost breakdown for each system as summarized in Table B-1. These costs include purchased cost of the component, balance of plant materials, and site labor. Table B-7 gives operating and maintenance costs in mills/kWh; costs include both labor and materials. The total operating and maintenance costs for our reference coal-fired power plant is 3.86 mills/kWh. Table B-8 is an economic summary including plant capital cost and cost of electricity. Cost of electricity for our 675 MW power plant in mid 1978 dollars is 46.3 mills/kWh @ 65% operating capacity, assuming a coal cost of $1.43/MBtu.

Table B-1

PLANT CAPITAL COST ESTIMATE SUMMARY (ECAS METHOD)
(675 MW Plant)

System	Cost in $10^3$$ (Mid 1978)
Land, Improvements, Structures and Miscellaneous Equipment	39,430
Fuel Handling and Processing	149,650
Fuel Cell System	84,981
Steam Bottoming Cycle	65,148
Electrical Plant Equipment	40,946
Total	380,155
A&E Services & Contingency (24.5%)	93,138
Escalation & Interest During Construction @ 48.7%	230,494
Total Installed Cost	703,787
$/kW Installed on a Mid 1978 Basis	1,043

COSTS ON THIS PAGE ARE IN YEAR MID 1978 DOLLARS

Table B-2

LAND, IMPROVEMENTS, STRUCTURES & MISCELLANEOUS EQUIPMENT
(ECAS Method)

Component	Component or Subsystem Costs ($10^3$$)	Balance of Plant Materials ($10^3$$)	Site Labor (Direct & (Indirect) ($10^3$$)	Total Installed Cost ($10^3$$)
Land and Land Rights	400	N/A	N/A	400
Improvements	N/A	580	695	1,275
Structures	935	9,230	11,365	21,530
Miscellaneous Plant Equipment				
Inter Island Piping	N/A	7,680	5,120	12,800
Balance	560	2,030	835	3,425
TOTAL	1,895	19,520	18,015	39,430

Table B-3

FUEL HANDLING AND PROCESSING
(ECAS Method)

Subsystem	Total Installed Cost ($10^3$$)
Coal Handling	11,150
Oxidant Feed	59,350
Gasification and Ash Handling	12,250
Gas Cooling	33,900
Acid Gas Removal and Sulfur Recovery	33,000
TOTAL	149,650

COSTS ON THIS PAGE ARE IN YEAR MID 1978 DOLLARS

Table B-4

FUEL CELL SYSTEM
(ECAS Method)

Component	Component or Subsystem Costs ($10^3$$)	Balance of Plant Materials ($10^3$$)	Site Labor (Direct & Indirect) ($10^3$$)	Total Installed Cost ($10^3$$)
Fuel Cell Stacks with Insulation	43,932	N/A	2,134	46,066
Fuel Cell Vessels	2,510	N/A	N/A	2,510
Burners and Aux.	740	N/A	113	853
Piping, Valves, Controls & Instruments	N/A	12,929	6,276	19,205
Fuel Cell Turbo-compressor	14,260	1,878	209	16,347
TOTAL	61,442	14,807	8,732	84,981

Table B-5

STEAM BOTTOMING CYCLE
(ECAS Method)

Component	Component or Subsystem Costs ($10^3$$)	Balance of Plant Materials ($10^3$$)	Site Labor (Direct & Indirect) ($10^3$$)	Total Installed Cost ($10^3$$)
Steam Turbine Generator	15,378	N/A	2,185	17,563
Heat Recovery Steam Generator	10,722	N/A	11,539	22,261
Condensers and Associated Equip.	1,225	N/A	470	1,695
Boiler Feed and Condensate System	N/A	2,573	327	2,900
Piping, Valves, Insulation	N/A	4,146	2,900	7,046
Cooling Tower System	7,250	1,634	4,799	13,683
TOTAL	34,575	8,353	22,220	65,148

COSTS ON THIS PAGE ARE IN YEAR MID 1978 DOLLARS

Table B-6

ELECTRICAL PLANT EQUIPMENT
(ECAS Method)

Component	Component or Subsystem Costs ($10^3$$)	Balance or Plant Materials ($10^3$$)	Site Labor (Direct & Indirect) ($10^3$$)	Total Installed Cost ($10^3$$)
Inverter	20,585	N/A	4,381	24,966
Main & Aux. Transformers	2,545	N/A	205	2,750
Motor Control Centers & Control Board	N/A	400	60	500
Isolated Phase Bus	N/A	320	130	450
Diesel Generator	N/A	190	40	230
Cables, Conduits & Trays	N/A	3,070	3,330	6,400
Steam Plant Accessory Electrical Equip.	N/A	380	1,420	1,800
Total Plant Controls & Instrumentation	N/A	1,540	1,160	2,700
Switchgear	N/A	750	400	1,150
TOTAL	23,130	6,690	11,126	40,946

Table B-7

OPERATING AND MAINTENANCE COSTS (mills/kWh)
(ECAS Method)

Item	Materials	Labor	Total
Coal Gasification & Desulfurization	0.35	0.64	0.99
Coal and Ash Handling	0.1	0.11	0.21
Fuel Cell Stacks	1.45	0.11	1.56
Catalytic Burner	0.11	--	.11
Turbocompressors	0.27	0.01	0.28
Balance of Plant	0.17	0.12	0.29
Steam Plant	0.08	0.24	0.32
TOTAL O&M (mills/kWh)	2.53	1.23	3.76

COSTS ON THIS PAGE ARE IN YEAR MID 1978 DOLLARS

Table B-8

COAL-FIRED MOLTEN CARBONATE FUEL CELL POWER PLANT
ECONOMIC SUMMARY
(ECAS Method)

Plant Capital Cost	$ 704.21	Million
Plant Capital	1,043.00	$/kW
Cost of Electricity (with capacity factor - 0.65)		
Capital	32.9	mills/kWh
Fuel*	9.6	mills/kWh
Operating and Maintenance	3.8	mills/kWh
TOTAL COE** (Mid 1978)	46.30	mills/kWh

*Coal Cost is assumed at $1.43/MBtu
**Cost of Electricity

COSTS ON THIS PAGE ARE IN YEAR MID 1978 DOLLARS

Cost Evaluation - EPRI Method

Table B-9 presents a cost breakdown structure derived from published data for each section of the plant, including material, labor, A&E fees, sales tax, and contingencies. (A&E fees, tax, and contingencies were calculated using assumptions outlined earlier.) The total plant investment for the 675 MW power plant is $803/kW and is summarized in Table B-10. Table B-11 gives a breakdown of capital charges, incremental costs for the replacement of the fuel cells and the equivalent total capital requirement (ETCR). The Total Capital Requirement (TCR) including capital charges is $935/kW. The increment for interim fuel cell replacement is $205/kW, and thus the Equivalent Total Capital Requirements (ETCR) is $1140/kW. Table B-12 gives operating cost breakdowns, coal cost, levelized fixed charges and cost of electricity on a first-year and 30-year levelized basis, at a 70% capacity factor. Cost of electricity, based on first-year costs, 46.7 mills/kWh, and on a 30-year levelized cost basis it is 58.4 mills/kWh.

Table B-9

COST BREAKDOWN
(EPRI Method)

Plant Section	Material ($10^3$$)	Labor ($10^3$$)	A&E Fee ($10^3$$)	Sales Tax ($10^3$$)	Total Cost ($10^3$$)	Total Cost ($/kW)	Percent	Contingencies Process ($10^3$$)	Contingencies Project ($10^3$$)	Total Plant Investment ($10^3$$)	Total Plant Investment ($/kW)
Coal Handling	6,250	4,900	1,271	312	12,733	18.86	3	-	1,273	14,006	20.75
Oxidant Feed	35,000*	24,350*	6,810	1,750	67,910	100.61	15	-	6,791	74,701	110.67
Gasification & Ash Handling	7,000*	5,250*	1,400	350	14,000	20.74	3	1,750	1,400	17,150	25.41
Gas Cooling	25,000*	8,900*	4,015	1,250	39,165	58.02	9	5,875	3,917	48,957	72.53
Acid Gas Removal (Selexol, Claus & Tail Gas)	25,000	8,000	3,925	1,250	38,175	56.56	9	38	3,818	42,031	62.27
Steam Bottoming Cycle	42,928	22,220	7,588	2,146	74,882	110.94	17	-	7,488	82,370	122.03
Fuel Cell Modules & Combustion Turbines	76,249	8,732	10,404	3,812	99,197	146.96	23	49,599	9,920	158,716	235.13
Inverter System	20,585	4,381	3,011	1,029	29,006	42.97	7	2,901	2,901	34,808	51.57
Electrical System	9,235	6,745	1,829	462	18,271	27.07	4	-	1,827	20,098	29.77
Land Improvements Structures & Miscellaneous Equipment	21,415	18,015	4,478	1,071	44,979	66.64	10	-	4,498	49,477	73.30
TOTAL	268,662	111,493	44,731	13,432	438,318	649.37	100	60,163	43,833	542,314	803.43

* Total cost of material & labor taken from AF642 Report
(the split of the total cost is assumed)

ALL COSTS ON THIS PAGE ARE IN YEAR MID 1978 DOLLARS
(Plant Output = 675 MW)

Table B-10

TOTAL PLANT INVESTMENT SUMMARY
(EPRI Basis)

	$10^3$$	$/kW
Process Plant Investment and Land, Improvements, Structures & Miscellaneous Equipment	483,318	649
Process Contingency	60,163	89
Project Contingency	43,833	65
TOTAL PLANT INVESTMENT	542,314	803

Table B-11

PLANT CAPITAL REQUIREMENT SUMMARY
(EPRI Basis)

	$10^3$$	$/kW
Capital Charges		
Prepaid Royalties	2,711	4
Preproduction Costs	13,170	19.5
Inventory Capital	4,758	7
Initial Catalyst & Chemicals Charge	292	0.43
Allowance for Funds During Construction	67,735	100
Total Capital Charges	88,666	131*
Total Plant Investment	542,314	803
Total Capital Requirement (TCR)	630,980	934*
Increment for Interim Replacement of Fuel Cells	138,251	204
Equivalent Total Capital Requirement (ETCR)	769,231	1138*

* Costs are in whole $/kW.

ALL COSTS ON THIS PAGE ARE IN YEAR MID 1978 DOLLARS

Table B-12

BUSBAR POWER COST
(70% Capacity Factor)
(EPRI Basis)

Net Production		
Net Power, MW		675
Byproduct Ammonia, ST/D		-
Byproduct Sulfur, ST/D		174
Equivalent Total Capital Requirement ($10^3$$)		
Total Capital Requirement (TCR)		630,980
Increment over TCR for Interim Fuel Cell Modules		138,251
	ECTR =	769,231
	First-Year Cost	30-Year Levelized Cost
Fixed Operating Cost ($10^3$$)		
Operating Labor	2,081	
Maintenance Labor	4,072	
Maintenance Materials	6,109	
Administrative & Support Labor	1,846	
Total Fixed O&M Costs	14,108	26,608
Variable Operating Cost (Excluding Coal) ($10^3$$)		
Catalysts & Chemicals	200	
Other Consumables (if any)	684	
Ash Disposal	124	
Variable Maintenance (if any)	-	
Total Variable O&M Costs	1,008	1,901
Coal Cost ($10^3$$ @ $1.43/MBtu)	39,848	75,153
Byproducts Credits ($10^3$$)	-	-
Total Operating Costs ($10^3$$)	54,964	103,662
Levelized Fixed Charges ($10^3$$)	138,462	138,462
kWh Produced in One Year		
$= 675 \times 10^3 \times 24 \times 0.7 \times 365$		
$= 4{,}139 \times 10^6$		
Total Cost of Electricity (mills/kWh)		
Fixed Charges	33.4	33.4
Operating Costs	13.3	25.0
Cost of Electricity (mills/kWh)	46.7	58.4

ALL COSTS ON THIS PAGE ARE IN YEAR MID 1978 DOLLARS

Capital Cost Evaluation Comparison

Table B-13 shows a comparison between three MCFC coal plant cost evaluations:

- EPRI RP-1085-1 Coal Plant (this study), using ECAS based accounting method.
- EPRI RP-1085-1 Coal Plant (this study), using EPRI suggested accounting method.
- UTC-ECAS Coal Plant (1976 DOE study), using ECAS based accounting method.

A review of the sources for this study (Table B-1) will show that a significant amount of the costing base for the RP 1085-1 cost evaluation is taken from the ECAS study. Thus a comparison of the capital cost evaluations becomes a comparison of cost accounting methods to a large extent. Such a comparison has value in that it will permit a judgment as to the impact of selecting a particular method for subsequent studies.

Comparison of the ECAS method evaluations in Table B-13 (UTC-ECAS study and this study) shows significant differences in the fuel handling and processing, fuel cell, and steam bottoming subsystems.

Table B-13

CAPITAL COST COMPARISON
(Mid-1978 $)

	RP-1085-1 ECAS Method		RP-1085-1 EPRI Method		UTC-ECAS**	
	$/kW*	%	$/kW*	%	$/kW*	%
Land, Improvements, Structures and Misc. Equipment	108	10.4	85	9.1	109	15.1
Fuel Handling & Processing	401	39.4	339	36.3	176	24.5
Fuel Cell System	233	22.3	273	29.3	209	29.0
Steam Bottoming Cycle	179	17.1	142	15.2	111	15.4
Electrical Plant Equipment	112	10.8	95	10.1	115	16.0
TOTAL	1042***	100.0	934***	100.0	720***	100.0

NOTES

* Per plant kW
** Escalated 3 years at 6.5% p.a.
*** Inclusive of all adders including contingencies

The difference in the fuel handling and processing system costs center around the acid gas removal and gasifier oxidant systems. The UTC-ECAS study assumes an iron oxide system operating at elevated temperatures, whereas this study uses the low temperature Selexol system.

The UTC-ECAS study did not incorporate an oxygen-blown gasifier. In this study, the requisite oxidant feed system accounts for $163/kW, using the ECAS method. However, improved plant efficiency produces a reduction in fuel costs.

The fuel cell subsystem cost is greater in this study than in the UTC-ECAS study because of a reevaluation of the turbocompressor costs. A review of the machinery costs against currently available published data indicated that an appropriate upward revision was required. The steam bottoming subsystem cost in this study is significantly larger than the ECAS method, again based on a review of newly available literature.

The more significant comparison to be made is between the two RP-1085-1 study evaluations using the ECAS and the EPRI accounting methods. These studies use the identical data bases for the evaluation, and thus the differences are exclusively in the various adders assumed. To aid in understanding this, a summary of the adders is shown below:

	Millions of $, 1978	
	ECAS Method	EPRI Method
A&E & Contingency	93.1	162.2
Construction Funds Allowance	230.5	67.7
	323.6	229.9

As can be seen, there is significant departure on the costs of escalation and interest during construction. Part of this difference stems from the underlying assumption of construction times; ECAS assumes five years, whereas the EPRI method assumes three years. Thus the ECAS adder is 48.7%, whereas the EPRI method adder is 12.5%.

When comparing the individual subsystem, proportional differences greater than that noted above can be found. Of particular note are the fuel handling and processing and the fuel cell subsystems. The ECAS method assumes a single contingency figure for the whole plant, which has been uniformly distributed among the subsystems in Table B-13. The EPRI method assigns differing contingencies to each subsystem. In the case of the fuel handling and processing subsystem, EPRI-method contingency is modest (10.1% for the acid gas removal); for the fuel cell subsystem it is quite large (50% for the fuel cell modules).

Cost of Electricity Comparison

Table B-14 compares the cost of electricity computed by the ECAS method with that computed by the EPRI method.

Table B-14

COST OF ELECTRICITY COMPARISON

	mills/kWh	
	ECAS	EPRI
Plant Construction Capital	32.9	27.4
Fuel	9.6	9.6
O&M	2.2	3.7
Fuel Cell Replacement	1.6	6.0
TOTAL	46.3	46.7

A 5% overall variance exists because of differing capacity factor assumptions; ECAS assumes 65% and EPRI assumes 70%. Above this, significant variance can be seen in the capital costs. In addition, a major difference exists in the O&M costs and the fuel cell replacement costs as assigned by the EPRI method.

Capital cost variance has been discussed earlier and was shown to be related most significantly to the assumption relating to the cost of capital during the construction period, and to a lesser extent, on the contingency allowance assumptions.

The most striking difference in the COE comparison is the cost attributed to an allowance for the replacement of the fuel cells.

The ECAS method simply assumes that the fuel cells have to be purchased again every six years, and that the cost is escalated by 6.5% per annum. In addition, the combined effect of the replacement purchases is reduced to present worth, using an annual factor of 6.5%. This sum of money is then distributed among the kWh produced per annum.

The EPRI method assumes a similar replacement scheme and a similar cost escalation. However, the treatment of raising the capital is more complex. It is assumed that every six years (replacement time) the fuel cells are replaced and the cost is treated as fresh capital investment, similar to a new plant.

It is apparent that this accounting difference may well be a major issue in consideration of the power plant economics. It is closely interrelated not only with the way in which the utilities raise money for periodic maintenance needs, but also with the method by which such replacement is accomplished. If the requirement to completely refurbish the plant periodically forces the utility into a full capital purchase situation, with all its high costs, then that maintenance concept may require reconsideration. For example, a continuing refurbishment by on-site labor may prove to be a more attractive alternative if the utility is more economically able to provide a steady stream of maintenance funds.

Appendix C

OIL-FIRED POWER PLANT COSTING
(ECAS and EPRI Methods)

Cost Evaluation - ECAS Method

Table C-1 is a capital cost summary which gives the installed cost for each plant system, including A&E services and contingencies. On a mid 1978 basis, the total installed cost for the reference case 4.5 MW oil-fired power plant is 511 $/kW. Tables C-2, C-3, C-4, C-5 and C-6 each give a component cost breakdown for each system summarized in Table C-1. Operating and maintenance costs are given in Table C-7, showing that the total O&M cost for the oil-fired power plant is 10.5 mills/kWh. Table C-8 is an economic summary including plant capital cost and cost of electricity. The cost of electricity for the 4.5 MW power plant is 67.0 mills/kWh for an assumed 50% capacity factor.

Cost Evaluation - EPRI Method

Table C-9 gives cost breakdowns for each section of the plant including material, labor, A&E and other fees, sales tax and contingencies. The total plant investment for the 4.5 MW oil-fired plant is 562 $/kW, as summarized in Table C-10. Table C-11 gives a breakdown of capital charges, incremental cost for the replacement of the fuel cells, and the Equivalent Total Capital Requirement (ETCR). The Total Capital Requirement (TCR) for this plant is 642 $/kW with a fuel cell replacement cost of 170 $/kW, thus the ETCR amounts to 811 $/kW. Table C-12 gives operating cost breakdowns, oil cost, levelized fixed charges and cost of electricity all on a first-year and 30-year levelized basis for an assumed capacity factor of 50%. Total operating costs are $909,400/year including $737,700/year for fuel. Thirty-year levelized costs are $1,715,100/year total operating cost, which includes $1,391,000/year for fuel.

The cost of electricity is 79.5 mills/kWh with a 30-year levelized cost of 120.4 mills/kWh for a 50% capacity factor as detailed in Table C-12.

Table C-1

PLANT CAPITAL COST ESTIMATE SUMMARY
(4.5 MW Plant)
(ECAS Method)

System	Cost in $10^3$$
Land, Improvements, Structures & Miscellaneous Equipment	177
Fuel Processor System	416
Fuel Cell System	598
Fuel Cell Turbocompressor	180
Electrical Plant	350
TOTAL	1721
A&E Services & Contingency	366
Total Installed Cost	2087
$/kW Installed on a Mid-1978 Basis	464

Table C-2

LAND, IMPROVEMENTS, STRUCTURES & MISCELLANEOUS EQUIPMENT
(ECAS Method)

Component	Component or Subsystem Costs ($10^3$$)	Balance of Plant Materials ($10^3$$)	Site Labor (Direct & (Indirect) ($10^3$$)	Total Installed Cost ($10^3$$)	$/kW
Land and Land Rights	29.0	NA	NA	29.0	6.4
Improvements	NA	3.9	4.6	8.5	1.9
Structures	2.0	21.3	26.7	50.0	11.1
Miscellaneous Plant Equipment					
Inter Island Piping	NA	32.0	34.2	66.2	14.7
Balance	3.8	13.9	5.7	23.4	5.2
TOTAL	34.8	71.1	71.2	177.1	39.4

COSTS ON THIS PAGE ARE IN YEAR MID 1978 DOLLARS

Table C-3

FUEL PROCESSOR SYSTEM
(ECAS Method)

Component	Component or Subsystem Costs ($10^3$$)	Balance of Plant Materials ($10^3$$)	Site Labor (Direct & (Indirect ($10^3$$)	Total Installed Cost ($10^3$$)	$/kW
Oil Reformer (ATR)	55.2	16.9	8.3	80.9	17.9
Heat Exchangers	77.3	N/A	11.6	88.9	19.8
Misc. Vessels	11.6	N/A	3.9	15.5	3.4
Instrumentation and Electrical	N/A	57.4	28.7	86.1	19.1
Piping and Misc.	N/A	58.7	26.3	85.0	18.9
Sulfur Sorbent	N/A	60.0	N/A	60.0	13.3
TOTAL	144.1	193	78.8	416.4	92.4

Table C-4

FUEL CELL SYSTEM
(ECAS Method)

Component	Component or Subsystem Costs ($10^3$$)	Balance of Plant Materials ($10^3$$)	Site Labor (Direct & (Indirect) ($10^3$$)	Total Installed Cost ($10^3$$)	$/kW
Fuel Cell Stacks, with Insulation	446	N/A	21	467	103.8
Fuel Cell Vessels	26	N/A	N/A	26	5.8
Burner and Auxiliary Startup Burners	8	N/A	1	9	2.0
Piping, Valves, Controls & Instrumentation	N/A	64	32	96	21.3
TOTAL	480	64	54	598	132.9

COSTS ON THIS PAGE ARE IN YEAR MID 1978 DOLLARS

Table C-5

FUEL CELL TURBOCOMPRESSOR SYSTEM
(ECAS Method)

Component	Component or Subsystem Costs ($10^3$$)	Balance of Plant Materials ($10^3$$)	Site Labor (Direct & Indirect) ($10^3$$)	Total Installed Cost ($10^3$$)	$/kW
Fuel Cell Turbocompressor	156	21	3	180	40.0
TOTAL	156	21	3	180	40.0

Table C-6

ELECTRICAL PLANT EQUIPMENT
(ECAS Method)

Component	Component or Subsystem Costs ($10^3$$)	Balance of Plant Materials ($10^3$$)	Site Labor (Direct& Indirect) ($10^3$$)	Total Installed Cost ($10^3$$)	$/kW
Inverter	211	N/A	45	256	56.9
Main & Auxiliary Transformers	17.1	N/A	1.4	18.5	4.1
Motor Control Centers & Control Board	N/A	3	.4	3.4	0.8
Isolated Phase Bus	N/A	2.1	.9	3.0	0.7
Cables, Conduits & Tray	N/A	20.7	22.5	43.2	9.6
Total Plant Controls & Instrumentation	N/A	10.3	7.8	18.1	4.0
Switchgear	N/A	5.1	2.7	7.8	1.7
TOTAL	228.1	41.2	80.7	350	77.8

COSTS ON THIS PAGE ARE IN YEAR MID 1978 DOLLARS

Table C-7

OPERATING AND MAINTENANCE COSTS
(ECAS Method)
50 Capacity Factor

Item	Materials mills/kWh	Labor mills/kWh	Total mills/kWh
Fuel Processor System	6.29	.47	6.76
Fuel Cell Stacks	2.86	0.16	3.02
Catalytic Burner	0.16	N/A	0.16
Turbocompressor	0.27	0.01	0.28
Balance of Plant	0.17	0.12	0.29
TOTAL O&M	9.75	0.76	10.51

Table C-8

OIL-FIRED MOLTEN CARBONATE FUEL CELL ECONOMIC SUMMARY
(ECAS Method)
4.5 MW Plant - 50% Capacity Factor

Plant Capital Cost	2.087 MM$
Plant Capital Cost	464 $/kWh
Cost of Electricity (with capacity factor = 0.50)	
Capital	19.05 mills/kWh
Fuel*	37.40 mills/kWh
Operating & Maintenance	10.51 mills/kWh
Cost of electricity in mid 1978	66.96

*Fuel Cost is Assumed at $4.74/MBtu in Year 1978 Dollars.

COSTS ON THIS PAGE ARE IN YEAR MID 1978 DOLLARS

Table C-9

OIL-FIRED PLANT COST BREAKDOWN
(EPRI Method)

Plant Section	Cost Breakdown Without Contingencies: Material ($10^3$$)	Labor ($10^3$$)	Fees ($10^3$$)	Sales Tax ($10^3$$)	Total Cost ($10^3$$)	Total Cost ($10^3$$)	Percent	Contingencies: Process ($10^3$$)	Project ($10^3$$)	Total Plant Investment: ($10^3$$)	$/kW
Fuel Processing System	260	79	40.4	13	392.4	87.2	20.93	44.8	58.9	496.1	110.2
Fuel Cell System	538	54	73	26.9	691.9	153.8	33	331.8	103.8	1125.9	250.4
Turbocompressor	177	3	22.4	8.9	211.3	47.0	11.3	-	31.7	243.0	54.0
Inverter System	211	45	30.9	10.6	297.5	66.1	15.91	-	44.6	342.1	76.0
Electrical System	58	36	10.9	2.9	107.8	24.0	5.76	-	16.2	124.0	27.6
Improvement, Structures & Miscellaneous Equipment	84.6	63.5	16.9	4.2	169.2	37.6	9.05	-	25.4	194.6	43.2
TOTALS	1329	281	194.5	66.5	1870.1	413.6	100.00	376.0	280.6	2526.7	561.4

COSTS ON THIS PAGE ARE IN YEAR MID 1978 DOLLARS
(Plant Output 4.5 MW)

Table C-10

PLANT INVESTMENT SUMMARY
(EPRI Method)

	$10^3$$	$/kW
Process Plant Investment and Land, Improvements, Structures & Miscellaneous Equipment	1870	414
Process Contingency	376	84
Project Contingency	281	62
TOTAL PLANT INVESTMENT	2527	562

Table C-11

PLANT CAPITAL REQUIREMENTS SUMMARY
(EPRI Method)

	$10^3$$	$/kW
Total Plant Investment	2527	562
Capital Charges		
Prepaid Royalties	9	2.0
Preproduction Costs	96	21.4
Inventory Capital	143	31.8
Initial Catalyst & Chemicals	83	18.4
Allowance to Funds During Construction	-	-
Land	29	6.4
Total Capital Charges	360	80.0
Total Capital Requirements (TCR)	2887	642
Increment for Interim Replacement of Fuel Cells	763	169
Equivalent Total Capital Requirement (ETCR)	3650	811

COSTS ON THIS PAGE ARE IN YEAR MID 1978 DOLLARS

Table C-12

BUSBAR POWER COST AT 50% CAPACITY FACTOR
Oil-Fired Power Plant
EPRI Method)

Net Production		
Net Power, MW-AC		4.5
Equivalent Total Capital Requirement (ETCR) ($10^3$$)		
Total Capital Requirement (TCR)	2887	
Increment Over TCR for Interim Fuel Cell Modules ETCR	763	
ETCR	3650	

Heat Rate = 7890 Btu/kWh	First Year Cost	30-Year Levelized Cost
Fixed Operation Cost ($10^3$$)/Year		
Operating Labor	2.6	4.9
Maintenance Labor	15.0	28.3
Maintenance & Materials	22.4	42.2
Administrative & Support Labor	5.3	10.0
Total Fixed O&M Costs	45.3	85.4
Variable Operating Cost ($10^3$$)/Year		
Catalyst and Chemicals	126.0	237.6
Waste Disposal	.4	.8
Total Variable O&M Costs	126.4	238.4
Cost of Oil ($10^3$$)/Year	737.7	1391.3
Byproducts Credits ($10^3$$)/Year	-	-
Total Operating Costs ($10^3$$)/Year	909.4	1715.1
Levelized Fixed Charges ($10^3$$)/Year		
Total Capital Requirement	519.7	519.7
Increment Over TCR for Interim Fuel Cell Modules	137.7	137.7
Total Levelized Fixed Charges	657.4	657.4
Total Cost of Electricity		
($10^3$$)/Year	1566.8	2372.5
mills/kWh	79.5	120.4

COSTS ON THIS PAGE ARE IN YEAR MID 1978 DOLLARS

Plant Capital Cost Comparison

Table C-13 shows a comparison between the two MCFC oil plant evaluations - the ECAS Method and the EPRI Method as described earlier. The comparison is shown (both capital cost and cost of electricity) in order to evaluate the impact of cost accounting method.

Table C-13

COST EVALUATION COMPARISON
TOTAL CAPITAL REQUIREMENT

	ECAS Method*		EPRI Method**	
	$/kW	%	$/kW	%
Land Improvements Structures, Misc.	47.7	10.3	43.2	6.7
Fuel Handling and Processing	112.1	24.2	110.2	17.2
Fuel Cell Subsystem	161.1	34.7	250.4	39.0
Turbocompressor	48.5	10.5	54.0	8.4
Electrical Subsystem	94.3	20.3	103.6	16.2
Capital Charges	-	-	80.0	12.5
TOTAL	464	100.0	641.4	100.0
Cost of Electricity At 50% Capacity Factor	ECAS	mills/kWh	EPRI	
Plant Construction Capital	19.05		26.36	
Fuel	37.43		37.43	
O&M	7.49		8.71***	
Fuel Cell Replacement	3.02		6.97	
TOTAL	66.99		79.7	

*Contingencies included
**Fuel cell replacement not included in total capital requirement (TCR)
***Due to high cost of sulfur sorbent

COSTS ON THIS PAGE ARE IN YEAR MID 1978 DOLLARS

Evaluation of the comparison shows the following findings:

- The differences in contingency factors for the fuel cell subsystem alone (particularly the 50% process contingency of the EPRI Method) add about 100 $/kW to the EPRI-Method Cost.

- Many capital charges are considered in the EPRI-Method but do not appear explicitly in the ECAS-Method; i.e., prepaid royalties, pre-production costs, inventory capital. These additional capital charges add about 40 $/kW to the EPRI-Method Cost. Note that interest during construction charges has not been added for either method.

- An additional 5% sales tax adds more than 20 $/kW to the EPRI-Method Cost.

- A&E fees, taxes and contingency average 21.75% for the ECAS-Method but averages 34.94% for the EPRI-Method.

- Apart from the obvious capital cost contribution difference in the Cost of Electricity, the same disparity in the cost for fuel cell replacement is noted in the oil-fired plant as in the coal-fired plant (discussed in Section 2).

Appendix D

DEVELOPMENT OF AN MCFC FINITE SLICE (NODAL) MODEL

INTRODUCTION

During 1979, a GE computer simulation of the molten carbonate fuel cell subsystem (utilizing a lumped parameter representation of the fuel cell) was extended by the development of a finite slice model of the cell in order to provide a more detailed representation of the characteristics of the fuel cell module. For example, the more detailed model permits examination of the impact of major flow path alternatives: co-flow, crossflow and counterflow. An additional objective for the development of the model was to retain the flexibility and economic use associated with the lumped parameter model. Specific assumptions are made for the process behavior characteristics at each slice in the following categories:

- Anode and Cathode Gas Conditions
- Electrochemistry
- Heat Transfer Considerations

Of particular interest are the heat/energy balance constraints for each slice, permitting assessment of the distribution of the following temperatures within the cell:

- Cell Temperature
- Anode Gas Temperature
- Cathode Gas Temperature

The model was used to perform parametric study of cell operating characteristics and overall MCFC system operating characteristics, which are discussed at the end of this section.

FUEL CELL SUBSYSTEM CONFIGURATION

The fuel cell subsystem is considered to consist of the following elements, as indicated in Figure D-1 (flow configuration selectable, however):

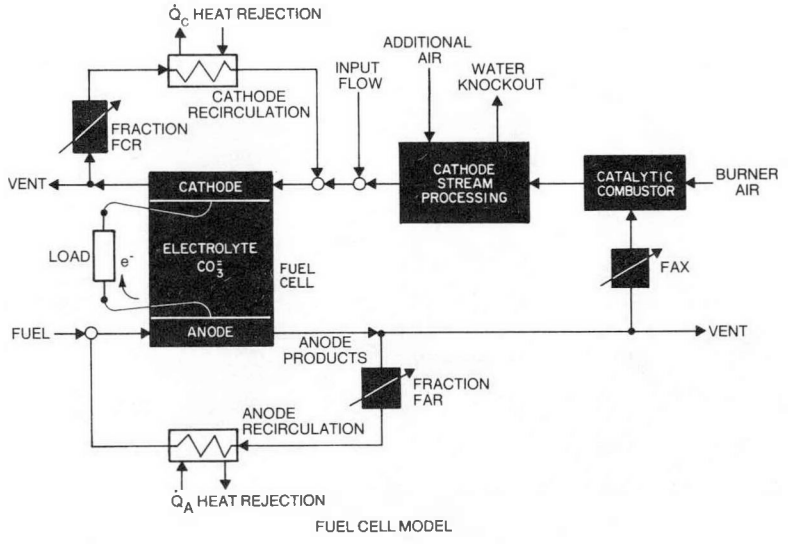

Figure D-1. Fuel Cell Subsystem

Note: Model/Simulation can apply to co-flow, counterflow, or cross flow configuration, as selected by input data.

- Fuel Cell: anode, cathode, electrolyte
- Adjustable anode recirculation, venting and heat rejecting provision
- Catalytic combustor for anode products
- Cathode stream processing, water knockout, additional air
- Adjustable cathode recirculation, venting and heat rejection provision

The fuel cell subsystem configuration thus considered may be used for simulation of either the oil-fired or the coal-fired plant by suitable selection of parametric values for the above elements, permitting the development of a single model to simulate the performance characteristics of the fuel cell subsystem.

The configuration of the fuel cell itself is selectable, by input data, to represent operation of a single (isolated) cell or a cell which is part of a stack (see Figure D-2). Thus, the fuel cell representation for the subsystem simulation includes characteristics such as anode and cathode gas flow areas, equivalent diameters, and common surface area for anode to cathode gas heat transfer through the separator plates (stack operation).

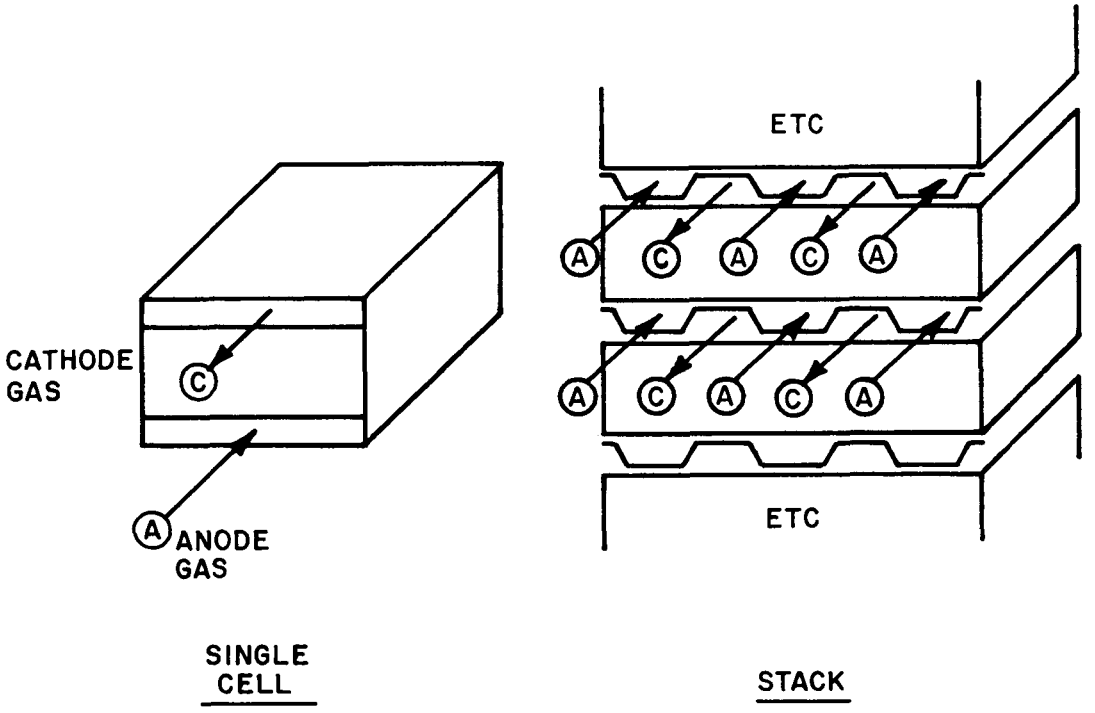

Note: Counterflow arrangement shown.

Figure D-2. Typical Fuel Cell Configuration, Single Cell or Part of Stack

ANALYSIS APPROACH

The analysis can be considered as comprised of two separate, but related procedures:

- MCFC Subsystem Calculations
- Fuel Cell (Component) Calculations

The analysis procedure for the MCFC subsystem is generally similar to the approach described earlier in EPRI EM-1097. The fuel composition, flow rate, anode/cathode recirculation fractions, cell area, fuel utilization, and several other parameters are defined (independent variables), as indicated in Table D-1. In addition to mass balance calculations, energy balance calculations are used to determine process stream conditions at a number of points in the subsystem, such as anode and cathode exit, and catalytic burner exit. The gas temperatures into the anode and cathode are defined parameters, and the associated heat rejection requirements are calculated.

Table D-1

MODEL/SIMULATION INPUT DATA REQUIRED

MNENOMIC	PARAMETER	UNITS
WIDCEL	Cell Width	cm
PATM	Pressure	atm
RESDVJ	Polarization Resistance	Ohm-cm^2
CFI	Fuel Component Species Mole Fractions	---
FITOT	Fuel Flow Rate	moles/h
TFUEL	Fuel Temperature	deg F
UTILIZ	Anode (Hydrogen) Utilization	---
IFUSYS	Flag, 1=System,0=Per Pass Utilization	---
TABIN	Anode Inlet Gas Temperature Required	deg F
FRACAR	Fraction, Anode Recirculation	---
FRACAB	Fraction, Products to Burner (not vented)	---
FBATOT	Burner Air Flow	moles/h
TBAIR	Burner Air Temperature	deg F
CCAUX	Cathode System Aux. Input Concentrations	---
FICAUX	Cathode Aux. Flow Rate (if used)	moles/h
TICAUX	Cathode Aux. Input Gas Temperature	deg F
FRACCR	Fraction, Cathode Recirculation	---
TCBIN	Cathode Inlet Gas Temperature Required	deg F
HXFAD	Anode Heat Transfer Coeff. (if constant)	Btuh/ft^2
HXFCD	Cathode Heat Transfer Coeff. (if constant)	Btuh/ft^2
IHXDAT	Flag, 1-Constant, 0=Calculate Heat Transfer Coeff.	---
YFPA	Height, Flow Path for Anode Gas	cm
YFPC	Height, Flow Path for Cathode Gas	cm
SIGA	Ratio, Flow Area Frontal Area, Anode	---
SIGC	Ratio, Flow Area Frontal Area, Cathode	---
RASAC	Ratio, Anode-Cathode HX Area/Cell Area	---
DIAEQA	Equivalent Flow Diameter, Anode	cm
DIAEQC	Equivalent Flow Diameter, Cathode	cm

The fuel cell calculation procedure determines the distribution of current within the cell and associated temperatures for an energy balance at each location (slice). Assuming a polarization voltage drop proportional to current density, a constraint is applied requiring that the cell terminal voltage be the same at each slice (uniform terminal voltage). Additional considerations and constraints are discussed under Process Assumptions.

The calculated anode and cathode gas exit temperatures are then used in the subsystem calculations. Because assumed temperatures are required earlier, the overall subsystem approach takes the form of an iterative calculation to achieve a heat/energy balance.

PROCESS ASSUMPTIONS

Specific assumptions are made for the process behavior characteristics at each slice in the following categories:

- Anode and Cathode Gas Conditions
- Electrochemistry
- Heat Transfer Considerations

It was decided to defer refinement of the representation of the polarization effect, which remains represented as a voltage drop proportional to current density. In this way, efforts were concentrated upon developing the simulation approaches and solution techniques required to satisfy the numerous constraints and boundary conditions for each slice. Figure D-3 shows the choice of slice representation for the cell, as a function of flow configuration.

Gas Conditions

For each cell element, or slice, the bulk gas conditions for the anode and cathode are considered to be the average of the inlet and exit concentrations (anode gas in shift equilibrium, homogeneous water-gas shift reaction). The anode equilibrium changes only as a function of temperature. Also, the pressure is assumed constant from slice to slice. The gas concentrations at the reaction site are assumed to be governed by bulk gas conditions. Other than equilibrium, gas composition changes are considered to be associated solely with electrochemistry (no other chemical reactions). Methane, if present, is considered as an inert gas, not entering into the reactions.

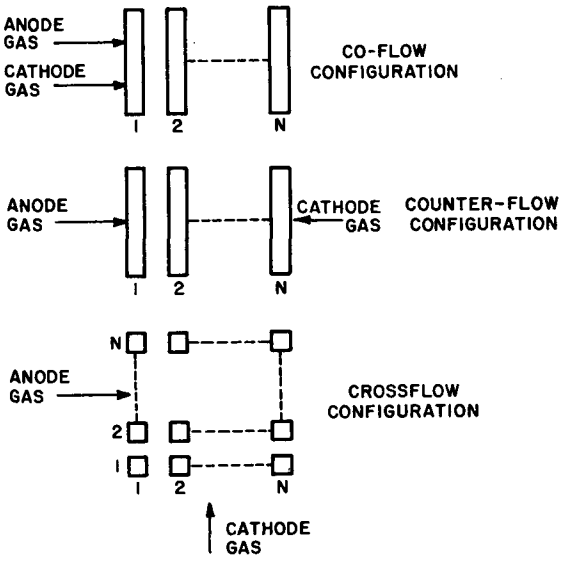

Figure D-3. Fuel Cell Representation, Finite Slice Model

Electrochemistry

The electrochemical reactions for a slice are assumed to be a function of the average bulk gas compositions (and partial pressures), based on averaging inlet and outlet conditions for the slice. The reversible cell potential, from the Nernst equation, is based on these values. The polarization voltage drop is subtracted from the reversible cell potential to obtain the terminal voltage. The electrolyte and electrodes for a given slice are considered to be at the same temperature (TCELL). The electrochemical reaction is assumed to occur within the electrolyte/electrode, at the temperature of the electrolyte/electrode.

Heat Transfer Considerations

Because the reaction location is assumed to be entirely within the electrolyte/electrode, all the heat of reaction not delivered as electrical power ($T\Delta S+I^2Rp$) is considered to be generated within the solid/liquid. Thus, it is assumed that no heat is released directly to (or within) the anode and cathode gas streams by the reaction itself. For each slice the temperature within the cell (solid/liquid) is assumed to be uniform.

Heat transfer to the anode and cathode gas from the solid/liquid is assumed to be governed by convective heat transfer relationships. No lateral (node to node)

heat transfer in the electrode or electrolyte is considered. The heat transfer considerations within a slice are shown in Figure D-4. Simple convective heat transfer relationships are assumed, $\frac{Q}{A} = H(T_{CELL}-T_{GAS})$. Initially, a constant value of 10 Btuh/sq ft/deg F was used for the heat transfer coefficient. More recently, under support of DOE Contract DE-AC01-80ET17019, refinements were included to permit use of calculated heat transfer coefficient values, as a function of flow geometry and gas tranport properties (viscosity, thermal conductivity, etc.). Adjacent cells in a stack are considered to be identical, permitting provision for anode to cathode gas heat transfer to be included, $\frac{Q}{A} = U\ (T_A-T_C)$. These variable heat transfer considerations are summarized in Figure D-5 and Table D-2.

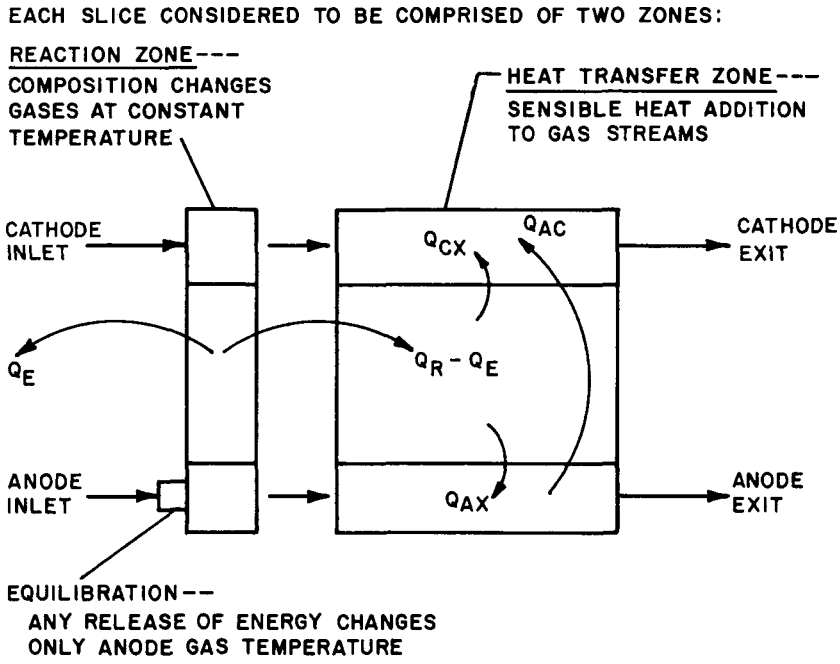

Q_E = ELECTRICAL POWER OUTPUT, TERMINAL VOLTAGE TIMES CURRENT

Q_R = HEAT OF REACTION IN ELECTROLYTE/ELECTRODE

Q_{AX} = CORRECTIVE HEAT TRANSFERRED FROM CELL TO ANODE GAS

Q_{CX} = CORRECTIVE HEAT TRANSFERRED FROM CELL TO CATHODE GAS

Q_{AC} = HEAT TRANSFERRED FROM ANODE TO CATHODE GAS (STACK CONFIGURATION)

Figure D-4. Heat Transfer Considerations Within a Slice

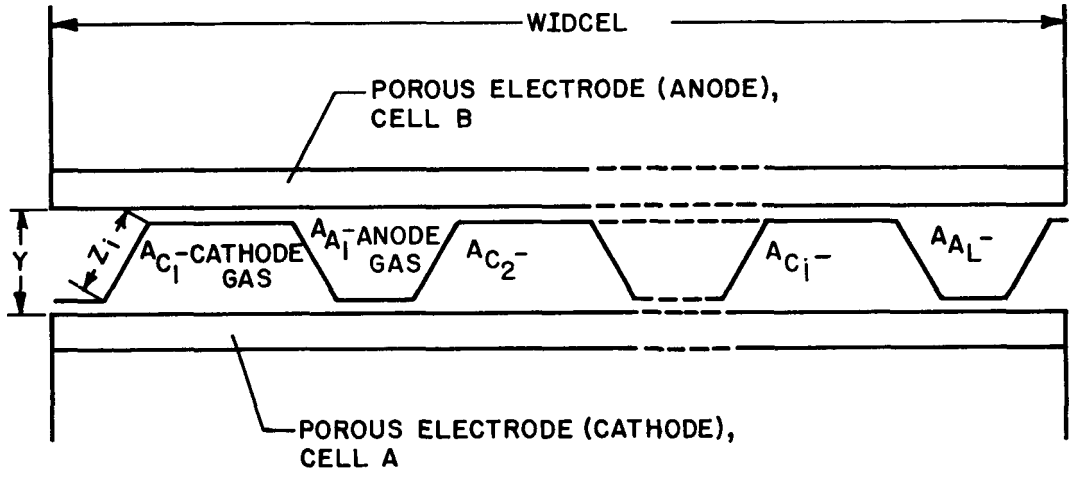

SPECIFIED DATA

Y = HEIGHT OF FLOW PATH

SIGA = RATIO OF ANODE FLOW AREA TO TOTAL AREA $= \dfrac{\Sigma A_{A_i}}{Y * WIDCEL}$

SIGC = SIMILARLY, FOR CATHODE AREA

RASAC = RATIO OF SURFACE AREA TO CELL AREA, FOR ANODE/CATHODE GAS HEAT TRANSFER $= \dfrac{\Sigma Z_i}{WIDCEL}$

DIAEQA = FOR ANODE, EQUIVALENT FLOW DIAMETER $= \dfrac{4 * AREA}{WETTED\ PERIMETER}$

DIAEQC = SIMILARLY FOR CATHODE

Figure D-5. Cell Geometry Parameters for Heat Transfer Coefficient Calculation

Table D-2

VARIABLE HEAT TRANSFER CALCULATION PROCEDURE

- For a given gas mixture (e.g., average anode gas composition), calculate gas properties:
  - Viscosity
  - Thermal Conductivity
  - Prandtl Number
  - Molecular Weight
  - Density
- Determine gas flow per unit area, G
- Calculate Reynolds Number

$$N_R = \frac{G * \text{Equivalent Diameter}}{\text{Viscosity}}$$

- Calculate effective flow distance parameter as a function of cell slice location, equivalent diameter, Reynolds Number and Prandtl Number.

$$\text{Dist} = \frac{X}{\text{DIAEQ} * N_R * N_P}$$

- Interpolate to find local Nusselt Number as a function of the effective flow distance (from Engineering Heat Transfer, W.H. Giedt, p. 152, Van Nostrand, 1957).
- Calculate local heat transfer coefficient based on Nusselt Number, Thermal Conductivity and Equivalent Diameter.

$$h = N_N * \text{COND/DIAEQ}$$

SIMULATION DESCRIPTION

The digital computer simulation of the MCFC subsystem, utilizing the finite slice fuel cell model, is organized on a modular basis. The solution procedure and the associated modules representing the process are indicated in Figure D-6 and Table D-3 respectively.

There is a good deal of similarity to the simulation approach for the earlier lumped parameter model, including the input data requirements:

- Specify overall utilization or cell utilization of (H_2 + CO).
- Specify recirculation amounts (may be zero).
- Specify air flow and fraction of anode products to catalytic burner and cathode (may be zero).
- Specify auxiliary flow input to cathode system (additional air, water knockout).

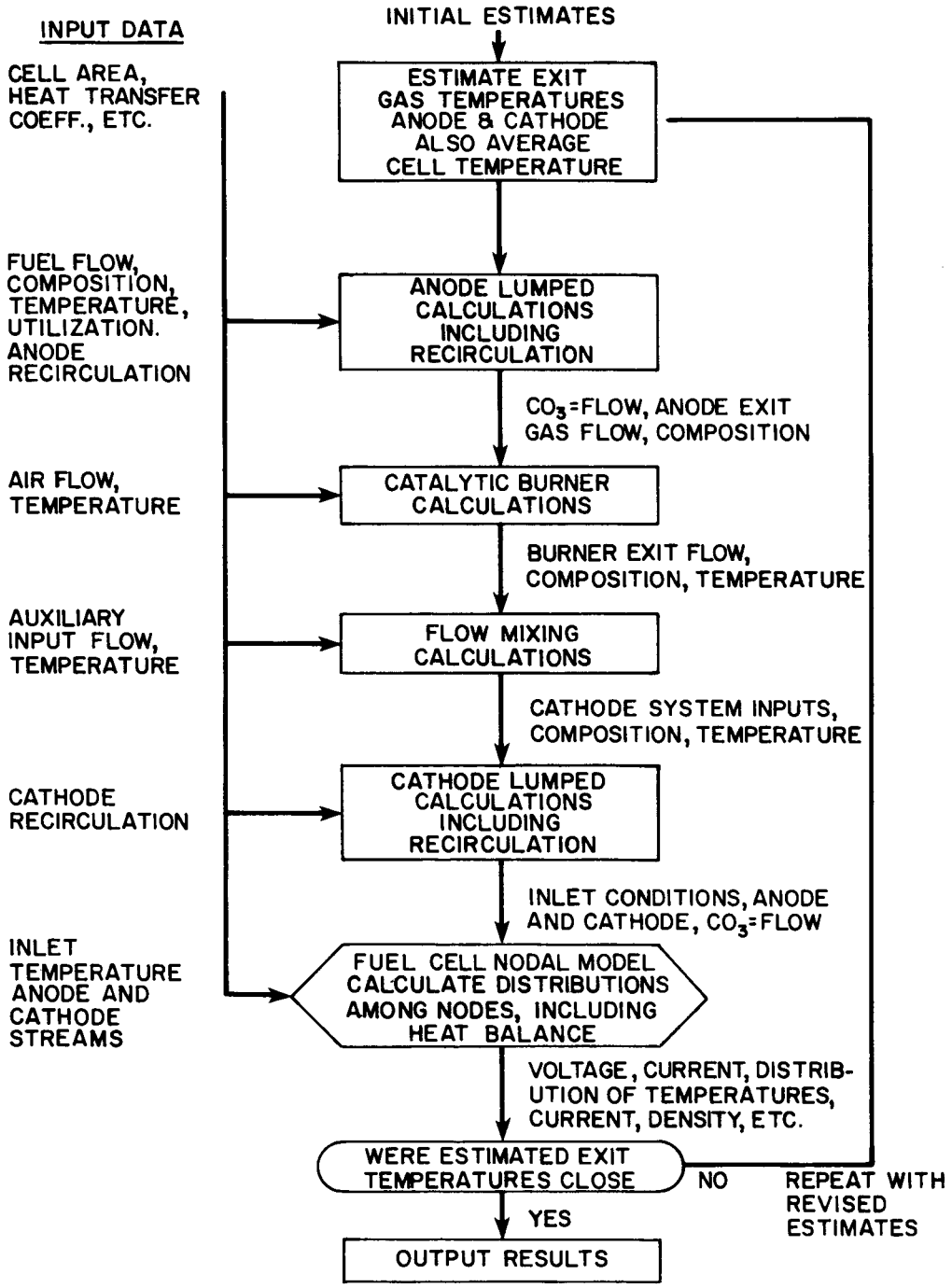

Figure D-6. Overall MCFC Subsystem Simulation Solution

Table D-3

OVERALL MCFC FINITE SLICE MODEL FORMULATION

- MODULAR APPROACH, INCLUDING:
  - EQUIL: Equilibrium Subroutine
  - ELECAL: Electrochemical Calculation
  - QBAL: Overall Nodal (Slice) Heat Balance
  - QBLNØD: Heat Balance Nodal (Slice) Iteration
  - NODE: Single Node (Slice) Model
  - FCELL: Entire Cell Calc., Co-Flow
  - FCLCTR: Entire Cell Calc., Counter-Flow
  - FCLXFL: Entire Cell Calc., Cross-Flow
  - ANDLMP: Anode Lumped Parameter Calculation
  - CATLMP: Cathode Lumped Parameter Calculation
  - BURNER: Catalytic Combustor Calculation
  - FLOMIX: Flow Mixing Subroutine
  - TOTAL: Flow Totalizing Calculation
  - CONCEN: Concentration Calculation
  - SUBSYS: MCFC Overall Subsystem Solution

For the solution of the finite slice fuel cell representation, iterative procedures are employed to satisfy the heat (energy) and mass balance constraints for each slice. In addition, the terminal voltages at all slices are required to be the same. The total carbonate flow ($CO_3^=$) and electrical current are calculated by the lumped anode model, based on specified utilization and fuel composition. The total carbonate ion flow is divided among the slices. As the slice-to-slice calculations proceed, the calculated terminal voltage for each slice is noted. Based on these values, the average terminal voltage is calculated, and the $CO_3^=$ flow is reapportioned among slices, either increasing or decreasing for each slice in proportion to its voltage "error" from the average value. The iteration repeats the

slice-to-slice calculations until convergence, with:

- Heat and mass balance satisfied at all times.
- Terminal voltage same at all slices.
- Total $CO_3^=$ flow equal to the total from the lumped anode model.

The calculation iteration procedure, utilizing an adaptive secant method, is well behaved, with rapid convergence.

The simulation program results, by category, are enumerated in Table D-4.

RESULTS AND TEST CASES

Preliminary results from the finite slice model indicate that the higher cell efficiency associated with counterflow operation is accompanied by a temperature profile within the cell having undesirable peaks and gradients, compared to those for co-flow operation. Also, the calculated temperature profiles are at variance with the assumptions made in the earlier lumped parameter model, where it was assumed that the temperature of the two exit gas streams from the cell are essentially at the same temperature as the cell itself, regardless of flow configuration. Therefore, previous conclusions and associated system performance implications regarding heat removal in the anode and cathode gas streams were imprecise.

To illustrate the use of the finite slice model, an oil-fired plant configuration was chosen which had the characteristics shown in Figure D-7 and Table D-5. For this case, runs were made with the finite slice model for counterflow, co-flow, and crossflow configurations, to be compared to the results from the earlier lumped parameter model. The comparative results are summarized in Table D-6. It can be seen that the lumped and finite slice model predictions for cell voltage and efficiency, for counterflow operation, are within 1.5 percent. However, there are large differences in predicted anode and cathode gas exit temperatures (236 deg. F and 78 deg. F) and maximum cell temperature (110 deg. F). For co-flow operation, differences in the predicted temperatures are smaller, but the predicted cell voltage and efficiency from the finite slice model are lower (2.7 percent) than the earlier values from the lumped parameter model. The crossflow results are in closest agreement with earlier predictions, but the anode gas exit temperature is also lower than was expected and the crossflow case exhibited the largest value of maximum cell temperature (1421 deg. F).

Table D-4

SIMULATION PROGRAM RESULTS
(Categories)

- SINGLE VALUED QUANTITIES
  - Voltage
  - Current
  - Power
  - Current Density
  - Efficiency
  - Heat Rejected
  - Temperatures
  - Cathode Utilization
  - Total $CO_3^=$ Flow
- FLOW VECTORS (MOLES/HR, CONCENTRATIONS)
  - Anode Inlet (Before and After Shift Equilibrium)
  - Anode Exit
  - Burner Exit
  - Cathode system In
  - Cathode Inlet
  - Cathode Exit
- SLICE PARAMETERS(Each Slice)
  - Anode Gas Temperatures
  - Cathode Gas Temperatures
  - Cell Temperatures
  - Current Density
  - Anode Utilization
  - Cathode Utilization
  - Anode Gas Constituents, Concentrations
  - Cathode Gas Constituents, Concentrations

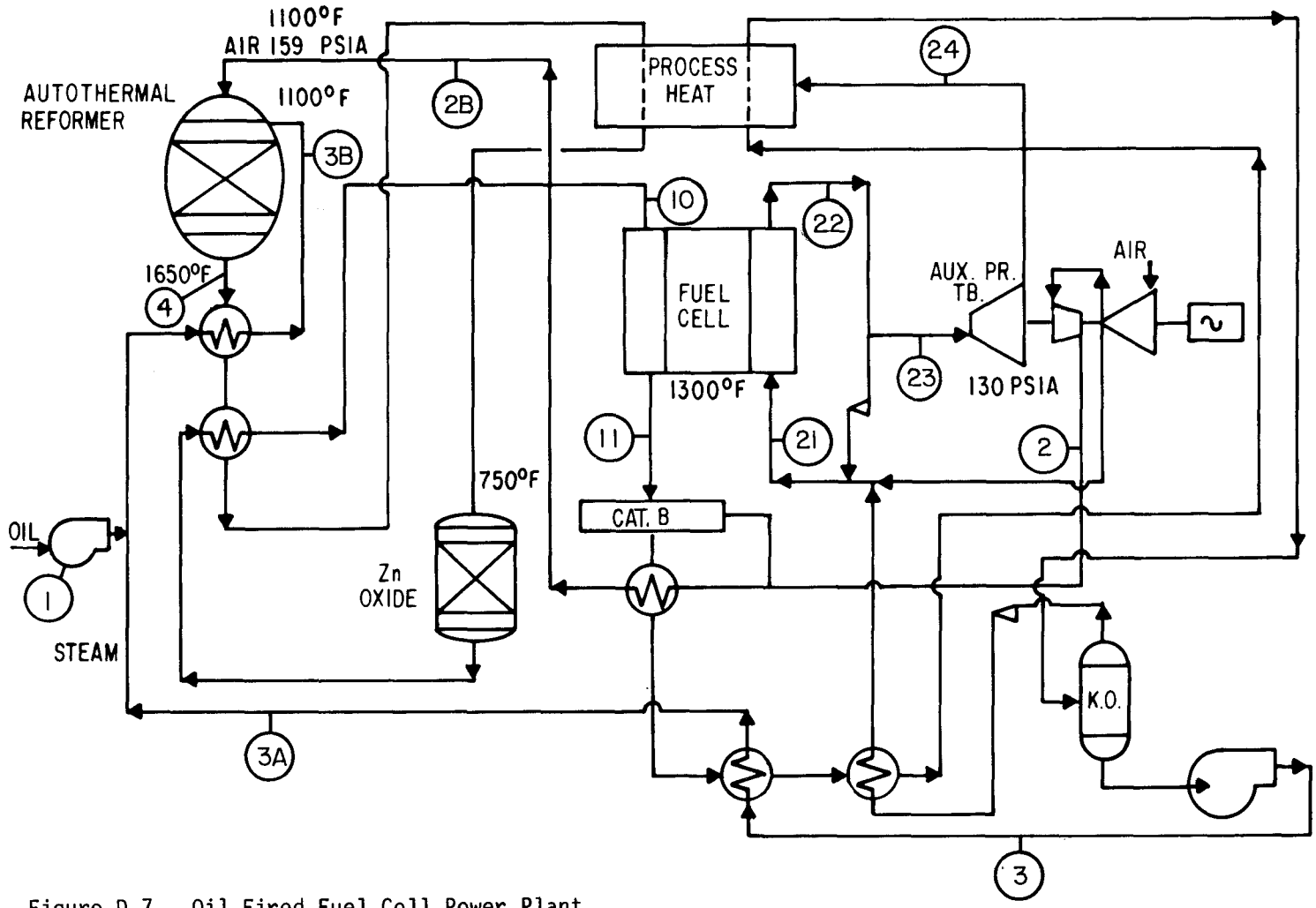

Figure D-7. Oil-Fired Fuel Cell Power Plant

Table D-5

OIL-FIRED PLANT MATERIAL AND ENERGY BALANCE

Stream Number	1	3A	2B	4	10	11	21	22	23	24
Stream ID	Oil	Steam	Air to Reformer	Reformer Exit	Anode Inlet	Anode Exit	Cathode Inlet	Cathode Exit	Turbine Inlet	Vent
Temperature (^{o}F)	77	572	1100	1650	1000	1300	1000	1300	770	250
Pressure (psia)	14.7	162	159	149	134	133	134	133	130	15
Gas Composition (Mole Fraction)										
O_2			.2100	0	0	0	.1641	.1450	.1450	.1450
CO				.1337	.1337	.0205	.0000	.0000	.0000	.0000
H_2				.2899	.2901	.0262	.0000	.0000	.0000	.0000
CO_2				.0718	.0718	.3954	.1065	.0432	.0432	.0432
CH_4				.0012	.0012	.0009	.0000	.0000	.0000	.0000
N_2			.7810	.3020	.3020	.2220	.6875	.7651	.7651	.7651
A_R			.0090	.0035	.0035	.0026	.0079	.0088	.0088	.0088
H_2S				.0002	.0000	.0000	.0000	.0000	.0000	.0000
H_2O		1.0000		.1977	.1977	.3324	.0341	.0379	.0379	.0379
Total Flow $\frac{lb\ mole}{h}$		202.19	249.80	646.48	646.58	879.34	3442.15	3092.82	3092.82	3092.82
Total Flow lb/h	1841.63	3642.56	7234.25	12718.13	12714.08	26692.72	103709.57	89729.56	89724.56	89724.56
Enthalpy Flux $\frac{MBtu}{h}$	35.507	4.64	1.85	44.41	40.88	20.98	26.69	30.94	17.92	6.09

Table D-6

COMPARISON OF RESULTS, FINITE SLICE
(NODAL) MODEL VS. LUMPED PARAMETER MODEL

		CASE				
		Lumped Model		Finite Slice Model		
		A	B	C	D	E
Voltage (note 1)	volts	0.810	0.807	0.823	0.785	0.813
Power (note 1)	watts	1614	1635	1666	1591	1647
Cell Efficiency (note 2)		0.462	0.460	0.469	0.448	0.464
Anode Exit Gas Temp.	deg. F	1300*	1300*	1064	1316	1152
Cathode Exit Gas Temp.	deg. F	1300*	1300*	1378	1314	1353
Average Cell Temp.	deg. F	1300*	1300*	1262	1242	1224
Maximum Cell Temp.	deg. F	1300*	1300*	1410	1315	1421

Cases: A = Lumped Parameter Model, Counterflow
B = Lumped Parameter Model, Co-flow
C = Finite Slice Model, Counterflow
D = Finite Slice Model, Co-flow
E = Finite Slice Model, Crossflow

Note 1. For single cell having area of 12544 cm^2 (112x112 cm). For reference current density of 161.5 mA/cm^2, current = 2025.8 amperes.

Note 2: Cell efficiency = Electrical Power Out/Fuel HHV

*Note: Temperatures for lumped parameter model are assumed values.

These results from the finite slice model can be examined in closer detail. Plots of certain nodal parameters (temperatures, current density and cumulative fuel utilization) are given in Figures D-8 through D-10. It can be seen that the anode gas temperature rises very quickly and peaks about 20% of the distance along the flow path. The temperature then falls, very much dominated by the (cooler) incoming cathode stream. The maximum current density is also experienced near the anode inlet, 37% higher than the average value of 161.5 mA/cm^2.

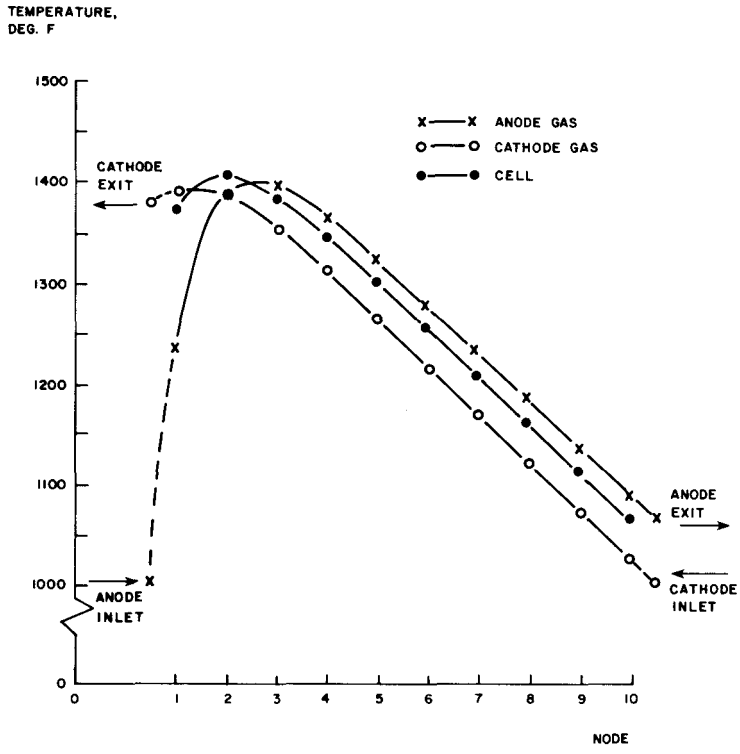

Figure D-8. Temperature vs. Node, Counterflow

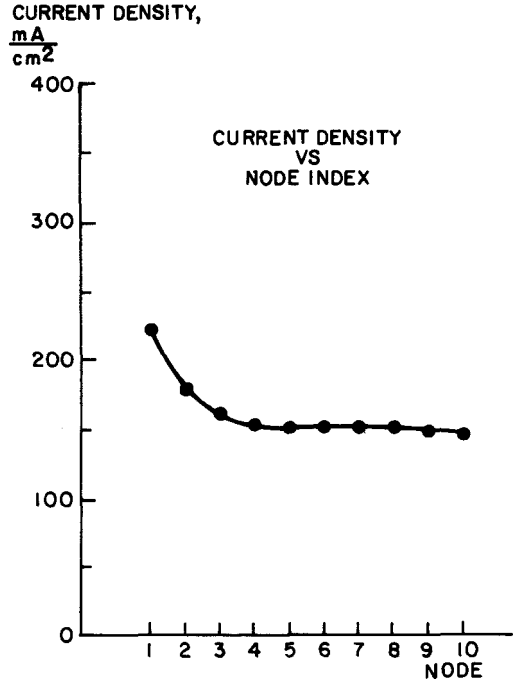

Figure D-9. Current Density vs. Node, Counterflow Configuration

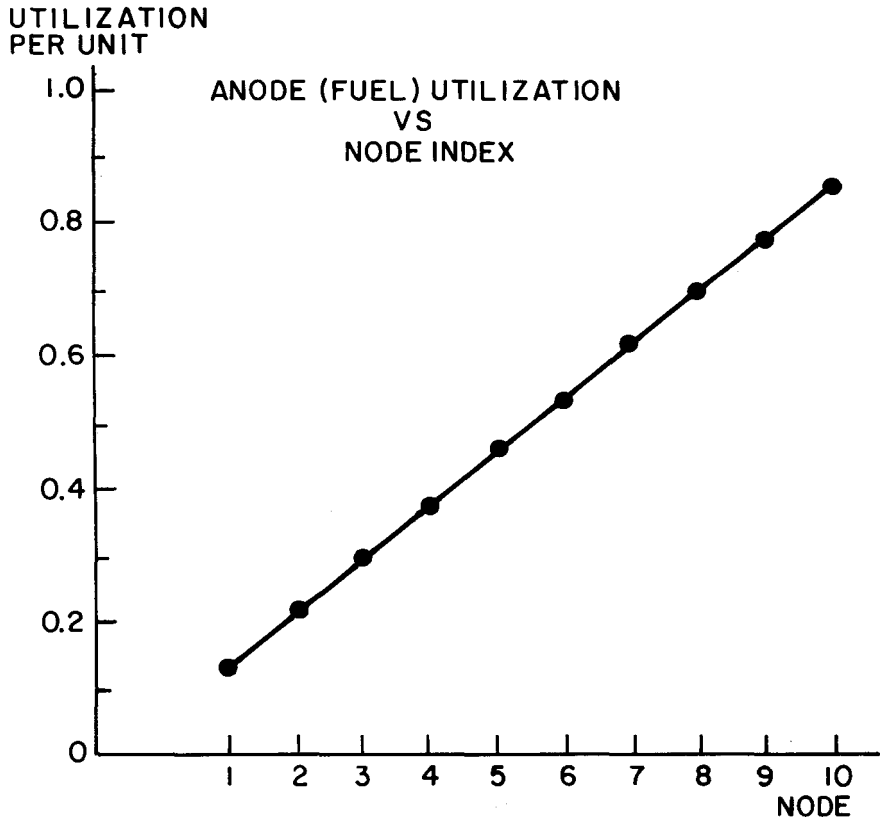

Figure D-10. Anode (Fuel) Utilization Counterflow

In contrast, model results for the co-flow configuration reference oil-fired case show a temperature profile which approaches lower peak values, as shown in Figure D-11. The current density (Figure D-12), however, is much less uniform than for the counterflow case, with associated higher i^2R losses and lower cell efficiency.

Simulation was performed for the crossflow cell configuration, for the same reference oil fired case. A constant value of heat transfer coefficient, 10.0 Btu/(h ft^2 deg F), was assumed for calculating the sensible heat transferred between the cell/electrolyte and the gases. However, provision also exists in the simulation for calculation of the heat transfer coefficients at each slice (node), as indicated earlier. To illustrate use of the fuel cell model to apply to a stack configuration, an example is used including a separator plate configuration selected to give approximately equal pressure drops from inlet to exit for both the anode and

cathode gas streams. The fractional flow areas are thus chosen to give roughly equal values of G^2/o (flow density squared divided by gas density). For the counter-flow case considered previously, the average flow and density values are:

Anode Flow = 7.04 lb/h

Cathode flow = 34.44 lb/h

Anode Density = 24.98 lb/mole

Cathode Density = 29.47 lb/mole

For equal pressure drops the flow area ratio required is 4.5 (cathode to anode). Based on approaching this value, separator plate ratios of flow area/frontal area were selected:

$\sigma_A = 0.2$ anode

$\sigma_C = 0.8$ cathode

Assuming a channel depth of 0.254 cm (0.1 inch) and flow channel widths of 2.0 cm and 0.5 cm for the cathode and anode paths, respectively, repeated across the 112 cm active cell width, equivalent flow diameters were calculated. Also the ratio of active area for anode to cathode gas heat transfer across the separator plate was calculated, assuming a 45 degree forming angle. The assumed geometry and corresponding input data for the computer simulation are shown in Figure D-13. A test of the subroutine which determines gas transport properties and associated heat transfer coefficients, based on this flow geometry and the gas flow vectors corresponding to slice (node) number 1 of the counter flow example, shows:

Anode $h = 30.7$ Btu/(h deg F ft^2)

Cathode $h = 12.7$ Btu/(h deg F ft^2)

Although the anode gas heat transfer coefficient is significantly higher, primarily because of the thermal conductivity of hydrogen, the anode flow rate and effective heat transfer area are both much less than for the cathode, so the cathode side will dominate the heat transfer considerations.

The resultant predicted temperature profiles for the counterflow cell in a stack configuration, with variable heat transfer coefficients calculated, are shown in Figure D-14. The array of calculated heat transfer coefficients are normalized to the total cell area (instead of the effective heat transfer surface areas for

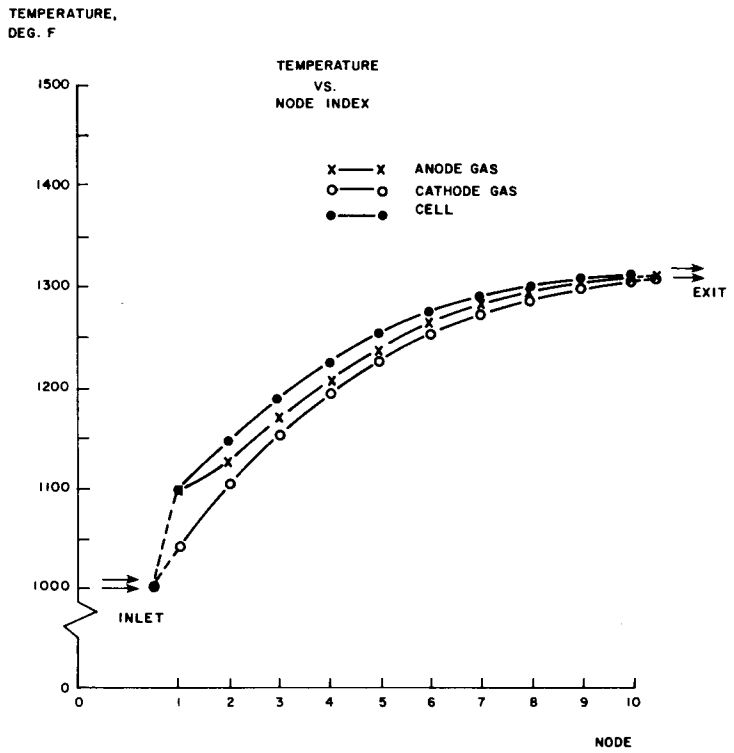

Figure D-11. Temperature vs. Node, Co-Flow

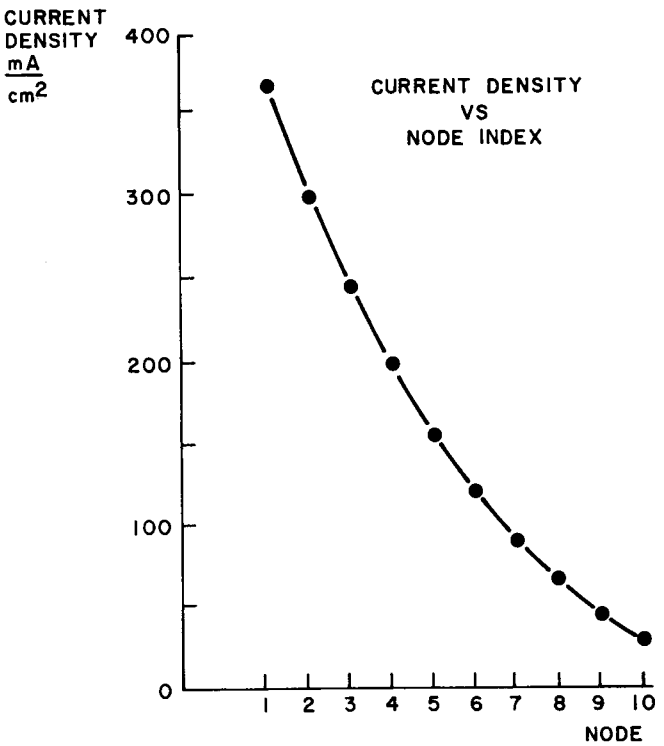

Figure D-12. Current Density vs. Node, Co-Flow Configuration

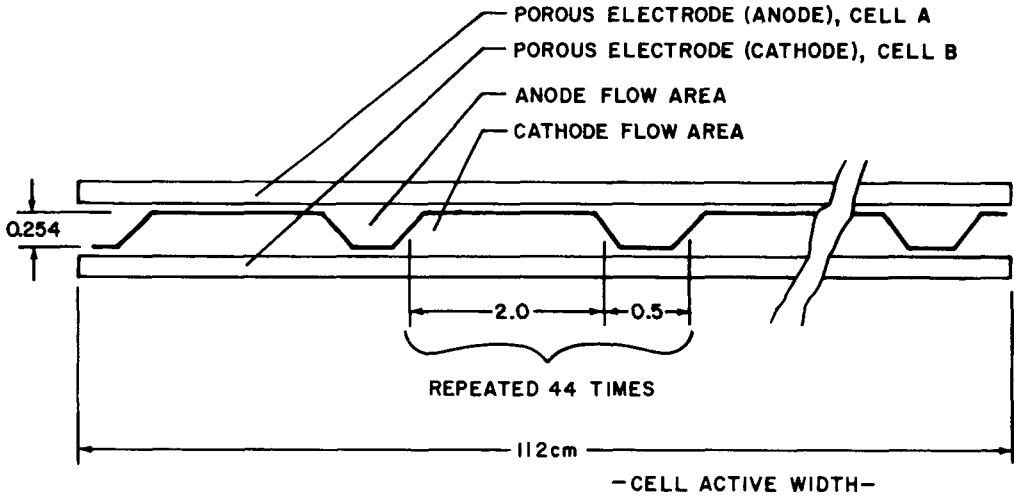

$\sigma_A = 0.2$
$\sigma_C = 0.8$
} RATIOS, FLOW AREA TO FRONTAL AREA

$$\text{DIAEQA} = \frac{4*\text{AREA}}{\text{WETTED PERIMETER}} = \frac{4(0.5)0.254}{1.0+0.508\sqrt{2}} = 0.296\,\text{cm}$$

$$\text{DIAEQC} = 0.431\,\text{cm}$$

$$\text{RASAC} = \frac{44*2*(0.254\sqrt{2})}{112} = 0.28$$

Figure D-13. Assumed Flow Channel Geometry

this example; 20% for the anode, 80% for the cathode, and 28% for the anode-to-cathode surfaces). As expected, the temperature profiles are closer together than those calculated earlier for an individual cell.

The choice of the number of model elements for the simulation was arbitrarily selected to be 10 slices. Exercises were subsequently performed to determine the sensitivity of the simulation to the number of slices selected for the fuel cell representation. These results are summarized in Figure D-15, in terms of performance and cost. It is concluded that whereas a 10-slice model is adequate for accurate prediction of overall performance, a 20-slice model is a better compromise choice in order to more accurately represent slice-to-slice process characteristics without an exessive increase in computer costs.

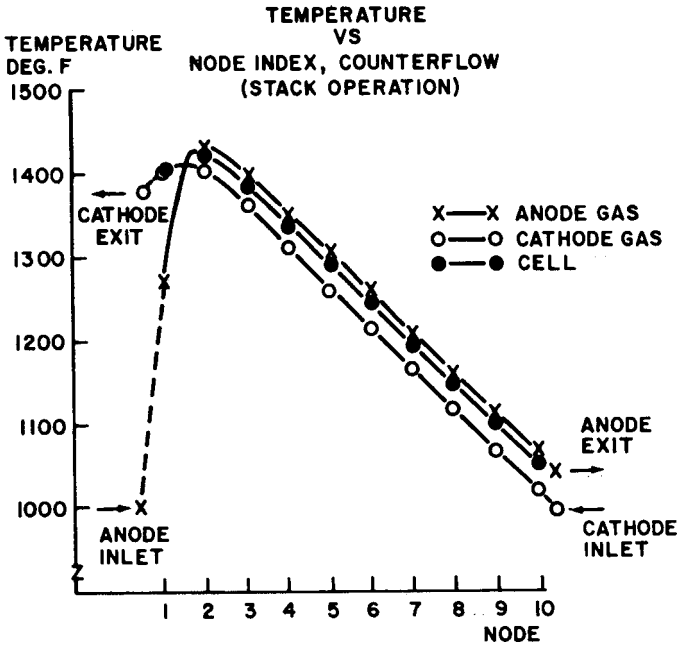

Figure D-14. Temperature vs. Node, Counterflow (Stack)

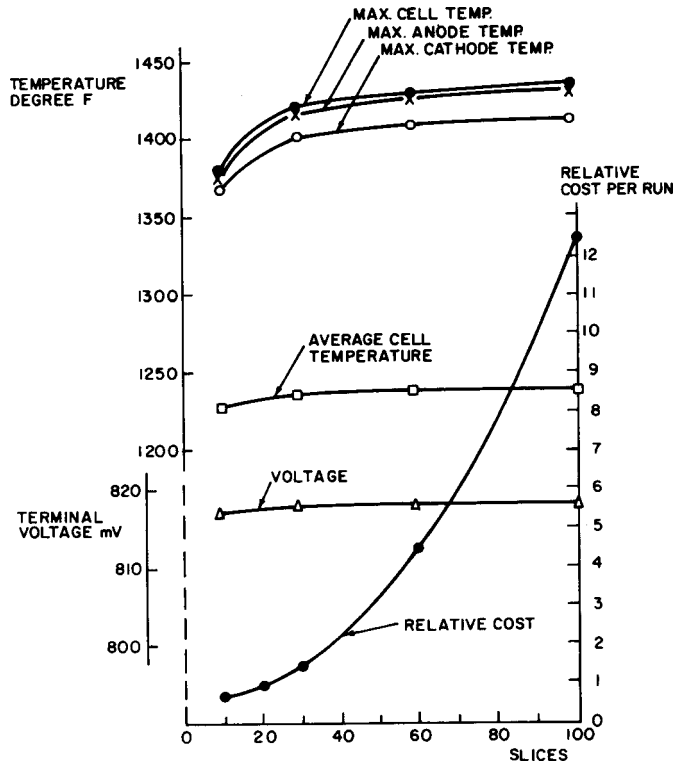

Figure D-15. Model Sensitivity to Number of Slices (Counterflow Configuration)

CONCLUSIONS FOR THE NODAL MODEL

The MCFC subsystem simulation, using the finite slice model of the fuel cell, is a useful tool for evaluating the performance and integrated system characteristics of the fuel cell power plant. The model is an excellent compromise between certain coarse approximations of the earlier lumped model and the precision of extremely detailed mechanistic models, which consider pore characteristics, calculated diffusion rate limiting effects, etc.

- Preliminary results from the finite slice model indicate that co-flow operation has cell efficiency comparable to that for counter-flow operation and does have a temperature profile with undesireable peaks and gradients.
- Previous conclusions and associated performance implications regarding heat removal in the anode and cathode gas streams were imprecise.
- Lumped parameter and finite slice model predictions for cell voltage and efficiency, for counterflow operation, are within 1.5%.

MCFC PARAMETRIC INVESTIGATION

Parametric runs were made using the MCFC subsystem simulation with the finite slice fuel cell model. The results provide a preliminary indication of subsystem operational interrelationships as well as the detailed behavior of key fuel cell parameters under different conditions. Three cell flow configurations were investigated: co-flow, counterflow, and crossflow. For each of these configurations, 12 computer runs were made, with an input data matrix having four values of fuel flow (1.0, 0.75, 0.50, 0.25 per unit), each being evaluated for three values of anode utilization (0.85, 0.70, 0.60). The resulting cases are designated A1-C12 as shown in Table D-7.

The basic subsystem configuration being evaluated is the oil-fired reference design case as described in the interim report (3-1). Results from these parametric runs for each flow configuration are presented here in the form of subsystem performance operational maps and distributions of key parameter values within the cell. It is intended that the form of these preliminary results comprise a trend-indicating framework from which subsequent detailed system investigations can proceed, leading to a more complete understanding of anticipated operational characteristics.

Table D-7

PARAMETRIC RUNS - CASE DESIGNATION

Anode (Fuel) Utilization	Fuel Flow (Note 1)	Flow Configuration		
		Co-flow	Counterflow	Crossflow
0.85	1.0	A1	B1	C1
	0.75	A2	B2	C2
	0.50	A3	B3	C3
	0.25	A4	B4	C4
0.70	1.0	A5	B5	C5
	0.75	A6	B6	C6
	0.50	A7	B7	C7
	0.25	A8	B8	C8
0.50	1.0	A9	B9	C9
	0.75	A10	B10	C10
	0.50	A11	B11	C11
	0.25	A12	B12	C12

Note 1. Flow magnitude indicated as fraction of design value. Air flow to catalytic combustor is varied in proportion, as is the magnitude of water knockout ahead of cathode.

A comparison of the results for the three flow configurations leads to a number of observations and conclusions about the indicated trends:

- For a given utilization (e.g., 0.85), cell efficiency increases as fuel flow (and power output) are decreased. This increase in efficiency is most marked for the counterflow configuration, and is least for co-flow case.

- As flow is decreased (at constant utilization), the terminal voltage changes least for the co-flow configuration (about three percent for a seventy-five percent decrease in fuel flow). For the counterflow configuration, the voltage increases approximately 13% under this condition.

- The distribution of local current density in the cell is most uniform for the counterflow configuration, and the pattern is relatively unaffected by a reduction in fuel flow.

- The distribution of temperatures within the cell is an important consideration and differs significantly as a function of flow configuration. An optimum choice of design point operating conditions and turn-down approach is not possible without careful consideration of the temperature distributions.

These and other observations are examined in more detail in the discussion of the results of the parametric runs which follow. It is concluded that use of the finite slice (nodal) model of the fuel cell in the MCFC subsystem simulation is an excellent means of providing necessary understanding of the overall operational trends in the integrated plant systems environment.

CELL PERFORMANCE

Cell efficiency, here defined as the ratio of electrical power output to the high heating value of the incoming fuel (in comparable units), is an important parameter affecting the performance of the overall plant. Results from the parametric runs have been plotted for the three flow configurations and are shown in Figures D-16, D-17 and D-18 for co-flow, counterflow and crossflow, respectively. Efficiency is plotted versus fuel flow (fraction of design value) for several values of utilization. Lines of constant power are indicated. It can be seen that cell effciency increases somewhat as flow is decreased, if operating at constant anode (fuel) utilization. This effect is most pronounced for the counterflow case. Since the counterflow case exhibits the highest design point efficiency, it therefore exhibits an even higher part load efficiency, as indicated. It should be noted, however, that the considerations associated with comparing the various flow configurations are complex. Care must be taken not to place excessive significance on consideration of only the comparative cell performance data. Other important factors include cell operating characteristics and distribution of parameters within the cell.

CELL OPERATIONAL CHARACTERISTICS

The operation of the plant will involve establishing conditions required to achieve the desired electrical power output. The relationships between fuel cell electrical power output and fuel flow, for several values of utilization,are given in Figures D-19, D-20 and D-21 (for the three flow configurations). Lines of constant current are shown. These figures show that increasing the power output and maintaining a desired utilization is achieved by a coordinated increase in fuel flow and electrical current drawn from the cell. The basic shape of these curves for the three flow configurations does not vary significantly.

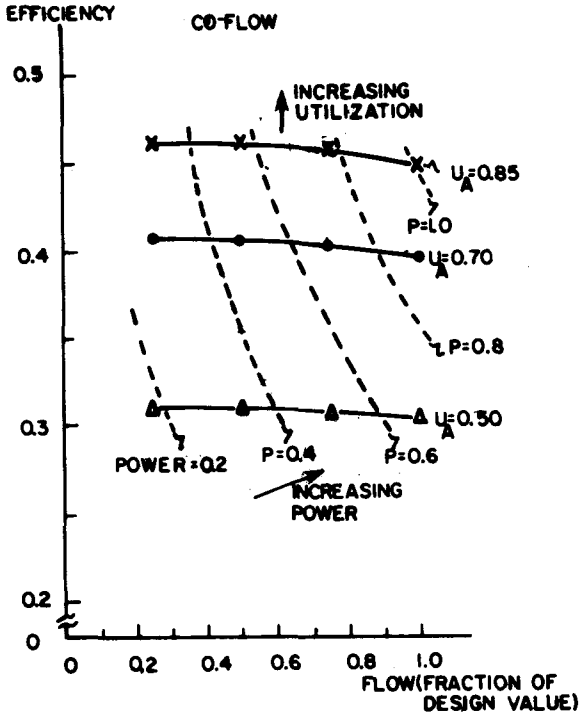

Figure D-16. Efficiency vs. Flow, Co-Flow Configuration

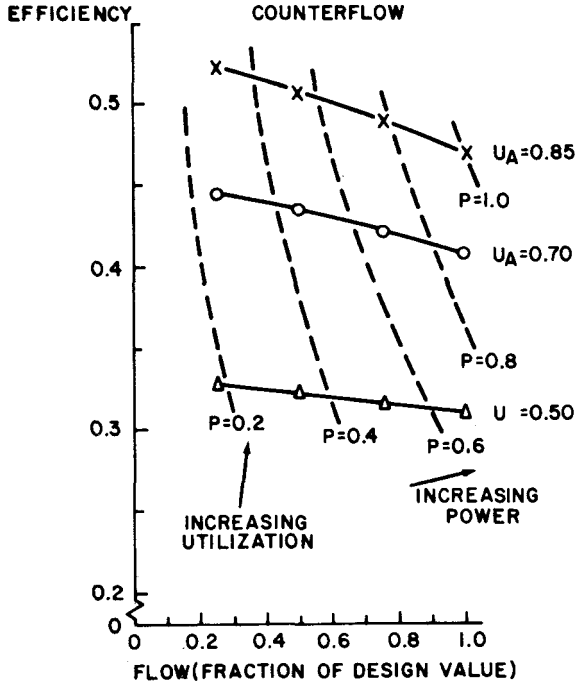

Figure D-17. Efficiency vs. Flow, Counterflow Configuration

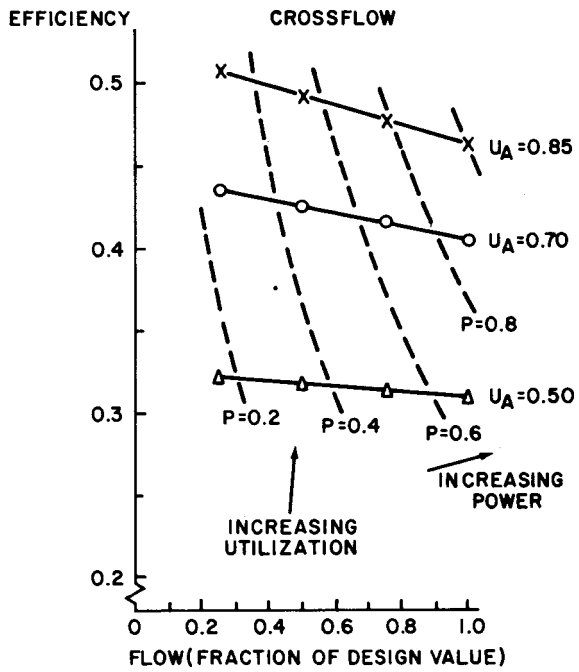

Figure D-18. Efficiency vs. Flow, Crossflow Configuration

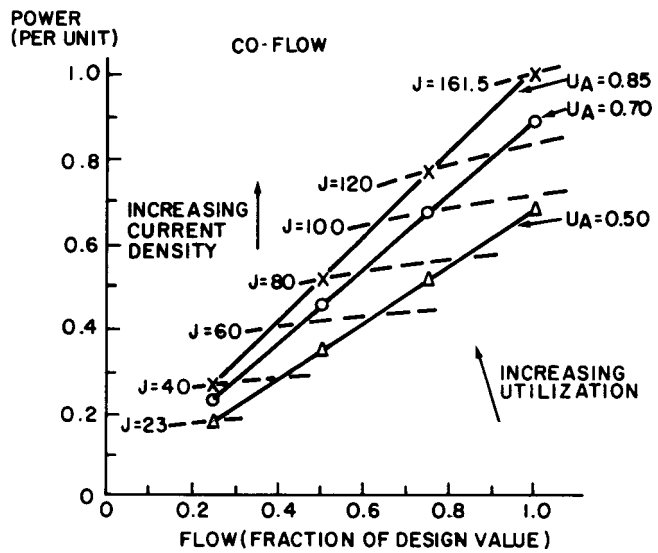

Figure D-19. Power vs. Flow, Co-Flow Configuration

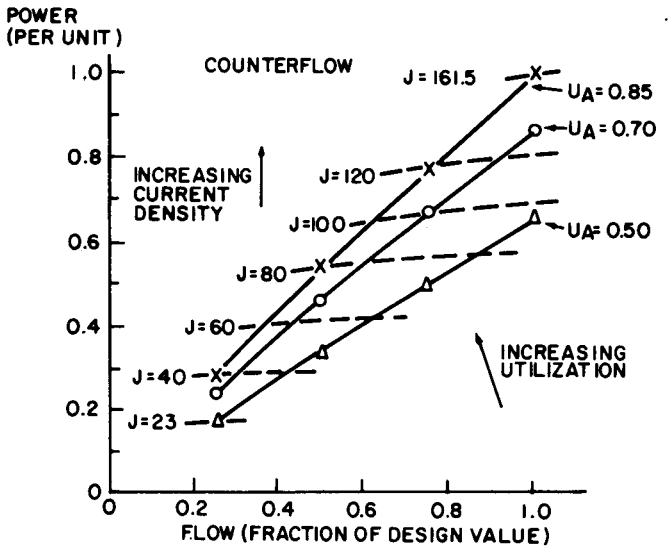

Figure 20. Power vs. Flow, Counterflow Configuration

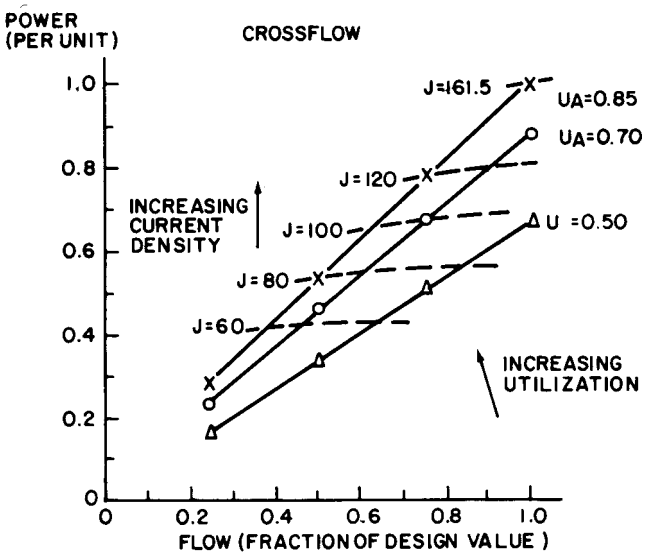

Figure D-21. Power vs. Flow, Crossflow Configuration

The behavior of cell voltage as a function of flow rate is shown in Figures D-22, D-23 and D-24, with lines of constant power indicated. For operation at constant utilization, the voltage increases. This increase is most notable for the counter-flow operation (related to the cell performance characteristics discussed previously). It will be noted that for a given flow rate, the co-flow voltage variation with utilization is larger than for the other flow configurations. As expected, the curves of current density versus flow rate, for defined utilization values, are identical. As shown in Figures D-25, D-26 and D-27, only the lines of constant power differ for the three configurations.

The parametric variations and trends shown here are significant to the degree they impact upon the plant design requirements and operational techniques. Care must be taken regarding establishing compatible interfaces, for example, between the fuel cell and the inverter subsystem. Studies of the form discussed here will be useful in defining the required detailed design characteristics.

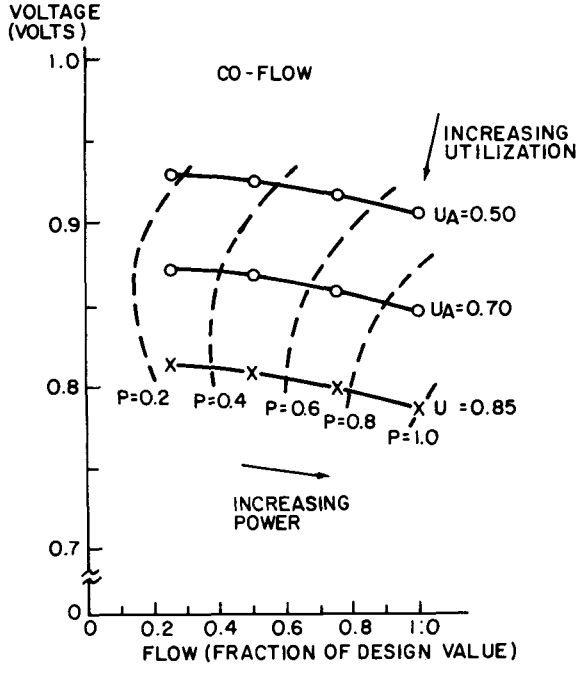

Figure D-22. Voltage vs. Flow, Co-flow Configuration

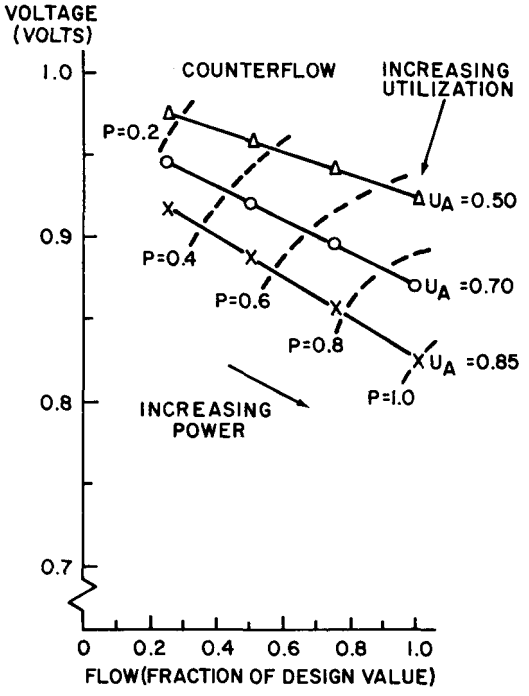

Figure D-23. Voltage vs. Flow, Counterflow Configuration

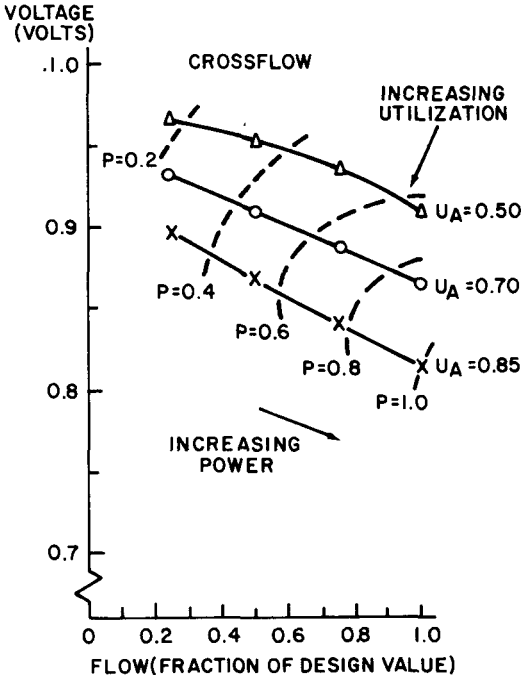

Figure D-24. Voltage vs. Flow, Crossflow Configuration

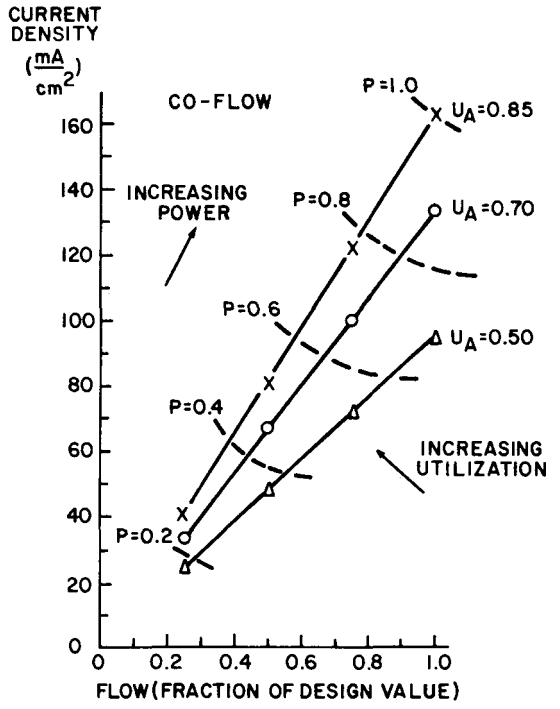

FigureD-25. Current Density vs. Flow, Co-Flow Configuration

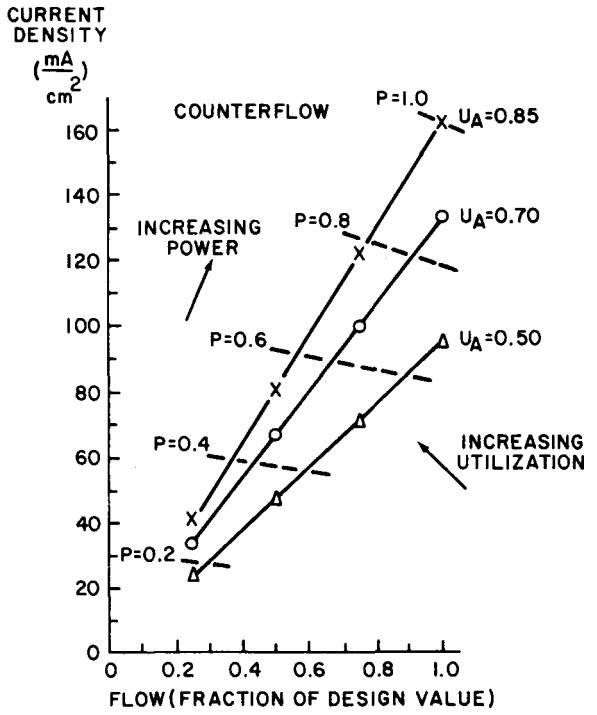

Figure D-26. Current Density vs. Flow, Counterflow Configuration

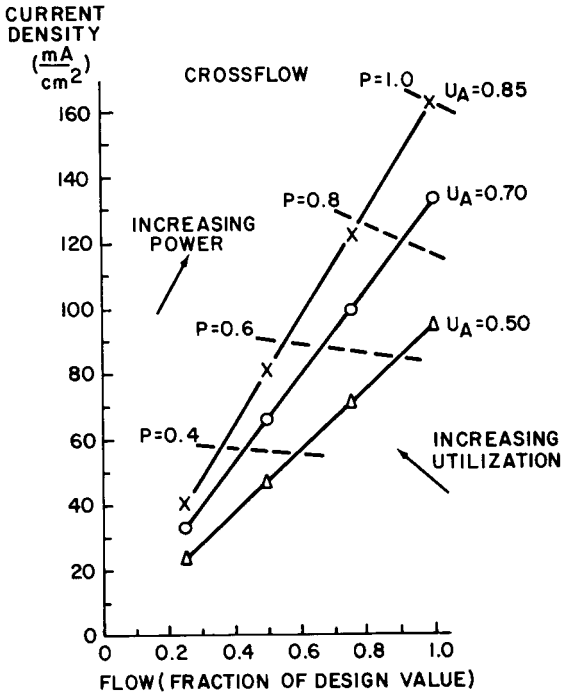

Figure D-27. Current Density vs. Flow, Crossflow Configuration

DISTRIBUTION OF PARAMETERS WITHIN THE CELL

Discussions thus far have pertained to operation of the cell based on parameters observed outside the cell itself. Equally important, or perhaps more so, are considerations associated with the distribution of local parameters within the cell. For the co-flow and counterflow results presented here, 20 slices (or nodes) were used to represent the cell. For the crossflow configuration, a 10 x 10 slice matrix was used (100 elements). Each slice is constrained to satisfy mass and energy balances, as well as requiring the terminal voltage to be uniform. The resulting predicted distribution of parameters within the cell provides insight into cell behavior, distinguishing between good characteristics and trends which are likely to lead to cell deterioration or other operational difficulties.

The distribution of three parameters in the cell (among the model slices,or nodes) was investigated: Cumulative anode utilization, local current density, and cell/electrolyte temperature. Figures D-28 through D-36 show the cumulative anode (fuel) utilization as a function of anode flow distance for the three flow configurations.

For each of these cases, the overall utilization is 0.85 and the effect of varying fuel flow (and power output) is shown by the family of curves. An interesting phenomenon is observed for the co-flow configuration, with the non-linearity of the utilization curve increasing significantly as fuel flow is decreased. As indicated, portions of the cell nearest the anode inlet are most active. Specifically, below 75% of the rated flow over 90% of the electrochemical activity occurs in the first half of the cell. At half flow, and especially at 25% flow, significant portions of the cell have essentially no activity for the co-flow case. In contrast, the counterflow case (Figure D-26) displays a rather linear cumulative utilization characteristic as a function of flow distance, and is little affected by the magnitude of the flow. This is indicative of a more uniform spatial distribution of electrochemical activity within the cell for this case. The crossflow configuration is intermediate between these two. The soundness of these predicted trends is related to the degree of validity of the process assumptions used in the model. Significant variations from these, for instance the proportionality between current density and polarization on a local basis, could have a significant impact on the relationships found here. Further work in these areas will help to strengthen the usefulness of the fuel cell model and confirm the validity of the simulation results.

Conclusions

The results of the parametric runs indicate the usefulness of the simulation of the fuel cell subsystem utilizing the finite slice (nodal) model of the fuel cell to provide an indication of trends in the process/operational interrelationships. Predicted behavior of key fuel cell parameters, such as distribution of current density and cell temperature, provides information helpful for the establishment of design criteria and operational strategies consistent with process constraints. The influence of flow arrangement is seen as a major factor. Advantages associated with a particular configuration, such as uniformity of current density for counterflow is typically accompanied by less desirable characteristics, such as large temperature gradients. Further system studies, using parametric studies of the type presented here, should be useful in arriving at preferred arrangements and operating conditions satisfying both system needs and process constraints.

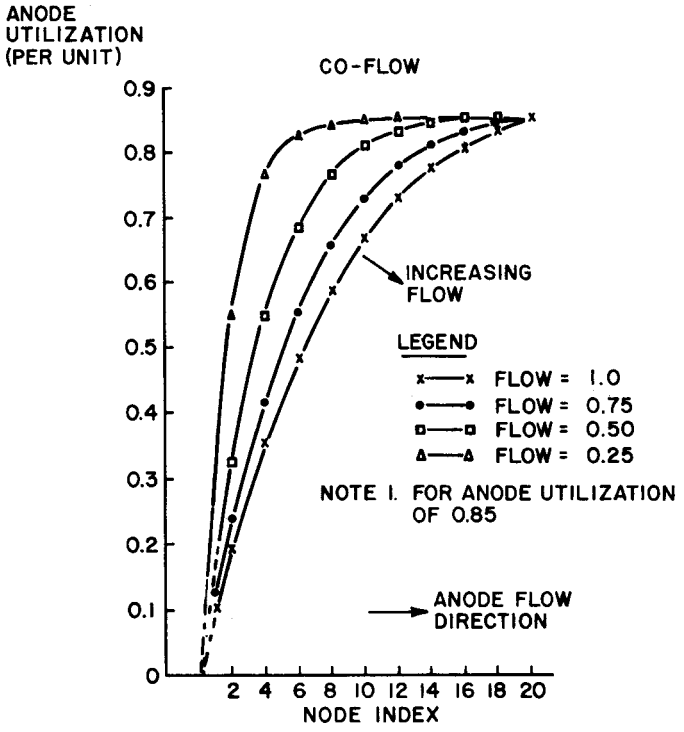

Figure D-28. Anode Utilization vs. Distance, Co-Flow Configuration

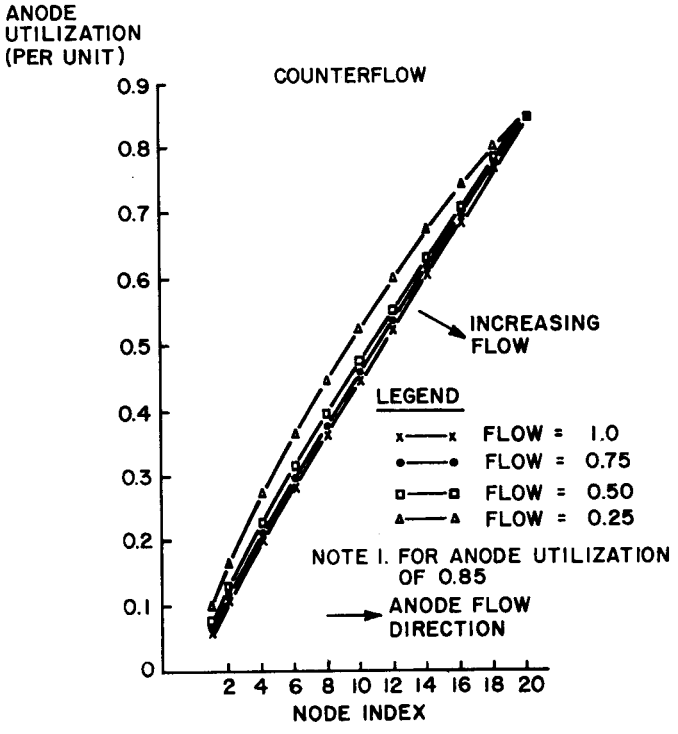

Figure D-29. Anode Utilization vs. Distance, Counterflow Configuration

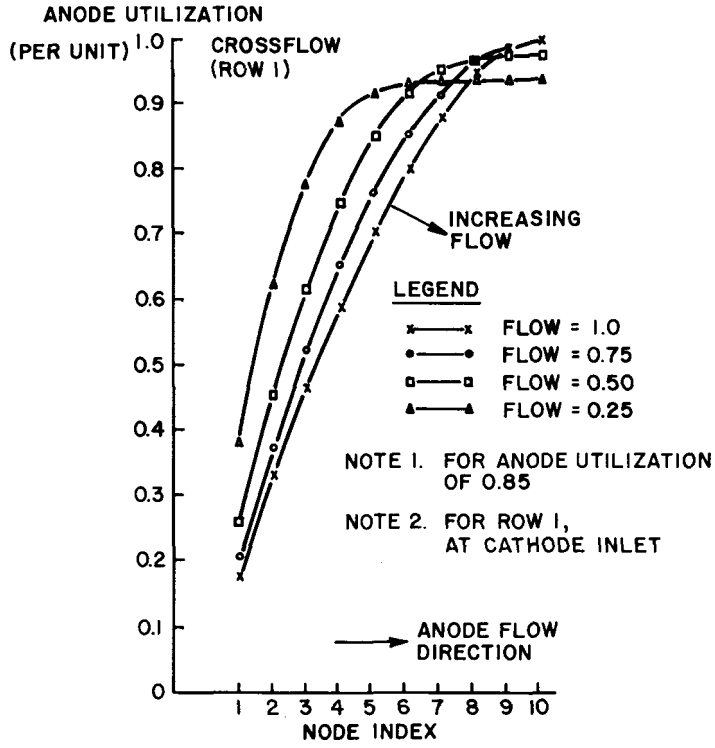

Figure D-30. Anode Utilization vs. Distance, Crossflow Configuration

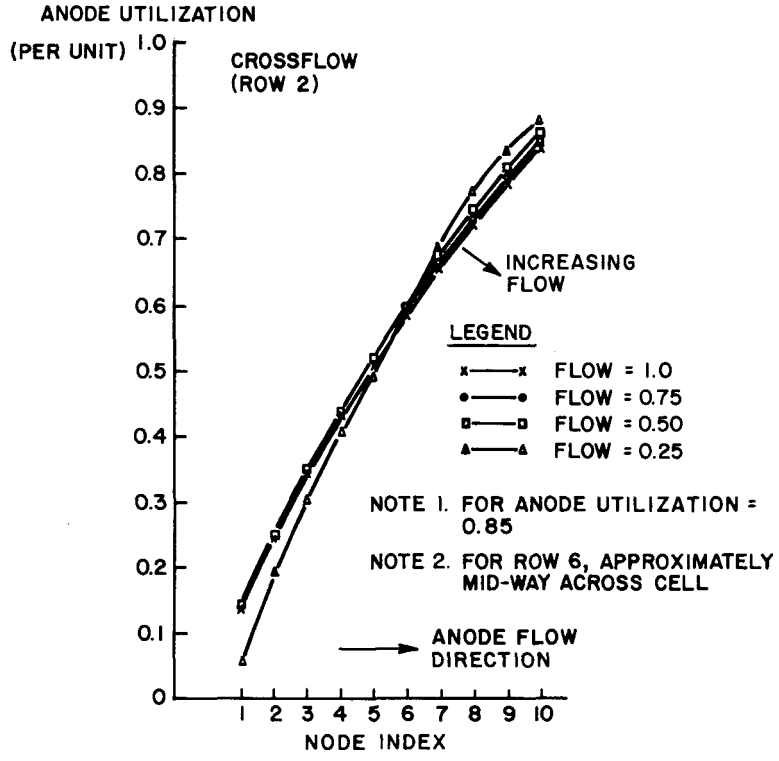

Figure D-31. Anode Utilization vs. Distance, Crossflow Configuration.

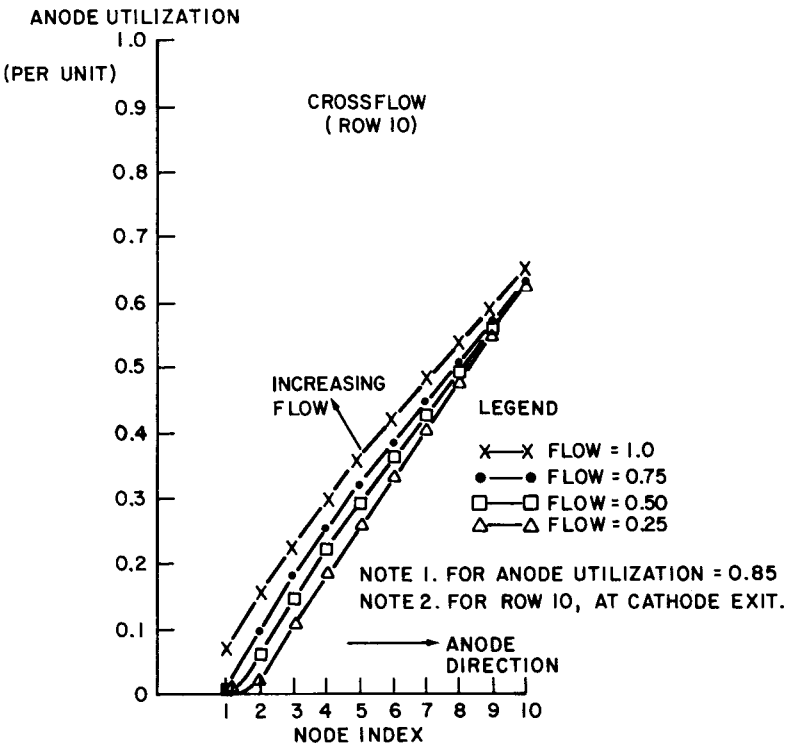

Figure D-32. Anode Utilization vs. Distance, Crossflow Configuration

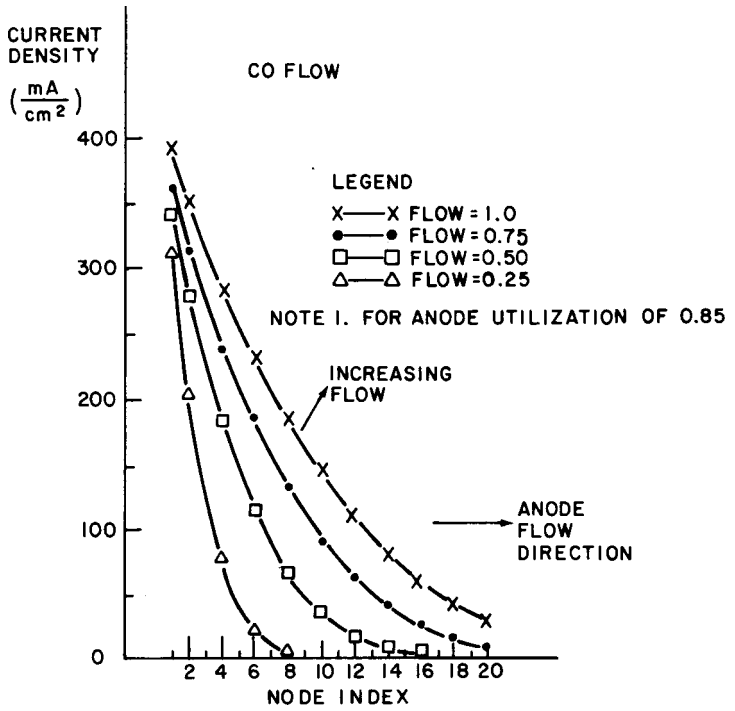

Figure D-33. Current Density vs. Distance, Co-Flow Configuration

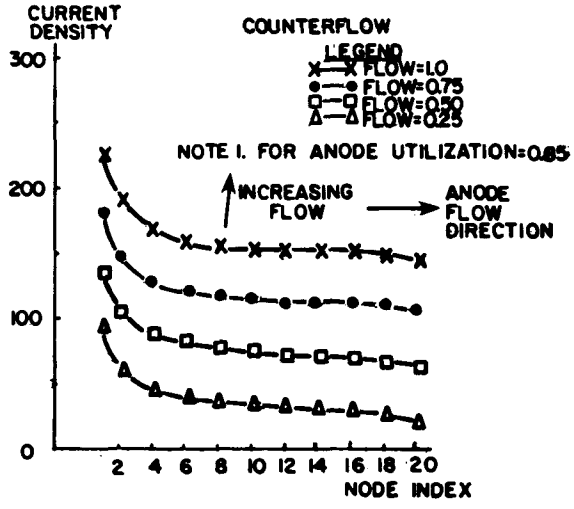

Figure D-34. Current Density vs. Distance, Counterflow Configuration

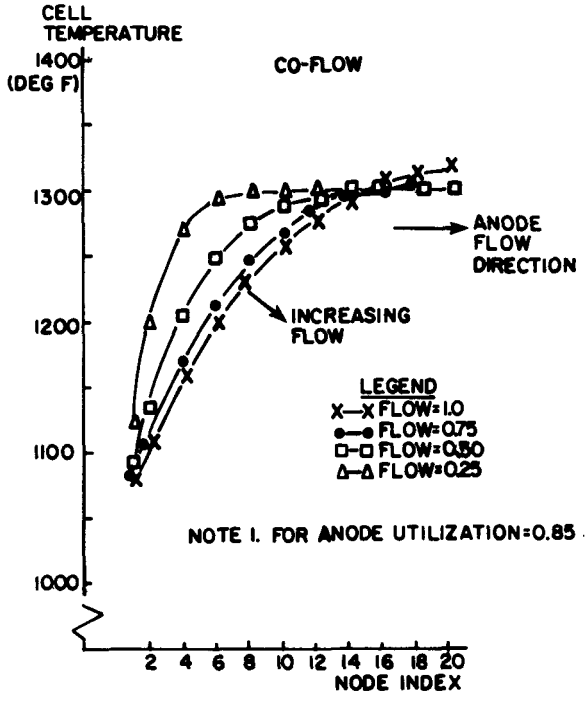

Figure D-35. Cell Temperature vs. Distance, Co-Flow Configuration

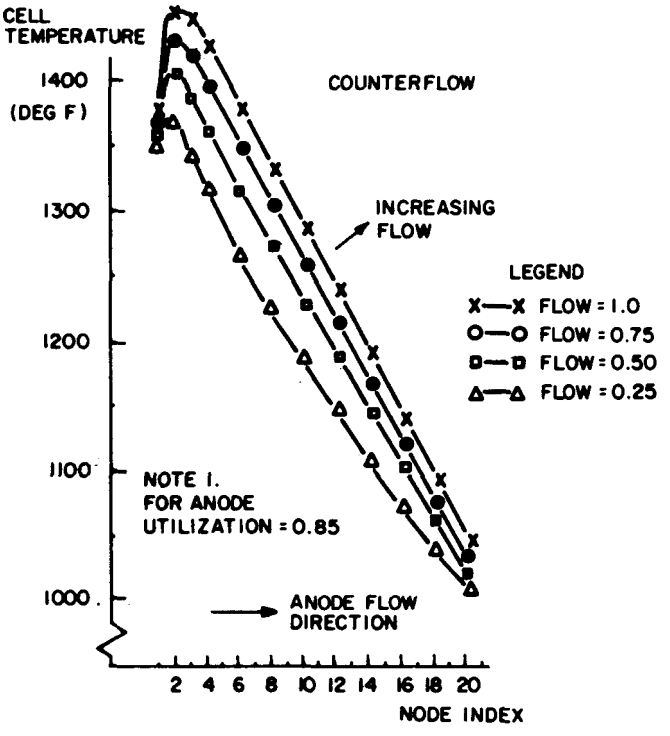

Figure D-36. Cell Temperature vs. Distance, Counterflow Configuration

PARAMETRIC STUDY OF STEAM INJECTION AND RECIRCULATION ON CELL PERFORMANCE

A parametric study has been performed to investigate the use of steam injection and anode recirculation as methods of preventing carbon formation and the resultant effect of these conditions on cell performance. The fuel composition used in the reference coal-fired plant nominally contains 0.0227 water vapor by volume (mole fraction), thus a range of several additional fuel gas compositions were calculated to reflect net water vapor contents of 0.10, 0.20, 0.25, 0.30 and 0.40 by mole

fraction. The nodal fuel cell model was used to determine the minimum amount of anode recirculation necessary to prevent carbon formation for each of these fuel gas compositions. The anode inlet was maintained at 1300°F; cathode recirculation and cathode inlet temperatures were used to control the cell temperatures to within the allowable range. The fuel cell nodal model utilized for this evaluation was a 10 node representation of the cell. The model also included constant heat transfer rates of 10 Btu/h-ft^2-°F between the gas streams and the electrolyte.

DISCUSSION OF RESULTS

The general results of this study indicated that as water vapor content of the fuel stream is increased, less anode recirculation is required to prevent carbon formation. This trend continues until the water vapor content reaches 0.25-0.30, at which point anode recirculation is no longer necessary to prevent carbon formation. However, operation at the lower threshold of this range, 0.250 water vapor with no anode recirculation, results in peak cell temperatures of approximately 1350°F which is undesirable since this could result in electrolyte evaporation. As the water vapor content is increased above 0.250, with no anode recirculation, the peak cell temperatures decrease. Conversely, increasing the anode recirculation to 0.1 at this point (0.250 water vapor) results in an acceptable peak cell temperature, since the cell can operate at a lower temperature without carbon formation. Thus at any water content, tradeoffs exist between cell operating temperature, anode recirculation and carbon formation.

In conjunction with the general observation concerning the decrease in required anode recirculation with increasing steam content, the efficiency of the cell (at the minimum anode recirculation to prevent carbon formation) increases with increasing steam content reaching a peak in the area of 0.20-0.30 water vapor content and decreases above 0.30 water vapor content. Several cells were investigated with water vapor contents of 0.250 and various anode recirculations less than 0.2. The highest efficiency found was 47.31% at 0.25 water vapor content and 0.15 anode recirculation. However, it was observed that this efficiency was not significantly higher from either the 0.2 water vapor/0.2 anode recirculation case (47.26%) or the 0.3 water vapor/0 anode recirculation case (47.24%). It should be noted that these efficiencies were reached by modifying the cathode inlet and recirculation rates to result in cell operating parameters just above the carbon formation limit, and thus represent the maximum attainable efficiencies under those conditions.

The general trend of the results indicate that a family of curves exist for each cell configuration, with each curve representing an efficiency vs. water vapor content curve for a fixed recirculation ratio. Certain portions of the cell operation curve (such as 0 anode recirculation with water vapor contents of 0.250 or below) represent cell operating conditions which are unacceptable. Due to the overlap of the curves, numerous operating conditions can be found with differing anode recirculation rates and efficiencies. The curve shown in Figure D-37 shows the results of the highest efficiencies found for each value of fuel water vapor content studied. It is evident that in the range of 0.20-0.30 water vapor content, the peak efficiency does not vary significantly, and above and below this range the cell efficiency decreases. A sample mass/energy balance is shown in Figure D-38 and Table D-8 for the peak efficiency case load, 0.250 water vapor content, 0.15 anode recirculation, 0.5 cathode recirculation and inlet temperature of 1300°F and 1003°F, respectively. The example shown is based on a fuel gas flow rate of one mole per second, and Figure D-39 illustrates the internal cell temperature distribution for this particular fuel cell.

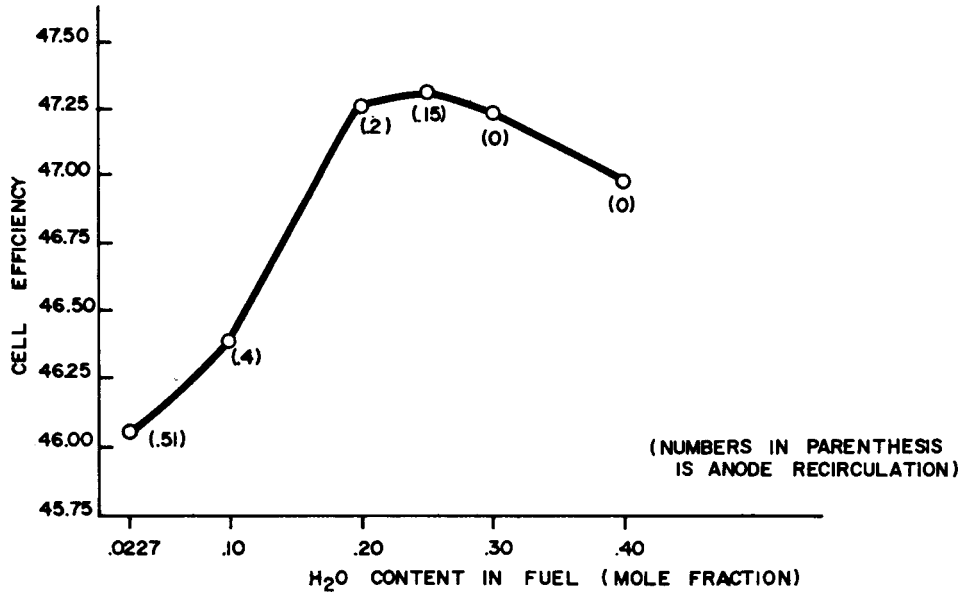

Figure D-37. Cell Efficiency vs. Water Vapor Content

Based on this observation that peak cell efficiencies occur over a relatively broad range of water vapor/anode recirculation conditions, it becomes advantageous to utilize those cell operating conditions which provide the best integration with

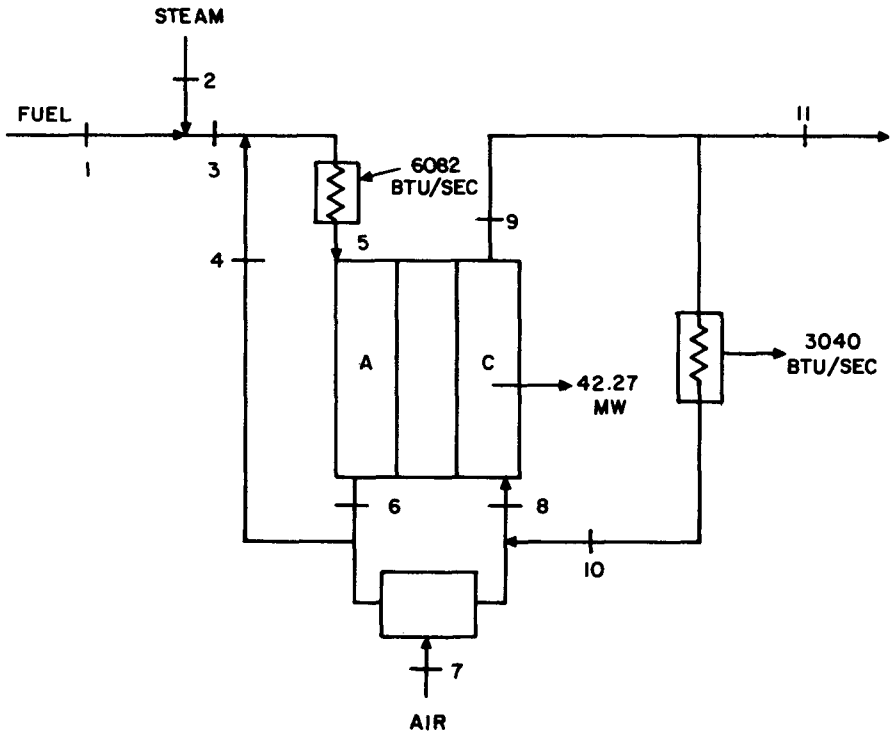

Figure D-38. Nodal Fuel Cell Model with Steam Injection

the overall plant system. These considerations should also extend to the impact of cell operating conditions on overall plant size and general impact on capital costs. In addition it should be recognized that each combination of cell operating parameters has a "margin" of operation limited by carbon formation and peak cell temperatures, and that this range of acceptable cell operating parameters will be important in the context of an integrated fuel cell plant.

In summary, the nodal fuel cell model has indicated that water vapor injection can be used either alone, or in conjunction with anode recirculation, as a means of preventing carbon formation at the anode inlet. The use of water vapor injection generally results in an increase in cell efficiency up to a value of approximately 0.30 water vapor, with peak efficiencies in the range of 0.20-0.30 water vapor, and anode recirculation of 0.2 or less.

Within this range of operating conditions, the peak cell efficiencies do not appear to be significantly different, and the choice of operating conditions should be based on overall systems considerations and economics, considering the impact on steam turbine and gas turbine outputs.

Table D-8

NODAL FUEL CELL MODEL WITH STEAM INJECTION SUBSYSTEM FLOW DATA

Stream Number	1	2	3	4	5	6	7	8	9	10	11
	Fuel	Steam	Fuel Mixture	Anode* Recirc.	Anode Inlet	Anode Exit	Air Inlet	Cathode Inlet	Cathode Exit	Cathode** Recirc.	Cathode System Exit
Temperature (^{o}F)	652	652	652	1043	1300	1043	485	1003	1270	1219	1270
Pressure psia	100	100	100	100	100	99	100	100	99	100	99
Gas Composition (Mole Fraction)											
CO	.5397		.442	.0265	.3292	.0265					
H_2	.3668		.2815	.0391	.2283	.0391					
CO_2	.0708		.0543	.6395	.1826	.6395		.1009	.0657	.0657	.0657
O_2							.210	.1532	.1420	.1420	.1420
N_2							.790	.6757	.7177	.7177	.7177
H_2O	.0227	1.00	.250	.2949	.2598	.2949		.0702	.0746	.0746	.0746
Flow (moles/sec)	.7675	.2325	1.00	.2808	1.2808	1.8722	6.475	15.1413	14.2543	7.1272	7.1271
Total Flow (#/sec)	14.87	4.19	19.06	9.63	28.69	64.18	186.80	447.27	411.66	205.83	205.83
Enthalpy Flow Btu/sec x 10^3	88.721	5.585	94.306	6.604	106.993	44.034	19.480	130.540	153.391	73.652	76.695

* Anode Recirculation Rate = 0.2802 ÷ 1.8722 = 0.15

** Cathode Recirculation Rate = 7.1272 ÷ 14.2543 = 0.50

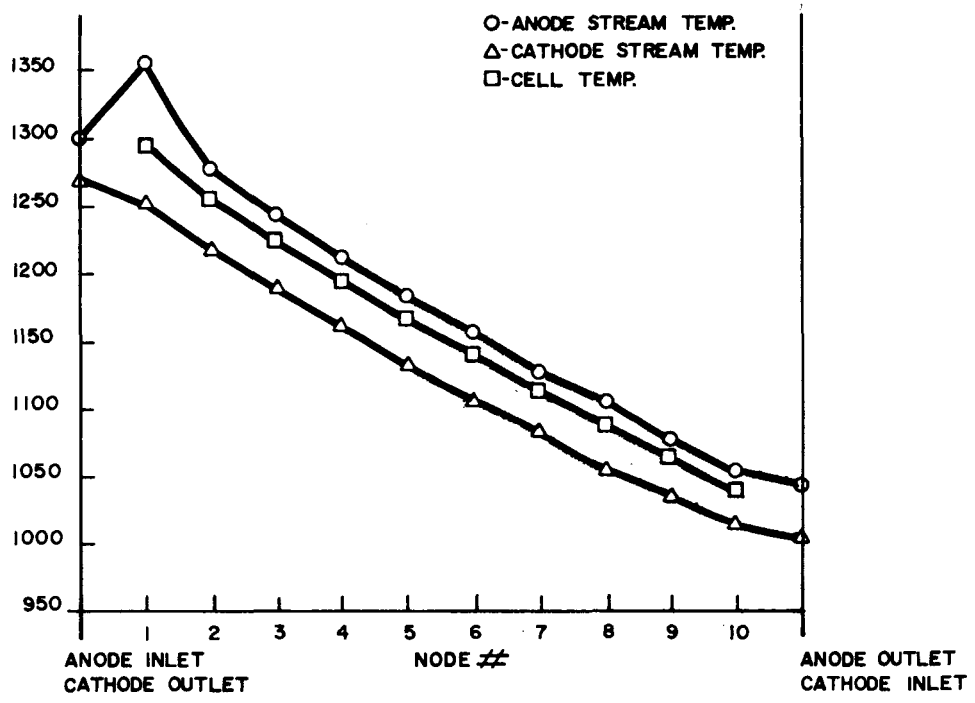

Figure D-39. Internal Cell Temperature Distribution

Appendix E

ALTERNATE OIL-FIRED MCFC POWER SYSTEM CYCLES

INTRODUCTION

Previous studies of the oil-fired MCFC cycle for dispersed power plant application, which have been conducted by General Electric under EPRI Contract (3-1) and (3-2), have defined conditions under which the EPRI performance goal of .455 ratio between fuel cell AC output and oil fuel HHV input might be obtained. These studies were based upon the cycle illustrated in Figure E-1 and were also based on certain assumptions regarding fuel cell performance, including the following:

- Polarization constant of fuel cell - .7 ohm/cm^2
- Fuel cell current density level - 161 mA/cm^2
- Fuel cell temp. - 130 ^oF
- Maximum H_2 and CO fuel util. = .85

Key parameters governing the system fuel cell output ratio were found to be the reformer fuel conversion ratio (HHV of CO and H_2 in product gas/HHV of oil fuel fired) and the fuel cell voltage; the efficiency ratio being proportional to the product of these two quantities. These parameters in turn were found to be closely related to the air/carbon and steam/carbon ratios at which the autothermal reformer is operated. If the reformer is assumed to operate in accordance with chemical equilibrium it was found that the reformer fuel conversion ratio increases as the air/carbon ratio decreases and that the reformer fuel conversion ratio is also influenced, to a lesser degree, by the steam/carbon ratio, increasing slightly with the latter ratio. Fuel cell voltage improves as air/carbon ratio and steam/carbon ratio decreases and as pressure increases.

Attainment of the .455 efficiency goal seems to require operation at air/carbon and steam/carbon ratios both in the vicinity of 1.5. On an equilibrium basis the principal constraint upon selection of the air/carbon and steam/carbon ratios is that this selection must be made at a carbon-free operation condition. In practice this

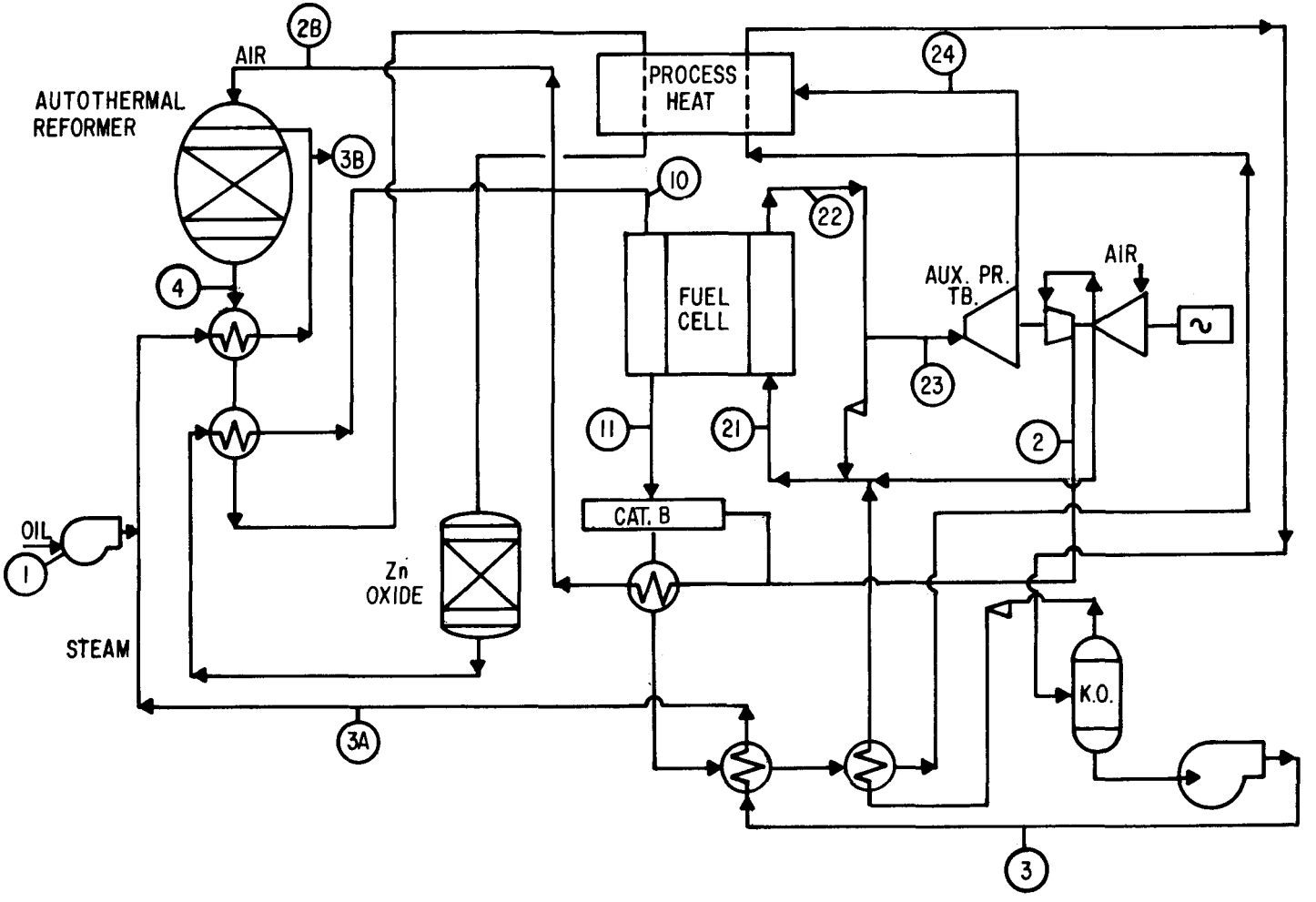

Figure E-1. Oil-Fired MCFC Power Plant Flow Stream Numbers

constraint is substantially more severe than that imposed by ideal chemical equilibrium operation. This is illustrated by Figure E-2, which indicates that autothermal reforming of No. 2 fuel oil is, at the present state-of-the-art, limited to operation at an air/carbon ratio not less than approximately 1.9. Also, indications are that operation at a minimal air/carbon ratio is improved, (with respect to chance of carbon, and with respect to close approach to equilibrium) by the use of a steam/carbon ratio of 2 or more. Reference (E-3) indicates that the most favorable operating condition achieved to date by JPL Investigators is that of air/carbon = 1.9, steam/carbon = 3.0. It is hoped both of these ratios can be reduced by further advancements in the state-of-the-art and, if so, the goal of .455 may be met.

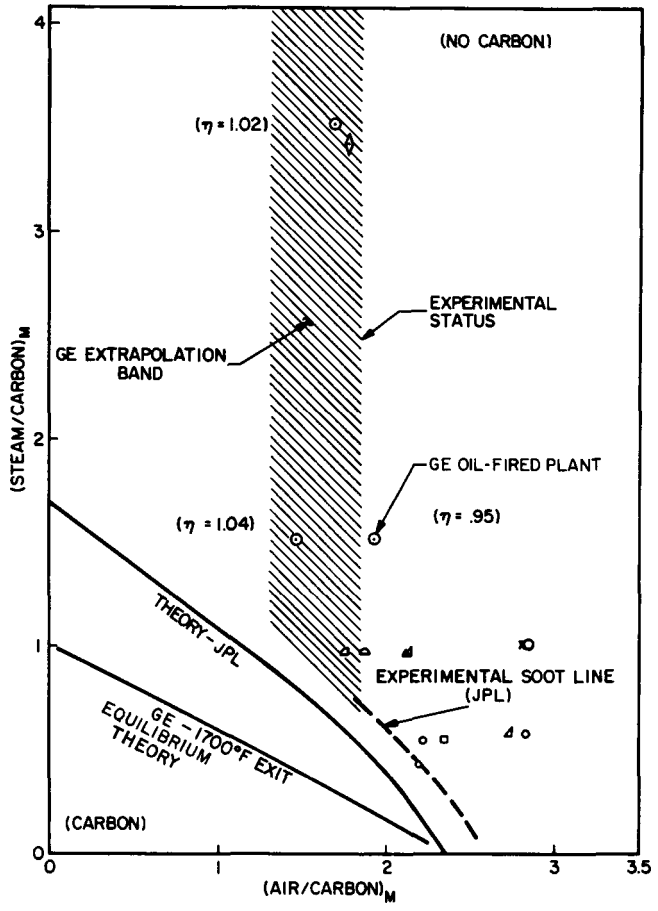

Figure E-2. Autothermal Reformer Soot Line

The work reported herein consists of the following:

- A different cycle design approach from that of the previous GE studies has been investigated in order to define new theoretical possibilities for achievement of high fuel cell performance in the oil-fired plant. Two alternate forms of a cycle employing an oil steam reformer thermally coupled by heat transfer to a combustor of anode discharge gas have been defined. This approach provides a much more effective feed-back of energy from the fuel cell anode discharge to the fuel processor than is provided by the cycle of Figure E-1. The result is a dramatic increase in the reformer fuel conversion ratio and in the ratio of fuel cell output to fuel heating value input.

  Although the No. 2 oil/steam reformer component required by this approach is not yet realizable as a practical device, these cycles indicate new levels of fuel cell and overall cycle efficiency which are theoretically achievable with No. 2 oil fuel, and which may be, at the present state of the steam reforming art, actually achievable with methane and light hydrocarbon fuels.

  Theoretical fuel cell efficiency ratios and overall cycle efficiency ratios in excess of .50 and .60, respectively, are indicated for this approach with No. 2 oil fuel.

- Parametric analysis of the autothermal reformer cycle has been conducted to show both theoretical and practical limits upon efficiency, and has been expanded to include electrical output of the gas turbine generator in addition to the fuel cell output. The purpose here is to evaluate the tradeoffs between the gains from operating at difficult reformer conditions which can potentially provide peak fuel cell performance and the gains in gas turbine performance which can be achieved by operating the reformer at less critical values of the air/carbon and steam/carbon ratios. This approach shifts the focus of attention to the overall cycle performance as opposed to the previous concentration on the performance of the fuel cell alone.

  The results of this analysis indicate that overall cycle efficiency ratios above 55% can be achieved at autothermal reformed operating conditions which are comfortably within the state-of-the-art. The results also show that, although an approximate 3 1/2 point gain in fuel cell efficiency ratio is theoretically achievable through reduction in reformer air/carbon ratio from 1.9 to 1.5, the overall cycle gain achievable is approximately 2 points, because of compensation loss in gas turbine output.

STUDY OBJECTIVES

The objectives of the study presented herein are the following:

- Definition and evaluation of an advanced oil-fired molten carbonate fuel cell power plant cycle which has a theoretical capability for

a substantially higher fuel cell output ratio than that provided by cycles similar to Figure E-1 which employ an autothermal reformer type of fuel processor. The salient feature of this advanced cycle is a steam reformer for No. 2 oil which is thermally coupled to an anode discharge gas-fired combustor.

Two variations of this theoretical cycle have been defined. One of these provides a maximum fuel cell output ratio, and the other provides maximum efficiency of the overall system including the bottoming cycle gas turbine generator.

- Evaluation of the efficiency potential of a practical oil-fired MCFC power plant cycle, incorporating an autothermal reformer fuel processor, and of the limitations, upon this potential which are imposed by the differences between theoretical and practical state-of-the-art constraints upon operating parameters. As in the case of the theoretical cycle the practical cycle evaluation considers both fuel cell output ratio limits and overall cycle efficiency limits which include the contribution of the bottoming cycle gas turbine.

THEORETICAL CYCLE EMPLOYING A NO. 2 FUEL OIL/STEAM REFORMER

The conceptual advantages of a steam reformer fuel processor over an air-blown autothermal reformer include the following:

- The chemical energy of the unburned fuel in the anode discharge stream can be utilized in a combustor which is thermally coupled to the reformer to supply the heat required by the reforming reaction. By means of the reforming process the heating value content of the reformed fuel ($CO + H_2$) which is available at the anode inlet is made substantially higher than the heating value content of the oil fuel feed. Thus the fuel which is available for electrochemical reaction is higher than that which can be provided by an autothermal reformer fuel processor for which the heating value content of the reformed fuel is slightly less than, or at best equal to, the heating value content of the oil supply.

- The steam reformer product gas has higher concentrations of H_2 and CO than does the air-blown autothermal reformer product which suffers from N_2 dilution. This results in higher fuel cell voltage, and output ratio, at a given level of current density.

  Thermal energy liberated in the combustor in excess of that required by the reforming reaction is available for conversion in the bottoming cycle, just as in the case of the autothermal reformer cycle which utilizes a catalytic combustor downstream of the fuel cell anode.

For these reasons the steam reformer oil-fired cycle has a theoretical potential for higher efficiency than the practical autothermal reformer cycle. The following section of the report is directed toward definition and parametric analysis of the steam reformer cycle approach.

Steam Reforming Reference Cycle A

The first "theoretical" cycle is shown in Figure E-3. Flow stream quantities and composition breakdowns are shown in Table E-1. In this cycle the oil fuel processor is a stream reformer to which heat is transferred from a closely integrated anode discharge gas combustor. With this arrangement chemical energy in the anode discharge stream is added to the chemical energy of the oil fuel through the reforming reactions so as to produce a reformer product with a H_2+ CO heating value content substantially higher than the heating value of the oil fuel fed to the reformer. In this manner the heating value content of the electrochemically reacted fuel is maximized.

Principal components of the system are the integrated reformer-combustor fuel processor, the fuel cell, and the pressurizing gas turbine. Steam for the reformer is generated by heat exchange with turbine discharge gas, is then mixed with heated oil and the steam-oil mixture is further heated in a special preheater by anode discharge gas, and then by reformer combustor discharge gas. Anode discharge gas is cooled by heat transfer with the steam/oil mixture and also by regenerative heat exchange with the same (anode disch.) stream returning from a dehumidifying cooler. The dehumidified anode discharge gas is then passed to the reformer combustor through a regenerative heat exchanger coupled to the reformer product gas stream. Reformer product gas is passed to the anode inlet through two regenerative heat exchangers, a feed water heater, and a ZnO scrubber. Combustor discharge gas is cooled in the steam/oil and air preheater heat exchangers and is then passed to the cathode inlet where it is mixed with air from the gas turbine compressor. This mixed stream is heated to a temperature of 109 ^{o}F by mixture with recirculated cathode discharge gas. The net cathode discharge stream is passed to the gas turbine inlet.

The reference Cycle A energy balance summary is presented in Table E-2. Heat extracted from the anode discharge stream in the temperature range of 100 ^{o}F to 265 ^{o}F can be used for process heating if a suitable cogeneration application is available. Also, additional process heat at a maximum temperature of 380 ^{o}F is available from the HRSG discharge stream.

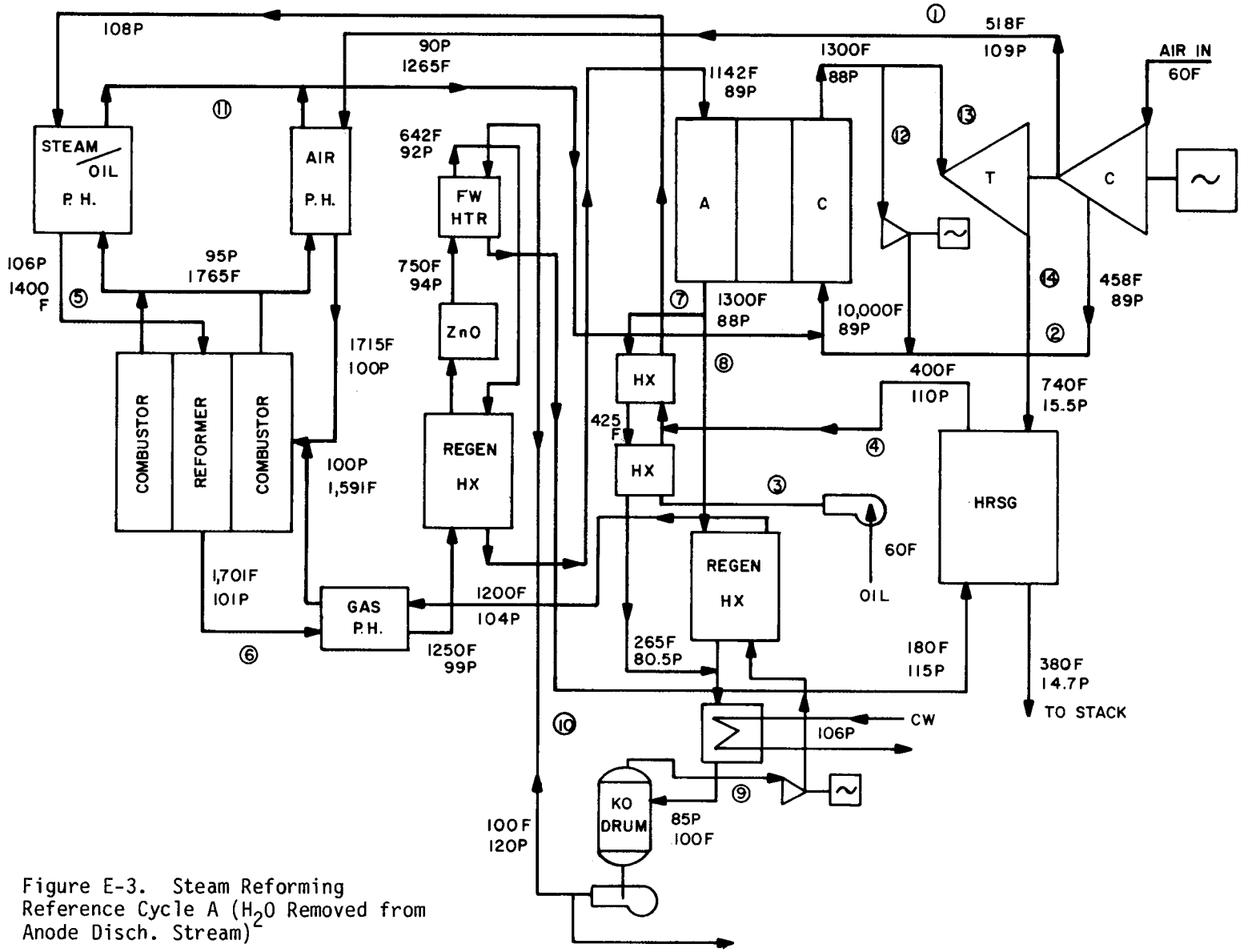

Figure E-3. Steam Reforming Reference Cycle A (H_2O Removed from Anode Disch. Stream)

TABLE E-1

STEAM REFORMER REF CYCLE A (Fig. E-3)
Flow Stream Compositions

Flow Stream	Description	#/mole inlet gas	Total mole/mole inlet gas	Mole/mole of Total Inlet Gas						
				O_2	N_2	H_2	CO	CH_4	CO_2	H_2O
1	Air to Reformer Combustor		0.4466	0.0938	0.3528					
2	Air to Cathode		3.4094	0.7160	2.6934					
3	Oil to Heat Exchanger	3.161								
4	Steam to Heat Exchanger	10.351								
5	Steam/Oil Mixture to Reformer	13.513								
6	Reformer Gas to Anode		0.9998			0.4910	0.1620	0.0010	0.0668	0.2790
7	Anode Discharge A		0.7420			0.364	0.2330	0.0004	0.2328	0.2394
8	Anode Discharge B		0.9541			0.651	0.0418	0.0006	0.4174	0.4292
9	Anode Discharge C		0.8265			0.1015	0.0651	0.0010	0.6500	0.0089
10	Feedwater	10.351								
11	Reformer Combustor Discharge		1.1901	0.0085	0.3528				0.7164	0.1124
12	Cathode Recycle		3.9200	0.4918	3.0860				0.2298	0.1124
13	Turbine Inlet Gas		3.9200	0.4918	3.0860					
14	Turbine Discharge Gas		3.9200	0.4918	3.0860				0.2298	0.1124

Table E-2

STEAM REFORMER REF CYCLE A
Cycle Energy Balance

Oil HHV Input			1.0
FC DC Output		.539	
Gas Turbine Shaft Output		.096	
Water Removal Heat Loss		.236	
Stack Loss		.129	
		1.000	1.00
FC AC Output	.528		
Gas Turbine Gen AC Output	.094		
Gross Electrical Output	.622		
Estimated Parasitic Power	.02		
Net Electrical Output	.612		

As indicated by Table E-2 the fuel cell AC output ratioed to the oil HHV input is .528 and the gas turbine generator output ratio is .094. After subtraction of estimated parasitic losses of .01, the net electrical output is .612.

Steam Reforming Reference Cycle B

The second "theoretical" cycle is shown in Figure E-4. Flow stream quantities and composition breakdowns are shown in Table E-3. This cycle differs from that of Figure E-3, principally by the absence of the dehumidifying heat exchanger train in the anode discharge stream. Because of this the fuel cell is forced to operate at a lower anode fuel utilization in order to supply sufficient heating value content in the anode discharge streams to heat up the water vapor in the anode discharge to the final combustion temperature. This reduces the fuel cell output ratio. However, this effect is more than offset by increased gas turbine output resulting from the presence of the water vapor mass flow in the turbine.

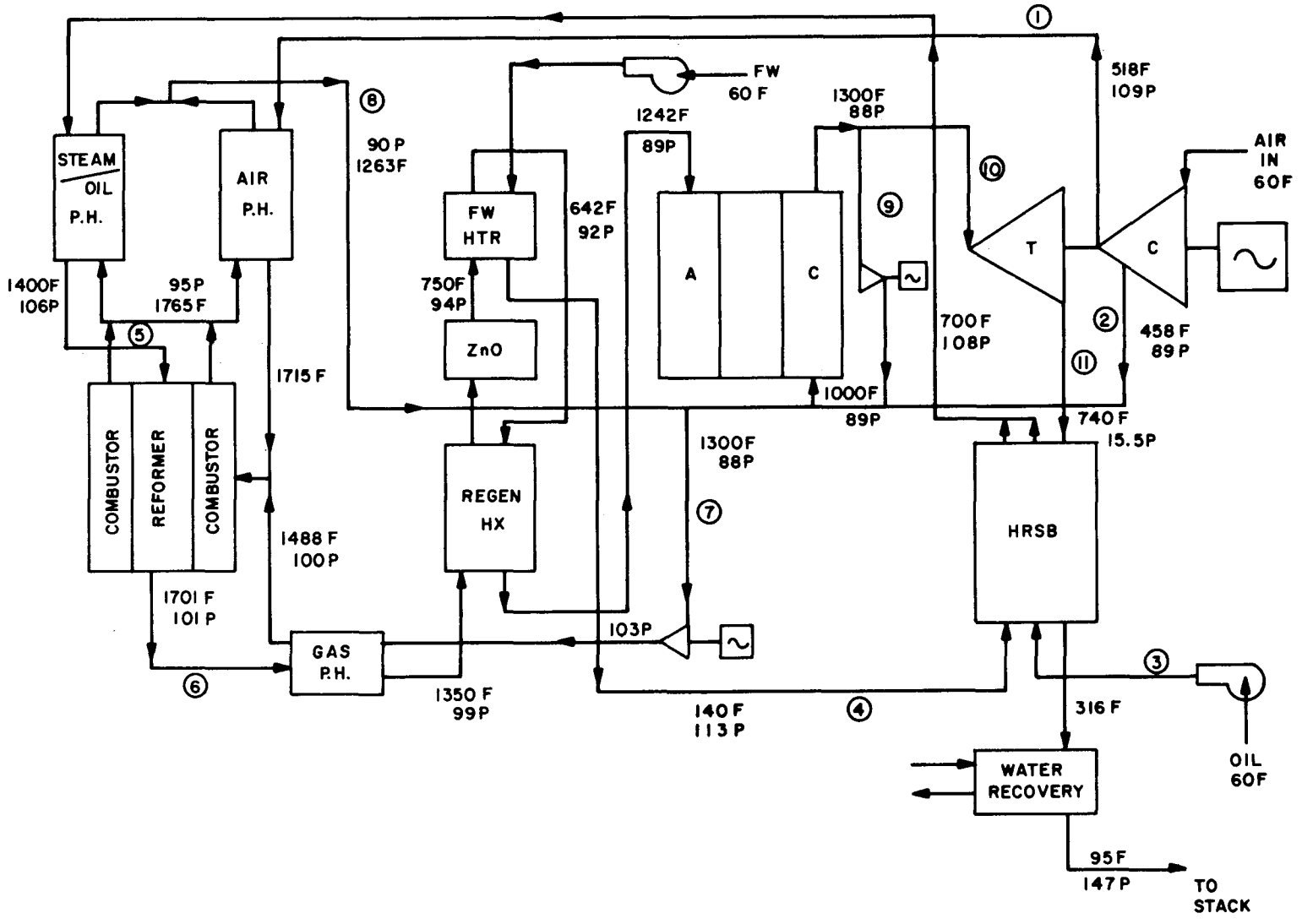

Figure E-4. Steam Reforming Reference Cycle B
(H_2O Not Removed From Anode Disch. Stream)

TABLE E-3

STEAM REFORMER REF CYCLE B (Fig. E-4)
Flow Stream Compositions

Flow Stream	Description	#/mole inlet gas	Total mole/mole inlet gas	Mole/mole of Total Inlet Gas O_2	N_2	H_2	CO	CH_4	CH_2	H_2O
1	Air to Reformer Combustor		0.51336	0.1078	0.4056					
2	Air to Cathode		2.8973	0.6084	2.2889					
3	Oil to Heat Exchanger	3.162								
4	Feedwater to Heat Exchanger	10.351								
5	Steam/oil Mixture to Reformer	13.513								
6	Reformer Gas to Anode		0.9999			0.4911	0.1620	0.0010	0.0668	0.2790
7	Anode Discharge		1.4610			0.1183	0.0737	0.0010	0.6162	0.6518
8	Reformer Combustor Discharge		1.8783	0.0098	0.4056				0.6909	0.7720
9	Cathode Recycle		2.3857	.2265	1.5739				0.1343	0.4510
10	Turbine Inlet Gas		4.0835	0.3877	2.6940				0.2298	0.7720
11	Turbine Discharge		4.0835	0.3877	2.6940				0.2298	0.7720

The cycle energy balance is summarized in Table E-4. The fuel cell output ratio is .50 and the gas turbine generator output is .147. After subraction of estimated parasitic losses of .023, the net electrical output is .614.

Some process heat is potentially available from the HRSG discharge stream. Water recovery for supply of steam to the reformer is effected in this system by water spray cooling/condensing of the HRSG discharge.

Table E-4

STEAM REFORMING REF CYCLE B
Cycle Energy Balance

Oil HHV Input		1.00
FC DC Output	.51	
Gas Turbine Shaft Output	.15	
Stack Loss	.34	
	1.00	1.00

FC AC Output	.50
Gas Turbine Gen AC Output	.147
Gross Output	.647
Estimated Parasitic Power	.023
Net AC Output	.624

Steam Reforming Cycle Parametric Analysis

In Figures E-5 through E-12 the results of a parametric study of fuel cell output ratio, $\frac{\text{fuel cell AC output}}{\text{oil fuel HHV input}}$ for a cycle having the configuration shown in Figure E-3 are presented. Since this ratio is proportional to the product of reformer energy conversion ratio $\frac{\text{CO \& } H_2 \text{ product HHV}}{\text{oil HVV}}$, fuel cell ($CO + H_2$) utilization, and fuel cell voltage, the variation of fuel cell output ratio can be explained by variation of the other three parameters. These four parameters are

presented as functions of the reforming temperature and reformer steam/carbon ratio in Figures E-5, E-6, E-7 and E-8 (based on six atmospheres fuel cell pressure) and in Figures E-9, E-10, E-11, and E-12 (based on three atmospheres pressure).

Reformer fuel conversion ratio improves with increasing reformer temperature and with increasing steam/carbon ratio, since increases in these parameters promote completion of the reforming reactions. Fuel cell voltage improves with reforming temperature as a result of increasing hydrogen concentration in the product gas. Voltage also improves as steam/carbon ratio is dropped, except for the case of steam/carbon = 1.5, for which it is necessary to use anode recirculation to avoid carbon formation.

However, the effects of increasing reforming temperature and steam/carbon ratio on reformer fuel conversion ratio are offset by a reverse effect on fuel cell H_2 + CO utilization which drops as temperature and steam/carbon ratio are increased. As temperature and S/C are increased it is necessary to fire more fuel in the reformer combustor; thus less fuel is available for electrochemical reaction in the fuel cell itself. Also, at lower temperatures the anode discharge gas contains more CH_4 which can be used as combustor fuel, and the CO and H_2 are conserved for electrochemical conversion.

The overall result, shown in Figures E-6 and E-10, is that the theoretical fuel cell output ratio increases as reforming temperature is reduced in the range of $1400^{o}F$-$1700^{o}F$. The fuel cell output ratio is relatively insensitive to steam/carbon ratio, except where this ratio is so low that anode recirculation is necessary to prevent carbon at the anode inlet. Fuel cell output ratio is increased with a change in pressure from 3 to 6 atmospheres as a result of improved fuel cell voltage.

All of the above results are based upon operation of the steam reformer in accordance with chemical equilibrium. Close approach to such performance in a #2 fuel oil/steam reformer (through future development) is more promising at relatively high temperature level. This reasoning has guided the selection of reference Cycles A and B at a reforming temperature of $1700\ ^{o}F$, although better theoretical performance is indicated by the parametric analysis at lower reforming temperatures.

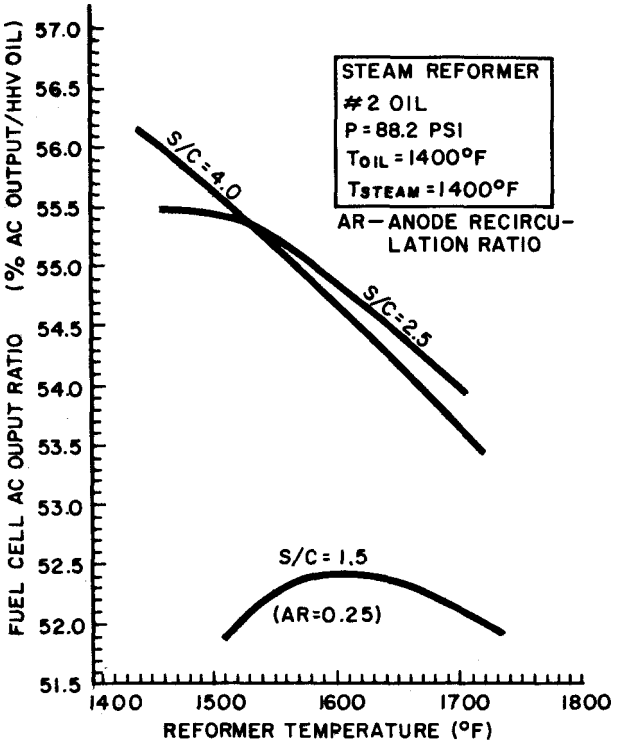

Figure E-5. Fuel Cell AC Output Ratio vs. Reformer Temperature and Steam/Carbon (S/C) Ratio

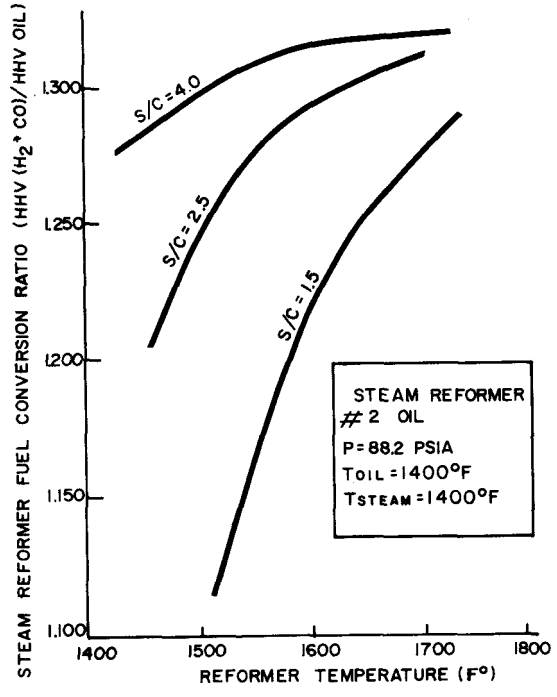

Figure E-6. Steam Reformer Fuel Conversion Ratio vs. Reformer Temperature and Steam/Carbon (S/C) Ratio

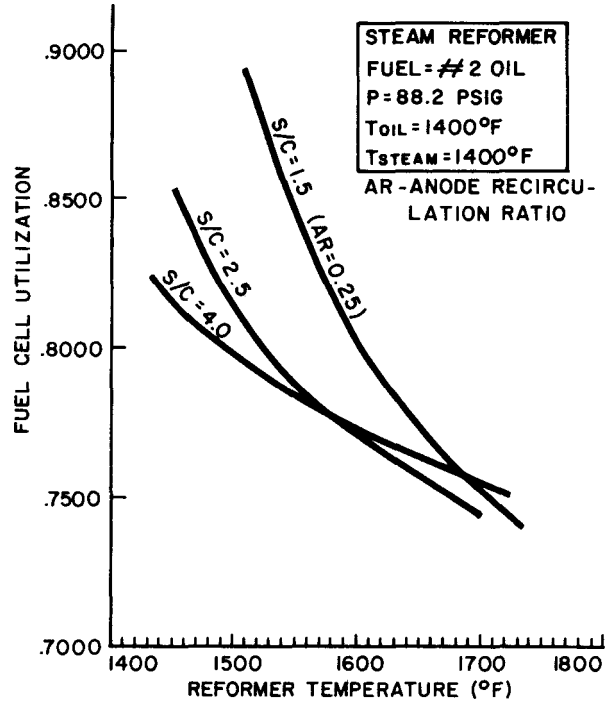

Figure E-7. Fuel Cell Utilization vs. Reformer Temperature and Steam/Carbon (S/C) Ratio

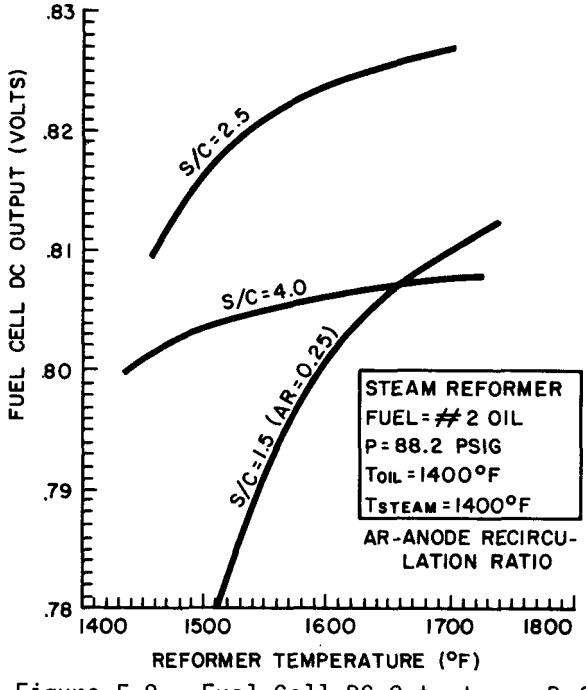

Figure E-8. Fuel Cell DC Output vs. Reformer Temperature and Steam/Carbon (S/C) Ratio

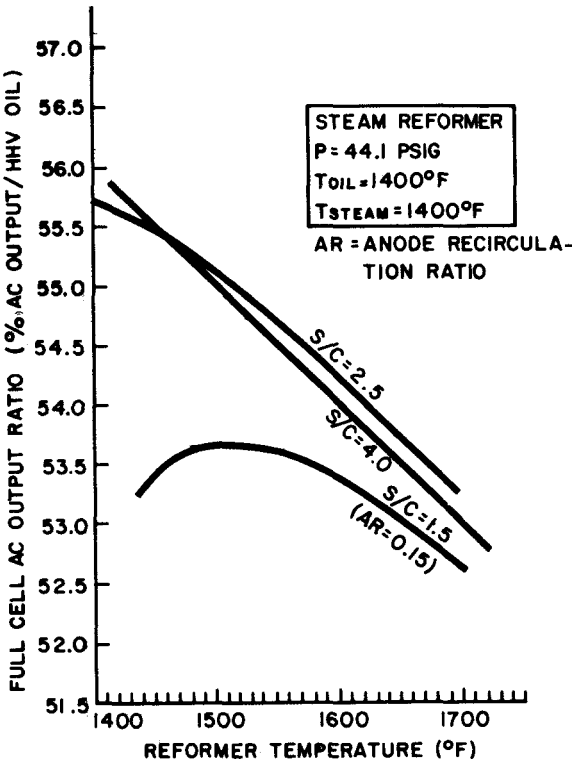

Figure E-9. Fuel Cell AC Output Ratio vs. Reformer Temperature and Steam/Carbon (S/C) Ratio

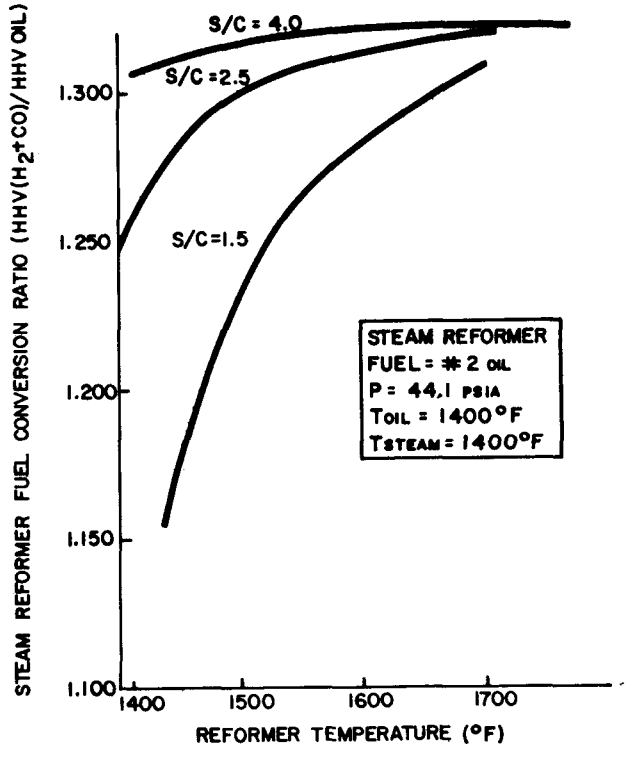

Figure E-10. Steam Reformer Fuel Conversion Ratio vs. Reformer Temperature and Steam/Carbon (S/C) Ratio

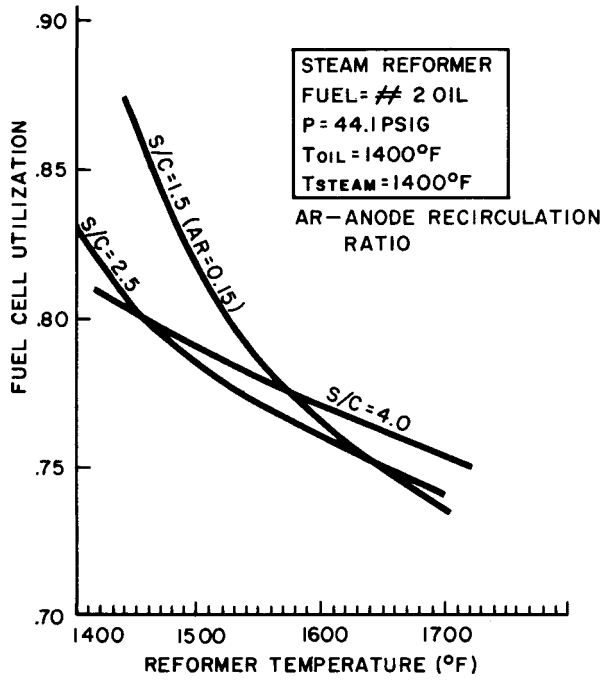

Figure E-11. Fuel Cell Utilization vs. Reformer Temperature and Steam/Carbon (S/C) Ratio

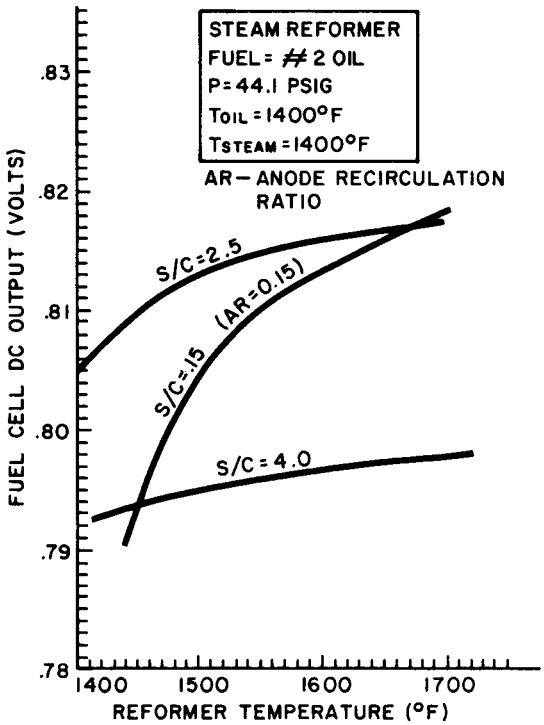

Figure E-12. Fuel Cell DC Output vs. Reformer Temperature and Steam/Carbon (S/C) Ratio

AUTOTHERMAL REFORMER CYCLES

The autothermal reformer cycle ("practical cycle") is shown in Figure E-13. Flow stream quantities and composition breakdowns are shown in Table E-5. In this cycle the autothermal reformer fuel processor is supplied with a steam/oil mixture heated in a HRSG behind the gas turbine, and by regenerative heat transfer with the ATR product gas. Air is also supplied to the ATR from the gas turbine compressor and is preheated by heat transfer with the catalytic combustor discharge stream. A regenerative heat exchanger, ZnO Scrubber and feedwater heater are employed in the reformer discharge gas stream flowing to the anode in the same manner as in the previously described cycles.

In this reference cycle the ATR operates at state-of-the-art levels of air/carbon and steam/carbon ratios (1.9 and 3.0). The system energy balance is summarized in Table E-6. The fuel cell output ratio is .417 and the gas turbine-generator output is .164. Net electrical output after subtraction of estimated parasitic powe of .015 is .566. Water recovery for generation of reformer steam is accomplished by spray cooling/condensing of the HRSG discharge stream.

Autothermal Reformer Parametric Analysis

Parametric analysis of the autothermal reformer cycle has been conducted in accordance with three different procedures:

(1) The plant efficiency has been evaluated as a function of ATR air/carbon and steam/carbon ratios for cycle pressure ratios of 3 and 6. This analysis is based on operation of the ATR in accordance with chemical equilibrium.

(2) The plant efficiency has been evaluated in a manner similar to (1) above except that differences resulting from ATR operation with a 100 ^{o}F approach to equilibrium as opposed to equilibrium operation have been calculated. This has been done for a steam/carbon ratio of 1.5 over a range of air/carbon ratio from 1.5 to 1.8.

(3) The ATR reference cycle efficiency has been evaluated as a function of pressure ratio. Fixed parameters of this cycle are air/carbon = 1.9, steam/carbon = 3.0, and steam/oil/air preheat temperature = 1400 ^{o}F.

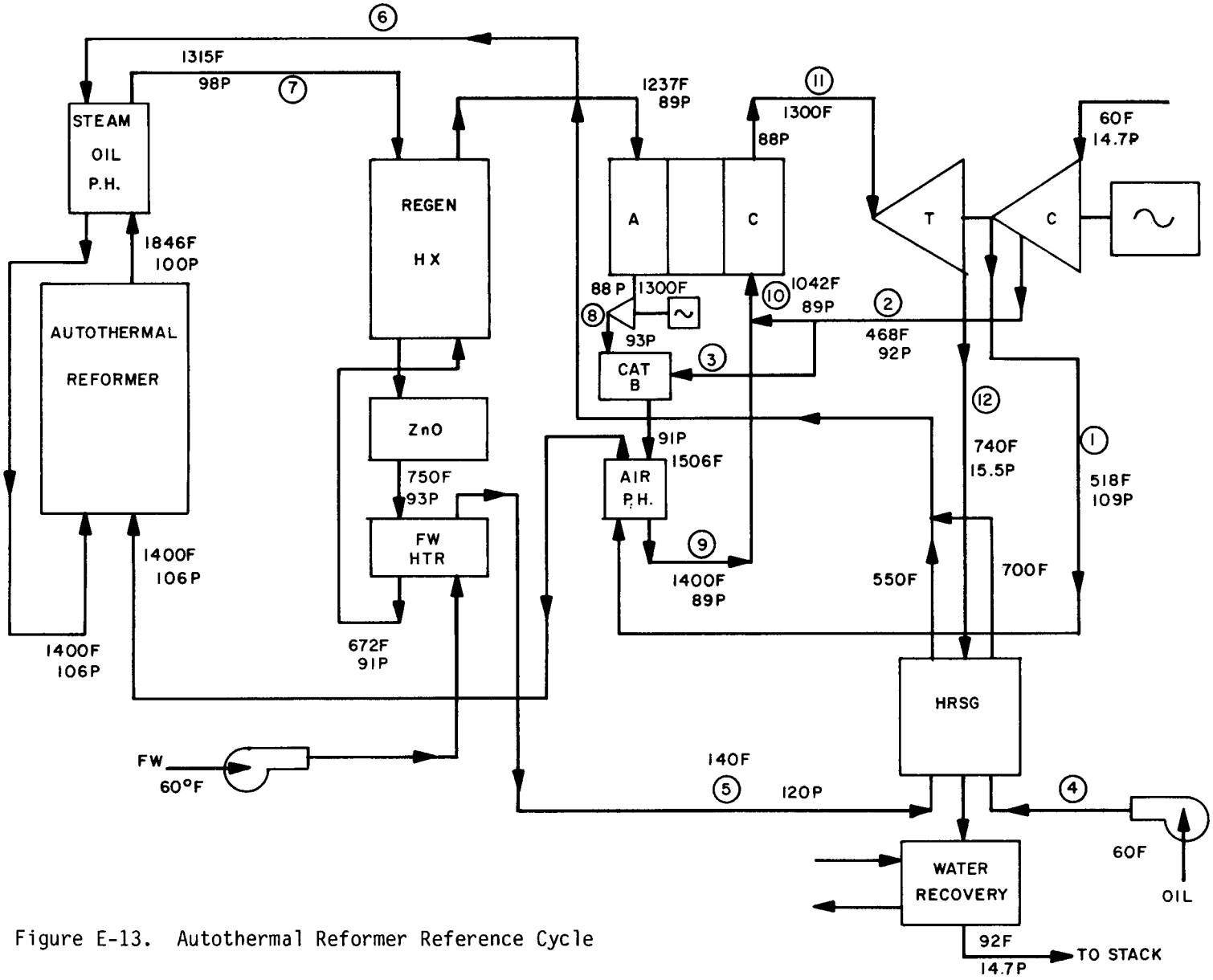

Figure E-13. Autothermal Reformer Reference Cycle

TABLE E-5

AUTOTHERMAL REFORMER CYCLE (Fig. E-5)
Flow Stream Compositions

Flow Stream	Description	#/mole inlet gas	Total mole/mole inlet gas	Mole/mole of Total Inlet Gas O_2	N_2	H_2	CO	CH_4	CO_2	H_2O
1	Air to Reformer		0.3000	0.0630	0.2370					
2	Air to Cathode		1.5920	0.3343	1.2577					
3	Air to Catalytic Combustor		0.7598	0.1596	0.6002					
4	Oil to Heat Exchanger	2.163								
5	Feedwater to Heat Exchanger	8.496								
6	Steam/Oil Mixture to Reformer	10.659								
7	Reformer Gas to Anode		0.9974		0.2340	0.2403	0.0825	0.00001	0.0745	0.3661
8	Anode Discharge		1.2717		0.2340	0.03277	0.01565	0.00001	0.4157	0.5736
9	Catalytic Combustor Discharge		1.2717	0.1355	0.8348				0.4314	0.6064
10	Cathode Inlet		3.5995	0.4697	2.0920				0.4314	0.6064
11	Turbine Inlet		3.1929	0.3375	2.0920				0.1570	0.6064
12	Turbine Discharge		3.1929	0.3375	2.0920				0.1570	0.6064

Table E-6

AUTOTHERMAL REFORMER
Cycle Energy Balance

Oil HHV Input			1.00
FC DC Output		.426	
Gas Turbine Shaft Output		.167	
Stack Loss		.407	
		1.00	1.00
FC AC Output	.417		
Gas Turbine Gen AC Output	.164		
Gross Electrical Output	.581		
Estimated Parasitic Power	.015		
Net Plant Output	.566		

Results of the analysis described in paragraph (1), page E-18, are presented in Figures E-14 through E-25. These figures show the following:

- Autothermal reformer fuel conversion ratio, $\frac{\text{HHV of CO + } H_2 \text{ product}}{\text{HHV of oil fuel}}$ increases as air/carbon ratio is reduced and, to a minor degree, as steam/carbon ratio is increased in the range of 1.5 to 3.0. At the lowest value of steam/carbon ratio, 1.5, performance improves as pressure is reduced in the range of 3 to 6 atmospheres because a lower anode recirculation rates is required to prevent carbon formation at the the anode inlet.

- The fuel cell output ratio increases as air/carbon ratio and steam-carbon ratio decrease to limits at which anode recirculation is required to prevent carbon formation subject to the carbon formation limit. These effects result from the effect of air/carbon ratio on reformer fuel conversion, and from increases in fuel cell voltage resulting from increased hydrogen concentration (reduced concentration of inert species), and from increased pressure.

- The bottoming cycle gas turbine output ratio increases as air/carbon and steam/carbon ratios are increased. This is a compensating effect to the trends stated above for fuel cell output. It results from the increase in turbine mass flow and from increased heat input

to the bottoming cycle as fuel cell output is reduced. Gas turbine output, however, like fuel cell output, increases with pressure in the range of 3 to 6 atmospheres.

- The overall cycle efficiency increases as air/carbon ratio and steam-carbon ratio are reduced. However, the effect on the overall cycle is substantially less than the effect on the fuel cell alone, because of the compensating influence of the reversed trend of gas turbine output. Overall cycle efficiency, as shown in Figures E-17, E-21, and E-25, does not include system auxiliary power.

- Overall cycle efficiency increases with pressure level in the range of 3 to 6 atmospheres. This results from the favorable effects of increased pressure on both fuel cell and gas turbine.

- At air/carbon and steam/carbon ratios of approximately 1.5, pressure 6 atmospheres, fuel cell output ratios in excess of the goal of .455 can be theoretically attained. Corresponding values of overall cycle efficiency, before parasitic power, are in excess of .60. An increase in air/carbon ratio from 1.5 to 1.9 and an increase in steam/carbon ratio from 1.5 to 3.0 results in about a 2 point loss in overall cycle efficiency.

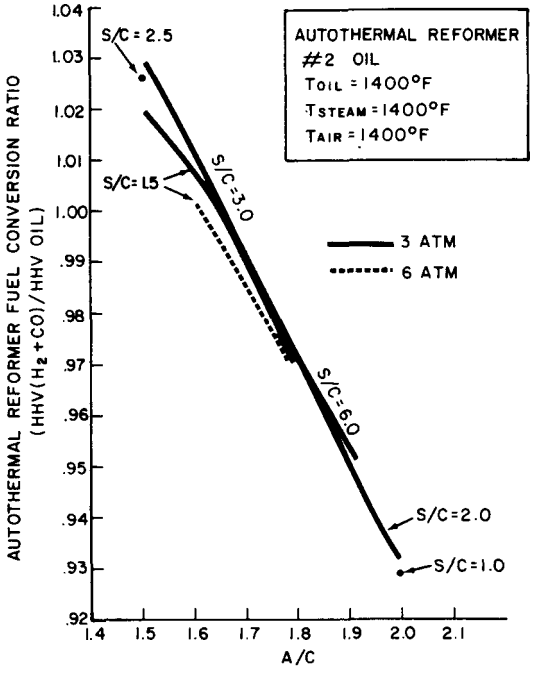

Figure E-14. Autothermal Reformer Fuel Conversion Ratio vs. Air/Carbon (A/C) Ratio, Steam/Carbon (S/C) Ratio, and Cycle Pressure

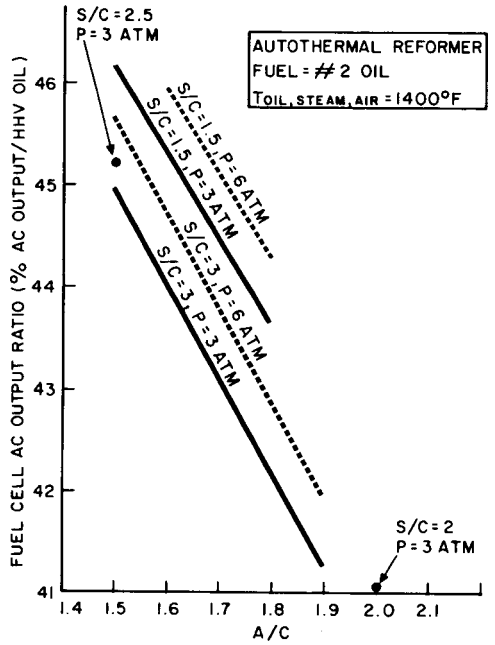

Figure E-15. Fuel Cell AC Output Ratio vs. Air/Carbon (A/C) Ratio, Steam/Carbon (S/C) Ratio, and Cycle Pressure

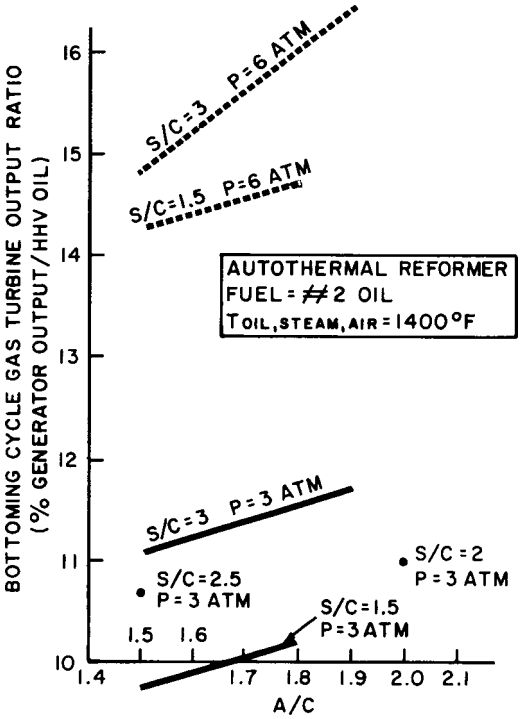

Figure E-16. Bottoming Cycle Gas Turbine Output Ratio vs. Air/Carbon (A/C) Ratio, Steam/Carbon (S/C) Ratio, and Cycle Pressure

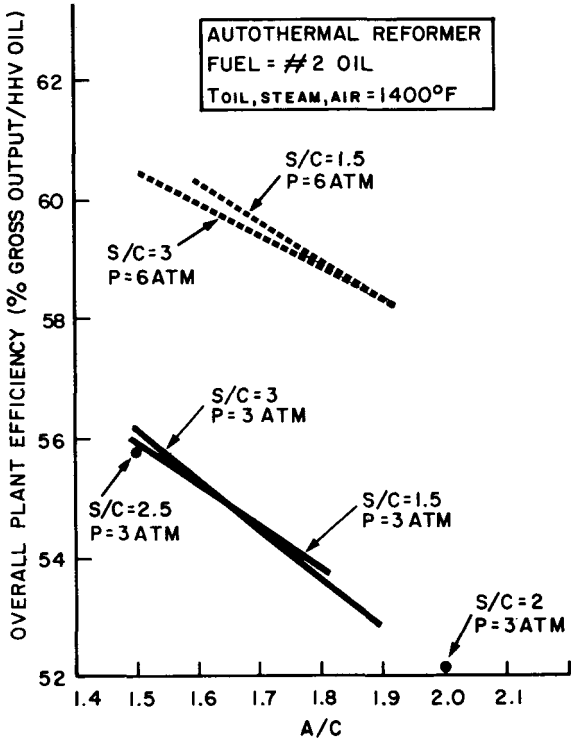

Figure E-17. Overall Plant Efficiency vs. Air/ Carbon (A/C) Ratio, Steam/Carbon (S/C) Ratio, and Cycle Pressure

Results described in paragraph (2), page E-18, are presented in Figures E-18 through E-21. These figures shows the following:

- At a steam/carbon ratio of 1.5, air/carbon ratio of 1.5, the loss in reformer fuel conversion ratio resulting from 100 ^{o}F approach to equilibrium is approximately 2 points at a pressure of 3 atmospheres and 2.5 points at 6 atmospheres. The corresponding drops in fuel cell output ratio are approximately .75 points and 1.0 point.
- Performance loss due to 100 ^{o}F approach to equilibrium decreases as air/carbon ratio increases. The loss is negligible at an air/carbon ratio of 1.8 or higher.
- Approach to equilibrium operation results in a small increase in gas turbine output which partially cancels the effect on fuel cell output.

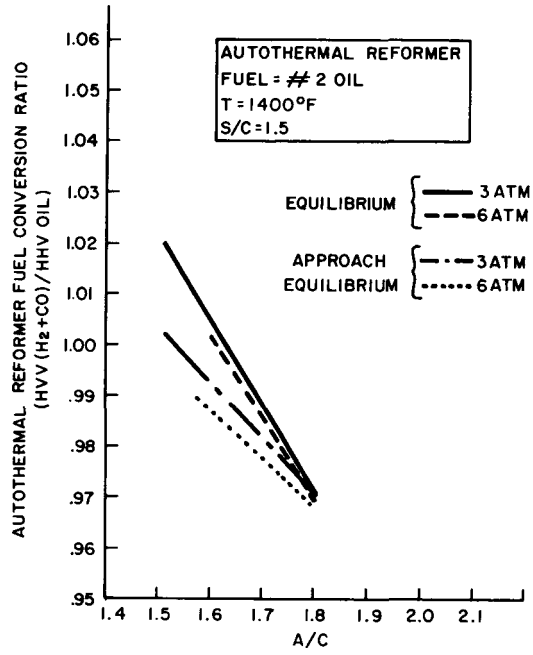

Figure E-18. Autothermal Reformer Fuel Conversion Ratio vs. Air/Carbon (A/C) Ratio, and Cycle Pressure

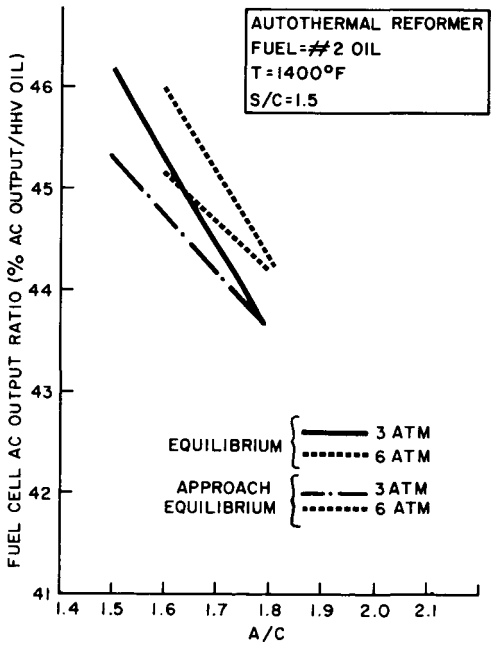

Figure E-19. Fuel Cell AC Output Ratio vs. Air/ Carbon (A/C) Ratio, and Cycle Pressure

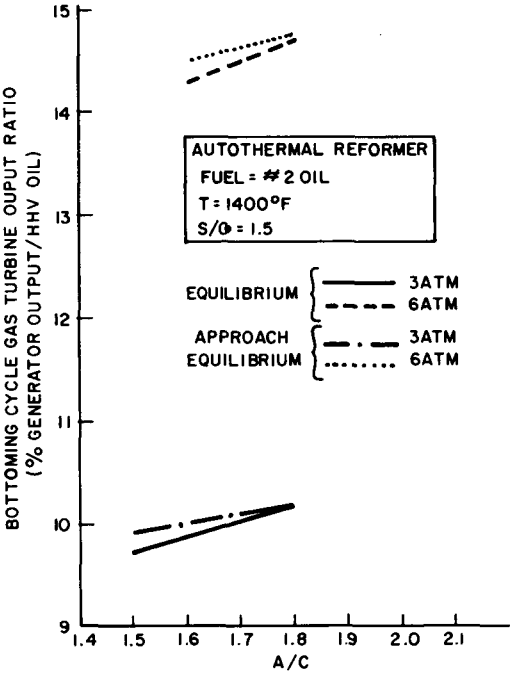

Figure E-20. Bottoming Cycle Gas Turbine Output Ratio vs. Air/Carbon (A/C) Ratio, and Cycle Pressure

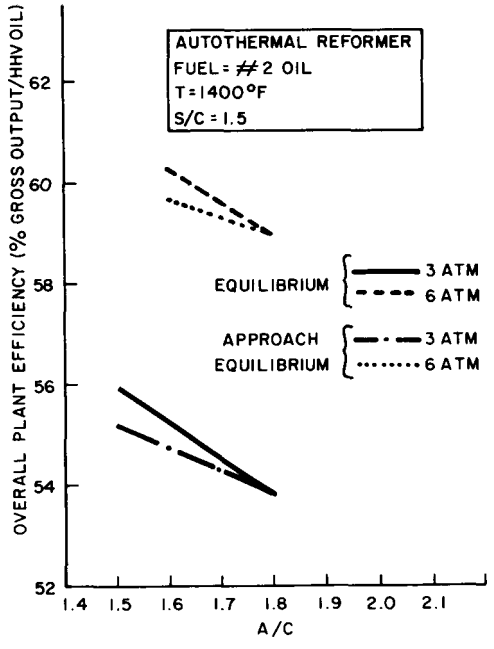

Figure E-21. Overall Plant Efficiency vs. Air/Carbon (A/C) Ratio, and Cycle Pressure

Results of the analysis described by (3) above are presented in Figures E-22 through E-25. These figures show that the fuel cell output and the overall cycle efficiency increase with pressure in the range of 3 to 12 atmospheres. However, the rise in efficiency above a pressure of 6 atmospheres is very small. This results both from the effect of pressure on fuel cell voltage and from the effect of pressure on cycle excess air ratio and gas turbine output. Cycle excess air is shown to peak at a level of 205% at a pressure of 6 atmospheres. Above this pressure gas turbine output falls, although fuel cell output continues to rise. With the ATR cycle at air/carbon = 1.9 and steam/carbon = 3.0 carbon formation at the fuel cell anode inlet does not occur at any pressure level below 16 atmospheres.

CONCLUSIONS

Conclusions derived from the study results may be summarized as follows:

- The steam reforming cycle offers a theoretical potential for oil fired MCFC power plant efficiencies in the range of 60 to 65%, with 50 to 56% obtainable from the fuel cell above. The theoretical efficiency potential is highest at relatively low levels of reforming temperature (1300 ^{0}F-1400 ^{0}F).

- Maximum fuel cell output ratio is obtained with a steam reforming cycle in which the anode discharge gas is dehumidified before supply to the reformer combustor. However, maximum overall plant efficiency is obtained with a cycle in which water vapor in the anode discharge is retained for expansion in the bottoming cycle gas turbine.

- The current state-of-the-art autothermal reformer cycle is capable of providing an overall practical cycle efficiency of 58% before auxiliary power if full advantage is taken of attainable gas turbine generator output, utilizing high efficiency turbomachinery.

- The autothermal reformer cycle efficiency increases sharply with increasing pressure in the range of 3 to 6 atmospheres, and increases only slightly with pressure above 6 atmospheres.

- Although significant gains in fuel cell output ratio (3 to 4 pts) are theoretically achievable by reduction of reformer A/C ratio from 1.9 to 1.5, and superimposed smaller gains are achievable by reduction of S/C ratio from 3 to 1.5, the corresponding potential overall plant efficiency gains are less (2 to 3 pts) because of offsetting changes in gas turbine output ratio.

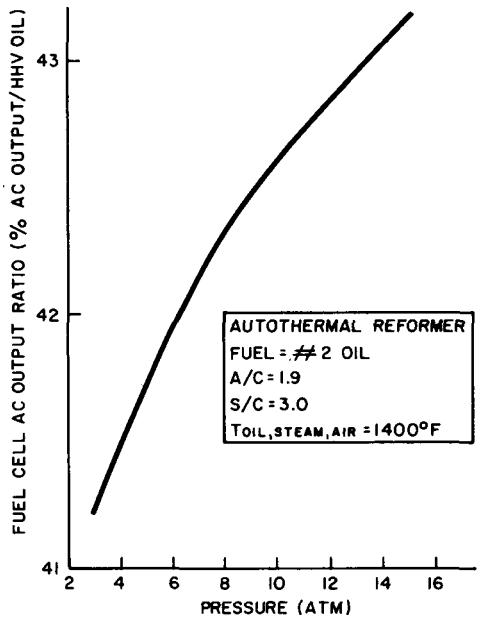

Figure E-22. Fuel Cell AC Output Ratio vs. Cycle Pressure

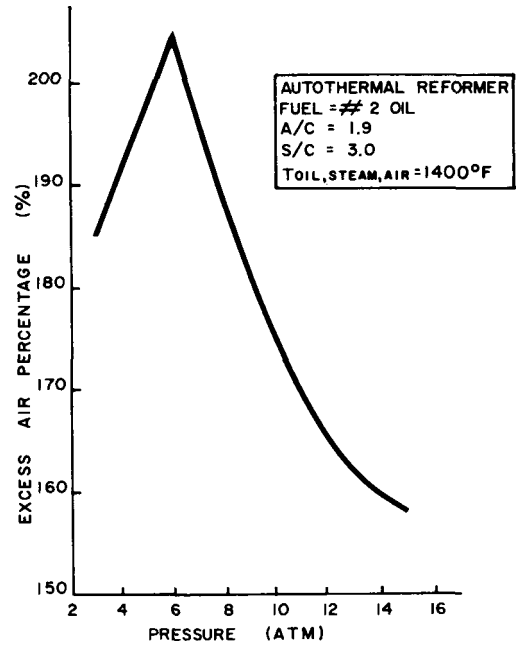

Figure E-23. Excess Air Percentage vs. Cycle Pressure

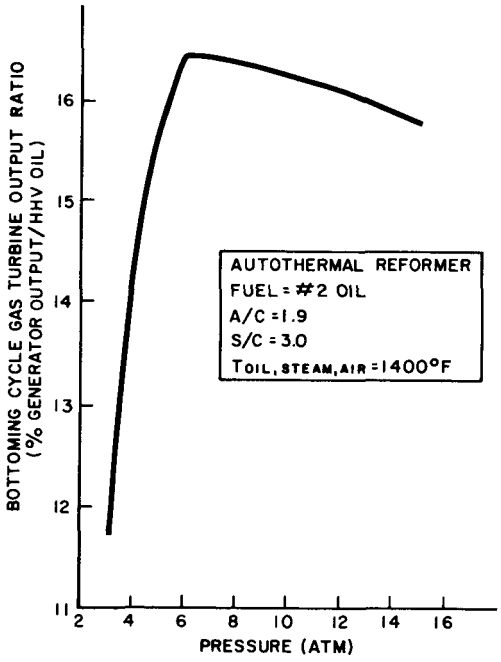

Figure E-24. Bottoming Cycle Gas Turbine Output Ratio vs. Cycle Pressure

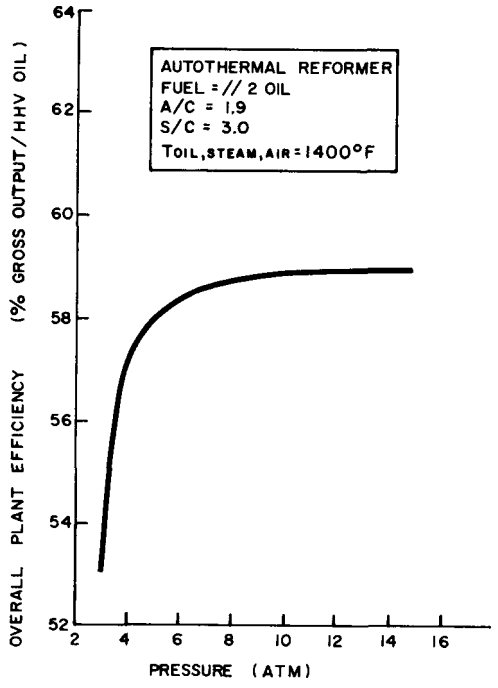

Figure E-25. Overall Plant Efficiency vs. Cycle Pressure

Appendix F

PERFORMANCE EVALUATION USING ALTERNATE GASIFIERS

Previous cycle definition/evaluation studies of the molten carbonate fuel cell combined cycle power plant conducted by General Electric (2-1 and 2-8), have established a reference system configuration and have determined its performance potential based on the use of the Texaco gasifier and a fully developed fuel cell stack component. This reference cycle configuration is illustrated in simplified form in Figure F-1.

Performance of the MCFC combined cycle system is significantly affected by variations in gasifier subsystem characteristics such as cold gas efficiency of H_2 and CO production, carbon utilization, specific consumption of steam and oxygen, and

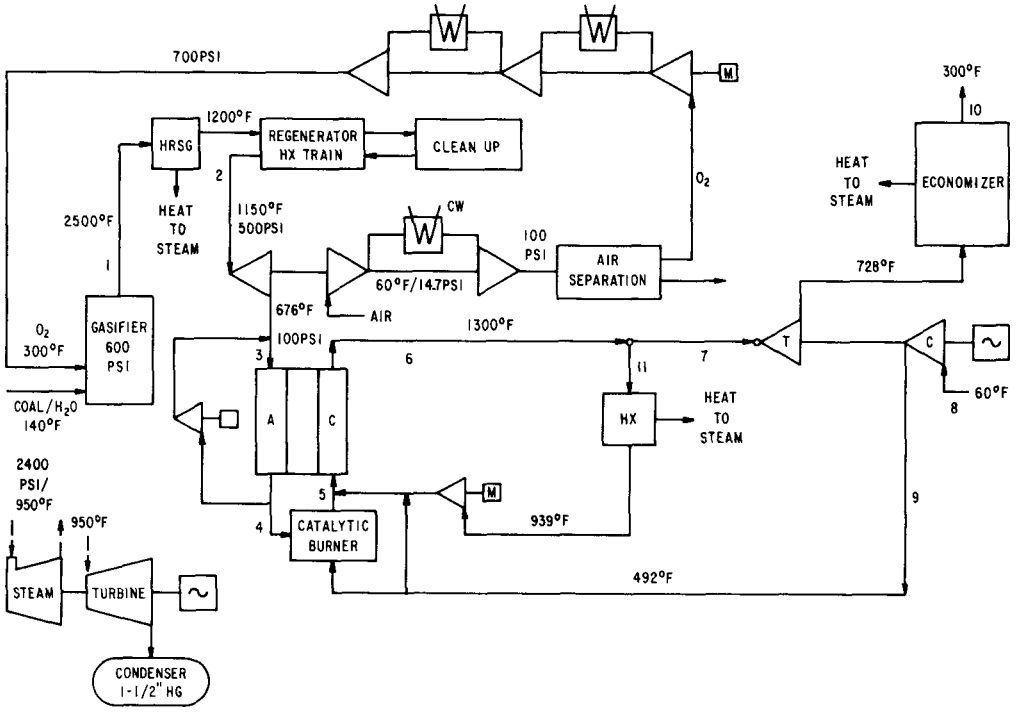

Figure F-1. Oxygen-Blown System with Partially Cascaded Bottoming Cycle

thermal efficiency of the gas cooling/reheating process. It was therefore of interest to determine combined cycle performance based on the use of alternate gasifiers and to establish on a comparative basis one of the major criteria for gasifier selection; i.e., the attainable system efficiency level.

The data presented herein summarize the results of MCFC combined cycle performance calculations for the reference cycle configuration of Figure F-1 as modified for use of four alternate gasifiers, Texaco, IGT U Gas, Shell Koppers, and British Gas Slagger. Gasifier performance data which have been used as a basis for these calculations are taken from References 2-3, 2-6 and 2-7. In addition, the calculations have been carried out in accordance with the following uniform assumptions:

1. Polarization constant of fuel cell = .7 ohm/cm^2.
2. Fuel cell current density level = 161 mA/cm^2.
3. Fuel cell temperature = 1300^{o}F.
4. (H_2 + CO) electrochemical utilization = .85.
5. Clean gas temperature at inlet of fuel gas expander (if such expander is used) = 750^{o}F.
6. Excess air ratio for overall oxidation of clean fuel gas = 100%.
7. Fuel cell pressure level = 100 psia at anode inlet.
8. Fuel cell anode recirculation ratio = minimum value consistent with carbon-free anode inlet gas equilibrium at 1300^{o}F temperature.
9. No methane forms within the fuel cell.
10. Fuel cell voltage is calculated in accordance with the model presented in (2-1).

Assumptions (6) and (7) are based on results presented in (2-8), which indicate that a fuel cell pressure of 7 atm and an overall excess air ratio of 100% provide approximately optimum system operating conditions. This study also investigated the variation in total plant investment and the total cost of electricity as it was modified by the use of each gasifier system. The work was meant to complement the cost studies for the oxygen-blown Texaco gasifier system studies reported in Appendix B and the work in Section 2; however, data will differ in minor respects due to slightly different assumptions.

ALTERNATE GASIFIER SYSTEM DEFINITION

Schematic diagrams for the four alternate systems are shown in Figures F-2 through F-5. These systems are briefly described herein.

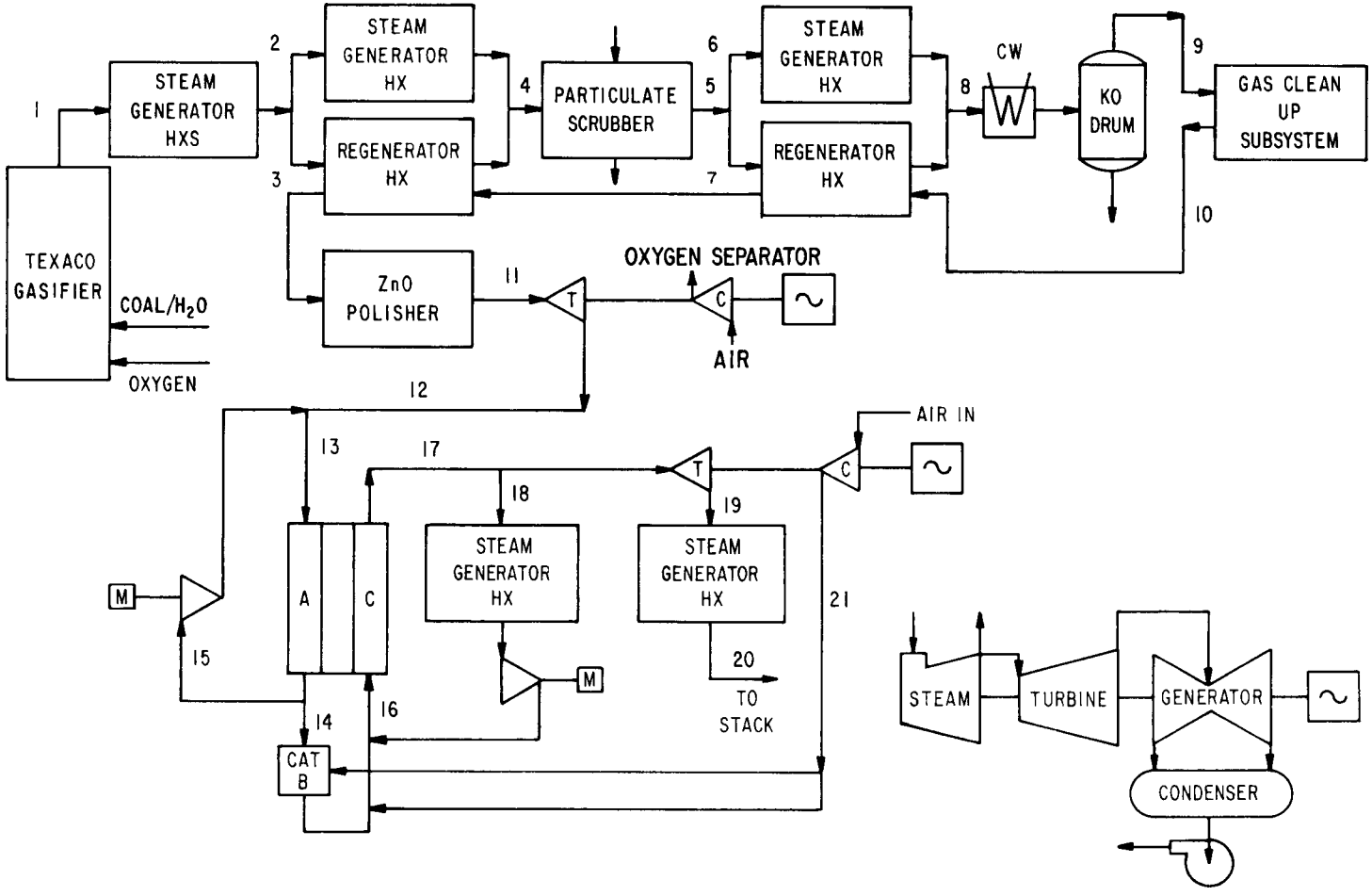

Figure F-2. MCFC Combined Cycle Power System (Texaco Gasifier)

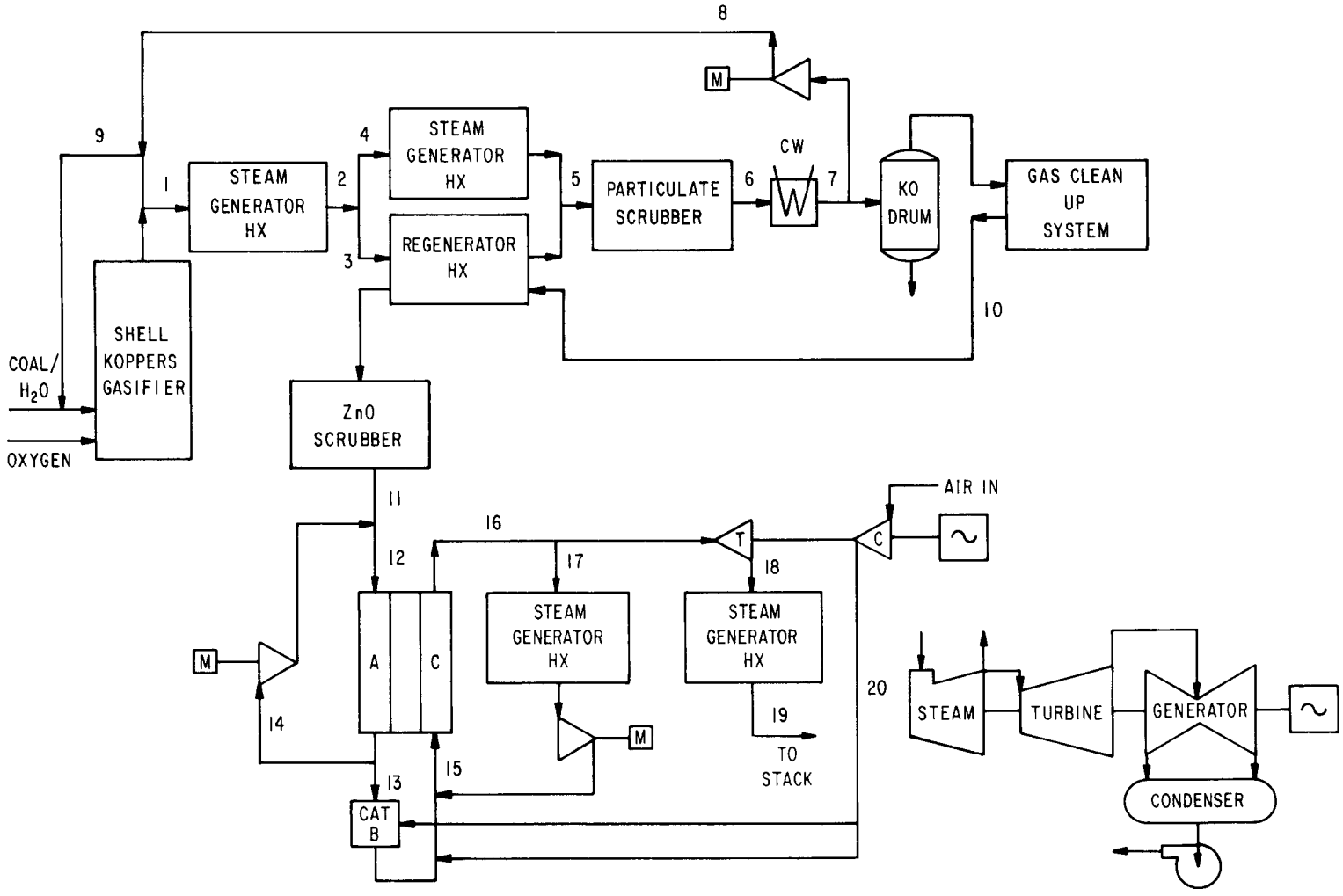

Figure F-3. MCFC Combined Cycle Power System (Shell Koppers Gasifier)

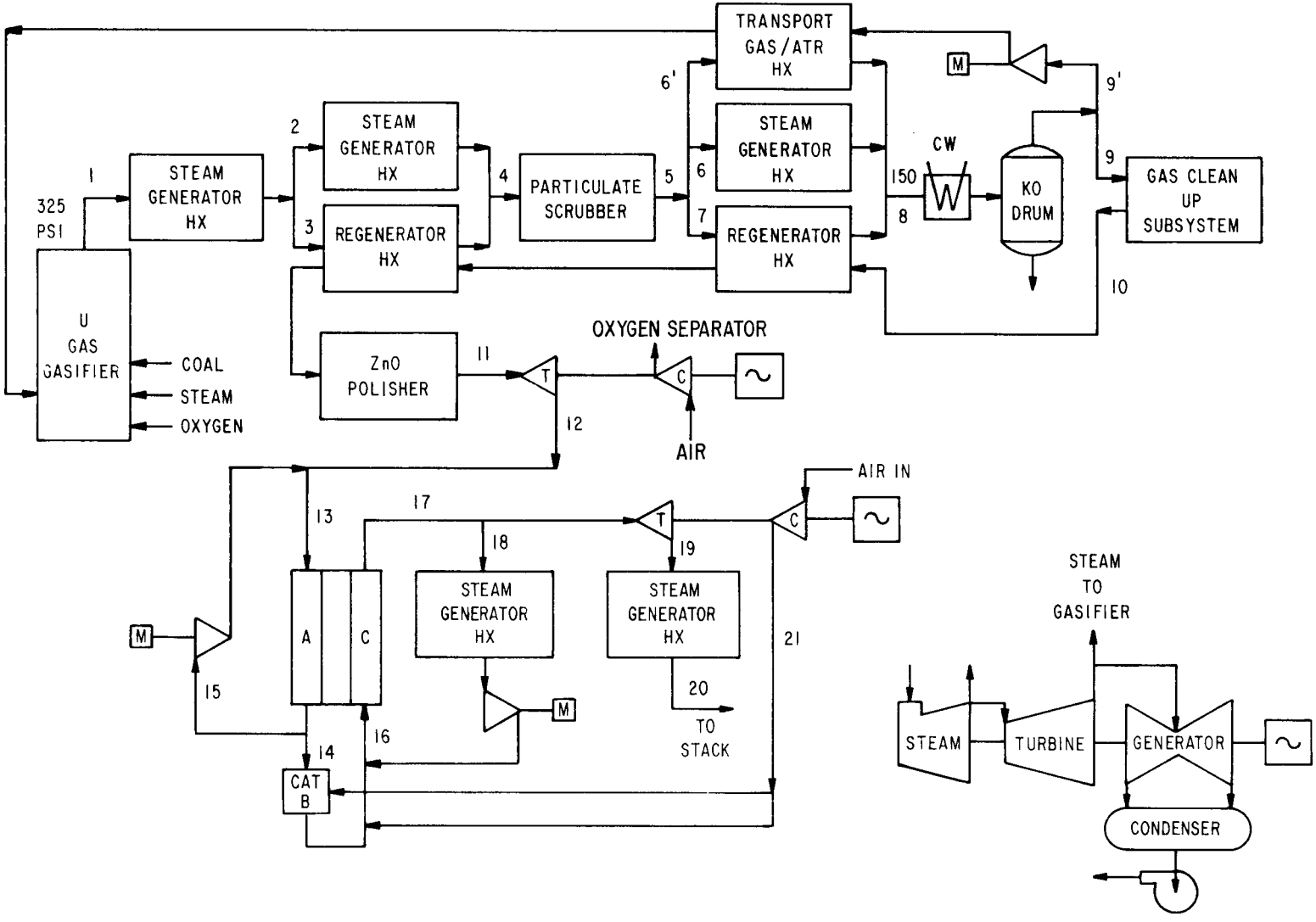

Figure F-4. MCFC Combined Cycle Power System (U-Gas Gasifier)

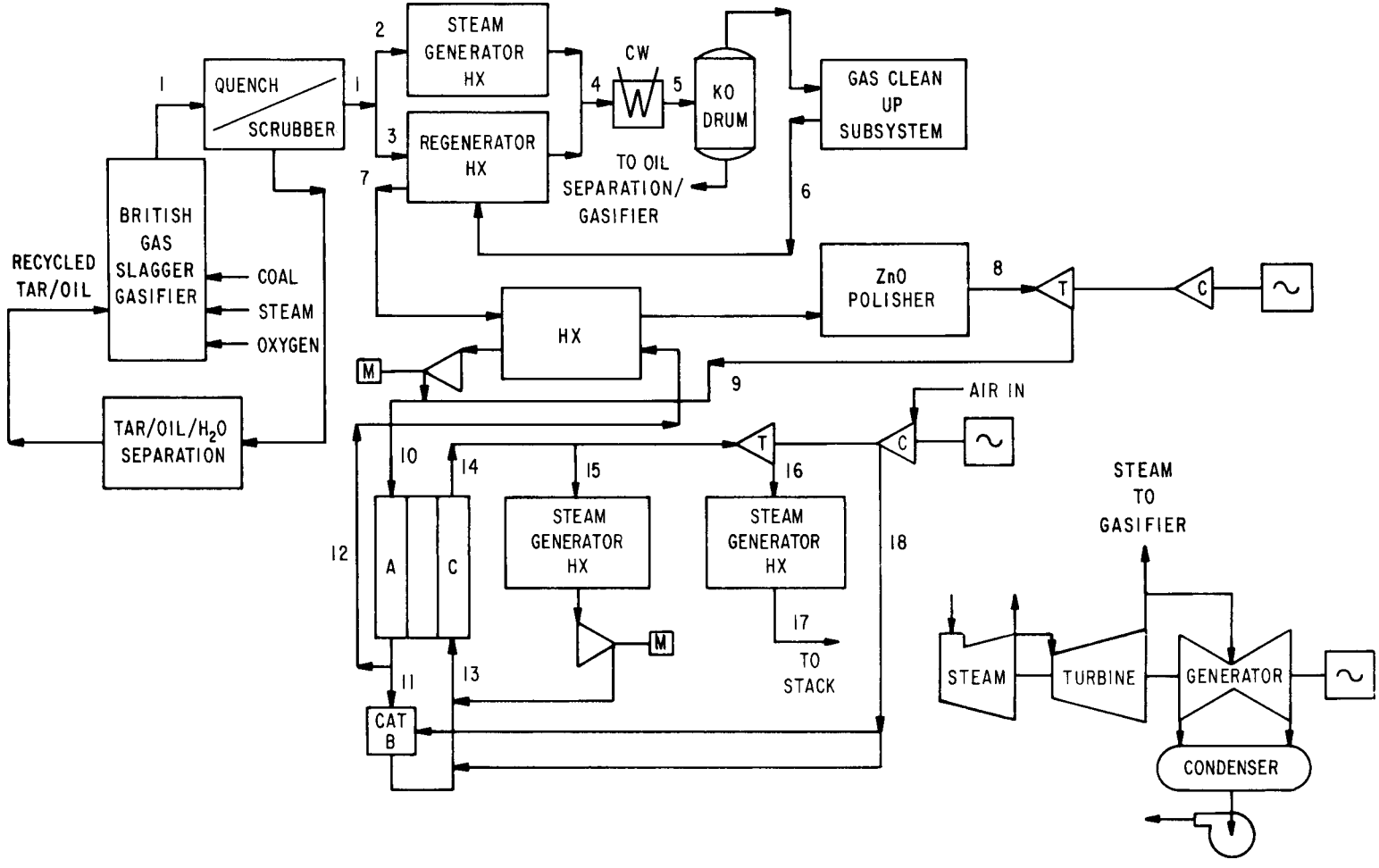

Figure F-5. MCFC Combined Cycle POWER System (U Gas Gasifier)

Texaco System

The system that uses the Texaco gasifier is shown in Figure F-2. The entrained bed gasifier is fed with a coal/water slurry and with oxygen. Product gas at a temperature of 2450^{O}F is passed through a heat recovery steam generator which incorporates a radiant section where slag is solidified and separated from the gas stream, and a following convection section. Downstream of this HRSG the raw gas stream is divided into two parts, one passing through a steam generator heat exchanger and the other passing through a regenerative heat exchanger for reheating clean gas. These heat exchangers are followed by a wet particulate scrubber in which the gas enters at a temperature slightly above its dew point. After this is a second parallel arrangement of steam generator and regenerative heat exchangers, followed by a gas cooler, knockout drum, and the acid gas removal subsystem.

Clean gas is regeneratively reheated to a temperature of 750 ^{O}F, is passed through a ZnO polishing scrubber, and is admitted to an expander turbine in which pressure is reduced to the fuel cell pressure. Anode inlet gas is heated and conditioned to a carbon-free equilibrium composition by recirculation of anode discharge gas. The anode discharge stream is mixed with air from the bottoming cycle gas turbine compressor, is passed through a catalytic burner, and is admitted to the cathode after mixture with additional air and with a stream of cooled cathode discharge gas. The cathode discharge stream, after being partially recirculated through a steam generator heat exchanger for removal of fuel cell waste heat, is admitted to the bottoming cycle gas turbine. Downstream of this turbine is an economizer (feed water heater) heat exchanger for recovery of exhaust heat ahead of the stack.

Shell Koppers System

The system configuration using the Shell Koppers gasifier, Figure F-3, is similar to that using the Texaco gasifier except for the following points:

- The dew point of the raw gas is lower, so that no temperature drop is available for a second pair of parallel heat exchangers downstream of the particulate scrubber.
- A portion of the cooled gas is recycled for cooling of the gasifier discharge well below the ash fusion point. The high temperature HRSG is therefore a convective type heat exchanger.

- Because of the relatively low pressure level of the gasifier, there is no fuel gas expander turbine.*

The gasifier is fed with pulverized coal, oxygen, and little or no steam. (Any steam required is generated as gasifier Shell coolant.) A small portion of the recycled gas is used in coal pneumatic transport.

U Gas System

The system configuration using the U Gas gasifier (Figure F-4) is very similar to the system of Figure F-2 (Texaco) except that a small flow of cooled gas is recirculated for use as transport gas for gasifier coal feed. Also steam is extracted from the steam turbine for supply to the gasifier. The gasifier is a fluidized bed type with two-stage internal cyclones which recirculate directly to the bed.

British Gas Slagger System

The system configuration employing the British Gas Slagger gasifier, shown in Figure F-5, differs from the other systems in that the gasifier effluent is directly subjected to a quench scrubbing process for tar removal.

Tar removed from the gas stream by this scrubber is separated from the water and is recycled to the gasifier. Other condensable hydrocarbons are removed in the primary stage of the gas clean-up system and are also recycled to the gasifier. A heat exchanger in the anode recirculation stream is employed for raising the temperature of the clean gas to a suitable level ($750^{o}F$) for ZnO polishing and for admission to the fuel gas expander turbine.

Mass Balance

Gas stream composition, pressure, and temperature data are also provided along with the total moles of gas per lb of coal. Mass flow rates balance throughout each power plant within a tolerance 0.5% or less except where:

*Information received after the calculations were completed indicates that the Shell Koppers gasifier is designed for pressure levels in the range of 20-40 Bar. Although the discrepancy between this pressure range and the level of 13.5 Bar used in the calculations, based on (3-7), will have an important effect upon the selection of the gas cleanup process and upon component costs, it has only a minor effect upon system performance. (It will tend to improve efficiency slightly due to an increase in total gas turbine output.)

- water condenses out of the gas stream when the temperature in the cooling system approaches the dew point.
- water removal occurs in the knockout drum.
- ethylene, ethane, hydrogen sulfide, carbonyl sulfide, or ammonia are removed in the gas cleanup system.

Energy Balance

The total enthalpy in the gas stream is the sum of the chemical energy (higher heating value) in the fuel gas, the sensible energy due to its temperature, and the latent heat due to water vapor. Fuel cell electrical output was calculated from the difference between the enthalpy flow in and the enthalpy flow out. These results were then compared to the fuel cell output based upon system performance parameters and a net plant output of 675 MWe. The two sets of values for fuel cell output agreed within 3% or less. The energy balance about the fuel cell is very sensitive to changes in the cathode inlet and outlet temperatures. After passing through the catalytic burner, no H_2, CO, and CH_4 is left in the gas and the gas stream chemical energy is zero. The sensible energy then becomes the largest contributor to the total enthalpy at the cathode.

RESULTS OF CALCULATIONS

Results of the comparative system performance calculations are presented in the following tables:

Tables F-1 through F-4	Gasifier Energy balances
Tables F-5 through F-8	System Flow Stream Composition/Pressure/Temp Data
Table F-9	System Gas Stream Energy Balance Summaries
Table F-10	System Performance Summaries

DISCUSSION OF RESULTS

The results presented herein illustrate the fact that the gasifier parameter of primary importance to MCFC combined cycle efficiency is the ratio of the heating value of the $CO+H_2$ in the product gas to the heating value of the coal. The output ratio $\frac{\text{Electrical Output}}{\text{Coal HHV Input}}$ of the fuel cell, the largest contributor to system output, is approximately proportional to this heating value ratio. The gas turbine generator output ratio is approximately proportional to the ratio of the total gas heating value to the heating value of the coal, since the turbine air/gas flows

Table F-1

TEXACO GASIFIER ENERGY BALANCE
(Based on Data From Ref. 2-3)

Energy Inputs	
Coal HHV	1.00
Coal Sensible Energy	.0019
Oxidant Sensible Energy	.00398
Water Sensible Energy	.00288
	1.00876

Energy Outputs	
Raw Gas HHV	.796
Raw Gas Sensible + Latent Energy	.2077
Heat Loss	.00506
	1.00876

Table F-2

SHELL KOPPERS GASIFIER ENERGY BALANCE
(Based on Data From Ref. 2-7)

Energy Inputs	
Coal HHV	1.00
Oxidant Sensible Energy	.0026
Recycled Gas HHV	.6854
Recycled Gas Sensible + Latent Energy	.0029
	1.6909

Energy Outputs	
Effluent + Recycled Gas Stream HHV	1.519
Effluent + Gas Stream Sensible + Latent Energy	.154
Heat Loss	.0179
	1.6909

Table F-3

U GAS GASIFIER ENERGY BALANCE
(Based on Data From Ref. 2-6)

Energy Inputs	
Coal HHV	1.00
Oxidant Sensible Energy	.0048
Steam	.0577
Transport Gas HHV	.0214
Transport Gas Sensible + Latent Energy	.00014
	1.08404

Energy Outputs	
Effluent Gas HHV	.8912
Effluent - Gas Sensible + Latent Energy	.12392
Heat Loss	.06892

Table F-4

BRITISH GAS SLAGGER GASIFIER ENERGY BALANCE
(Based on Data From Ref. 2-1)

Energy Inputs	
Coal HHV	1.000
Oxidant Sensible Energy	.0014
Steam	.00316
	1.033

Energy Outputs	
Gas HHV	.957
Gas Sensible + Latent Energy	.047
Heat Loss	.029
	1.033

Table F-5

TEXACO SYSTEM GAS STREAM FLOW RATES/COMPOSITION/PRESSURE/TEMPERATURE DATA
(flow rates for net output - 675 MWe)

Stream Number	1	2	3	4	5	6	7	8	9	10	11	12	13	14	15	16	17	18	19	20	21
Stream ID	Gasifier Exit	HRSG	Regen. HX	Scrubber Inlet	Scrubber Exit	HRSG	Regen. HX	Water Knockout	Clean up Inlet	Clean up Exit	Turbine Inlet	Turbine Exit	Anode Inlet	Burner Inlet	Anode Recir.	Cathode Inlet	Cathode Exit	HRSG	Econom. Inlet	Stack	Fuel Cell Air
Temperature (^{o}F)	2450	800	800	350	327	327	327	150	100	75	750	352	1062	1300	1300	1000	1300	1300	718	300	490
Pressure (psia)	600	592	592	585	570	570	570	562	555	530	500	100	100	99	99	100	99	100	15.3	14.7	101
Gas Composition (Mole Fraction)																					
H_2	.2884	→	→	→	→	→	→	.3487	.3506	.393	→	→	.1539	.0230	→						
CO	.4244	→	→	→	→	→	→	.5135	.5162	.578	→	→	.2414	.0568	→						
CH_4	.0008	→	→	→	→	→	→	.0009	.00098	.0011	→	→	.00077	.00068	→						
CO_2	.0871	→	→	→	→	→	→	.1052	.1057	.0161	→	→	.4716	.7211	→	.1649	.1154	→	→	→	
H_2O	.1788	→	→	→	→	→	→	.00693	.0017	.0008	→	→	.1247	.1926	→	.0698	.0767	→	→	→	
N_2	.0078	→	→	→	→	→	→	.00946	.0095	.0108	→	→	.00755	.0058	→	.6492	.7133	→	→	→	.79
H_2S	.0101	→	→	→	→	→	→	.01217	.01224												
COS	.0006	→	→	→	→	→	→	.00073	.00073												
NH_3	.002	→	→	→	→	→	→	.00239	.0024												
O_2																.116	.0945	→	→	→	.21
Total Gas Moles LB Coal	.1081	.020	.0881	.1081	.1081	.0858	.0223	.0894	.0889	.0793	.0793	.0793	.2241	.1448	.1448	1.0928	.9946	.58523	.40936	.40936	.3685
Total Gas Flow (10^3 lb mole/hr)	40.1863	7.4350	32.7513	40.1863	40.1863	31.8962	8.2900	33.2345	33.0487	29.4798	24.4798	29.4798	83.3094	53.8295	53.9295	406.2495	369.7435	217.5598	152.1800	152.1800	136.9902
Total Gas Flow (10^6 lb/hr)	.8207	.1518	.6689	.8207	.8207	.6514	.1693	.6957	.6922	.5315	.5315	.5315	2.5243	1.9927	1.9927	12.3563	10.8956	6.4113	4.4846	4.4846	3.9522
Gas Enthalpy Flow (10^6 Btu/hr)	4609.6	741.5	3267.2	3863.1	3855.9	3060.5	795.4	3683.9	3671.5	3516.4	3658.5	3573.9	5013.7	1434.7	1434.7	3574.6	4171.0	2454.3	983.9	493.1	417.1

Table F-6

SHELL KOPPERS SYSTEM
GAS STREAM FLOW RATES/COMPOSITION/PRESSURE/TEMPERATURE DATA
(flow rates for net output - 675 MWe)

Stream Number	1	2	3	4	5	6	7	8	9	10	11	12	13	14	15	16	17	18	19	20
Stream ID	Gasifier Exit	HRSG Exit	Regen HX	HRSG	Scrubber Inlet	Scrubber Exit	Water Knockout	Gasifier Recir.	Transport Gas	Cleanup Exit	ZnO Scrubber	Anode Inlet	Burner Inlet	Anode Recir.	Cathode Inlet	Cathode Exit	HRSG	Econom. Inlet	Stack	Fuel Cell Air
Temperature (^{o}F)	1650	800	800	800	140	120	100	100	100	91	750	1162	1300	1300	1000	1300	1300	720	300	490
Pressure (PSIA)	200	185	185	185	170	150	140	140	220	120	100	100	99	99	100	99	99	15.3	14.7	101
Gas Composition (mole fraction)																				
H_2	.277	→	→	→	→	→	.278	→	→	.282	→	.112	.01737	→						
CO	.647	→	→	→	→	→	.6497	→	→	.66	→	.2754	.06119	→						
CH_4	.002	→	→	→	→	→	.002	→	→	.002	→	.00143	.00111	→						
CO_2	.01	→	→	→	→	→	.01	→	→	.01	→	.49015	.7565	→	.1762	.13305	→	→	→	
H_2O	.011	→	→	→	→	→	.0068	→	→	.006	→	.09242	.1416	→	.0527	.05738	→	→	→	
N_2	.039	→	→	→	→	→	.0392	→	→	.04	→	.0286	.0222	→	.6576	.7155	→	→	→	.79
H_2S	.014	→	→	→	→	→	.0141	→	→											
O_2															.1134	.09405	→	→	→	.21
Total Gas Moles / LB Coal	.15926	.15926	.0873	.07196	.15926	.15926	.15859	.07155	.0017	.0857	.0857	.2392	.1542	.1541	1.2733	1.17035	.7373	.43305	.43305	.3879
Total Gas Flow (10^3 lb-mole/hr)	58.3871	58.3871	32.0055	26.3816	58.3871	58.3871	58.1415	26.2313	.6232	31.4189	31.4189	87.8776	56.5320	56.5320	466.8109	429.0679	270.3052	158.7626	158.7626	142.2099
Total Gas Flow (10^6 lb/hr)	1.2385	1.2385	.6789	.5596	1.2385	1.2385	1.2343	.5568	.0132	.6521	.6521	2.8121	2.1615	2.1615	14.3577	12.8474	8.0937	4.7538	4.7538	4.1028
Gas Enthalpy Flow (10^6 Btu/hr)	7619.2	7217.3	3956.2	3261.1	6929.1	6920.2	6909.4	3116.3	73.9	3648.7	3696.7	5258.4	1458.6	1458.6	3962.5	4704.0	2963.4	973.9	456.9	433.0

Table F-7

U GAS SYSTEM
GAS STREAM FLOW RATES/COMPOSITION/PRESSURE/TEMPERATURE DATA
Flow Rates for Net Output - 675 MWe)

Stream Number	1	2	3	4	5	6	6'	7	8	9	9'	10	11	12	13	14	15	16	17	18	19	20	21
Stream ID	Gasifier Exit	HRSG	Regen. HN	Scrubber Inlet	Scrubber Exit	HRSG	Transport Gas HX	Regen. HX	Water Knockout	Cleanup Inlet	Transport Gas	Cleanup Exit	Turbine Inlet	Turbine Exit	Anode Inlet	Burner Inlet	Anode Recir.	Cathode Inlet	Cathode Exit	HRSG	Econom. Inlet	Stack	Fuel Cell Air
Temperature (^{o}F)	1550	800	800	280	261	261	261	261	150	100	100	75	750	566	1102	1300	1300	1119	1300	1300	713	300	490
Pressure (psia)	325	320	320	315	300	300	300	300	295	280	280	250	200	100	100	99	99	100	99	99	15.3	14.7	101
Gas Composition (Mole Fraction)																							
H_2	.3079	→	→	→	→	→	→	→	.3457	.3489	→	.4075	→	→	.1635	.0245	→						
CO	.3627	→	→	→	→	→	→	→	.4073	.4111	→	.48015	→	→	.2071	.0514	→						
CH_4	.0588	→	→	→	→	→	→	→	.0660	.0666	→	.07782	→	→	.0565	.0443	→						
CO_2	.1311	→	→	→	→	→	→	→	.14719	.1485	→	.02342	→	→	.4325	.6656	→	.1224	.09279	→	→	→	
H_2O	.1206	→	→	→	→	→	→	→	.01250	.00339	→	.00172	→	→	.1336	.2088	→	.0855	.09016	→	→	→	
N_2	.00705	→	→	→	→	→	→	→	.00793	.008	→	.00935	→	→	.00679	.00533	→	.684	.72137	→	→	→	.79
H_2S	.01107	→	→	→	→	→	→	→	.01245	.01256	→												
COS	.000429	→	→	→	→	→	→	→	.000482	.000486	→												
NH_3	.000353	→	→	→	→	→	→	→	.00039	.0004	→												
O_2																		.1080	.0956	→	→	→	.21
Total Gas Moles Lb Coal	.10177	0.288	.07297	.10177	.10177	.0775	.00035	.02427	.09603	.087648	.002157	.07504	.07504	.07504	.2067	.13165	.13165	1.6427	1.5578	1.0876	.47015	.47015	.4284
Total Gas Flow (10^3 lb mole/hr)	40.5985	11.4890	29.1095	40.5985	40.5985	30.9166	.1396	9.6819	38.3087	34.9649	.8605	29.9353	29.9353	29.9353	82.4576	52.5183	52.5183	655.3125	621.4438	433.8697	187.5541	187.5541	170.8990
Total Gas Flow (10^6 lb/hr)	.8327	.2356	.5970	.8327	.8327	.6341	.0029	.1986	.7977	.7289	.0179	.5042	.5042	.5042	2.3639	1.8595	1.8595	19.3624	18.0076	12.5723	5.4348	5.4348	4.9304
Gas Enthalpy Flow (10^6 Btu/hr)	5009.3	1337.1	3388.2	4549.6	4543.5	3459.9	15.8	1083.6	4789.2	4308.7	105.8	4148.5	4298.4	4256.3	6535.3	2273.9	2273.9	6526.5	7116.5	4968.5	1246.4	633.2	520.3

Table F-8

BGC SYSTEM
GAS STREAM FLOW RATES/COMPOSITION/PRESSURE/TEMPERATURE DATA
(flow rates for net output - 675 MEe)

Stream Number	1	2	3	4	5	6	7	8	9	10	11	12	13	14	15	16	17	18
Stream ID	Gasifier Exit	HRSG	Regen. HX	Water Conden.	Water Knockout	Cleanup Exit	Recir. HX Inlet	Turbine Inlet	Turbine Exit	Anode Inlet	Burner Inlet	Anode Recir.	Fuel Cathode Inlet	Cathode Exit	HRSG	Econom. Inlet	Stack	Fuel Cell Air
Temperature (^{o}F)	820	280	280	150	100	100	250	750	531	1000	1300	1300	1119	1300	1300	729	300	492
Pressure (PSIA)	320	300	300	290	280	250	240	230	100	100	99	99	100	99	99	15.3	14.7	101
Gas Composition (mole fraction)																		
H_2	.2856	.25058	→	.29583	.29866	.3109	→			.11464	.019176	→						
CO	.5451	.47814	→	.5645	.56989	.59324	→			.23286	.05754	→						
CH_4	.0729	.0639	→	.07544	.076166	.079286	→			.056122	.04485	→						
C_2H_4	.0022	.00189	→	.00223	.002253	.002345	→			.00166	.001327	→						
C_2H_6	.0032	.00279	→	.003294	.003326	.003462	→			.00245	.001959	→						
CO_2	.0182	.01592	→	.01880	.01898	.00267	→			.48118	.7139	→	.13656	.10489	→			
H_2O	.0467	.16384	→	.01282	.00338	.003531	→			.10786	.1586	→	.07034	.07454	→			
N_2	.0041	.003678	→	.00434	.00438	.004563	→			.00323	.00258	→	.68354	.72438	→			.79
H_2S	.0129	.01130	→	.01334	.01347													
COS	.0006	.000493	→	.000582	.000587													
NH_3	.0085	.007466	→	.008814	.008898													
O_2													.10955	.09618	→			.21
Total Gas Moles LB Coal	.085375	.07076	.02657	.082445	.081664	.07845	.07845	.07845	.07845	.23973	.138673	.16128	1.60409	1.51366	1.000	.51366	.51366	.4705
Total Gas Flow (10^3 lb-mole/hr)	32.1509	26.6471	10.0058	31.0475	30.7533	29.5430	29.5430	29.5430	29.5430	90.2785	52.2220	60.7355	604.0746	570.0201	376.5840	193.4361	193.4361	177.1828
Total Gas Flow (10^6 lb/hr)	.6455	.5280	.1983	.6255	.6202	.5644	.5644	.5644	.5644	2.8087	1.9289	2.2434	18.0805	16.7181	11.0449	5.6733	5.6733	5.1117
Gas Enthalpy Flow (10^6 Btu/hr)	4681.3	3341.8	1255.1	4489.5	4474.1	4233.8	4266.5	4380.1	4329.4	68.16.1	2252.5	2619.8	5862.3	6375.2	4211.9	1254.3	617.5	542.0

Table F-9

GAS FLOW STREAM ENERGY BALANCE SUMMARIES

		Texaco System	Shell Koppers System	U Gas System	British Gas Slagger System
Energy Outputs	Coal HHV	1.00	1.00	1.000	1.000
	Coal Sensible Energy	.0019	0.00	.000417	0.00
	Oxidant Sensible Energy	.0037	.0026	.00483	.0014
	Water Sensible Energy	.0065	-	-	-
	Steam Sensible/Latent Energy	-	-	.0557	.0316
	Total	1.0121	1.0026	1.06095	1.033
Energy Inputs	Fuel Cell DC Output	.344	.3625	.2945	.314
	Bottoming Cycle Gas TB Shaft Output	.070	.0748	.0874	.096
	Fuel Gas Expander Shaft Output	.0186	-	-	-
	Heat Transferred to Steam	.4372	.4300	.45705	.431
	Heat Losses in Gas Cooling/Cleanup	.008	.004	.007	.046
	Stack Loss	.1084	.1018	.1340	.135
	Gasifier Heat Loss	.012	.015	.02	.011
	Miscellaneous Heat Loss	.0139	.0145	.061	-
	Total	1.0121	1.0026	1.06095	1.033

Table F-10

SYSTEM PERFORMANCE SUMMARIES
Basis: One Unit Coal HHV

	Texaco System	Shell Koppers System	U Gas System	British Gas Slagger System
Fuel Cell AC Output	.338	.357	.290	.309
Bottoming Cycle Gas TB Gen Output	.069	.0737	.0861	.094
Steam Turbine Gen Output	.166	.1634	.160	.155
Plant Gross Electrical Output	.573	.5941	.536	.558
Parasitic Power				
Pwr for O_2 Plant Air Compressors in Excess of Pwr Supplied by Fuel Gas Expander	.0135	.035	.023	.019
Pwr for O_2 Compressors	.0230	.014	.011	.009
Pwr for Anode/Cathode RC Blowers	.005	.005	.005	.005
Misc Pwr for Coal Handling/Cleanup/ Steam Auxiliaries/Misc	.025	.025	.025	.025
Total Parasitic Pwr	.0665	.079	.064	.058
Net Plant Output	.573 - .065 = .5065	.5941 - .079 = .5151	.536 - .064 = .472	.558 - .058 = .500

are proportional to the total quantity of fuel gas handled by the system. Gas turbine generator gross output also increases with the pressure ratio of the fuel gas expander. Heat transferred to the steam is the difference between the coal energy input and the sum of fuel cell and gas turbine generator outputs plus losses, including the largest loss, stack loss. The stack loss ratio increases with the ratio of total gas heating value to the heating value of the coal.

The calculated results, which are consistent with the above principles, show that the Shell Koppers gasifier provides the highest fuel cell output ratio and the highest overall system efficiency. The Shell Koppers performance is followed closely by Texaco. British Gas Slagger, which has the highest total gas cold gas efficiency but with a lower $CO+H_2$ cold gas efficiency than that of the entrained bed gasifiers, is third. U Gas, with the lowest $CO+H_2$ cold gas efficiency, is fourth.

Because the system using the Shell Koppers gasifier has no fuel gas expander, the gas turbine generator output ratio is lower than that of the Texaco system. Information received from Shell subsequent to completion of the calculations indicates that the Shell Koppers gasifier can be designed for pressure levels up to 40 Bar. Operation at this pressure level would result in an increase in the gas turbine generator gross output, and a small increase in the efficiency of the Shell Koppers system.

Steam turbine generator output is highest for the Texaco and Shell Koppers systems, which do not require a supply of turbine extraction steam for gasification.

COMPARATIVE ECONOMICS

Cost estimates were made for each of the gasifier systems. All capital cost estimates are based on publicly available literature. No detailed estimates were performed.

The selection of realistic scaling factors is the crucial step in this study. The choice of a particular scaling factor was based upon a number of considerations. Among these were the need to reconcile the fundamental technical or operational differences between alternate plant subsystems. There were also variations in plant equipment which had to be accommodated. The elements of cost and their corresponding scaling factors are listed in Table 2-1.

A short description of the subsystems and their scaling factors is given below:

- Oxidant feed system costs reflect two functions of this subsystem: the compression and separation of air, and the compression of oxygen. The cost of the first function is keyed to the oxygen feed rate, and the cost of the second function is keyed to the gasifier operating pressure. Both of these key parameters differ greatly among the alternate gasifiers, unlike the coal feed rate which is almost the same.

- The gasification, gas cooling, and gas cleanup subsystems involve different operating conditions, and these costs were taken directly from economic studies of integrated gasifier combined cycle systems. These cost figures were adjusted to the requirements of a fuel cell power plant using the fact that the reference system had a Texaco type gasifier. Contingency costs were added to bring the cost estimates in line with the accounting standards of the reference fuel cell power plant.

- The steam bottoming cycle is scaled using the heat to steam to account for differences in the steam generating equipment between power plants.

- Turbocompressor costs are scaled by the molar flow rate.

- Adjustments are made for differences in power plant equipment not accounted for elsewhere. This includes deducting the cost of a regenerative heat exchanger and a turbocompressor set from the Shell gasifier power plant cost estimate.

The total plant investment and the total cost of electricity for the five power plants are summarized in Tables F-11, F-12 and F-13, respectively. Despite some big differences in individual cost categories, the total plant investments of all the power plants vary by no more than 10%. The total cost of electricity differs by less than 6%. Within the limitations of the time available and the accuracy of this study, no one system stands out as a clear winner or loser on the basis of either the total plant investment or the total cost of electricity.

Table F-11

TOTAL PLANT INVESTMENT
(EPRI Method, 10^3\$)

Plant Section	Texaco	BGC	U Gas	Shell	Refer
Coal Handling	14,018	14,201	15,043	13,825	14,006
Oxidant Feed	75,297	41,289	53,302	58,419	74,701
Gasification & Ash Handling	17,175	35,549	21,502	43,224	17,150
Gas Cooling	48,996	63,040	22,619	25,592	48,957
Acid Gas Removal (Selexol, Claus & Tail Gas)	39,846	33,083	37,867	29,998	42,031
Steam Bottoming Cycle	95,523	94,168	99,860	93,959	82,370
Fuel Cell Modules & Combustion Turbines	159,210	160,224	154,766	165,618	158,716
Inverter System	34,924	32,877	32,179	36,289	34,808
Electrical System	20,098	20,098	20,098	20,098	20,098
Land Improvements, Structures & Miscellaneous Equipment	47,479	45,581	45,646	44,008	49,477
TOTALS	552,566	540,110	502,882	531,030	542,314

All plant outputs = 675 MW

ALL COSTS ON THIS PAGE ARE IN MID 1978 DOLLARS
(All plant outputs = 675 MW)

Table F-12

PLANT CAPITAL REQUIREMENT
(EPRI Method, 10^3\$)

	Texaco	BGC	U Gas	Shell	Refer
Total Plant Investment	552,566	540,110	502,882	531,030	542,314
Total Capital Charges	90,342	88,305	82,219	86,821	88,666
Total Capital Requirement	642,908	628,415	585,101	617,851	630,980
Increment for Interim Replacement of Fuel Cells	140,864	137,689	128,198	135,374	138,251
Equivalent Total Capital Requirement	783,772	766,104	713,299	753,225	769,231

Table F-13

BUSBAR POWER COST
(EPRI Method, 70% Capacity Factor)

	Texaco	BGC	U Gas	Shell	Refer
Net Power (MW)	675	675	675	675	675
ECTR ($1000)	783,772	766,104	713,299	753,225	769,231
Fixed Operating Cost ($1000/yr)	14,108	14,108	14,108	14,108	14,108
Variable Operating Cost ($1000/yr)	1,009	1,022	1,082	992	1,008
Coal Cost ($1000/yr)	39,884	40,402	42,799	39,333	39,848
TOTAL Operating Cost ($1000/yr)	55,001	55,532	57,989	54,433	54,964
Levelized Fixed Charges ($1000/yr)	141,079	137,899	128,394	135,581	138,462
KWh Produced in 1 Year	4.139×10^9	4.139×10^9	4.139×10^9	4.139×10^9	4.139×10^9
Total Cost of Electricity (mills/kWh)					
Fixed Charges	34.1	33.3	31.0	32.7	33.4
Operating Costs	13.3	13.4	14.0	13.2	13.3
Cost of Electricity	47.4	46.7	45.0	45.9	46.7

Table F-14

COMPARATIVE SUMMARY OF ALTERNATE SYSTEM PARAMETERS

	Texaco	U Gas	Shell Koppers	British Gas Slagger
$\frac{\text{HHV } (H_2+CO+CH_4)}{\text{HHV Coal}}$	.772	.846	.81	.927
$\frac{\text{HHV } (CO+H_2)}{\text{HHV Coal}}$	.770	.664	.805	.708
Temp. of Gasifier Effluent	2450°F	1150°F	1650°F after cooled gas quench	820°F
Gasifier Pressure	600 psia	325 psia	200 psia*	320 psia
$\frac{\text{\# Water or Steam}}{\text{\# Coal}}$	Water in Slurry	.505	Water in Slurry	.298
$\frac{\text{\# } O_2}{\text{\# Coal}}$	.84	.62	.934	.469
F.C. DC Voltage	.775	.767	.778	.769
$\frac{\text{F.C. AC Output}}{\text{Coal HHV Input}}$	.338	.290	.357	.314
$\frac{\text{Gas Tb Gen. Output}}{\text{Coal HHV Input}}$	.087	.091	.074	.094
$\frac{\text{Steam Tb Gen. Output}}{\text{Coal HHV Input}}$	.166	.160	.163	.155
$\frac{\text{Gross Electric Output}}{\text{Coal HHV Input}}$	.591	.541	.594	.563
$\frac{\text{Auxilliary Power}}{\text{Coal HHV Input}}$	.0845	.069	.079	.063
$\frac{\text{Net Electric Output}}{\text{Coal HHV Input}}$	.5065	.472	.515	.500

*Shell Koppers gasifiers could be designed for pressures up to 600 psia.

CONCLUSIONS

A comparative summary of the major performance parameters of the alternate systems is presented in Table F-14.

With respect to the comparative MCFC combined cycle system efficiency potentials offered by application of the four alternate gasifiers which have been evaluated, the following conclusions may be stated:

- The Shell Koppers and Texaco high temperature entrained bed gasifiers have a significant performance advantage for the MCFC combined cycle application over the U Gas (fluidized bed) gasifier, and a small advantage over the British Gas Slagger (moving bed) gasifier. The superior performance of the entrained bed gasifier relates directly to a higher $CO+H_2$ cold gas efficiency.

- The British Gas Slagger gasifier, operating with total recycle of tar and condensable hydrocarbons, has a very high overall product gas cold gas efficiency (0.95), and also a moderately high $CO+H_2$ cold gas efficiency (0.70). These characteristics result in a potential for 0.50 efficiency of a combined cycle system using this gasifier.

- A wide range of gasifiers appears to be acceptable from a cost standpoint since the results for the BGC gasifier power plant show that the cost of recovering condensable hydrocarbons (tars, oils, phenols, naphtha) has a negligible effect on the overall capital cost and the cost of electricity.

- The U Gas gasifier power plant has the lowest cost of electricity despite higher operating expenses because of the lower capital needs of its gasification, gas cooling subsystems.

- Capital cost variations dominate the economics of each of these power plants compared to the fuel, operating and maintenance expenses. Fixed charges amount to approximately 70% of the total cost of electricity and vary twice as much as the operating charges (10% vs. 5%) between different power plants.